University of Glasgow

Li, Yueming (2025) *Searching novel pharmacological tools for the pharmacology of orphan G protein-coupled receptor GPR84.* PhD thesis.

https://theses.gla.ac.uk/85101/

Searching novel pharmacological tools for the pharmacology of orphan G protein-coupled receptor GPR84

Yueming Li

MSc BSc

Submitted in fulfilment of the requirements for the Degree of
Doctor of Philosophy

School of Molecular Biosciences

College of Medical, Veterinary and life Science

University of Glasgow

September 2024

Abstract

G protein-coupled receptors (GPCRs), a large group of cell-surface receptors, are involved in numerous physiological and pathological processes. Among GPCRs, the pro-inflammatory orphan receptor GPR84, a member of the Class A receptor family, is an attractive drug target for inflammatory diseases and metabolic disorders. However, there remains a significant lack of GPR84 compounds, particularly GPR84 antagonists that can be used in mouse model studies as available GPR84 antagonists display marked species selectivity for human GPR84. The most direct method to overcome this challenge is through the screening and characterization of novel compounds for both human and mouse GPR84 to discover antagonists with similar affinities for both species. Compound 271 was characterized as a competitive orthosteric antagonist for both human and mouse GPR84, and the key residue Arg172^{ECL2} in the orthosteric binding pocket is not necessary for the binding of compound 271. However, previous studies have shown that the mutation of Arg172^{ECL2} to alanine or lysine abolished the function of medium-chain fatty acids while having no effect on the potency of the allosteric agonist 3,3'-diindolylmethane in GPR84. Therefore, studying the binding pocket of an antagonist to GPR84 would be essential for understanding the structural determinants of ligand recognition and receptor modulation. In addition to this time-consuming method of screening a large number of compounds, generating a novel transgenic mouse strain expressing 'chimeric' human orthologue-like GPR84 could be another solution. Similar potencies of agonists at human and mouse orthologues, along with the high similarities between these two orthologues, provide a foundation for this idea. Herein, stable cells expressing each of HA-human GPR84, HA-mouse GPR84 or HA-humanised GPR84 were generated to characterize and compare the pharmacology of these forms using each of cAMP assays, radioligand binding assays and immunoblotting. Encouragingly, the ability of human GPR84 species selective antagonists compound 020, compound 140, compound 837 and GLPG1205 to block the activation of HA-humanised GPR84 was similar to that of HA-human GPR84. The phosphosite-specific antiserum pT263-pT264 recognized the 2-HTP induced phosphorylation of these three forms of receptors, which suggests that this antiserum can be used to detect the phosphorylation of GPR84 in *ex vivo* studies in the future. However, HA-human GPR84 was constitutively phosphorylated at residues Ser^{221} and Ser^{224} while HA-

humanised GPR84 was phosphorylated in a 2-HTP-dependent manner at these two residues. This result suggests that the differences between HA-human GPR84 and HA-humanised GPR84 still need to be considered carefully in future studies.

In addition to lacking useful compound tools for pre-clinical models, basic research around GPR84 signalling also need to be improved. GPCR phosphorylation plays an important role in GPCR signalling and regulates the downstream signal transduction including desensitization and internalization of receptors. Thus, studying which GRK(s) might be involved in GPR84 phosphorylation is important for further understanding the signalling of the receptor. It was found that both GRK2 and GRK3 are involved in GPR84 phosphorylation, and $G\alpha_i$ probably influences the GRK subtypes that phosphorylate GPR84. Moreover, the recruitment and binding of arrestin 3 to GPR84 may not depend on GPR84 phosphorylation. The internalization of GPR84 was also tracked using BRET-based 'Bystander' assays and immunocytochemical staining experiments.

In summary, the studies presented herein characterize novel GPR84 antagonists and suggest the development of a 'chimeric' human orthologue-like GPR84 mouse model to explore the therapeutic potential of blocking this receptor. Moreover, the understandings on GPR84 phosphorylation and internalization mechanisms are also improved. The results in this thesis may help to better understand the therapeutic potential of GPR84.

Table of Contents

List of Tables

List of Figures

List of Publications

Ieremias L, Kaspersen MH, Manandhar A, Schultz-Knudsen K, Vrettou CI, Pokhrel R, Heidtmann CV, Jenkins L, Kanellou C, Marsango S, <u>Li Y</u>, Bräuner-Osborne H, Rexen Ulven E, Milligan G, Ulven T. Structure-Activity Relationship Studies and Optimization of 4-Hydroxypyridones as GPR84 Agonists. J Med Chem. 2024 Mar 14;67(5):3542-3570. doi: 10.1021/acs.jmedchem.3c01923. Epub 2024 Feb 21. PMID: 38381650.

Acknowledgement

First and foremost, I would like to thank Professor Graeme Milligan for his continuing support, encouragement and guidance throughout my PhD project and my academic career. I am very grateful for the opportunity to learn from such a great scientist. I would also like to thank all the postdocs and technicians, especially Dr. Sara Marsango, Laura Jenkins and Dr. Li-Chiung Lin for all the supports and kindness.

I could not have reached this point without the great support of my parents and my sister. Thank you for all the financial supports, unconditional love and encouragement which gives me the courage to live alone in UK and finish such a PhD project. I would also want to thank Qizai and Qiuren for accompanying me through every day and night in Glasgow. Thanks to myself for being strong enough physically and mentally to finish this PhD project.

Finally, I want to thank all the kind and welcoming Scottish people for giving me this wonderful experience in Glasgow. People make Glasgow.

Author's Declaration

I declare that, except where explicit reference is made to the contribution of others, this dissertation is the result of my own work and has not been submitted for any other degree at the University of Glasgow or any other institution."

Signature: Yueming Li

Name: Yueming Li   Date: 09/09/2024

Abbreviations

ANOVA	Analysis of variance
AP2	Adaptor protein 2
ATP	Adenosine triphosphate
BRET	Bioluminescence resonance energy transfer
BCA	Bicinchoninic acid
BSA	Bovine serum albumin
cAMP	Cyclic adenosine monophosphate
cDNA	Complementary deoxyribonucleic acid
CNS	Central Nervous System
CPM	Counts per minute
DAG	Diacylglycerol
DAPI	4',6-diamidino-2-phenylindole
DMEM	Dulbecco's modified eagle's medium
DMSO	Dimethyl sulfoxide
DOX	Doxycycline
DPM	Disintegrations per minute
dNTP	Deoxynucleoside triphosphate
ECL	Extracellular loop
EDTA	Ethylene diamine tetra acetic acid
ERK	Extracellular signal-regulated kinase
eYFP	Enhanced yellow fluorescent protein
FBS	Foetal bovine serum
FRET	Fluorescence resonance energy transfer
GABA	γ-Aminobutyric acid
GAP	GTPase-activating protein
G-protein	Guanine nucleotide-binding protein
GDP	Guanosine diphosphate
GTP	Guanosine-5'-triphosphate
GTPase	Guanine nucleotide triphosphatase
GPCR	G protein-coupled receptor
GRK	G protein-coupled receptor kinase

HA	Haemagglutinin
HEK293	Human embryonic kidney cell line 293
HTRF	Homogeneous time-resolved fluorescence
IBD	Inflammatory bowel disease
ICC	Immunocytochemistry
ICL	Intracellular loop
IFN-γ	Interferon γ
IL	Interleukin
IP3	Inositol 1,4,5-triphosphate
K$_d$	Dissociation constant
KO	Knock out
LPS	Lipopolysaccharide
MCFAs	Medium chain fatty acids
mRNA	Messenger ribonucleic acid
NAM	Negative allosteric modulator
NLuc	Nanoluciferase
PAM	Positive allosteric modulator
PEI	Polyethylineimine
PTX	Pertussis toxin
RT	Room temperature
RGS	Regulators of G protein signalling
SAR	Structure-activity relationship
SDS-PAGE	Sodium dodecyl sulphate polyacrylamide gel electrophoresis
TM	Transmembrane domain
TNFα	Tumour necrosis factor α
WB	Western blot
WT	Wild type

Chapter 1   Introduction

1.1 G protein-coupled receptors

1.1.1 Structural features and classification of GPCRs

G protein-coupled receptors (GPCRs) comprise the largest class of cell surface proteins in the human genome with over 800 members (Yang et al., 2021, Lagerstrom and Schioth, 2008). They are widely distributed in the central nervous system, immune system, cardiovascular system, retina, and many other organs and tissues, and they can be activated by endogenous ligands including odours, hormones, neurotransmitters and chemokines (Yang et al., 2021, Alexander et al., 2017). As GPCRs are widely expressed in various tissues, they are the most commonly targets in drug development, and it is estimated that around 34% of marketed drugs target GPCRs (Sriram and Insel, 2018, Guo et al., 2022, Addis et al., 2024).

GPCRs are made up of seven transmembrane α-helices, thus GPCRs are also named 7TMRs. The N-terminus and three extracellular loops (ECLs) are located extracellularly, while the C-terminus and three intracellular loops are located intracellularly. Broadly, extracellular regions of the receptor interact with endogenous ligands, and intracellular regions respond to the signals from extracellular regions by conformational rearrangements. Based on phylogenetic criteria, GPCRs are divided into five main families: Rhodopsin (Class A), Secretin (Class B1), Adhesion (Class B2), Glutamate (Class C) and Frizzled (Class F) (Alexander et al., 2017, Fredriksson et al., 2003).

The class A or rhodopsin family (**Figure 1.1 A**) is the largest family of GPCRs and contains approximately 700 GPCRs in humans. These receptors can be activated by various endogenous ligands including peptides, amines, purines, proteins, and lipids which results in the Rhodopsin family receptors being the most frequently drugged targets (Yang et al., 2021, Lagerstrom and Schioth, 2008). Compared to the other four GPCRs families, rhodopsin family receptors have a shorter N-

terminus which rarely plays a role in ligand binding. There are two types of extracellular regions in rhodopsin family receptors: those that block ligand-binding pockets and those that allow water to access ligand-binding pockets (Venkatakrishnan et al., 2013). Thus, endogenous ligands tend to bind in the pockets formed by the transmembrane domains (TMD), which potentially interact with ECLs. In addition, there are several highly conserved residues in this family which play important roles in receptor function and structure. The E(D)RY motif at the C-terminal end of transmembrane helix 3 (H3) and residues on H6 form conserved interhelical cytoplasmic hydrogen bond networks involved in the activation of these receptors (Vogel et al., 2008). In addition, the tyrosine (Y) of the NPxxY motif in TM7 is also involved in the activation of Class A receptors (Urizar et al., 2005).

Class B GPCRs family contains the secretin receptors (Class B1, **Figure 1.1 B**) and the adhesion receptors (Class B2, **Figure 1.1 C**), with 15 members and 33 members respectively (Yang et al., 2021). Secretin subfamily members have large extracellular domains (ECDs), which allows them to bind to various peptide hormones including vasoactive intestinal peptide (VIP), pituitary adenylate cyclase-activating peptide (PACAP), corticotropin-releasing factor (CRF), parathyroid peptide hormone (PTH), growth hormone-releasing hormone (GHRH), calcitonin gene-related peptide (CGRP), glucagon, and glucagon-like peptides (GLPs) (Yang et al., 2021, Lagerstrom and Schioth, 2008). As class B1 receptors have a longer N-terminal extracellular domain than class A receptors, two disulphide bonds help to maintain the structural stability (Unson et al., 2002). Similar to the secretin family, adhesion receptors also have long and various N-termini which contain a GPCR autoproteolysis-inducing (GAIN) domain. The GAIN domain has a GPCR proteolytic site (GPS) and generates two non-covalently attached subunits: an N-terminal fragment (NTF) and a 7TM containing C-terminal fragment (CTF). Adhesion receptors are distinguished from other GPCRs because of their roles in migration and cell adhesion (Lagerstrom and Schioth, 2008, Hamann et al., 2015, Yang et al., 2021, Vizurraga et al., 2020).

The glutamate (Class C, **Figure 1.1 D**) receptor family consists of 22 members including 8 metabotropic glutamate receptors (GRMs), 2 gamma-aminobutyric acid (GABA) B receptors (GABA$_B$Rs), a calcium-sensing receptor (CASR), 3 sweet and umami taste receptors (TAS1R1–3), GPRC6A and seven orphan receptors. Receptors in this family have a large ECD and exist as obligate constitutive dimers which are important for receptor activation. The ECD contains a conserved venus fly trap (VFT) and cysteine-rich domains (CRD) involved in the ligand binding process. The ligand binding mechanism of the extracellular region involves the two lobes of this region that create a cavity that binds glutamate, subsequently activating the receptor (Yang et al., 2021, Lagerstrom and Schioth, 2008, Fredriksson et al., 2003).

The frizzled (Class F, **Figure 1.1 E**) receptor family is composed of 10 frizzled receptors (FZD1–10) and a smoothened receptor (SMO). Frizzled receptors have a conserved CRD in the extracellular part which can interact with Wnt glycoproteins and activate the downstream signalling (Yang et al., 2021). SMO signalling proceeds via the G$_i$ signalling pathway (Riobo et al., 2006). Because of the general lack of full-length structures and complexity in signalling pathways, more studies are needed to fully understand the receptors of this family.
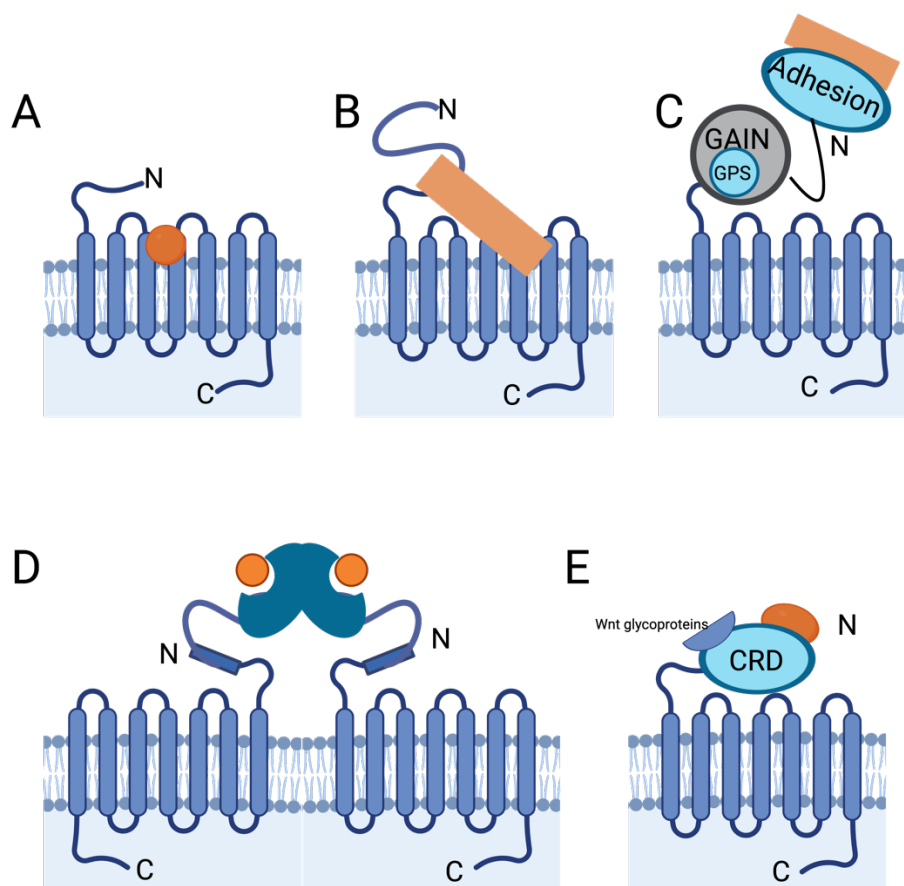
Figure 1.1 GPCR families and their structural features.
All G protein-coupled receptor (GPCR) families share a basic transmembrane helix structure, with an extracellular N-terminus and an intracellular C-terminus. However, they have various extracellular regions which leads to different ligand binding modes (ligands show in orange). A) Rhodopsin family (Class A) has a short N-terminus and the ligand binding pocket normally formed by TMs. B) Secretin family (Class B1) receptors have a long N-terminus and normally involved in ligand binding. C) Adhesion family (Class B2) receptors have a GPCR autoproteolysis-inducing (GAIN) domain, which catalyses the cleavage of the N-terminus and promotes the separation of the adhesion domain. D) Glutamate family (Class C) receptors exist in dimeric forms, and the cysteine-rich domains (CRD) domains keep the stabilisation of dimers. Venus fly trap domain (VFD) is for ligand binding. E) Frizzled (Class F) family receptors contain CRD which is bound with WNT glycoproteins for ligand binding.

1.1.2 GPCR ligand pharmacology

GPCRs have been studied as important targets in drug discovery for decades. GPCRs also play an irreplaceable part in the modern medicines market with over 40% drugs targeting GPCRs directly or indirectly (Hauser et al., 2017, Yang et al., 2021). Therefore, studying the ligand pharmacology of GPCRs is necessary for the development of many new drugs. To evaluate ligands targeting GPCRs, affinity and efficacy are the parameters that are normally considered (Kenakin et al., 2006, Kenakin, 2013). The affinity of ligands reflects the ability of the ligand to bind the receptor. Ligand affinities can be measured directly as a dissociation

constant (K_d) using radiolabeled ligands by saturation or competition binding assays or fluorescent ligands in bioluminescence resonance energy transfer (BRET)-based assays (Rossi and Taylor, 2011, Hulme and Trevethick, 2010). Competition binding assays can also detect whether two ligands share the same binding sites, or they bind to distinct sites. The efficacy of ligands is the ability of a ligand to produce physiological or molecular responses through the receptor, which is normally defined as the maximal response (E_{max}) obtained from concentration-response curves in functional assays by inducing receptor conformational changes that trigger the interactions between receptors and signalling effector proteins (Kenakin, 2013).

A 'two-state' model was proposed to explain the conformational changes of GPCRs which illustrated that a GPCR maintains either an inactive or active state. Although this model explains the different functional activities of GPCRs in response to the treatment of different ligands, development on GPCR structures has revealed that GPCRs can have multiple conformational states (Kenakin, 2013, Heo and Feig, 2022). In the absence of ligands, most of receptors prefer an inactive conformation which is normally not related to cellular activity. However, some receptors can maintain a conformation that leads to cellular responses in a ligand-independent manner, such as constitutive receptor phosphorylation. Ligand binding to the receptor causes conformational changes and leads to ligand-dependent signalling pathways (Kenakin, 2013, Latorraca et al., 2017). Based on the receptor state after ligand binding, orthosteric ligands can be divided into agonists, inverse agonists and neutral antagonists. Based on the efficacy of activation caused by agonists, they can be further divided into full, partial, or super agonists (**Figure 1.2**). Full agonists generate effects equal to the maximum efficacy of the endogenous ligands. Partial agonists produce lower efficacy than full agonists while super agonists produce higher efficacy than full agonists. Inverse agonists stabilize receptors in an inactive conformation and reduce their constitutive activity. Neutral antagonists block or compete with agonists (or inverse agonists) without inducing conformational changes in the receptors or signalling responses and do not alter the constitutive activity of the receptors (Kenakin, 2004, Nutt et al., 2017, Milligan et al., 2017b).
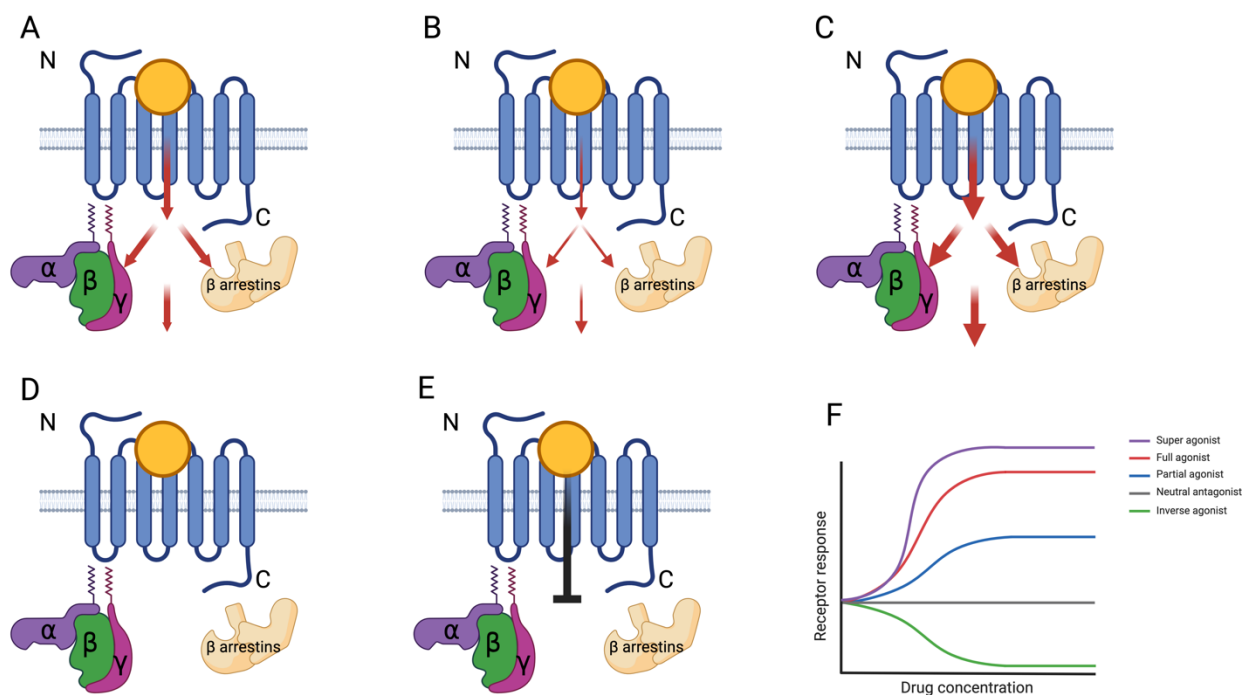
Figure 1.2 Pharmacology of orthosteric GPCR ligands.
Different types of orthosteric ligands lead to different extent of activation. A) full agonists, B) partial agonists, C) super agonists, D) neutral antagonists, E) inverse agonists, F) Representative response-concentration curves for each type of orthosteric ligands. Ligands are shown in orange

In addition to orthosteric ligands, allosteric ligands that bind to distinct sites from orthosteric sites have attracted research interest because they can induce different receptor conformational changes and affect the affinity and/or maximum efficacy of co-bound orthosteric agonists (Smith and Milligan, 2010). To evaluate the interactions between allosteric ligands and co-bound orthosteric ligands on receptors, the affinity cooperativity factor (α) and the activation (efficacy) cooperativity factor (β) are proposed. The affinity cooperativity factor evaluates how the binding of an allosteric ligand affects the affinity of an orthosteric ligand. The activation cooperativity factor describes how the binding of an allosteric ligand affects the efficacy of an orthosteric ligand. If α or β >1, the affinity/efficacy of the co-bound orthosteric ligand is increased; if α or β <1, the affinity/efficacy of the co-bound orthosteric ligand is decreased; if α or β =1, the affinity/efficacy of the co-bound orthosteric ligand is not affected by the binding of the allosteric ligand. Allosteric ligands that increase the affinity and/or efficacy of co-bound orthosteric ligands are called positive allosteric modulators (PAMs) while those allosteric ligands that decrease the affinity and/or efficacy of co-bound orthosteric ligands are called negative allosteric modulators (NAMs)

(Kenakin, 2017, Chen et al., 2022a). PAMs can be divided into PAM agonists (ago-allosteric modulators) and PAM antagonists. PAM agonists show the properties of both PAMs and agonists, thus they can activate receptors with or without the orthosteric agonists that they modulate. PAM antagonists act as antagonists and reduce the efficacy of the agonists that they modulate. NAM agonists work as NAMs and agonists, thus they can activate receptors with or without the agonists that they modulate. Furthermore, NAM agonists increase efficacy when the orthosteric ligands are at low concentrations that do not activate the receptor, while they decrease efficacy when the orthosteric ligands are at concentrations that activate the receptor (Kenakin, 2017, Kenakin and Strachan, 2018). Moreover, PAMs/NAMs can show combinations of the effects mentioned above. Because of these complex possible effects, allosteric modulators have attracted the intertest in drug discovery and disease treatment (Conn et al., 2009). Details of allosteric pharmacology are shown in **Figure 1.3** and **Figure 1.4**.
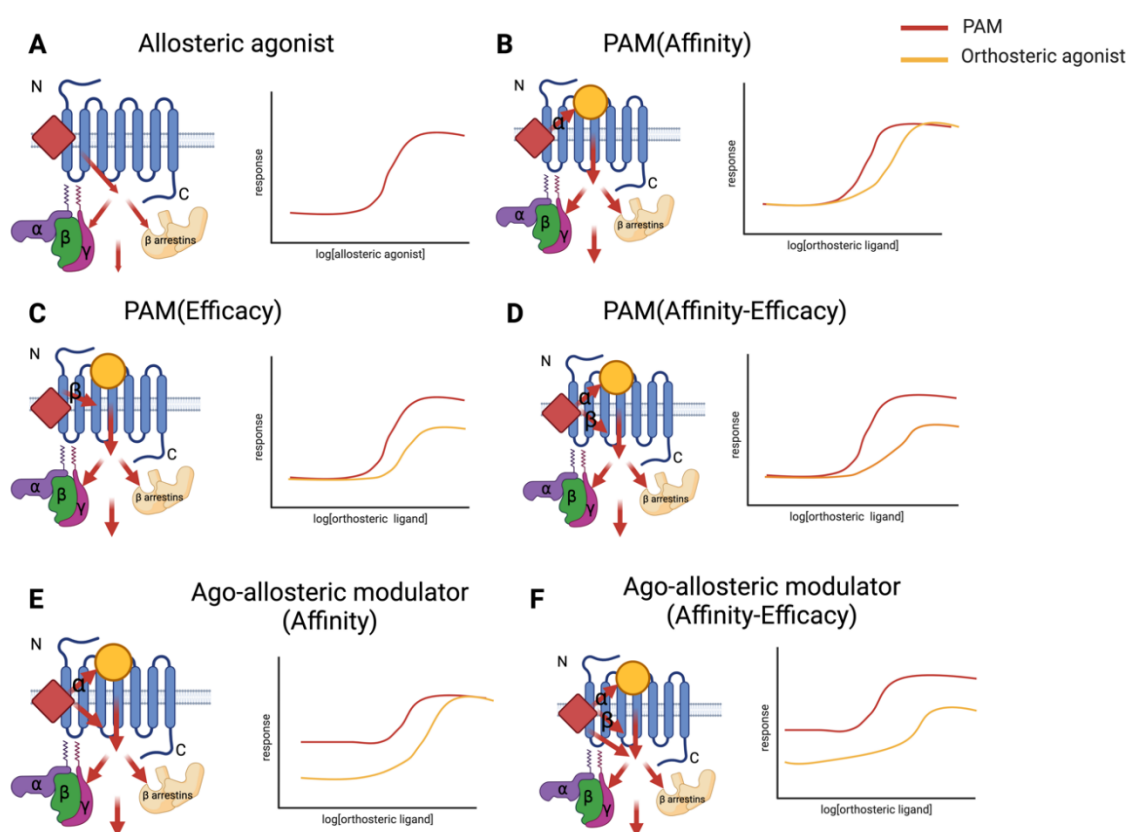
Figure 1.3 Allosteric agonism and pharmacology of positive allosteric modulators (PAMs).
Allosteric agonists display the properties of agonists in their own right and/or modulate the affinity (α) and/or efficacy (β) of orthosteric ligands. Allosteric agonists are shown as red squares and orthosteric agonists are shown as yellow circles. The presented response-concentration curves show effects in the absence (yellow) or presence (red) of PAM agonists. A) Allosteric agonists induce receptor activation alone. PAMs modulate orthosteric agonists B) Affinity, C) Efficacy, D)

Affinity and Efficacy without displaying agonistic effects. PAMs can also show agonistic effects and modulate orthosteric agonists E) Affinity or F) Affinity and Efficacy.
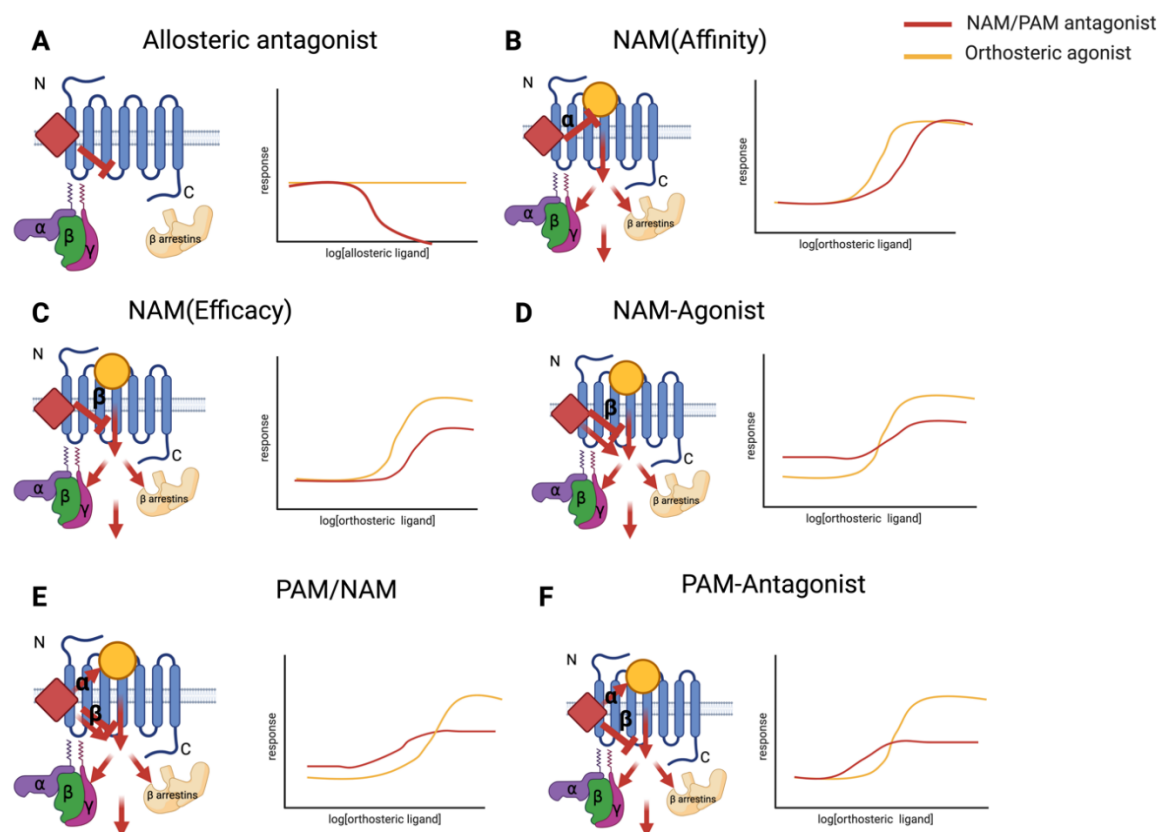
Figure 1.4 Pharmacology of GPCR Negative Allosteric Modulators (NAMs) and combined PAM-NAM.
NAMs display the properties of agonists or antagonists in their own right and/or modulate the affinity (α) and/or efficacy (β) of orthosteric ligands. NAMs/PAM antagonists are shown as red squares and orthosteric agonists are shown as yellow circles. The presentative response-concentration curves show effects in the absence (yellow) or presence (red) of allosteric ligands. A) Allosteric antagonists inhibit receptor activation alone. NAMs modulate orthosteric agonists B) Affinity, C) Efficacy. D) NAM-agonists negatively modulate the efficacy of orthosteric agonists and display agonistic effects. E) PAM/NAM and F) PAM-antagonist positively modulate the affinity of orthosteric agonists and negatively modulate the efficacy of orthosteric agonists

Compared to orthosteric ligands, allosteric ligands potentially have higher selectivity and less toxicity. Orthosteric binding pockets are normally conserved within a receptor family, whereas allosteric binding sites exhibit greater variability among receptor subtypes. Although receptor subtypes share high sequence similarity, small differences in their allosteric binding pockets can be selectively targeted by allosteric ligands. The unique and less-conserved allosteric binding sites reduce the risk of cross-reactivity with other receptors (He et al., 2019, Chen et al., 2022a, Han et al., 2020). Moreover, some allosteric ligands modulate biased receptor signalling which can tailor therapeutic effects to desired

outcomes (Cheng et al., 2023, Moore et al., 2024). The design of allosteric drugs has attracted significant attention as they can provide more precise therapeutic effects with fewer side effects. However, this is also challenging because identifying and characterizing allosteric binding sites are difficult. Cryo-electron microscopy (cryo-EM) methods are the most popular technology nowadays to study the range of GPCR activation states bound by ligands or G proteins (Carroni and Saibil, 2016). Up to now, there are approximately 1160 GPCR structures available including active, inactive and receptors in complex with ligands or G proteins (GPCRdb, https://gpcrdb.org/structure). Developments on GPCR structures directly improve the understanding of basic receptor mechanisms including signal transduction and conformational changes. Moreover, complex structures of receptors bound with ligands reveal how different ligands including orthosteric agonists and allosteric agonists interact with receptors and help to design more specific and effective drugs by targeting precise receptor conformations.

1.1.3 GPCR-mediated signalling

1.1.3.1 Heterotrimeric G proteins

Heterotrimeric guanine nucleotide-binding proteins (G proteins) are composed of three subunits: $G\alpha$, $G\beta$ and $G\gamma$ and play important roles in GPCR signalling. It is generally believed that G proteins are associated with signal transduction from the extracellular environment into cells. G proteins are classified based on the $G\alpha$ diversity. $G\alpha$ is the largest subunit and can be divided into 4 families which are $G\alpha_s$ ($G\alpha_s$ and $G\alpha_{olf}$), $G\alpha_{i/o}$ ($G\alpha_{i1}$, $G\alpha_{i2}$, $G\alpha_{i3}$, $G\alpha_{oA}$, $G\alpha_{oB}$, $G\alpha_{t1}$, $G\alpha_{t2}$, $G\alpha_g$ and $G\alpha_z$), $G\alpha_q$ ($G\alpha_q$, $G\alpha_{11}$, $G\alpha_{14}$, $G\alpha_{15}$ and $G\alpha_{16}$) and $G\alpha_{12/13}$ ($G\alpha_{12}$ and $G\alpha_{13}$) (Simon et al., 1991a, Maggio et al., 2021). The $G\alpha$ subunit contains a Ras-like GTPase domain and an α-helical domain which can bind GDP/GTP (Sprang et al., 2007). The activation of $G\alpha_s$ activates adenylyl cyclase enzymes (AC) while $G\alpha_i$ inhibits the activation of AC. $G\alpha_q$ activates phospholipase C enzymes and $G\alpha_{12}$ activates the small GTPase Rho (Maggio et al., 2021). The distribution of different $G\alpha$ is distinct. $G\alpha_s$, $G\alpha_{i1/2/3}$, $G\alpha_{12/13}$, $G\alpha_q$ and $G\alpha_{11}$ are expressed in most of cell types. $G\alpha_{olf}$ is only expressed by olfactory sensory neurons. $G\alpha_{oA/B}$ are expressed in neurons. $G\alpha_{t1/2}$ are expressed in rods and cones of the eyes and $G\alpha_g$ is expressed by taste receptor cells. $G\alpha_z$ is expressed in neuronal tissues and in platelets. $G\alpha_{14}$ is mainly

expressed in the kidney, lung and liver while $G\alpha_{15/16}$ are only expressed by hematopoietic cells (Syrovatkina et al., 2016). There are 5 distinct Gβ and 12 Gγ, and Gβ Gγ are normally exist as constitutive dimers in order to maintain stability and anchor the Gα subunit (Dingus et al., 2005).

1.1.3.2 G protein dependent GPCR signalling

In the resting condition, GPCRs maintain conformational states between activation and inactivation, and the Gα of heterotrimeric G proteins is bound with GDP. After activation by extracellular stimuli, GPCRs undergo conformational changes which regulate signalling cascades. Heterotrimeric G proteins are recruited to the receptor and the interaction of Gα-GDP is replaced by Gα-GTP. This change leads to the dissociation of G proteins from the activated receptor and the dissociation of Gα from G$\beta\gamma$ subunits. Then Gα and G$\beta\gamma$ may mediate various downstream signalling pathways separately. In order to terminate the activation state of heterotrimeric G proteins, GTP is hydrolysed to GDP by the guanine nucleotide triphosphatase (GTPase) activity of the Gα which can be accelerated by GTPase activating proteins (GAPs) such as Regulators of G Protein Signalling (RGS). Then the Gα-GDP subunit re-associates with G$\beta\gamma$ dimer and the reformed heterotrimeric G protein can bind to another activated receptor and initiate another signalling cycle (Simon et al., 1991a, Syrovatkina et al., 2016, Watson et al., 1996). Several regulatory process can terminate the activation state of GPCR such as GPCR phosphorylation, β-arrestin coupling and endocytosis (Luttrell and Lefkowitz, 2002).

Initially, Gα was believed to be the primary factor that mediates receptor signalling. After GPCR activation, intracellular effector enzymes are activated which causes changes of second messenger levels. The activation of Gα_s activates AC enzymes which increase the second messenger cyclic adenosine monophosphate (cAMP) levels. cAMP binds and activates protein kinase A (PKA) which leads to phosphorylation of downstream substrates or protein synthesis. In contrast to Gα_s, Gα_i inhibits AC and thus decrease the cAMP levels. Gα_q activates phospholipase Cβ (PLCβ) which hydrolysis phosphatidylinositol 4,5-bisphosphate

(PIP2) into 1,4,5-trisphosphate (IP3) and diacylglycerol (DAG). The increase of IP3 raises the concentration of cytoplasmic Ca^{2+}. For conventional protein kinase C (cPKCs), Ca^{2+} and DAG bind to cPKCs, enabling the translocation of cPKCs to the plasma membrane. However, the activation of novel PKCs (nPKCs) requires DAG but is Ca^{2+} independent. The activation of atypical PKCs (aPKCs) does not require either DAG or Ca^{2+}. Once activated, PKCs can modulate various cellular responses, including the activation of the Na^+/H^+ Exchanger (NHE) which affects intracellular pH (Arshavsky et al., 2002, Maggio et al., 2021, Rhee, 2001, Simon et al., 1991a). $G\alpha_{12/13}$ regulates the GTPase Rho by activating Rho-specific guanine nucleotide exchange factors (RhoGEFs), and thus regulates a downstream protein kinase (ROCK) pathway (**Figure 1.5**) (Maggio et al., 2021, Patel et al., 2014).

In addition to signalling pathways mediated by $G\alpha$, $G\beta\gamma$ dimers also mediate receptor signalling in their own right (**Figure 1.5**). The broad function mediated by $G\beta\gamma$ signalling is attributed to $G\beta$ and $G\gamma$ subtype diversity. $G\beta\gamma$ dimers can regulate many effectors such as phospholipases, AC, G protein-coupled receptor kinases (GRKs), and ion channels. For example, $G\beta_1/\gamma_1$ can stimulate phospholipase C activity without the presence of an activated $G\alpha$ subunit. $G\beta\gamma$ dimers activate the muscarinic-gated potassium channel in heart (Dingus et al., 2005, Tennakoon et al., 2021, Ford et al., 1998, Milligan and Kostenis, 2006, LOGOTHETIS et al., 1987). Although G protein dependent GPCR signalling pathways in a broad sense are not difficult to understand, various factors contribute to its complexity. As previously mentioned, the combinations of different heterotrimeric subunits would potentially regulate different cellular responses. The complex combinations are affected by GPCRs and the cell types. Moreover, GPCRs can active more than one type of G proteins which can then activate numerous downstream effectors and lead to significantly amplified downstream pathways.
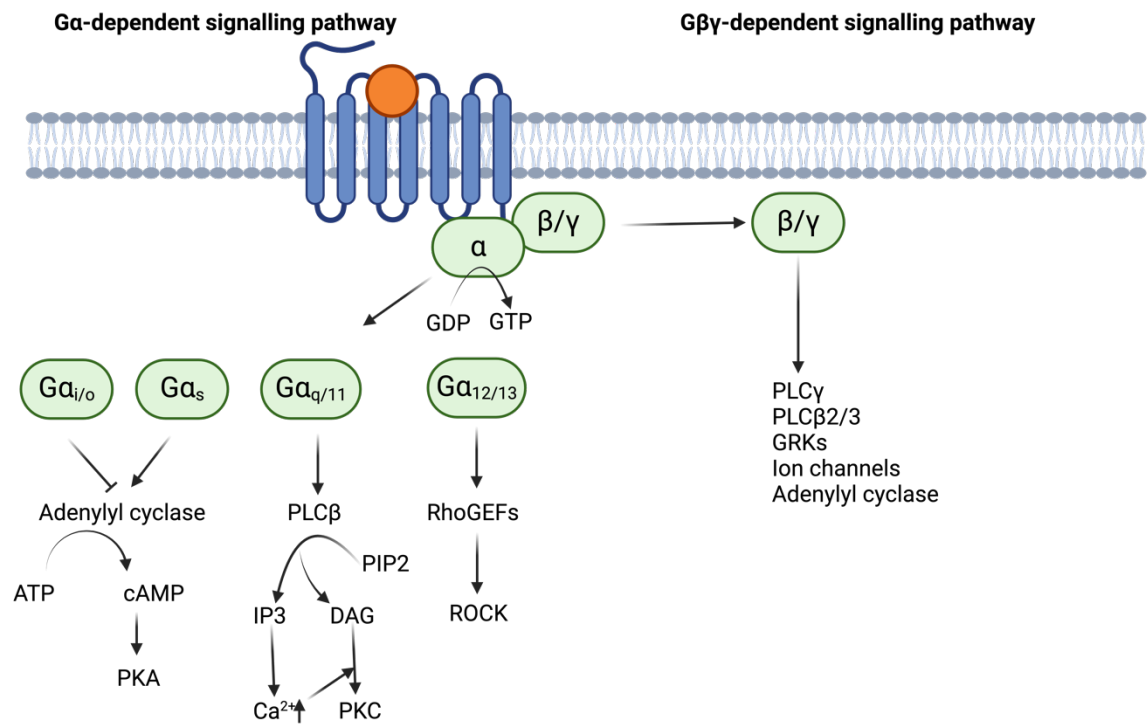
Figure 1.5 G protein dependent signalling pathways.
After the binding of ligand (orange circle), GPCRs undergo conformational changes and lead to the binding of heterotrimeric G proteins. Gα release GDP and bound with GTP. Then Gα-GTP separate from Gβγ dimer. Different Gα subunits mediate various signalling pathways. Gα$_{i/o}$ inhibits adenylyl cyclase while Gα$_s$ stimulates adenylyl cyclase, resulting in changes of intracellular cAMP levels, which then regulate PKA activity. Gα$_{q/11}$ regulates PLCβ signalling pathway. Gα$_{12/13}$ activates Rho GTPases, which then regulate ROCK signalling pathway. Gβγ dimers regulate a range of different signalling pathways.

1.1.3.3 G protein independent GPCR signalling

In addition to the classic G protein dependent signalling pathways, GPCRs also can trigger G protein independent signalling pathways. One of such mechanism involves β-arrestins (Whalen et al., 2011). There are 4 members in the arrestin family: non-visually related arrestin 2 (β-arrestin 1), arrestin 3 (β-arrestin 2) and visually related arrestin 1 and arrestin 4. β-arrestins are widely expressed by various tissues to regulate hundreds of non-visual GPCRs. However, arrestin 1 and arrestin 4 are only expressed by rod and cone photoreceptors and regulate the termination of phototransduction. Although arrestins were first discovered in the visual system where they interact with GRKs and regulate GPCR desensitization, they are now generally believed to regulate a variety of cellular processes, including receptor trafficking, internalization and potentially mitogen-activated protein kinases (MAPKs) signalling (Smith and Rajagopal, 2016, Luttrell and Lefkowitz, 2002, Gurevich and Gurevich, 2006, Lohse and Hoffmann, 2014).

Extracellular signal-regulated kinase (ERK) is a protein kinase in the family of MAPKs. It has been proposed that G protein dependent ERK activation occurs in the nucleus while β-arrestins dependent ERK activation happens in the cytosol. Moreover, G protein dependent ERK activation is transient while β-arrestins dependent ERK activation is slower but lasts longer. β-arrestins can also regulate the PI3K-AKT pathway and NF-κB pathway (Eishingdrelo et al., 2015, DeWire et al., 2007). Although these signalling pathways mediated by β-arrestins are described as "G protein independent" signalling, current evidence suggests that these pathways also require functional G proteins (Grundmann et al., 2018). This conclusion was also proved by the results in *Chapter 5*. Additionally, β-arrestins can modulate G protein signalling through the formation of a 'megaplex', a complex comprising a GPCR, a G protein, and β-arrestin. This complex facilitates sustained G protein signalling after internalization into endosomes (Thomsen et al., 2016). In the Cryo-EM structure of megaplex, all three components adopt their active conformations simultaneously. Unlike at the plasma membrane, the β-arrestin does not block the receptor core in the endosomal compartment (Nguyen et al., 2019, Nguyen and Lefkowitz, 2021). These findings challenge the traditional view that β-arrestins binding solely desensitizes GPCRs by preventing further G protein activation and provide a basis for prolonged intracellular signalling, which has significant implications for understanding GPCR function and drug development.

1.1.3.4 GPCR phosphorylation, desensitization and internalization

Phosphorylation is a process that regulates activated GPCRs and may uncouple G proteins from the receptor and recruit β-arrestins to the intracellular face of receptors. The desensitization and internalization of receptors normally happen after receptor phosphorylation (Tobin, 2008, Luttrell and Lefkowitz, 2002, Lefkowitz, 2004). GPCRs can be phosphorylated by second messenger dependent kinases including PKA or PKC in an agonist-independent way (Yang et al., 2017). GRKs also play important roles in the processes of GPCR phosphorylation, and they regulate GPCR phosphorylation in an agonist-dependent manner **(Figure 1.6)** (Yang et al., 2017). GRKs are members of the AGC kinase family and can be divided into three groups based on their sequence homology: GRK1 and GRK7, GRK2 and GRK3, GRK4, GRK5 and GRK6 (Komolov and Benovic, 2018, Benovic, 2021). GRKs

share sequence homology and domain organization in which a central catalytic domain, that is located within a Regulator of G protein signalling homology (RH) domain, is surrounded by a short N-terminal α-helical domain (αN-helix) and a variable C-terminal lipid-binding region. The N-terminal domain regulates receptor recognition on intracellular membranes. The C-terminal region facilitates membrane localization through different mechanisms: prenylation for GRK1 and GRK7, palmitoylation for GRK4 and GRK6, and direct lipid binding by either a pleckstrin homology (PH) domain in GRK2 and GRK3, or a polybasic/hydrophobic domain in GRK5 (Komolov and Benovic, 2018, Gurevich et al., 2012, DebBurman et al., 1995). GRK1 and GRK7 are mainly expressed in vertebrate rod and cone photoreceptors. GRK4 is highly expressed in testis although it is also present in proximal tubule cells in kidneys, in the brain and uterus myometrium. GRK2, GRK3, GRK5 and GRK6 are ubiquitously expressed and regulate the downstream signalling of most GPCRs (Gurevich et al., 2012, Gurevich and Gurevich, 2019, Matthees et al., 2021). After the activation of an GPCR, GRKs are recruited to the intracellular loops of the receptor and catalyse the phosphorylation of serine (Ser) and threonine (Thr) residues on ICLs and the C-terminus and promote the recruitment of β-arrestins (**Figure 1.6**). Different GRKs phosphorylate different sites on a given receptor and these effects is called 'phosphorylation barcoding'. Recruited β-arrestins can 'read' the unique 'phosphorylation barcodes' and this process is suggested to lead to different functional consequences (Tobin et al., 2008). Moreover, the phosphorylation of GPCRs can be regulated by β-arrestin conformational changes. The phosphate-binding concave surface of β-arrestins can be converted into a special β-arrestin conformation by reading different 'phosphorylation barcodes', and these special conformations can lead to different downstream effects (Yang et al., 2015). In summary, GPCRs are activated and form a specific receptor conformation which is recognized by one or more specific GRKs that potentially forms a unique phosphorylation barcode. Then the phosphorylation barcode is read by the recruited β-arrestins, which in turn causes the specific conformational changes of β-arrestins, and finally leads to the formation of intracellular β-arrestins mediated signalling networks by specific proteins. After the phosphorylation of a receptor by GRKs, β-arrestins prevent further binding of G proteins to inactivate receptors, a process called receptor desensitization (Rajagopal and Shenoy, 2018). Furthermore, the recruited β-arrestins can act as scaffolding proteins and recruit

trafficking proteins including clathrin, adapter protein 2 (AP-2) and NSF that promotes the endocytosis and internalization of receptors. As with many topics in GPCR signalling, details may vary between cell types, and recent years have seen considerable re-evaluation of the contributions of arrestins and G proteins to signalling outcomes. For example, recent studies indicate that $G\alpha_i$ can associate with β-arrestins to scaffold MAPK, even in receptors not traditionally linked to $G\alpha_i$ signalling (Smith and Pack, 2021). The signalling of atypical chemokine receptor 3 (ACKR3) can be regulated by modulators independently of both G proteins and β-arrestins (Hicks et al., 2024). These studies re-evaluate the roles of β-arrestins and G proteins in noncanonical GPCR signalling and expand the novel biological insights. Understanding these mechanisms may offer new therapeutic strategies and guide the direction of drug design (Shchepinova et al., 2020).Normally, internalized receptors are degraded in lysosomes or dephosphorylated and recycled to the cell membrane (GoodmanJr et al., 1996, Gurevich et al., 2012). Moreover, just as discussed above, internalized receptors can still undergo G protein signalling in the endosomal compartment (Thomsen et al., 2016, Nguyen et al., 2019, Nguyen and Lefkowitz, 2021) (**Figure 1.6**).
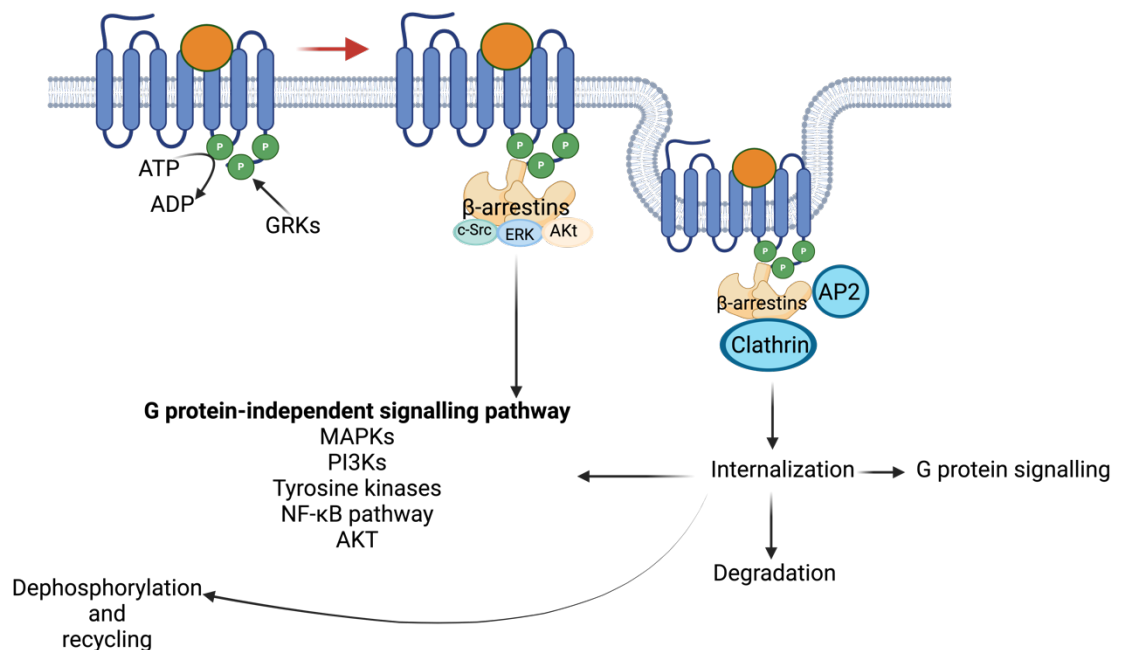
Figure 1.6 G protein independent signalling pathways.
Serine and/or threonine residues on the intracellular loops and C-terminus of activated GPCRs are phosphorylated by GRKs, which causes the recruitment of β-arrestins. The interactions of β-arrestins and AP2/clathrin lead to internalization. Then internalized receptor will be

dephosphorylated and recycled to the cell surface, degraded in lysosomes or mediated sustained G protein signalling. β-arrestins can also mediate signalling pathways by interacting with various kinases

1.1.3.5 GPCR 'biased' signalling

Traditionally, GPCR activation was thought to activate all associated signalling pathways in a balanced way. However, with the development of GPCR ligand pharmacology, the first 'biased' agonist was discovered. Such ligands can induce receptors to selectively bind to specific G protein subunits and lead to a 'biased' downstream signalling pathway (Gurwitz et al., 1994). 'Biased signalling' is a ligand-dependent activation in which a certain pathway is favoured over others and can lead to selective physiological responses. In recent years, studies on 'biased signalling' have mainly focused on either G protein biased signalling or β-arrestin biased signalling (Gurevich and Gurevich, 2020, Kolb et al., 2022). Many cases reveal that biased signalling could increase drug efficacy while avoiding adverse effects (Whalen et al., 2011, Luttrell et al., 2015, Rankovic et al., 2016).
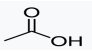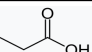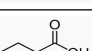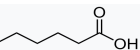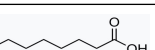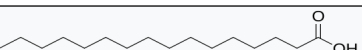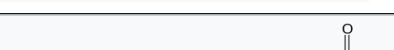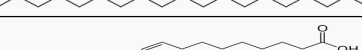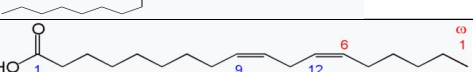
Biased agonists could be orthosteric or allosteric ligands based on their binding sites. The mechanism of biased signalling can be explained by conformational selection. It was found that GPCRs have significantly different conformations in G protein dependent signalling and in G protein independent signalling. The binding of different ligands could lead to different conformations of a GPCR which thus recruits different downstream signal molecules (Mary et al., 2013, Park et al., 2016). Upon ligand binding, if G proteins are recruited, different subtypes of heterotrimeric G proteins could mediate different pathways. If the specific conformation of the GPCR is recognized by one or more specific GRKs and forms a unique phosphorylation barcode at the C-terminus of the receptor, the 'phosphorylation barcodes' hypothesis mentioned above can explain the phenomenon of biased signalling. If β-arrestins are recruited to the receptor which may cause the conformational changes of β-arrestins and finally lead to the intracellular β-arrestins mediated signalling. Overall, the mechanism of biased signalling is complex but studying ligand-dependent biased signalling would be beneficial for drug development.

1.2 Free fatty acid (FFA) receptors

1.2.1 Fatty acids

Fatty acids are composed of a carboxyl group attached to an aliphatic chain with various length. Therefore, fatty acids can be classified by the length of their aliphatic chain including short-chain fatty acids (SCFAs), medium-chain fatty acids (MCFAs) and long-chain fatty acids (LCFAs). SCFAs have 5 or less carbon chains, MCFAs have 6-12 carbon chains and LCFAs have 13 or more carbon chains (Milligan et al., 2017b). Except for the chain length, fatty acids can be divided into saturated fatty acids (SFAs), monounsaturated fatty acids (MUFAs), and polyunsaturated fatty acids (PUFAs). The position of unsaturated carbons is important for function. The chemical structures of various fatty acids are presented as examples in **Table 1-1**.

Table 1-1 The chemical structures of various fatty acids

SCFAs	Acetic Acid		
	Propionic Acid		
	Butyric Acid		
MCFAs	Caproic Acid		
	Caprylic Acid		
	Capric Acid		
	Lauric Acid		
LCFAs	Palmitic Acid		**SFAs**
	Stearic Acid		
	Oleic Acid		**MUFAs**
	Linoleic Acid		**PUFAs**

SCFAs are produced through bacterial fermentation of fiber in colon or the oxidation of alcohol in liver (Lundquist et al., 1962, den Besten et al., 2013). Certain species of bacteria prefer to produce specific SCFAs and this may affect health and diseases including metabolic diseases, cardiovascular diseases and neuropsychiatric diseases (Karlsson et al., 2013, Generoso et al., 2021, Lu et al., 2022). MCFAs and LCFAs are obtained either from dietary fats or are synthesized in the liver (Ulven and Christiansen, 2015). MCFAs can be rapidly oxidized to

produce energy and LCFAs can be stored in adipose tissue as triglycerides which provides a long-term energy reserve. Although humans are able to synthesis fatty acids, the lack of key enzymes make some of these 'essential'. For example, PUFAs can only be obtained from the diet. It is normally believed that PUFAs have positive effects on metabolic and cardiovascular health (Lee et al., 2009, Carpentier et al., 2006). In addition to these roles, non-esterified fatty acids, (also called free fatty acids), can act as the precursors of many signalling molecules and act directly as ligands of various cell surface and intracellular receptors (Milligan et al., 2017b). It was found that the free fatty acids can affect the stabilization of glucose level, the development and differentiation of adipose tissue and immune responses. Thus, they are studied for their therapeutic potential for treating type 2 diabetes (T2DM), metabolic disorders and inflammation related diseases (Holliday et al., 2011, Hidalgo et al., 2021).

1.2.2 GPCRs activated by free fatty acids

Free fatty acid receptors (FFARs) are GPCRs that can be bound and activated by endogenous free fatty acids. The FFARs family contains FFA1 (GPR40), FFA2 (GPR43), FFA3 (GPR41) and FFA4 (GPR120) (Stoddart et al., 2008b, Karmokar and Moniri, 2022). FFA1 and FFA4 are activated by MCFAs and LCFAs while FFA2 and FFA3 are activated by SCFAs. In addition to these members, there are additional GPCRs can be activated by FFAs such as GPR84, Olfr78 in mouse or OR51E2 in human and HCA_2 (Milligan et al., 2017b). FFA1, FFA2, and FFA3 are structurally related, displaying between 30% and 40% sequence similarity with each other. All of them are encoded in tandem on chromosome 19 in humans. By contrast, FFA4 is encoded on chromosome 10 and shares very little sequence similarity with them. However, they still share the same traditional GPCR structure, which is composed of seven-transmembrane α-helices, the N-terminus and three ECLs, the C-terminus and three intracellular loops (Venkatakrishnan et al., 2013, Alexander et al., 2017).

The FFARs are members of the rhodopsin-like group of GPCRs. FFA1 can be activated by MCFAs and LCFAs and is expressed in beta and alpha cells of the pancreas as well as enteroendocrine K, L, and I cells of the gastrointestinal tract.

These cells are related to the regulation of blood glucose levels and insulin secretion. Since FFA1 is expressed in these cells, targeting FFA1 could be a possible way to treat diabetes. Moreover, FFA1 is also expressed by skeletal muscle, heart, liver, bone, brain, and monocytes which suggests that FFA1 may be a target for treating inflammation. The signalling of FFA1 by MCFAs or LCFAs is mainly transduced via $G_{q/11}$ followed by phospholipase C hydrolysis of PIP2. IP3 and DAG are produced and the intracellular Ca^{2+} level is increased (Briscoe et al., 2003, Stoddart et al., 2007). In addition, signalling of FFA1 can may also proceed through the G_i pathway, but this seems to be restricted to specific cell types such as breast cancer cell lines and keratinocytes (Yonezawa et al., 2004, Fujita et al., 2011). The recruitment of arrestin-2 and arrestin-3 also follows FFA1 activation. TAK-875 (Fasiglifam) is a partial agonist of FFA1 and displayed beneficial effects on glycaemia and HbA1c levels in diabetic patients (Kaku et al., 2015) but was withdrawn from clinical trials due to liver toxicity. The binding of TAK-875 in an FFA1 cryo-EM crystal structure demonstrated the binding pocket to be located between TMIII-TMIV and the ECL2 regions of the receptor. A hydrogen-bond interaction between Arg^{258} and Glu^{172} on ECL2 provides the roof of the binding cavity. Additionally, synthetic ago-positive allosteric modulators such as AP8 bind to a distinct pocket which is located on the surface of the 7TM above ICL2 (Srivastava et al., 2014, Ho et al., 2018, Zhang et al., 2023a).

Although sharing 30% sequence similarity with FFA1, FFA2 and FFA3 are activated by SCFAs instead of LCFAs (Milligan et al., 2017b). As SCFAs are mainly produced through bacterial fermentation of fiber, both FFA2 and FFA3 are expressed in the gut. Expression of FFA2 and FFA3 also have been described in adipose tissues and in pancreatic β-cells which regulate insulin secretion (Mishra et al., 2020, Milligan et al., 2017b). FFA2 is expressed by various immune cells with particularly high expression in monocytes and neutrophils, which suggests that FFA2 might be related to immune responses (Maslowski et al., 2009, Mishra et al., 2020). By contrast, FFA3 is mainly expressed in the neurons of sympathetic ganglia and the enteric nervous system which affects sympathetic nervous system activity and metabolic responses (Inoue et al., 2012, Nohr et al., 2015). The signalling of FFA2 is transduced via $G_{i/o}$ and $G_{q/11}$ while the signalling of FFA3 is transduced by $G_{i/o}$

(Le Poul et al., 2003, Alvarez-Curto and Milligan, 2016). The binding pockets of FFA2 and FFA3 are in the cavity comprising transmembrane helices TMV, TMVI and TMVII. Highly conserved residues Arg180[5.39] and Arg 255[7.35] are important. In FFA3, His[140] in TMIV was found to be important for SCFAs binding. FFA2 has a smaller binding pocket compared to FFA1 (Stoddart et al., 2008a, Zhang et al., 2023a). In humans, propionic and butyric acids are effective activators of both FFA2 and FFA3. Various synthetic ligands including the orthosteric agonist compound 1, allosteric agonist AZ1729 and the inverse agonist CATPB have been used to study the functional and structure of FFA2. 4-CMTB is also an allosteric agonist of FFA2 whose binding site needs to be defined (Milligan et al., 2021). However, studies on synthetic ligands targeting FFA3 are still limited.

Similar to FFA1, FFA4 is a class A family receptor that can be activated by LCFAs and particularly by PUFAs (Milligan et al., 2017b). FFA4 is expressed by various tissues including lower intestine, lung, spleen and adipose tissues (Miyauchi et al., 2009, Oh et al., 2010). Thus, FFA4 is found to be related with lung inflammation, metabolism and immune responses (Oh et al., 2010, Milligan et al., 2017b, Milligan et al., 2017a). The signal transduction pathway mediated by G proteins for FFA4 is associated with the $G_{q/11}$ and $G_{i/o}$. The recruitment of β-arrestin 2 has also been observed in FFA4 signalling (Milligan et al., 2017b, Husted et al., 2020). Endogenous agonists such as docosahexaenoic acid (DHA), ALA and palmitic acid and synthetic agonists such as NCG21, TUG-891, and GSK137647A all can activate FFA4. NCG21 and TUG-891 show higher potency at human FFA4 than FFA1 (Hudson et al., 2013, Milligan et al., 2017a). Both DHA and TUG-891 bind to a pocket formed by extracellular regions of TM3–7 of FFA4 and the N-terminal of FFA4 directly interacts with the ligands. However, binding sites of these two compounds are not exactly same (Zhang et al., 2023a).

1.3 G protein-coupled receptor 84 (GPR84)

1.3.1 GPR84 is a pro-inflammatory orphan receptor

GPR84 is also a member of the Class A receptor family and first discovered in 2001. The gene encoding human GPR84 is located on chromosome 12q13.13 and its

coding sequence is not interrupted by introns. GPR84 contains 396 amino acids (Wittenberger et al., 2001). Human GPR84 shares 85% protein sequence identity with murine GPR84 with most of the differences between these orthologues located within ICL3 (Wittenberger et al., 2001, Jenkins et al., 2021). If proteins share high similarity in sequence, they are likely to have similar structures. Both human and mouse GPR84 have a short N-terminus and C-terminus, and they both have a conserved disulphide bridge between ECL1 and ECL2. Although GPR84 is a Class A GPCR, the conserved D(E)RY motif, a key feature of class A GPCRs, is replaced by $G^{117}RY$ motif (Wittenberger et al., 2001, Yousefi et al., 2001).

Following the discovery of GPR84, it was found that MCFAs could activate the receptor *in vitro* and the 10-carbon chain decanoic acid was observed as the most potent endogenous agonist (Wang et al., 2006). However, GPR84 is still officially identified as an 'orphan' receptor because the potency of MCFAs to activate GPR84 is modest (Wang et al., 2006, Suzuki et al., 2013, Recio et al., 2018, Marsango et al., 2020). Besides, limited evidence supports that GPR84 mediates physiological function of MCFAs (Luscombe et al., 2020, Marsango and Milligan, 2023). GPR84 is mainly expressed by immune cells such as neutrophils, macrophages, dendritic cells, T cells, B cells and microglial cells in CNS. In immune cells, GPR84 promotes secretion of pro-inflammatory mediators including tumor necrosis factor alpha (TNFα), VEGF, IL-6, IL-12B, CCL2, CCL5, and CXCL1 (**Figure 1.7**) (Gaidarov et al., 2018, Recio et al., 2018, Mancini et al., 2019). Although the basal expression of GPR84 in immune cells is low, the expression of GPR84 is upregulated by acute inflammatory stimuli such as lipopolysaccharide (LPS), as observed in bone-marrow derived macrophages, resident peritoneal macrophages, RAW264.7 cells, mouse microglial cells and human monocyte derived macrophages. As GPR84 transcript is up-regulated in many pro-inflammatory conditions, GPR84 has become a therapeutic target for treating inflammation-related diseases (Yousefi et al., 2001, Venkataraman and Kuo, 2005, Wang et al., 2006, Bouchard et al., 2007, Luscombe et al., 2020, Wojciechowicz and Ma'ayan, 2020). In addition, the expression of GPR84 is also detected outside the immune system in cells such as adipocytes, epithelial cells, fibroblasts, and podocytes (Nagasaki et al., 2012, Abdel-Aziz et al., 2016, Marsango et al., 2020).

GPR84 expression can be detected in the gastrointestinal tract, liver, adipose tissues and lungs (Yousefi et al., 2001, Kose et al., 2020, Karpe et al., 2011, Nguyen et al., 2020). The expression of GPR84 in these tissues may reflect the presence of resident immune cells, but this idea needs to be further studied (Marsango and Milligan, 2023).
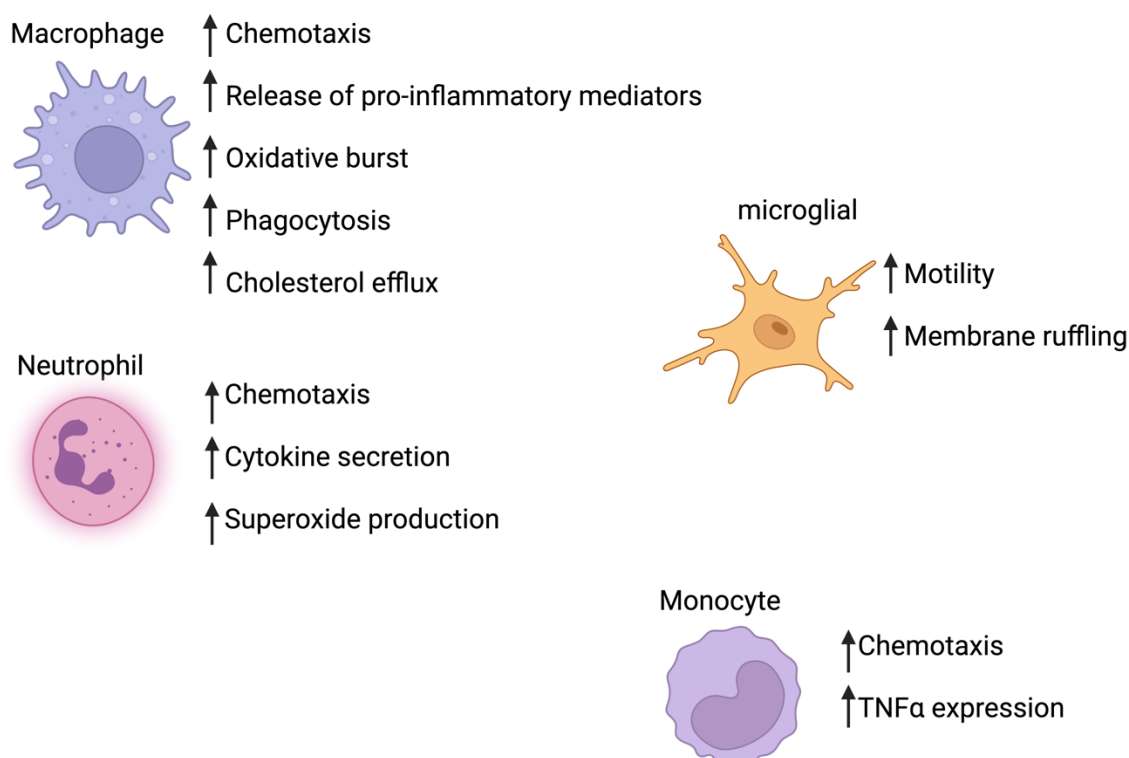
Figure 1.7 Functions of GPR84 in inflammatory conditions.
GPR84 activation generates pro-inflammatory responses in different cell types (Marsango et al., 2020).

1.3.2 GPR84 ligands

1.3.2.1 Orthosteric agonists

Tool compounds are important and necessary for studying the function and biology of GPR84. As discussed above, it is widely accepted that GPR84 can be activated by endogenous MCFAs, especially decanoic acid (C10), undecanoic acid (C11) and lauric acid (C12). 2- or 3- hydroxylated MCFAs are reported to be more potent than non-hydroxylated MCFAs (Suzuki et al., 2013). However, GPR84 cannot be activated by SCFAs, LCFAs or medium chain fatty acid amides (Marsango et al.,

2020). However, due to the modest potency of MCFAs, natural product-derived and synthetic compounds have been developed as tool compounds for GPR84.

Embelin (2,5-dihydroxy-3-undecyl-1,4-benzoquinone) is a natural product derived from the fruits of *Embelia ribes* which is used as traditional medicine for treating chronic diseases and inflammatory diseases (Lu et al., 2016, Gaidarov et al., 2018). It was firstly identified as a GPR84 agonist in 2007, and subsequently assessed in various assays (Hakak et al., 2007, Southern et al., 2013, Pillaiyar et al., 2017). Embelin is composed of a polar dihydroxybenzoquinone head group and an 11-carbon alkyl chain tail. Changing length of the carbon chain affects the potency of compounds. If the alkyl chain length is 7 or 8, the potency is increased; if the alkyl chain length is very short (C3) or very long (C15), the potency is lost. Embelin acts as a partial agonist to promote the $G\alpha_{i2}$ signalling pathway and ERK1/2 phosphorylation (Gaidarov et al., 2018). However, embelin has many biological activities and lacks selectivity for GPR84. For example, it is also an inhibitor of X-linked inhibitor of apoptosis protein (XIAP) and an activator of caspase 9 (Nikolovska-Coleska et al., 2004).

6-OAU (6-(octylamino) pyrimidine-2,4(1H,3H)-dione) was identified as a GPR84 agonist in 2013. It is composed of a polar head group and alkyl tail (Suzuki et al., 2013, Recio et al., 2018). 6-OAU can activate $G\alpha_{i/o}$ signalling pathways. It also promotes recruitment of β-arrestins, and GPR84 internalization and desensitization (Suzuki et al., 2013, Zhang et al., 2016). 6-OAU is able to induce GPR84-mediated inflammatory responses and promote the production of pro-inflammatory cytokines such as IL-8, TNF-α, IL-6 and IL-12B (Suzuki et al., 2013, Recio et al., 2018). Compared to embelin, 6-OAU is a selective agonist targeting GPR84 and has been used as a tool compound to study the pharmacology of GPR84 (Recio et al., 2018). Based on such studies and structure-activity relationship (SAR) investigations, a series of 6-OAU analogues have been generated by modifying the uracil head. This identified more potent agonists such as PSB-1584 (6-hexylamino-2,4(1H,3H)-pyrimidinedione) and the G protein biased PSB-17365 (6-((p-bromo-phenylethyl)amino)-2,4(1H,3H)-pyrimidinedione) (Pillaiyar et al., 2018).
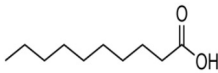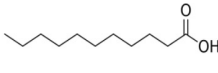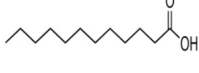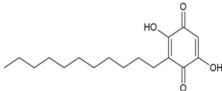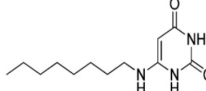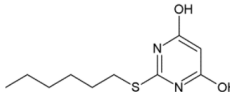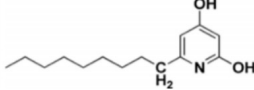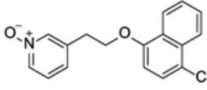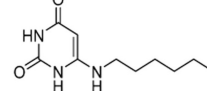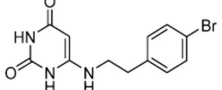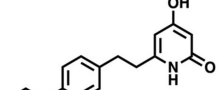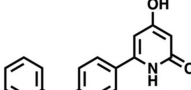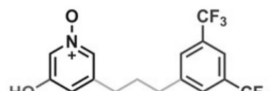
2-HTP (2-(hexylthio)pyrimidine-4,6-diol) (also known as ZQ-16 or 'compound 1'), is a potent and selective agonist at GPR84 and discovered via high-throughput screening (Zhang et al., 2016). To optimize this compound, compound LY-237 (compound51, 6-nonylpyridine-2,4-diol) was characterized as, at that time, the most potent agonist of GPR84 (Liu et al., 2016). Both 2-HTP and LY-237 are potent and selective agonists at GPR84 which has enabled their use for pharmacological and physiological characterization of GPR84. It is obvious that embelin, 6-OAU, 2-HTP and LY-237 have structure similarity with a lipophilic tail and 6-membered cyclic headgroups. Although LY-237 is a very potent GPR84 agonist, it has some unfavourable physicochemical properties. With further studies on SAR investigations around LY-237, TUG-2099 (4s, 4-Hydroxy-6-(4-propylphenethyl)pyridin-2(1H)-one) and TUG-2208 (42a, 4-Hydroxy-6′-phenoxy-[2,3′-bipyridin]-6(1H)-one) were synthesised and characterized as highly potent GPR84 agonists. Moreover, these compounds displayed improved physicochemical properties, including reduced lipophilicity, good to excellent solubility, *in vitro* permeability, and microsomal stability, making them valuable tools for exploring the pharmacology of GPR84 (Ieremias et al., 2024).

Cryo-EM structures of GPR84 in complex with LY-237 (PDB ID:8J19 from Protein Data Bank), 3-OH-C12 (PDB ID:8J18 from Protein Data Bank) and 6-OAU (Zhang et al., 2023b) have been available which helps to study the orthosteric binding sites. In the structure of LY237-GPR84-Gα_i complex, the ECL2 and the N-terminus of GPR84 form a roof-like structure over the compound binding pocket. The ECL2 presents a β-hairpin structure to extend towards TM1 (Liu et al., 2023). Similar cryo-EM structures were also observed in the 6-OAU-GPR84-G$_i$ complex (Zhang et al., 2023b). Moreover, both of these two structures contain two disulfide bonds in the extracellular domain of the GPR84 structure keep the structural stability of GPR84. One is the highly conserved disulfide bond between C168 of ECL2 and C93$^{3.25}$ of TM3, which is related to class A GPCR cell surface delivery and function. The other non-conserved disulfide bond is formed between C166 of ECL2 and C11 of the N-terminal, which is important to correct GPR84 folding. Although the non-

conserved disulfide bond is unusual in lipid receptors, it has been proposed in a previous modeling study (Mahindra et al., 2022). Single mutants that change amino acids at these sites to Ala abolished the activation of GPR84 to LY-237 or 6-OAU (Liu et al., 2023, Zhang et al., 2023b). Besides, another residue $H352^{7.35}$ of GPR84 which does not interact with 6-OAU but also potentially necessary for protein folding (Zhang et al., 2023b). It was found that $R172^{ECL2}$, $W360^{7.43}$, $Y69^{2.53}$, $S169^{ECL2}$, $F101^{3.33}$ and $F335^{6.51}$ of GPR84 are important for the binding of both LY-237 and 6-OAU (Zhang et al., 2023b, Liu et al., 2023), and $W360^{7.43}$, $F101^{3.33}$ and $F335^{6.51}$ were also proved important to orthosteric antagonists binding (Mahindra et al., 2022). The important role of $R172^{ECL2}$ in orthosteric binding pocket has also been indicated in many studies (Al Mahmud et al., 2017, Marsango et al., 2022). The cryo-EM structure of 3-OH-C12-GPR84-$G\alpha_i$ complex is similar to the LY-237 bound structure, but the interaction between 3-OH-C12 and $W360^{7.43}$ (Liu et al., 2023). These cryo-EM structure studies revealed the binding modes of orthosteric agonists and provided invaluable insights for structure-based drug design.

DL-175 (3-(2-((4-chloronaphthalen-1-yl)oxy)ethyl)pyridine 1-oxide) is a further example of an orthosteric agonist at GPR84. It was found that DL-175 can inhibit cAMP accumulation but cannot promote β-arrestins recruitment which suggests that DL-175 is a G protein signalling biased agonist. However, the rapid metabolism of DL-175 limits its use *in vivo* studies (Lucy et al., 2019). By optimizing DL-175 structure through SAR studies, compound 68 (3-(3-(3,5-Bis(trifluoromethyl)phenyl)propyl)-5-hydroxypyridine 1-oxide) and compound 69 (3-(3-(4-Chloro-3-(trifluoromethyl)phenyl)propyl)-5-hydroxypyridine 1-oxide) were generated which displayed excellent potency, high G protein signaling bias, and an appropriate *in vivo* pharmacokinetic profile. Thus, these new compounds should be more suitable for *in vivo* experiments than DL-175 (Wang et al., 2024).

Table 1-2 Orthosteric agonists targeting GPR84
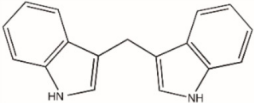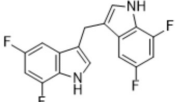
GPR84 agonists	Chemical structure	IUPAC Name
decanoic acid (C10)		decanoic acid
undecanoic acid (C11)		undecanoic acid
lauric acid (C12)		lauric acid
Embelin		2,5-dihydroxy-3-undecyl-1,4-benzoquinone
6-OAU		6-(octylamino) pyrimidine-2,4(1H,3H)-dione
2-HTP (ZQ-16/ compound1)		2-(hexylthio)pyrimidine-4,6-diol
LY-237(compound 51)		6-nonylpyridine-2,4-diol
DL-175		3-(2-((4-chloronaphthalen-1-yl)oxy)ethyl)pyridine 1-oxide
PSB-1584		6-hexylamino-2,4(1H,3H)-pyrimidinedione
PSB-17365		6-((p-bromo-phenylethyl)amino)-2,4(1H,3H)-pyrimidinedione
TUG-2099		4-Hydroxy-6-(4-propylphenethyl)pyridin-2(1H)-one
TUG-2208		4-Hydroxy-6′-phenoxy-[2,3′-bipyridin]-6(1H)-one
compound 68		3-(3-(3,5-Bis(trifluoromethyl)phenyl)propyl)-5-hydroxypyridine 1-oxide
compound 69		3-(3-(4-Chloro-3-(trifluoromethyl)phenyl)propyl)-5-hydroxypyridine 1-oxide

1.3.2.2 Allosteric agonists

DIM (3,3'-methylenebis-1H-indole) is a metabolite of indole-3-carbinol which is produced by vegetables including broccoli and kale (Takeda et al., 2003, Wang et al., 2012). DIM is an allosteric agonist at GPR84, and it acts as a PAM agonist of C10 as well as other orthosteric agonists (Al Mahmud et al., 2017, Pillaiyar et al., 2017). Similar to the plant-derived agonist embelin, DIM is not a GPR84 specific agonist (Marques et al., 2014, Marsango et al., 2020). Although DIM displays higher potency than MCFAs, it is still a moderately potent activator. Due to low potency and lack of selectivity at GPR84, DIM is not a commonly used tool compound in studying GPR84 pharmacology.

PSB-16671 (di(5,7-difluoro-1H-indole-3-yl)methane) is a DIM analogue that is more potent than DIM. Similar to DIM, PSB-16671 also acts as an ago-allosteric modulator of C10. However, care must be taken in its use as PSB-16671 displays off-target liabilities (Pillaiyar et al., 2017).

Table 1-3 Allosteric agonists targeting GPR84

GPR84 agonists	Chemical structure	IUPAC Name
DIM		3,3'-methylenebis-1H-indole
PSB-16671		di(5,7-difluoro-1H-indole-3-yl)methane

1.3.2.3 Antagonists

A series of synthesized compounds that contain dihydropyrimidinoisoquinolinones were identified as GPR84 antagonists (Labéguère et al., 2014). An example of these compounds is GLPG1205 (9-cyclopropylethynyl-2-((S)-1-[1,4]dioxan-2-ylmethoxy)-6,7-dihydropyrimido[6,1-a]isoquinolin-4-one). It shows high potency in blocking the activation of GPR84 induced by DIM and has the characteristics of a non-competitive antagonist to both orthosteric and allosteric agonists at GPR84 (Al Mahmud et al., 2017, Labéguère et al., 2020). This high affinity antagonist progressed into clinical trials for the potential treatment of ulcerative colitis and

idiopathic pulmonary fibrosis (Labéguère et al., 2020, Strambu et al., 2023). However, positive primary clinical endpoints have not been achieved.

PBI-4050 (2-(3-pentylphenyl)acetic acid sodium) is an inverse agonist and the only orthosteric antagonist at GPR84. However, it displays very low affinity at GPR84, and it also displayed effects on FFA1 and FFA2 (Gagnon et al., 2018, Marsango et al., 2020). However, PBI-4050 has also been studied in clinical trials for treating idiopathic pulmonary fibrosis and is reported to reduce pulmonary hypertension, lung fibrosis in heart failure with reduced ejection fraction (Khalil et al., 2019, Nguyen et al., 2020).

Compound 837 (3-((5,6-Bis(4-methoxyphenyl)-1,2,4-triazin-3-yl)methyl)-1H-indole) is a high-affinity and highly selective competitive antagonist of human GPR84. It also acts as a competitive antagonist to 2-HTP at human GPR84. However, it displayed no antagonist function on mouse GPR84 (Jenkins et al., 2021). Based on a molecular docking study, it is predicted that compound 837 binds within the helical bundle forming direct contacts with helices 2, 3, 6, and 7 and extracellular loop 2 (ECL2). This docking pose was confirmed by initial mutagenesis studies (Mahindra et al., 2022). Based on this binding mode, a novel compound 42 (4-(4-(3-((1H-Indol-3-yl)methyl)-5-phenyl-1,2,4-triazin-6-yl)benzyl)morpholine) was synthesized and characterized which displayed potent antagonist activity and a favourable *in vivo* PK profile (Mahindra et al., 2022).

Compound 33 (Sodium Bis(1-chlorodibenzo[b,f]thiepin-10-yl) Phosphate), a novel phosphodiester compound, was newly identified as a GPR84 antagonist. It was found that compound 33 significantly alleviated colitis symptoms and reduced the disease activity index score in a dextran sodium sulphate (DSS)-induced mouse model of ulcerative colitis. This compound has been approved for clinical trials in China (Xiao et al., 2024, Chen et al., 2022b).

CLH536 displayed an antagonist function on GPR84 in calcium response assays by blocking the activation of GPR84-Gα_{16} stimulated by 6-OAU. This compound also has been assessed in a DSS model of colitis in mice. It was found that CLH536 reduced inflammatory cell infiltration and mucosal damage in these animals. CLH536 also limited the development of colitis (Zhang et al., 2022)

Interestingly, the potencies of orthosteric or allosteric agonists at human and mouse GPR84 are very similar, but this is not always the case for the characterized GPR84 antagonists (Marsango et al., 2020). The lower affinity of antagonists at mouse GPR84, including GLPG1205, has presented a challenge in studying the pharmacology and functions of GPR84 in mouse models. To fill this gap, searching for novel mouse GPR84 antagonists or generating a chimeric construct that can be blocked by available GPR84 antagonists would be helpful. These will be discussed in detail in *Chapter 3* and *Chapter 4*.

Table 1-4 Synthetic GPR84 antagonists

GPR84 antagonists	Chemical structure	IUPAC Name
PBI-4050		2-(3-pentylphenyl)acetic acid sodium
GLPG1205		9-cyclopropylethynyl-2-((S)-1-[1,4]dioxan-2-ylmethoxy)-6,7-dihydropyrimido[6,1-a]isoquinolin-4-one
Compound 837		3-((5,6-Bis(4-methoxyphenyl)-1,2,4-triazin-3-yl)methyl)-1H-indole
compound 42		4-(4-(3-((1H-Indol-3-yl)methyl)-5-phenyl-1,2,4-triazin-6-yl)benzyl)morpholine
Compound 33		Sodium Bis(1-chlorodibenzo[b,f]thiepin-10-yl) Phosphate
CLH536		Sodium Bis(dibenzo[b,f]thiepin-10-yl) Phosphate

1.3.3 GPR84-mediated signalling

1.3.3.1 G protein dependent signalling

The most well-characterized signalling pathway of GPR84 is mediated by $G_{i/o}$ proteins (Wang et al., 2006, Suzuki et al., 2013, Al Mahmud et al., 2017). In cAMP assays, GPR84 stimulation inhibited the production of forskolin-activated 3',5'-cylic AMP production in an agonist concentration-dependent manner and this was blocked by the pre-treatment with the G_i protein inhibitor pertussis toxin (PTX). Moreover, the binding of the GTP analogue [^{35}S] GTPγS to G_i induced by GPR84 agonists is blocked by PTX treatment (Wang et al., 2006, Gaidarov et al., 2018, Suzuki et al., 2013, Al Mahmud et al., 2017). Such results indicate that GPR84 signalling is mediated via G_i proteins, and orthosteric agonists including MCFAs, embelin, 6-OAU and 2-HTP, as well as the allosteric agonist DIM all activate the GPR84-G_i signalling pathway. GPR84 activation stimulated by 6-OAU and embelin also induces G_i-mediated ERK1/2 phosphorylation and PI3K-Akt phosphorylation in human and mouse macrophages, and such effects were lacking in macrophages or neutrophils from GPR84 knock out (KO) mice. Furthermore, 6-OAU-activated GPR84 increased the nuclear translocation of NF_k B subunit p65 in LPS-induced murine bone marrow-derived macrophages (BMDMs) but not in GPR84 KO murine BMDMs. NF_k B subunit p65 regulated macrophage migration, adhesion and phagocytosis. In LPS-treated BMDMs, GPR84 activation stimulated by 6-OAU caused the enhanced expression of pro-inflammatory mediators including cytokines (TNFα, IL6 and IL12B) and chemokines (CCL2, CCL5 and CXCL1), and these effects were prevented by PTX pre-treatment (Gaidarov et al., 2018, Recio et al., 2018). These studies suggest that GPR84-mediated pro-inflammatory effects reflect GPR84-G_i signalling.

cAMP levels in response to forskolin-induction in mouse GPR84 KO macrophages was higher than wild type mouse macrophages (Nicol et al., 2015). However, in interferon-γ (IFN- γ) and a fixed concentration of G_s agonists PGE$_2$ or an adenosine receptor activator HE-NECA treated human macrophages, GPR84 activation stimulated by embelin/ lauric acids/ undecanoic acids increased intracellular levels of cAMP in a concentration-dependent way, and this effect can be blocked

by PTX treatment. This result is probably because that $G\beta\gamma$-G_i subunits, rather than $G\alpha_i$-subunit, affect cAMP levels by activating different adenylate cyclase isoforms. In IFN-γ pre-treated human macrophages, embelin-activated GPR84 increased PGE_2 release and intracellular cAMP levels in a concentration-dependent and PTX/ COX2 inhibitor indomethacin sensitive manner. PGE_2 released in an autocrine/paracrine manner can stimulate AC and therefore increased cAMP levels. In addition, the PI-3 kinase inhibitor wortmannin blocked the Akt phosphorylation which indicates that $G\beta\gamma$-G_i subunits mediated this pathway (Gaidarov et al., 2018). Embelin-activated GPR84 upregulated the expression of ABCA1 and ABCG1 (cholesterol transporters) and stimulated cholesterol efflux in macrophages in a G_i-dependent way, which suggests the potential treatment of atherosclerosis by targeting GPR84 (Gaidarov et al., 2018).

Although GPR84 function is largely associated with activation of G_i proteins, there are also other G protein-mediated signalling pathways. Embelin-mediated GPR84 activation caused $G_{12/13}$-Rho signalling (Gaidarov et al., 2018) and although potentially not a key signalling pathway in physiology. HEK293 cells stably expressing GPR84 and $G\alpha_{16}$ have bene used to screen for and identify GPR84 ligands in a manner that measures calcium mobilisation (Zhang et al., 2016).

1.3.3.2 GPR84 phosphorylation, desensitization and internalization

As discussed before, agonist binding to a GPCR frequently causes the phosphorylation of serine and/or threonine residues located within the intracellular loops. Such receptor phosphorylation promotes the recruitment of β-arrestins and GPCR internalization, desensitization and degradation normally happen after receptor phosphorylation (Luttrell and Lefkowitz, 2002, Tobin, 2008, Calebiro et al., 2009). Many studies have illustrated that GPR84 activation by various agonists can induce the recruitment of β-arrestins (Southern et al., 2013, Zhang et al., 2016, Pillaiyar et al., 2017, Marsango et al., 2022). GPR84 activation stimulated by 2-HTP and 6-OAU caused β-arrestin 2 recruitment and led to the internalization and desensitization of GPR84 (Zhang et al., 2016). GPR84 desensitization in recombinant systems and GPR84 internalization in neutrophils also have been observed (Zhang et al., 2016, Gaidarov et al., 2018). Although it is

reported that 2-HTP mediated GPR84 desensitization was independent of the actin cytoskeleton (Sundqvist et al., 2018), detailed mechanisms of GPR84 phosphorylation, desensitization and internalization are still unclear. In a recently published study, it was found that the orthosteric agonists 2-HTP and 6-OAU induced GPR84 activation that promoted the recruitment of β-arrestin 2 and the phosphorylation of the receptor measured by the incorporation of [^{32}P], while orthosteric G_i-biased agonist DL-175 and the allosteric agonist PSB-16671 could not mimic these effects (Marsango et al., 2022). Such outcomes might be GRK isoform-dependent as pre-treatment of cells with the GRK2/3 selective inhibitor compound 101 blocked these effects (Marsango et al., 2022, Fredriksson et al., 2022). Two important 2-HTP-dependent phosphorylation sites of GPR84 (threonine^{263} and threonine^{264}) were identified, and the phosphorylation of these two sites were important for the recruitment of β-arrestin 1 and β-arrestin 2 as well as the internalization of receptor. The functions of constitutive phosphorylated sites serine221 and serine224 are still unclear (Marsango et al., 2022). Although it is known that GRK2 and/or GRK3 are important to GPR84 phosphorylation, the relationships between individual GRKs and GPR84 phosphorylation as well as internalization are still unclear, and this will be studied and discussed in *Chapter 5*.
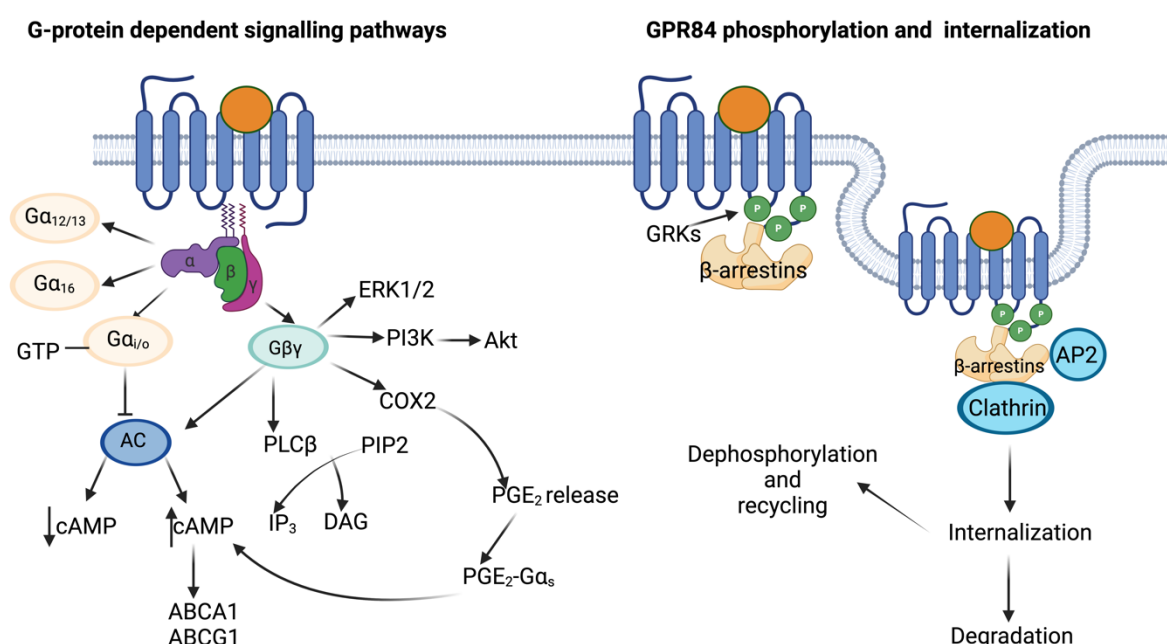
Figure 1.8 GPR84-mediated signalling pathways.
Activated GPR84 couples to $G\alpha_{i/o}$ which inhibits AC and causes the reduction of intracellular cAMP levels. By contrast, Gβγ activates AC and increases intracellular cAMP levels. Gβγ also mediates

PGE$_2$ release which promotes cAMP accumulation. Increased cAMP levels cause the increased expression of ABCA1 and ABCG1, which enhances cholesterol efflux in macrophages. G$\beta\gamma$ regulates ERK1/2 as well as activation of PI3K and PLCβ. Limited studies show that GPR84 signalling can be mediated via Gα_{16} and G$\alpha_{12/13}$. Moreover, the phosphorylation and internalization of GPR84 have been observed.

1.3.4 Therapeutic opportunities of targeting GPR84

1.3.4.1 In inflammatory diseases

As discussed before, GPR84 is mainly expressed by immune cells including macrophages and neutrophils, and the activation of GPR84 enhances the production of pro-inflammatory cytokines and chemokines. Therefore, GPR84 plays a role in mediating inflammatory responses and blocking GPR84 could be a therapeutic strategy to treat inflammation-related diseases such as ulcerative colitis (UC), idiopathic pulmonary fibrosis, inflammatory bowel diseases (IBD) and chronic neuropathic pain (Marsango et al., 2020, Labéguère et al., 2020, Nicol et al., 2015, Labéguère et al., 2014).

It was found that GPR84 was highly up-regulated in colon tissues of UC patients and DSS-induced mice (Zhang et al., 2022). In a DSS-induced mouse model of UC, GPR84 antagonist treatment can significantly reduce colitis symptoms and reduce the disease activity index as well as suppress colitis by reducing the polarization and function of pro-inflammatory macrophages (Zhang et al., 2022, Chen et al., 2022b, Labéguère et al., 2020). These studies suggests that blocking GPR84 would be a therapeutic way to treat UC. Indeed, the GPR84 antagonist GLPG1205 had been evaluated in clinical trials but failed to achieve primary efficacy end points in a phase II clinical trial in UC (Labéguère et al., 2020). This failure does not rule out the potential of blocking GPR84 as a treatment for UC. However, further studies are needed on the mechanisms of UC, as well as the physiological and pharmacological characterization of GPR84.

GPR84 is involved in the pathogenesis of fibrosis in many organs such as lung, kidney, heart and pancreas, and blocking GPR84 could be a therapeutic strategy

to treat idiopathic pulmonary fibrosis (Gagnon et al., 2018). Moreover, blocking GPR84 relieved steatohepatitis and hepatic fibrosis in chronic liver disease by reducing infiltrating monocyte derived macrophages (Puengel et al., 2020). Consistent with these findings, the GPR84 antagonist PBI-4050 displayed protective effects in a lung fibrosis model and stabilized the lung function of idiopathic pulmonary fibrosis patients in a phase II clinical trial (Gagnon et al., 2018, Khalil et al., 2019).

GPR84 is a potential target in treating neuro inflammatory pain. After peripheral nerve injury, wild type mice showed significant upregulation of GPR84 expression and pain hypersensitivity while GPR84 KO mice lacked pain hypersensitivity. Partial sciatic nerve ligation (PNL) caused the up-regulation of GPR84 mRNA and anti-inflammatory macrophage markers (Arg-1 and cytokine Il-10) in wild type mice while GPR84 KO mice displayed fewer peripheral macrophages-mediated inflammatory responses (Nicol et al., 2015). Similarly, GPR84 was upregulated in the brain in experimental autoimmune encephalomyelitis (EAE) mice which is a model of multiple sclerosis (Bouchard et al., 2007). GPR84 was identified as a potential therapeutic target for Alzheimer's disease through genetics-derived Mendelian randomization and integrative analyses of human brain transcriptomic and proteomic profiles (Qiu et al., 2024). However, inhibition of GPR84 might be harmful to the treatment of neurodegeneration such as Alzheimer's disease. Compared to wild type mice, GPR84 KO APP/PS1 (mouse model for Alzheimer's disease) mice displayed reduced cognitive performance and β-amyloid-induced microgliosis (Audoy-Remus et al., 2015). A GPR84 antagonist has been developed into a ^{11}C-PET ligand to monitor GPR84 upregulation in LPS-neuroinflammation (Kalita et al., 2023). This type of approach may be used more generally to detect early stages of neuro-inflammation.

1.3.4.2 In metabolic disorders

The levels of MCFAs will change in metabolic diseases such as diabetes and obesity (Page et al., 2009, Naja et al., 2024, Papamandjaris et al., 1998). GPR84 is expressed by adipocytes, indicating that it is likely related to metabolic regulation. It was found that GPR84 expression in macrophages was upregulated under high

glucose concentrations (Recio et al., 2018). Furthermore, GPR84 was involved in initiating insulin resistance in adipocytes under inflammatory circumstances. (Nagasaki et al., 2012). Similarly, another group found that GPR84 was related to glucose tolerance and reduced insulin plasma levels in mice and pancreatic islets (Montgomery et al., 2019). These studies indicate that modulating GPR84 activity might help improve insulin sensitivity in diabetic patients.

GPR84 also plays a role in lipid metabolism and the activation of GPR84 might be beneficial to the metabolic dysfunction associated with obese patients. Higher levels of hepatic triglycerides were observed in GPR84 KO mice that were fed a diet rich in MCFAs which indicates that the absence of GPR84 affected the ability to properly metabolize and store fats (Du Toit et al., 2018). It was also found that GPR84 KO mice displayed increased lipid accumulation in brown adipose tissue (BAT) and reduced BAT activity compared to wild type mice (Sun et al., 2023). Furthermore, GPR84 is involved in mitochondrial metabolism and the absence of GPR84 could cause impaired mitochondria and reduced O_2 consumption (Sun et al., 2023). The activation of GPR84 up-regulated intracellular Ca^{2+} levels which influenced mitochondrial respiration (Sun et al., 2023). By modulating mitochondrial Ca^{2+} levels and respiration, GPR84 activation could be a therapeutic treatment to metabolic disorders.

It was found that the expression of GPR84 in human chondrocytes was upregulated under an inflammatory condition stimulated by IL-1β. The activation of GPR84 may help preserve human osteoarthritis (OA) cartilage explants by promoting the expression of genes associated with cartilage anabolism, thereby preventing degeneration (Wang et al., 2021). It has been suggested that the activation of GPR84 by embelin would be beneficial in treating atherosclerosis (Gaidarov et al., 2018). By contrast, another group found that the upregulation of GPR84 might be associated with the pathogenesis of atherosclerosis (Recio et al., 2018). Therefore, the relationship between GPR84 and atherosclerosis need to be further studied.

1.3.4.3 In cancer

GPR84 could be a therapeutic target in cancer treatment because GPR84 signalling promotes macrophage phagocytosis (Recio et al., 2018, Lucy et al., 2019). It has been shown that GPR84 is expressed in tumour-associated macrophages (TAMs) and GPR84-G_i signalling regulated the macrophage phagocytosis of cancer cells (Kamber et al., 2021). By contrast, GPR84 promoted the accumulation and immunosuppressive function of MDSCs in both mouse and clinical samples which indicates that blocking GPR84 could be a potential treatment for cancer (Qin et al., 2023). Given these associations, it would be valuable for future studies to investigate whether GPR84 has therapeutic potential in cancer.

1.4 Aims

GPR84 is still identified as an 'orphan' receptor because the widely accepted endogenous ligands, medium chain fatty acids, display modest potency at GPR84. There is no doubt that GPR84 is involved in many physiological responses and various diseases. So far, better understanding of the basic biology and regulation of GPR84 have been achieved, and GPR84 antagonists have been evaluated in clinical trials. However, the outcomes of these clinical trials are not positive which probably because of lacking appropriate tools to study the physiological functions of blocking GPR84. Although some selective antagonists targeting human GPR84 are available, GPR84 antagonists that can be used in traditional rodent model studies are very limited. As discussed above, the phosphorylation of GPR84 is an important and complex process in which GRKs play an essential role. Although it has been known that GRK2 and/or GRK3 is involved in GPR84 phosphorylation, the relationship between individual GRKs and GPR84 phosphorylation is still not clear. Therefore, these questions are discussed in this thesis.

The aims and objectives of my PhD thesis are as follows:

i. Discovering and characterizing novel antagonists targeting both human and mouse GPR84

ii. Characterizing a newly designed 'chimeric' construct that can be blocked by available selective GPR84 antagonists

iii.   Studying the relationship between individual GRKs and GPR84 in receptor phosphorylation as well as internalization

Chapter 2   Materials and methods

2.1 Reagents

2.1.1 Pharmacological compounds

[^{35}S] GTPγS ([^{35}S]-guanosine-5'-O-(3-thio)triphosphate), from PerkinElmer Life Sciences

2-HTP 2-hexylthiopyrimidine-4,6-diol, from Sigma-Aldrich

6-OAU 6-n-octylaminouracil, from Sigma-Aldrich

DL-175 3-(2-((4-Chloronaphthalen-1-yl)oxy)ethyl)pyridine 1-oxide, from Tocris Bioscience

PSB-16671 di(5,7-difluoro-1H-indole-3-yl)methane, kindly provided by Galapagos NV

TUG-2097 6-(5-cyclohexylpentyl)pyridine-2,4-diol, gifts from Dr. Trond Ulven (Department of Drug Design and Pharmacology, Faculty of Health, University of Copenhagen, Universitetsparken 2, 2100 Copenhagen , Copenhagen, Denmark)

Compound 837 3-((5,6-Bis(4-methoxyphenyl)-1,2,4-triazin-3-yl)methyl)-1*H*-indole, synthesized as in Jenkins et al. (2021)

GLPG1205 9-Cyclopropylethynyl-2-((S)-1-[1,4]dioxan-2-ylmethoxy)-6,7-dihydropyrimido[6,1-a]isoquinolin-4-one, kindly provided by Galapagos NV

[^{3}H]140 3-((5,6-diphenyl-1,2,4-triazin-3-yl)methyl)-1*H*-indole) (40 Ci/mmol), produced by Pharmaron (Cardiff, UK)

Compound 020 4-(3-((1*H*-Indol-3-yl)methyl)-6-phenyl-1,2,4-triazin-5-yl)benzyl Acetate, synthesized as in Jenkins et al. (2021)

Compound 78 3-acetyl-N-(cyclohexylmethyl)-8-oxa-3-azatricyclo[7.4.0.0^{2,6}]trideca-1(9),10,12-triene-5-carboxamide, gifts from Dr.

Andrew G Jamieson (School of Chemistry, University of Glasgow, Joseph Black Building, University Avenue, Glasgow G12 8QQ, U.K.)

Compound 101, purchased from *Tocris Biosciences*

Compound 19, gift from Dr. David E. Uehling (Ontario Institute for Cancer Research, Canada) and Dr. Rodger E. Tiedemann (Princess Margaret Cancer Centre, Canada)

2.1.2 Primers

All primer sequences are from 5' to 3'.

HA-mGPR84

GATCGATCGGATCCGCCACCATGTACCCATACGATGTTCCAGATTACGCTTGGAACAGCTCAGATGCCAACTTCTCCTGCTACCATGAG (forward) and

GATCGATCGCGGCCGCTTAATGGAACCGGCGGAAACTCTGTGGCCCGCG (reverse)

HA-hGPR84-sBit

ACTGACTGACTGGCTAGCGCCACCATGGACTACAAGGACGACGATG (forward) and ACGTACGTGCTCGAGCCATGGAGCCTATGGAAACTCCGG (reverse)

HA-Halo-hGPR84

CCTGCAGGTATAGGCGCGCCAATGTGGAACAGCTCTGAC (forward) and

GACTACGTGCATGCGGCCGCTTAATGGAGCCTATGGAAACTCCGG (reverse)

HA-Halo-hGPR84 R172A

CCTGCAGCTTTGACGCCATCCGAGGCCGGCC (forward) and

GGCCGGCCTCGGATGGCGTCAAAGCTGCAGG (reverse)

2.1.3 Antibodies

Anti-HA high affinity primary (rat; 11867423001) from Sigma-Aldrich, dilution 1:10,000

Anti-rabbit IgG AlexaFluor488 secondary (goat; A-11034), **Anti-rat IgG AlexaFluor594 secondary** (goat; A-11007), dilution 1:250

Anti-pT263/pT264-GPR84 primary (rabbit, 7TM0120B), **Anti-pS221/pS224-GPR84 primary** (rabbit, 7TM0120A) and **GPR84-7TM structure primary** (rabbit, 7TM0120N) from 7TM antibodies, **mouse GPR84-ICL3 structure primary** (made by another lab member), dilution 1:2000

Anti-rabbit IgG IRDye 800CW secondary (goat; 926-32211) and **Anti-rat IgG IRDye 800CW secondary** (goat; 926-32219), dilution 1:10,000

2.1.4 Enzymes

DpnI (R6231) from Promega

PfuTurbo DNA Polymerase (600250-52) from Agilent Technologies

BamHI-HF (R3136S), **NotI-HF** (R3189S), **NheI-HF** (R3131S), **XhoI** (Xanthomonas holcicola; R0146S) and **AscI** (R0558S) from New England Biolabs

2.1.5 Other reagents

Ultima Gold XR (6013119) from PerkinElmer

NuPAGE 4-12%, Bis-Tris Gel (10 wells and 12 wells) (NP0321BOX; NP0322BOX), **NuPAGE MOPS SDS Running buffer (20×)** (NP0001) from Invitrogen

TWEEN-20 (P1379-500mL), **Ampicillin sodium salt** (A0166-25g), **Triton X-100** (T9284-500mL), **Paraformaldehyde** (P6148-500g), **Poly-D-lysine hydrobromide** (P6407-5mg), **Trypsin-EDTA** (0.25%) (T4049-100mL), **Penicillin-Streptomycin solution** (10,000U/mL 10mg/mL) (P0781-100mL) from Sigma-Aldrich

Pierce BCA Protein Assay kit (23227), **SYBR Safe DNA gel stain** (S33102), **HBSS (Ca2+, Mg2+, no phenol red) (10×)** (14065-049) and **DMEM (high glucose)**, (41965039 -500mL) from ThermoFisher

QIAprep Spin Miniprep kit (27106)

dNTP Solution mix (N0447S), **Gel loading dye** (6×) (B7024S), from New England Biolabs

Monoclonal Anti-HA–Agarose antibody (A2095-1ML) **Bovine Serum Albumin Fraction V (fatty acid free)** (3117057001) and **Bovine serum albumin Fraction V** (10735086001) from Sigma-Aldrich

cOmplete and cOmplete Mini EDTA-free protease inhibitor (4693132001, 4693159001), **PhosSTOP phosphatase inhibitor** (4906845001) from Roche

XL1-Blue Competent Cells (200249) from Agilent Technologies

Chameleon Duo Pre-Stained Protein Ladder (928-60000) from LICOR

VECTASHIELD Vibrance Antifade mounting medium with DAPI (H-1800) from Vector Laboratories

Tryptone (TRP02), **Yeast extract powder** (YEA02), **Agar** (AGA02) from Formedium

Hygromycin B Gold (100mg/mL) (ant-hg-5), **Blasticidin** (10mg/mL) (ant-bl-1) from InvivoGen

Agarose (1613102) from Bio-Rad Laboratories

Polyethyleneimine (PEI) (P3143-100mL) from Supelco

Amersham Protran 0.45µm nitrocellulose membrane (10600002) from Cytiva Life Sciences

Pertussis toxin from Bordetella pertussis from Invitrogen

Coelenterazine H from Nanolight technology

2.1.6 Media, buffers and solutions

Flp-In T-REx 293 stable cells medium - Dulbecco's Modified Eagle's Medium (DMEM,41965039), supplemented with 10% (v/v) foetal bovine serum (FBS), 1% (v/v) P/S, 5µg/mL blasticidin and 200µg/mL hygromycin B Gold

Flp-In T-REx 293 parental medium - DMEM (41965039), supplemented with 10% (v/v) FBS, 1% (v/v) P/S and 5µg/mL blasticidin

HEK293T medium – DMEM (41965039), supplemented with 10% (v/v) FBS, 1% (v/v) P/S

L-Broth medium - 1% (w/v) tryptone, 0.5% (w/v) yeast extract, 1% (w/v) NaCl

LB Agar plate – 1.5% (w/v) agar in LB medium, appropriate amount of antibiotic

[^{35}S]GTPγS buffer - 20mM HEPES, 5mM MgCl2, 160mM NaCl and 0.05% (w/v) Fatty Acids free BSA at pH7.6

Lysis buffer - 150mM NaCl, 50mM Tris-HCl (pH7.5), 5mM EDTA (pH 8.0), 1% (v/v) Nonidet P-40, 0.5% (w/v) Na-deoxycholat, 0.1% (w/v) sodium dodecyl sulphate (SDS)

SDS-PAGE running buffer – diluted from 50x NuPAGE MOPS, from Invitrogen

Phosphate-buffered saline (PBS) buffer - 137mM NaCl, 2.7mM KCl, 10mM Na$_2$HPO$_4$, 1.8mM KH$_2$PO$_4$ at pH7.4

Hank's balanced salt solution (HBSS) - without Ca^{2+} and Mg^{2+}, from ThermoFisher Scientific

Radioligand binding buffer – PBS buffer, 0.5% (w/v) Fatty Acids free BSA

SDS-PAGE loading buffer (Laemmli buffer) – 62.5nM Tris (at pH7.6), 2% (w/v) SDS, 20% (v/v) glycerol, 100mM dithiothreitol, 0.005% (w/v) bromophenol blue

TAE buffer - 40mM Tris-base, 20mM glacial acetic acid, 1mM EDTA at pH8.3

Tris-buffered saline (TBS) buffer - 20mM Tris-HCl, 150mM NaCl at pH7.4

TE buffer - 10mM Tris, 0.1mM EDTA at pH7.5

Transfer buffer - 25mM Tris-Base, 192mM glycine, 20% (v/v) methanol

Antibody solution (WB) - TBS supplemented with 0.1% (v/v) TWEEN-20 and 5% (w/v) BSA

Blocking solution (WB) - TBS supplemented with 5% (w/v) BSA

Blocking solution (ICC) - TBS supplemented with/without 0.05% (w/v) saponin, 1% (w/v) FA-free BSA and 3% (v/v) goat serum

2.2 Molecular biology

2.2.1 Site-directed mutagenesis – generation of HA-Halo-hGPR84 R172A mutant

To introduce specific mutation-point into the HA-Halo-hGPR84 construct, the Stratagene QuickChange method was employed. Mutagenesis primers were designed using PrimerX software (http://www.bioinformatics.org/primerx/) and custom generated by ThermoFisher Custom DNA Oligos Synthesis Services. The primers are listed in *section 2.1.2*. The mutagenesis reaction mixture contained 1.25μL 10mM dNTPs, 1.5μL 10μM forward primers, 1.5μL 10μM reverse primers and 5μL PfuTurbo buffer (10×). 100ng template plasmid DNA was added to the sample PCR tubes, but not to the control PCR tube which can detect whether primers bind to each other. Sterile water was added to bring the volume of the mixture to 49μL. Finally, 1μL (2.5 units) PfuTurbo DNA Polymerase was added to the mixture. After the preparation of mutagenesis mixture, the PCR process was performed in a MasterCycler 5333 thermal cycler. The programme for PCR was preheating the mixture to 95°C for 5mins, 16 cycles of 30s 95°C for denaturation, 1min 55°C for annealing and 14min 72°C for extension. Then samples were held at 4°C. Finally, methylated template DNA was digested by incubation with 10U DpnI for 4h at 37°C.

2.2.2 Plasmid cloning - generation of HA-hGPR84-sBit/HA-Halo-hGPR84/HA-mGPR84

To generate the desired constructs, primers were designed to introduce enzyme cutting sites for following subcloning. The primers are listed in *section 2.1.2*. The enzyme sites for HA-hGPR84-sBit were NheI and XhoI, the enzyme sites for HA-Halo-hGPR84 were ASCI and NotI, and the enzyme sites for HA-mGPR84 were BamHI and NotI.

The reaction mixture contained 10μL 0.25mM dNTPs, 2μL 0.5μM forward, 2μL 0.5μM reverse primers and 10μL PfuTurbo buffer (10×). 100ng template plasmid DNA was added to the sample PCR tubes, but not to the control PCR tube. Sterile water was added to bring the volume of the mixture to 99μL. Finally, 1μL (2.5 units) PfuTurbo DNA Polymerase was added to the mixture. After the preparation of reaction mixture, the PCR process was performed in a MasterCycler 5333 thermal cycler. The programme for PCR was preheating the mixture to 95°C for 5mins, 30 cycles of 1min 95°C for denaturation, 1min 55°C for annealing and 1.5min 72°C for extension. Then samples were held at 72°C for 10mins and 4°C overnight. 5μL PCR products and 1.25μL loading buffer(5X) were mixed and loaded to an agarose gel which detects whether the PCR works. If there was a band at the correct weight position, the PCR products left was purified using QIAquick PCR Purification Kit (28104).

The DNA template for HA-hGPR84-sBit was MOR-sBit (gift from C. Hoffmann), the template for HA-Halo-hGPR84 was HA-Halo-M1 (made by others in the lab), and the template for HA-mGPR84 was HA-humanised-GPR84 (made by others in the lab). 41μL purified PCR products/DNA template, 5μL enzyme cutting buffer (10x) and 2μL of each enzyme mentioned above were mixed to bring a total volume of 50μL. The mixture was kept at 37°C overnight for digestion. The mixture was purified by running an agarose gel, cutting the proper weight bands and gel extraction using QIAquick Gel Extraction Kit (28704). The purified digestion products from PCR and DNA template were then ligated by T4 DNA ligase enzyme for 2h at room temperature (RT). The ligation mixture was transformed into competent cells, miniprepped and sequenced.

2.2.3 Transformation of plasmids using competent cells

50μL XL-1 Blue competent cells were thawed on ice and aliquoted into pre-chilled 1.5 ml microcentrifuge tubes. Then 1μL (10-100ng) or 5μL ligation mixture was added to the tubes, which were then gently mixed and incubated on ice for 30mins. Tubes were then subjected to heat shock at 42℃ for 90 seconds, followed by 2mins incubation on ice immediately. 500μL preheated sterile L-Broth medium (LB) were added to tubes, and tubes were incubated in a shaking incubator (220 rpm) for 1h. 50-100μL transformed cells were plated on pre-warmed agar plates containing appropriate amount and type of antibiotics. Agar plates were incubated at 37℃ for 16h. On the following day, a single colony was picked and grown overnight in 5 ml of LB medium containing antibiotics in a shaking incubator at 37℃. Then bacterial cultures were purified using miniprep kit.

2.2.4 Plasmid DNA purification from bacterial culture

To purify plasmids, QIAprep Spin Miniprep kit (Qiagen) was used following the manufacturer's instructions. 5mL of the overnight bacterial culture was centrifuged at 4000rpm for 10mins at RT. Then the resulting pellets were re-suspended in 250μl Buffer P1 (with RNase A; 1:100 dilution) and the mixture should change to blue. 250μl Buffer P2 was added, and the mixture should change to clear. 350μL Buffer N3 was added, and the tube was centrifuged for 10mins at 13,000rpm. 800μl supernatant was added to a QIAprep 2.0 spin column and centrifuged for 1min at 13,000rpm. The flow-through was discarded and 750μl Buffer PE was added to the column. The column was centrifuged again for 1min at 13,000rpm. The flow-through was discarded and the empty column was centrifuged again for 1min at 13,000rpm. The spin column was transferred into a clean 1.5-mL microcentrifuge tube, and 100 μl nuclease-free water was added to the column. After 10mins incubation, the tube was centrifuged for 1min at 13,000rpm. After miniprep, samples were quantified and stored at -20˚C.

2.2.5 Sequencing

To confirm whether the newly generated plasmids are correct, they were sequenced. Sequencing was performed by the MRC PPU DNA Sequencing and Services (Medical Sciences Institute, School of Life Sciences, University of Dundee, Scotland). The primers used for sequencing are provided by the facility (the CMV

promoter for the forward and the BGH-poly(A) signal for the reverse primer), or specially designed for a certain construct.

2.3 Biochemistry and Cell biology

All cell culture work were conducted in class II biosafety cabinets following proper sterile rules and mycoplasma-free rules. The cells were incubated in an inCu saFe SANYO humidified incubator supplied with 5% CO2 at 37°C. All media were pre-warmed to 37°C in a water bath.

2.3.1 Mammalian cell culture and maintenance

Human embryonic kidney 293 cells (HEK293T cells) were maintained in DMEM (41965-039), supplemented with 10% (v/v) heat-inactivated fetal bovine serum (FBS) and 1% (v/v) penicillin/streptomycin (p/s).

Parental Flp-In T-REx-293 cells were maintained in DMEM (41965-039), supplemented with 10% (v/v) FBS, 1% (v/v) P/S and 5µg/mL blasticidin.

Flp-In T-REx 293 stable cells (inducible to express receptor) were maintained in DMEM (41965-039), supplemented with 10% (v/v) FBS, 1% (v/v) P/S, 5µg/mL blasticidin and 200 µg/ml hygromycin B. To express receptors of interest, these cells were treated with doxycycline (100 ng/ml) for 24 hours.

When cells in 75cm^2 flask (for example) were confluent to about 80%-90%, they need to be passaged. Medium was aspirated from the flask and cells were washed once with sterile PBS (137 mM NaCl, 2.7 mM KCl, 10 mM Na$_2$HPO4, 1.8 mM KH$_2$PO4, pH 7.4). Then, 1ml of trypsin-EDTA (0.25%) was added to the flask and incubated for 2-5mins in the hood at RT. Then the flask was tapped gently to detach cells from the flask. 9ml fresh medium was added to the flask to gently suspend cells. Various volumes of suspension were added to new flasks/dishes depending on the desired dilution of cells.

For long term storage, cells were stored at -80°C or -150°C. Cell culture medium was removed from the flask. Cells were washed with PBS and incubated with trypsin-EDTA to detach cells. Cells were resuspended with 10ml culture medium and centrifuged at 1200rpm for 5mins at RT. The resulting cell pellet was

resuspended in 1ml FBS with 10% (v/v) dimethyl sulfoxide (DMSO). The suspension was then transferred to a cryogenic tube and then stored at -80°C.

In order to recover cells, frozen cells were thawed in a water bath at 37°C. After complete thawing, cells were transferred to a 10ml falcon tube with 10ml pre-warmed culture medium and centrifuged at 1200rpm for 5mins at RT. Cell pellets were then resuspended with 10ml fresh culture medium and transferred to a 75cm^2 cell culture flask that was incubated in an incubator overnight. After 24h incubation, medium in the flask was discarded and replaced by fresh cell culture medium.

2.3.2 Transient transfection

To transiently express receptor of interest, HEK293T cells were plated in a 10cm cell culture dish and incubated for 24h in an incubator until approximately 80% confluency was achieved. On the day of transfection, 5µg plasmid DNA was diluted in 250µL of 150mM sterile NaCl. 30µg polyethyleneimine (PEI) was diluted in 250µL of 150mM sterile NaCl (DNA:PEI=1:6). Then diluted DNA and PEI were mixed, vortexed and incubated for 10mins at RT. The culture medium in the dish was replaced by fresh medium. The DNA-PEI mixture was dropped to the dish, gently mixed, and incubated for 24h in the incubator before downstream application.

2.3.3 Generation of Flp-In T-REx 293 stable cell lines

Flp-In T-REx 293 stable cell lines can be induced by doxycycline (DOX) to express desired receptor construct. Parental Flp-In T-REx 293 cells were plated in a 10cm cell culture dish and incubated for 24h in an incubator until approximately 80% confluency was achieved. Then cells were co-transfected with integration plasmid vector POG44 and desired pcDNA5/FRT/TO construct. 0.8µg pcDNA5/FRT/TO DNA and 7.2µg POG44 were diluted in 150mM sterile NaCl, and 48µg PEI was diluted in 150mM sterile NaCl (DNA:PEI=1:6). Negative control group without the pcDNA5/FRT/TO DNA plasmid was also included. Then diluted DNA and PEI were mixed, vortexed and incubated for 10mins at RT. The culture medium in dishes was replaced by fresh medium. The 500µL reaction mixture was dropped to the dish, gently mixed, and incubated for 24h in the incubator. After successful

transfection, Flp recombinase expressed from POG44 plasmid catalyses the recombination of FRT sites in the expression vector and the host genome.

After 24h incubation, cell culture medium was replaced by new parental Flp-In T-REx 293 culture medium. In the next day, transfected cells were split into 1:10 and 1:20 into 10 cm dishes. On the following day, growing medium was replaced with Flp-In T-REx 293 stable cells maintenance medium containing 200 μg/ml of hygromycin B to select successfully transfected cells. Then the medium was replaced every 2-3 days until visible hygromycin resistant colonies were observed (in about 2 weeks). Colonies were detached using 0.25% trypsin-EDTA, combined and transferred to a new flask. After passaging the cells, cells were induced by incubation with 100ng/mL DOX for 24h. Following induction, cells were tested using proper methods.

2.3.4 Membrane preparation

Membranes were prepared from Flp-In T-REx 293 stable cells treated with 100ng/ml DOX for 24h. After washing with cold PBS, cells were detached using a cell scraper and centrifuged at 1200rpm for 5mins at 4°C. The resulting pellets were then stored at -80°C for at least 1h. Pellets were resuspended in 2ml cold T/E buffer containing cOmplete Protease Inhibitor Cocktail (EDTA-free). The cell suspension was homogenized with 50 strokes in a 5ml hand-held homogenizer, followed by passing through a 25G needle 5 times. The suspensions were then transferred to a 10ml falcon tube and centrifuged at 4000rpm for 5mins at 4°C. The supernatant was then transferred to ultracentrifuge tubes and centrifuged at 50,000 rpm for 45mins at 4°C. The pellets were resuspended in cold T/E buffer containing protease inhibitor and passed through a 25G needle for 5 times. The concentration of membrane protein was measured using a Bicinchoninic acid (BCA) assay. Then membranes were aliquoted and stored at -80°C.

2.3.5 BCA assay

Membrane protein was quantified using BCA Protein Assay kit (Pierce, ThermoFisher) following recommended protocol. A series of BSA (fatty acid-free) concentrations between 0-2.0μg/μL was prepared and used as standards. 10 μl of each concentration of the standard was added to a 96-well clear flat bottom assay

plate. Membrane samples were diluted (1:10) and added to the same plate. BCA Reagent B and Reagent A (1:50) were mixed and 200μL mixture was added to the wells of standards and samples. The plate was then covered with a disposable seal and incubated at 37°C for 20mins. Then the absorbance was measured at 562nm using a plate reader (PHERAstar FS plate reader, BMG Labtech). The absorbance of standards was used to generate an absorbance-concentration standard curve, and the concentration of membrane protein was interpolated from the standard curve.

2.3.6 Immunoblotting

2.3.6.1 Lysate preparation

Flp-In T-REx 293 stable cells were induced to express the receptor of interest by 100ng/ml DOX for 24h. On the following day, culture medium was replaced by serum-free Flp-In T-REx 293 stable cells culture medium for at least 1h. Then cells were pre-treated with 10μM GRK2/3 inhibitor compound 101 for 30mins, or 10μM GPR84 antagonists for 15mins before cells were treated with agonists for 5mins. The concentration and treatment time were optimised from Marsango et al. (2022). Cells were detached in TBS and centrifuged at 1200rpm, 4°C for 5mins. The resulting pellets were resuspended in 500μL lysis buffer (150mM NaCl, 50mM Tris-HCl, 5mM EDTA, 1% (v/v) Nonidet P-40, 0.5% (w/v) Na-deoxycholate, 0.1% (w/v) SDS at pH7.4) containing cOmplete EDTA-free Protease Inhibitor Cocktail (Roche) and PhosSTOP Phosphatase Inhibitor Cocktail (Roche). Lysates were rotated at 4°C for 30mins and then centrifuged at 21,000×g, 4°C for 15mins. The supernatant was moved to a clean 1.5 mL microcentrifuge tube and quantified using BCA assay.

2.3.6.2 Immunoprecipitation

To enrich HA-tagged receptors, HA-trap agarose kit (Chromotek) was used according to the manufacturer's protocol. 25μL beads were washed three times in 500μL lysis buffer with centrifugations at 2,500×g at 4°C for 5mins between washes. After the last washing, 250μL lysis buffer was left in microcentrifuge tubes. The concentrations of protein samples were equalised and 250μL of samples were added to the washed beads. Samples were rotated at 4°C overnight. On the following day, samples were washed three times with lysis buffer without protease inhibitor cocktail and phosphatase inhibitor cocktail, with centrifugations at

2,500×g at 4°C for 5mins. After the third wash, beads were resuspended in 2x Laemmli buffer and eluted at 60°C for 10mins. Eluted samples were then centrifuged at 2500rpm, RT for 5mins. The supernatant was used for the following western blotting.

2.3.6.3 Western blotting

20µL/well eluted protein samples were loaded into a NuPAGE 4-12%, Bis-Tris gels (ThermoFisher) with 3µL Chameleon Duo Pre-Stained Protein Ladder (LICOR) as marker. Gels were run in 1x NuPAGE® MOPS SDS Running Buffer (Invitrogen) at 200V for 1h. Gels were then transferred to nitrocellulose membranes in a wet transfer system at 35V for 1h. The transfer cassette was in the order: sponge, pre-soaked 3mm filter paper, gel facing down, pre-soaked 0.45µm nitrocellulose membrane, filter paper, sponge, in transfer buffer (25mM Tris-Base, 192mM glycine, 20% (v/v) methanol). Once the transfer finished, the membrane was quickly washed once with TBS buffer and blocked in 10mL blocking solution (TBS supplemented with 5% (w/v) BSA) on a shaker for 1h at RT. Then blocking buffer was removed and 10mL diluted primary antibodies were added (primary antibodies were diluted in TBS with 0.1% (v/v) TWEEN and 5% (w/v) BSA at 1:2000 or 1:10,000). Membranes were incubated with the primary antibodies on a shaker at 4°C overnight.

On the following day, primary antibodies were removed, and membranes were washed three times with TBS-T (TBS with 0.1% Tween20) for 10 mins on a shaker at RT. Then 10mL diluted IRDye secondary antibodies were added (dilution 1:10.000) and incubated in dark on a shaker for 1h at RT. Membranes were then washed three times with TBS-T and left to dry in dark for 15mins. Finally, membranes were scanned using a LICOROdyssey 9260 fluorescent imaging system and the ImageStudio Software at 700 nm and 800 nm channels.

2.3.7 Immunocytochemistry (ICC)

2.3.7.1 Fixed cells

Flp-In T-REx 293 stable cells were cultured on poly-D-lysine-coated 16mm round coverslips in 12-well plates and incubated for 24 h at 37 °C. On the following day, 100ng/mL doxycycline was used to induce the expression of receptor overnight.

Then cells were starved in serum free Flp-In T-REx 293 cell culture medium for at least 1h. After that, cells were treated with antagonists or agonists and fixed with 4% (w/v) paraformaldehyde diluted in TBS containing PhosSTOP phosphatase inhibitor (Roche) for 10mins at RT. After fixation, cells were washed 3x15mins with TBS and blocked with blocking buffer (TBS with 1% (w/v) FA-free BSA and 3% (v/v) goat serum) for 2h at RT. Then blocking buffer was removed. Primary antibodies (diluted 1:250 in blocking solution) were added and incubated overnight at 4°C. Cells were washed 3x15mins with TBS and incubated with AlexaFluor secondary antibodies (dilution 1:250 in blocking solution) for 1h at RT in dark. Then cells were washed 3x15mins with TBS. Coverslips were mounted onto a microscopy slide with Vectashield Vibrance mounting medium with DAPI (4',6-diamidino-2-phenylindole) (Vector Laboratories) and sealed with nail polish. Imaging was performed with a Zeiss LSM 880 confocal equipped with a 63x/1.4 NA Plan Apochromat oil-immersion objective. Samples were excited by lasers (the wavelength is depended on the secondary antibodies).

2.3.7.2 Living cells

Flp-In T-REx 293 cells stably express HA-Halo human GPR84 were cultured on poly-D-lysine-coated 30mm round coverslips in 6-well plates and incubated for 24h at 37°C. After that, a final concentration of 100ng/mL doxycycline was used to treat the cells overnight. Then cells were labelled with HaloTag Ligands Alexa Fluor 488 (1mM, diluted 1:1000 in culture media) for 15mins at 37°C before washed twice with HBSS. Subsequently, coverslips were placed in a microscope chamber containing HBSS and images were acquired before and 15mins after agonist treatment using a Zeiss LSM 980 confocal equipped with a 63x/1.4 NA Plan Apochromat oil-immersion objective. Halotag ligand dye was excited using the 488-nm laser line and the emission light was detected over the wavelength range 500 to 560 nm using a GaASP detector. 3D best focus z stacks were created using Metamorph software to visualise the degree of receptor protein internalisation evoked for each treatment ligand

2.4 Functional assays

2.4.1 [^{35}S] GTPγS binding assay

The [^{35}S] GTPγS binding assay was employed to measure the level of G protein activation. [^{35}S] GTPγS is a radiolabelled analogue of GTP, but it is resistant to hydrolysis. After the activation of receptor by agonists, [^{35}S] GTPγS recruits to the receptor and remains bound to Gα. Therefore, the accumulation of [^{35}S] is proportional to the extent of G protein activation. The [^{35}S] GTPγS binding assay was performed following the protocol from Jenkins et al. (2021).

In a 96-deep well plate, 3µg/well membrane protein was preincubated with assay buffer (20mM HEPES, 5mM MgCl$_2$, 160mM NaCl and 0.05% (w/v) Fatty Acids free BSA at pH7.6) containing various concentrations of antagonists for 15mins at RT (when assessing antagonists). Then EC80 or various concentrations of agonists were added to the plate. The reaction was started by the addition of 50nCi/well of [^{35}S] GTPγS in assay buffer containing 1µM GDP. The reaction plate was incubated for 1h at 30°C. The reaction was stopped by rapid filtration through UniFilter-96 GF/C glassfibre filter-bottom plates (pre-soaked in cold PBS) using a UniFilter FilterMate Harvester (PerkinElmer). Filter plates were washed three times with cold PBS to remove unbound [^{35}S] GTPγS. The filter plate was dried for at least 2h at RT. Adhesive BackSeal was applied to the filter plate and 50µL/well MicroScintTM-20 scintillation cocktail (PerkinElmer) was added. The plate was then sealed and read by TopCount NXT scintillation counter (Packard). The radioactivity of the bound radioligand was counted as counts per minute (CPM), and CPM was plotted against log ligand concentrations using GraphPad Prism Software.

2.4.2 Radioligand [^{3}H]140 binding assay

[^{3}H]140 (3-((5,6-diphenyl-1,2,4-triazin-3-yl)methyl)-1H-indole) is an antagonist at human GPR84, which was used in saturation binding assays to assess the affinity of [^{3}H]140 at different Flp-In T-REx 293 stable cell lines or the affinity of other ligands. The [^{3}H]140 binding assay was performed following the protocol from Jenkins et al. (2021). Assays were applied in a total assay volume of 500µL assay buffer (PBS with 0.5% fatty acid free bovine serum albumin; pH 7.4) in 96-deep-

well plates. Because of the radioligand decay, the real concentration of [³H]140 was measured and calculated by the following formula:

$$\frac{standard(DPM)}{specific\ activity(\frac{DPM}{fmol})} \times \frac{1}{Assay\ volume(500\mu L)} = \frac{fmol}{\mu L} = \frac{nmol}{L} = nM$$

Saturation binding

3µg of membranes prepared from Flp-In T-REx 293 stable cells were incubated with various concentrations of [³H]140 were in the presence (non-specific) or absence (total binding) of 10µM unlabelled GPR84 antagonist compound 837 for 1h at 25℃. The reaction was terminated by rapid filtration through UniFilter-96 GF/C glassfibre filter-bottom plates (pre-soaked in cold PBS) using a UniFilter FilterMate Harvester (PerkinElmer). Filter plates were washed three times with cold PBS to remove unbound [³⁵S] GTPγS. The filter plate was dried for at least 2h at RT. Adhesive BackSeal was applied to the filter plate and 50µL/well MicroScintTM-20 scintillation cocktail (PerkinElmer) was added. Total and non-specific binding of [³H]140 was quantified as disintegrations per minute (DPM) using the TopCount NXT scintillation counter (Packard). The total and non-specific binding were calculated using the following formula:

$$Total\ or\ nonspecific\ binding = \frac{measured(DPM)}{specific\ activity(\frac{DPM}{fmol)}} \times \frac{1000}{Protein(\frac{\mu g}{well})}$$

Specific binding was calculated by subtracting non-specific binding from total binding. The saturation binding curve was generated by plotting these data against the calculated concentrations of [³H]140.

Competition binding (antagonist GLPG1205 and [³H]140)

3µg of membranes were incubated with a certain concentration of [³H]140 and various concentrations of unlabelled GLPG1205 for 1h at 25℃. The reaction was terminated by rapid filtration through UniFilter-96 GF/C glassfibre filter-bottom plates (pre-soaked in cold PBS) using a UniFilter FilterMate Harvester (PerkinElmer). Filter plates were washed three times and dried for at least 2h at RT. Adhesive BackSeal was applied to the filter plate and 50µL/well MicroScintTM-

20 scintillation cocktail (PerkinElmer) was added. The result was read by the TopCount NXT scintillation counter (Packard). Data was fitted to a one-site competition binding equation using GraphPad Prism Software.

2.4.3 Bioluminescence resonance energy transfer (BRET)-based β-arrestin-2 recruitment assay

HEK293T or G-protein knock out cells were plated in 10cm dishes and incubated in an incubator until 80% confluent. Cells were then transiently transfected with 1μg Flag-GPR84-eYFP and 4μg β-arrestin2-Rluc (Renilla-luciferase). As a negative control, cells in another dish were transfected with 1μg empty pcDNA5/FRT/TO plasmids and 4μg β-arrestin2-Rluc. After incubation overnight, 100μL/well cells were transferred to a white 96-well plate with 40μL/well of 50μg/mL Poly-D-lysine hydrobromide. The plate was incubated overnight. On the following day, the medium was aspirated, and cells were washed with 200 μL 1X HBSS twice. 80μL/well HBSS was added to the plate and incubated for 30mins at 37°C. Following HBSS incubation, 10μL/well coelenterazine-h substrate (NanoLight Technology, 5μM final concentration) was added and incubated for 10mins at 37°C. Finally, 10μL/well various concentrations of agonists were added and incubated for 5mins before reading on a PHERAstar FS plate reader at 535nm and 475nm. Data were calculated by the following formula:

$$mBRET = (\frac{sample\ 535nM}{sample\ 475nM} - mean\left(\frac{control\ 535nM}{control\ 475nM}\right)) \times 1000$$

Calculated mBRET was plotted against log concentrations of agonists using GraphPad Prism Software.

2.4.4 HTRF-based cAMP inhibition assays

The cAMP assay was carried out using a time-resolved FRET-based detection kit (CisBio) following the manufacturer's protocol. As GPR84 is a G_i-coupled receptor, the activation of GPR84 promoted by agonists will lead to the reduction of forskolin-induced cAMP levels. Flp-In T-REx 293 stable cells were induced to express the construct of interest by incubation with 100 ng/ml doxycycline for 24h. Then cells were resuspended with 1x stimulation buffer and 5μl of cell suspensions were added to a 384-well low volume plate (5000 cells/well). 5μl/well various

concentrations of agonists were added and incubated for 15mins at RT before the incubation with 1µM forskolin for 1h. 5µl cAMP-d2 and 5µl anti-cAMP cryptate in lysis buffer were added to each well and incubated for at least 1h in dark (1:20 dilution). The output was read by PHERAstar FS plate reader (BMGLabtech) at 620nm and at 665 nm. The 665 nm/ 620 nm ratio was multiplied by 10,000 and plotted against log concentrations of agonists using GraphPad Prism Software.

2.4.5 GRK Nanobit assay

The protocol was optimized from a published paper from Palmer et al. (2022). GRK knock out cells and GRK parental cells (gifts from Prof. Carsten Hoffmann, University of Jena) were plated in 10cm dishes and incubated until 80% confluent. On the day of transfection, 500ng LgBit-GRK, 50ng GPR84-sBit and 4450ng empty vector pcDNA5 was diluted in 250µL of 150mM sterile NaCl. 30µg polyethyleneimine (PEI) was diluted in 250µL of 150mM sterile NaCl (DNA:PEI=1:6). Then diluted DNA and PEI were mixed, vortexed and incubated for 10mins at RT. The culture medium in the dish was replaced by fresh medium. The DNA-PEI mixture was dropped to the dish, gently mixed, and incubated for 24h in the incubator. On the following day, 100µL/well cells were transferred to a white 96-well plate with 40µL/well of 50µg/mL Poly-D-lysine hydrobromide ($1x10^6$ cells/well). The plate was incubated overnight. On the following day, the medium was aspirated, and cells were washed with 200 µL 1X HBSS twice. 80µL/well HBSS was added to the plate and incubated for 30mins at 37°C. Following HBSS incubation, 10µL/well Nano-Glo Luciferase assay substrate (Promega, 1:80 dilution) was added and incubated for 10mins at 37°C. The plate was read by CLARIOstar (BMG LabTech) and the output1 was used as a baseline. Finally, 10µL/well various concentrations of agonists were added and incubated for 5mins. The plate was read again using CLARIOstar (BMG LabTech) and generate output2. The ratio of output2/output1 was plotted against log concentrations of agonists using GraphPad Prism Software.

2.4.6 'Bystander' BRET-based internalization assay

GRK parental cells were plated in 10cm dishes and grow until 80% confluent. 2.5µg human GPR84-Nluc and 2.5µg of the early endosome located marker mNG-FYVE in pcDNA3.1 were co-transfected into cells with PEI (DNA:PEI=1:6). On the next day,

100µL/well cells were transferred to a white 96-well plate with 40µL/well of 50µg/mL Poly-D-lysine hydrobromide and incubated overnight. Then cells were washed with 200 µL 1X HBSS twice and incubated with 80µL/well HBSS for 30mins at 37°C. 10µL/well Nano-Glo Luciferase assay substrate (Promega, 1:80 dilution) was added, and the plate was read every 2 to 2.5mins for 4 circles (baseline) by PHERAstar FS plate reader (BMGLabtech) before the addition of agonists. Then the plate was read every 2 to 2.5mins for an additional 1h or longer. The data was normalized to the baseline and plotted using GraphPad Prism Software.

2.5 Molecular modelling

The ligand docking was generated by Dr. Irina G. Tikhonova (School of Pharmacy, Medical Biology Centre, Queen's University Belfast). Compound 271 was docked into the AlphaFold model of the human GPR84 and mouse GPR84 using the Glide module of Schrodinger software (Friesner et al., 2004).

2.6 Data analysis and curve fitting

All data generated from different assays were analysed using GraphPad Prism software.

2.6.1 Functional agonist and antagonist assay analysis

Both agonist and antagonist functional assays were analysed by non-linear regression analysis (three parameters). The concentration-response curve displays a standard slope factor (Hill slope) of 1 to better fit data. The concentrations of ligands were plotted in logarithmic scale with the vehicle labelled as the lowest concentration.

For agonists, the model of curve fitting is showed below:

$$Response(Y) = Bottom + \frac{Top - Bottom}{1 + 10^{(logEC50-X)}}$$

Top is the maximal asymptote of the curve which reflects the maximal response (Emax), and therefore the agonist efficacy. Bottom is the response of the vehicle. logEC50 is the logarithm of the EC50. EC50 is the concentration of the agonist that

generates a half-maximal response, which reflects the potency of an agonist. X is the concentration of agonists. Normally, agonist potency was analysed as -logEC50 (pEC50) which is normally calculated from at least three independent experiments and displayed as mean±SEM.

For antagonists, the model of curve fitting is showed below:

$$Response(Y) = Bottom + \frac{Top - Bottom}{1 + 10^{(X - logIC50)}}$$

The IC50 is the concentration of the antagonist to reduce agonist-induced response by 50%. Normally, antagonist potency was analysed as -logIC50 (pIC50) which is normally calculated from at least three independent experiments and displayed as mean±SEM.

2.6.2 Radioligand binding assay analysis

Radioligand binding assays were used to directly measure the affinity of ligand at receptor. The specific binding data was calculated by subtracting the non-specific binding from the total binding. Then these data were fitted to a one site specific binding model (non-linear regression). The specific binding model of curve fitting is showed below:

$$Specific\ binding(Y) = \frac{B_{max} \times X}{K_d + X}$$

B_{max} is the maximum specific binding which reflects the total number of receptor binding sites (Bmax) of the sample, presented as fmol/mg protein. The equilibrium binding constant K_d is the radioligand concentration that occupies half of the receptor sites. X is the concentration of the radioligand.

2.6.3 'Schild' assay analysis

To study whether an antagonist is competitive or non-competitive to an agonist, 'Schild' assays are normally performed. A series of agonist concentration-response curves were set up with various fixed concentrations of antagonists, and the resulting data was fit to the Gaddum/Schild EC50 shift analysis program using GraphPad Prism software. The generated pA_2 value reflects the antagonist affinity

at the receptor. The 'schild' slope factor reflects how well the shifts correspond to the prediction of competitive interaction. If the 'schild' slope factor is 1, then the agonist and the antagonist are perfectly competitive.

2.6.3.1 Statistical analysis

For experiments only performed once, the results were presented as the mean from triplicate wells in one experiment. For experiments repeated three times, the results were presented as mean±SEM (standard error). To compare the data from different groups, two-tailed unpaired student's t-test or one-way analysis of variance (ANOVA) were performed. Tukey's post-hoc analysis was employed to compare the level of significance with a P value <0.05 being considered statistically significant.

Chapter 3   Characterization of novel antagonists of mouse GPR84
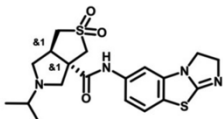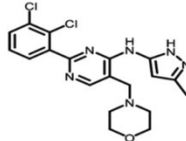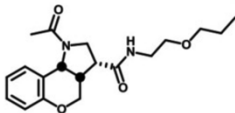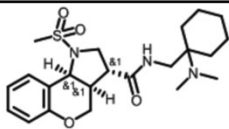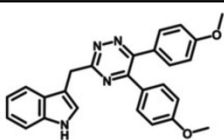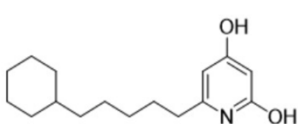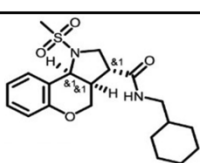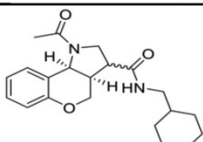
3.1 Introduction

Orphan receptor GPR84 is expressed by immune cells such as monocytes, macrophages and neutrophils, and it mediates the expression of pro-inflammatory mediators including IL-6, TNFα, KC-GROα and VEGF (Marsango and Milligan, 2023, Gaidarov et al., 2018). This suggests that blocking GPR84 could be a potential therapeutic opportunity in treating inflammation-related diseases such as ulcerative colitis, idiopathic pulmonary fibrosis and chronic inflammatory bowel disease (Jenkins et al., 2021, Marsango and Milligan, 2023). GLPG1205 is the most widely accepted and studied high affinity antagonist for GPR84. However, GLPG1205 is a non-competitive antagonist of both orthosteric agonists and allosteric agonists and displays relatively low potency at mouse GPR84 (Labéguère et al., 2020, Jenkins et al., 2021). Experiments using animal tissues including both *ex vivo* and *in vivo* are essential to understand the pharmacology of a GPCR and are required in the development of new drugs. However, the lack of suitable antagonists directly targeting mouse GPR84 has limited studies on understanding the therapeutic potential to block this receptor. Thus, finding a way to overcome this challenge would be important and necessary. High throughput screening would be the most direct way to solve this problem. In previous screening, 301,665 drug-like small molecules were screened against human GPR84 (Jenkins et al., 2021). Among these molecules, compound 837 displayed the highest potency in inhibiting human GPR84. However, compound 837 showed no significant inhibitory effect on mouse GPR84. Consequently, several compounds among them were selected based on their potency and chemical characteristic. These selected compounds were then tested against both human GPR84 and mouse GPR84 to compare their inhibitory effects across species. The chemical structures of compounds used in this chapter are listed in **Table 3-1.**

The initial aim of this chapter was to find novel and potent antagonists for mouse GPR84 by screening selected available compounds. In the light of the results, the

binding site(s) of such mouse-active GPR84 antagonists would be studied which would then facilitate the synthesis of further potent compounds.

Table 3-1 Chemical structures of GPR84 ligands used in this chapter

Compound	Chemical structure	IUPAC Name
Compound 195		2,2-dioxo-5-(propan-2-yl)-N-{7-thia-2,5-diazatricyclo[6.4.0.0^{2,6}]dodeca-1(8),5,9,11-tetraen-11-yl}-hexahydro-1H-2lambda6-thieno[3,4-c]pyrrole-3a-carboxamide
Compound 271		2-(2,3-dichlorophenyl)-N-(3-methyl-1H-pyrazol-5-yl)-5-[(morpholin-4-yl)methyl]pyrimidin-4-amine
Compound 275		3-acetyl-N-(2-propoxyethyl)-8-oxa-3-azatricyclo[7.4.0.0^{2,6}]trideca-1(9),10,12-triene-5-carboxamide
Compound 460		N-{[1-(dimethylamino)cyclohexyl]methyl}-3-methanesulfonyl-8-oxa-3-azatricyclo[7.4.0.0^{2,6}]trideca-1(9),10,12-triene-5-carboxamide
Compound 837		3-((5,6-Bis(4-methoxyphenyl)-1,2,4-triazin-3-yl)methyl)-1H-indole
TUG-2097		6-(5-cyclohexylpentyl)pyridine-2,4-diol
Compound 210		N-(cyclohexylmethyl)-3-methanesulfonyl-8-oxa-3-azatricyclo[7.4.0.0^{2,6}]trideca-1(9),10,12-triene-5-carboxamide
Compound 78		3-acetyl-N-(cyclohexylmethyl)-8-oxa-3-azatricyclo[7.4.0.0^{2,6}]trideca-1(9),10,12-triene-5-carboxamide

3.2 Results

3.2.1 Initial screens

Following previous work (Jenkins et al., 2021), 6 drug-like small molecules were screened against human GPR84-Gα_{i2} (hGPR84-Gα_{i2}) and mouse GPR84-Gα_{i2} (mGPR84-Gα_{i2}) each expressed stably in Flp-In TREx 293 cells. The ability of these

compounds to prevent stimulation of binding of [35S]GTPγS induced by 2-HTP was measured. In such [35S]GTPγS incorporation assays, this analogue of GTP binds to the α subunit of a G protein complex after receptor activation. The terminal S-substitution, in place of the γ phosphate of GTP, prevents effective hydrolysis of the molecule. The build-up of [35S]GTPγS-bound G proetin is proportional to the extent of receptor activation. Membranes prepared from Flp-In TREx 293 cells expressing hGPR84-Gα$_{i2}$ or mGPR84-Gα$_{i2}$ were pre-incubated with 10μM of the potential antagonists for 15mins prior to addition of agonist. Then [35S]GTPγS and GDP were added to the assay mixture and the reaction was incubated at 30°C for 1h. Non-linear regression curves were fitted to such data (**Figure 3.1**). It was found that all these 6 compounds, and compound 837 (Jenkins et al., 2021), could prevent activation of hGPR84-Gα$_{i2}$ promoted by 2-HTP, but only compound 271 displayed substantial inhibition at mGPR84-Gα$_{i2}$.
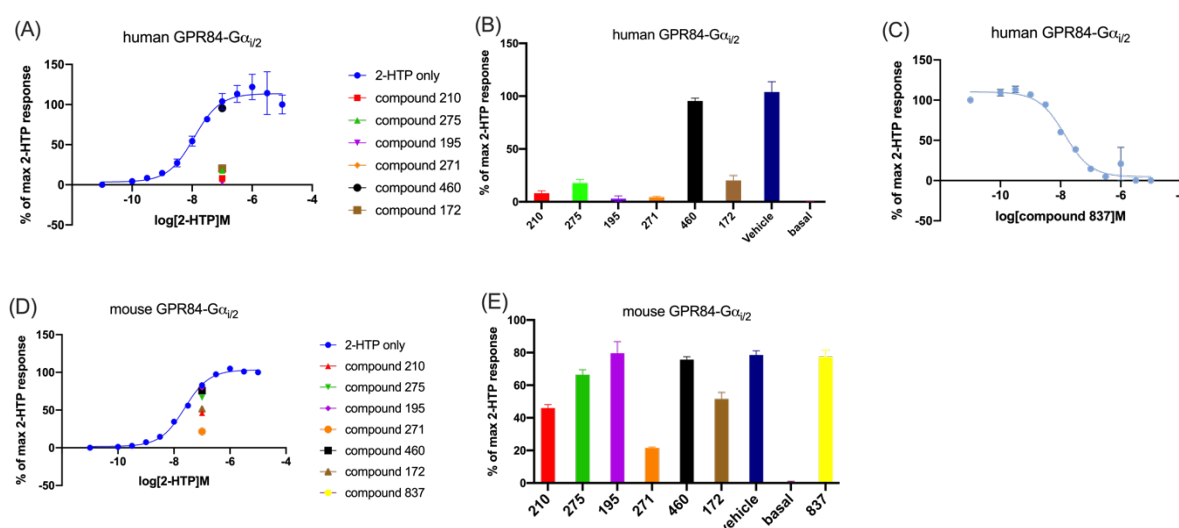
Figure 3.1 A novel mouse GPR84 antagonist was identified in [35S]GTPγS incorporation assays.

Membranes prepared from Flp-In TREx 293 cells induced to express hGPR84-Gα$_{i2}$ (A-C) or mGPR84-Gα$_{i2}$ (D-E). Membranes were pre-incubated with 10 μM of the compounds illustrated for 15mins before the addition of an EC$_{80}$ concentration of 2-HTP for 1h at 30°C. The lowest concentration of compounds displayed on the X-axis is actually 0M (vehicle only). The incorporation of [35S]GTPγS was measured. Data were normalised separately for each cell line. A, D) Concentration-response curves for 2-HTP are presented, along with the effect of 10 μM compounds on the EC$_{80}$ concentration (100 nM) responses of 2-HTP. B, E) Bar graphs comparing the ability of 10 μM compounds to inhibit the activation of hGPR84-Gα$_{i2}$ or mGPR84-Gα$_{i2}$ by 100 nM of 2-HTP. C) Concentration-response curve for compound 837 showing its inhibitory effect on hGPR84-Gα$_{i2}$ activation by 100 nM of 2-HTP. Each experiment was performed in duplicate, and results represent mean responses. Experiments were performed twice (n=2).

3.2.2 Compound 271 is a competitive orthosteric antagonist at both human and mouse GPR84

Initial screens showed that, at 10μM, compound 271 displayed the strongest inhibition of mouse GPR84. On this basis, compound 271 was selected for further characterization. The potency of compound 271 was measured in $[^{35}S]GTP\gamma S$ incorporation assays conducted using membranes of Flp-In TREx 293 cells expressing either hGPR84-$G\alpha_{i2}$ or mGPR84-$G\alpha_{i2}$ fusion proteins. 2-HTP is a potent orthosteric agonist of both human and mouse GPR84 (Jenkins et al., 2021, Marsango et al., 2020). Compound 271 was able to block activation of both human GPR84 and mouse GPR84 promoted by 2-HTP in a concentration-dependent manner, displaying pIC_{50} 6.74±0.22 and 5.64±0.19 respectively (mean±range, range = $(X_{max} – X_{min})/2$, n=2) (**Figure 3.2**). Compound 271 was able to fully block activation of hGPR84-$G\alpha_{i2}$ but at the highest concentration tested (10μM) blockade of the activation of mGPR84-$G\alpha_{i2}$ was incomplete (**Figure 3.2**). This reflects the lower pIC_{50} at mGPR84-$G\alpha_{i2}$ than at hGPR84-$G\alpha_{i2}$. It was not practical to use higher concentrations of compound 271. However, if it had been possible, it is expected that the activation of mouse GPR84 could have been fully blocked.
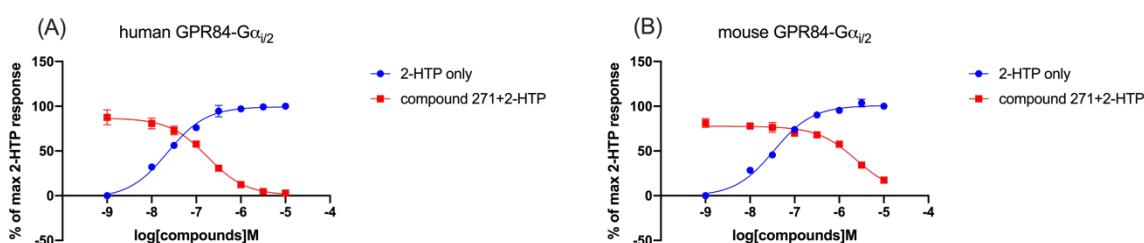
Figure 3.2 Compound 271 is an antagonist at both human and mouse GPR84.
Membranes prepared from Flp-In TREx 293 cells induced to express A) hGPR84-$G\alpha_{i2}$ or B) mGPR84-$G\alpha_{i2}$ were incubated with varying concentrations of compound 271 for 15mins before addition of 2-HTP (EC_{80}, calculated from **Figure 3.1**) for 1h at 30°C. The lowest concentration of compounds displayed on the X-axis is actually 0M (vehicle only). The incorporation of $[^{35}S]GTP\gamma S$ was measured. Response was normalised separately for each cell line. Experiments were performed twice (n=2).

'Schild' experiments were then applied to study whether compound 271 acted as a competitive antagonist or non-competitive antagonist to the orthosteric agonist 2-HTP. The results are typically plotted as a 'Schild' plot which is used to calculate the pA_2 value and determine the nature of inhibition. If the compound is a competitive antagonist, the concentration-response curve of the agonist will shift

to the right with increasing concentrations of the antagonist, but the maximum response remains unchanged. If the compound is a non-competitive antagonist, increasing antagonist concentration does not simply shift the agonist curve but instead reduces the maximum response of the agonist. Moreover, if the 'Schild' slope calculated from this model is closer to 1, the tested antagonist is more competitive with the used agonist. Measured EC_{50} (effective concentration 50%) of 2-HTP at both hGPR84-$G\alpha_{i2}$ and mGPR84-$G\alpha_{i2}$ was increased in a concentration-dependent manner by compound 271 in [^{35}S]GTPγS binding studies (**Figure 3.3**), with estimated affinity of compound 271 (pA_2) 7.6 and 6.5 respectively, and 'Schild' slope 1.02 and 0.87 respectively. Compound 271 was competitive with 2-HTP because the inhibitory effect of compound 271 was fully overcome with increasing concentrations of 2-HTP. Moreover, compound 271 'shifted' the concentration-response curve of human GPR84 more than that of mouse GPR84.
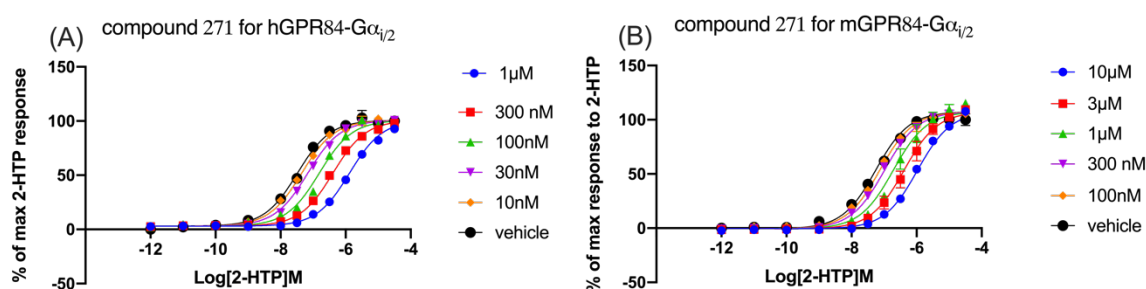
Figure 3.3 Compound 271 is a competitive orthosteric antagonist at both human GPR84 and mouse GPR84.
Membranes prepared from Flp-In TREx 293 cells induced to express A) hGPR84-$G\alpha_{i2}$ or B) mGPR84-$G\alpha_{i2}$ were incubated with varying concentrations of compound 271 for 15mins before addition of different concentrations of 2-HTP for 1h at 30˚C. The lowest concentration of compounds displayed on the X-axis is actually 0M (vehicle only). The incorporation of [^{35}S]GTPγS was measured. Response was normalised separately for each cell line. Each experiment was performed in triplicate. Data are from a single experiment (n=1).

A chemically distinct agonist TUG-2097 (Ieremias et al., 2024) was also used in the 'Schild' assay, and data showed that compound 271 also acted as a competitive antagonist to agonist TUG-2097 at both hGPR84-$G\alpha_{i2}$ and mGPR84-$G\alpha_{i2}$. The estimated affinity of compound 271 (pA_2) was 6.9 and 6.3 respectively, and the 'Schild' slope was 0.94 and 0.82 respectively (**Figure 3.4**).
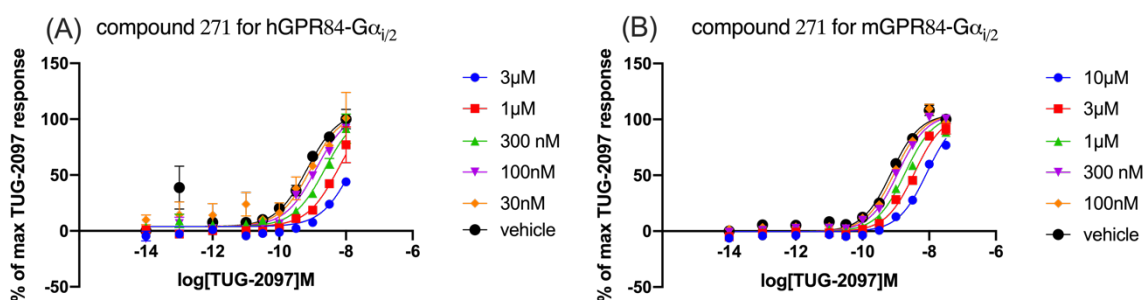
Figure 3.4 Compound 271 is a competitive antagonist of agonist TUG-2097 at human GPR84 and mouse GPR84.
Membranes prepared from Flp-In TREx 293 cells induced to express A) hGPR84-Gα_{i2} or B) mGPR84-Gα_{i2} were incubated with varying concentrations of compound 271 for 15mins before addition of different concentrations of TUG-2097 for 1h at 30°C. The lowest concentration of compounds displayed on the X-axis is actually 0M (vehicle only). The incorporation of [^{35}S]GTPγS was measured. Each experiment was performed in triplicate. Data are from a single experiment (n=1).

Because compound 271 acted as a competitive orthosteric antagonist for both human GPR84 and mouse GPR84, we wished to assess its mode of binding as this might help to design more potent mouse GPR84 antagonists in the future. A ligand docking study (**Figure 3.5**) was performed by the group of Irina G Tikhonova (Queen's University Belfast). The structure of human GPR84 was tested effectively in the docking of agonist (Marsango et al., 2022). Compound 271 could be docked into the same pocket of human GPR84 as 2-HTP (Al Mahmud et al., 2017, Jenkins et al., 2021), which is consistent with its competitive mode of binding and this was also the case for mouse GPR84 although interactions within the pocket were different, presumably reflecting the 10 times lower affinity of this compound at mouse GPR84 (**Figure 3.5 A**). The published human GPR84 cryo-EM structure is similar to other Class A rhodopsin-like GPCRs (Zhang et al., 2023b, Liu et al., 2023). The ECL2 and the N-terminus of GPR84 form a roof-like structure which makes ligands cannot access the orthosteric site from the extracellular milieu. The ECL2 presents a β-hairpin structure to extend towards TM1. Two disulfide bonds in the extracellular domain of the GPR84 structure keep the structural stability of GPR84. One is the highly conserved disulfide bond between C168 of ECL2 and C93$^{3.25}$ of TM3, which is related to class A GPCR cell surface delivery and function. The other disulfide bond is formed between C166 of ECL2 and C11 of the N-terminal, which is important to correct GPR84 folding (Zhang et al., 2023b, Liu et al., 2023). Previously published homology model identified a key residue Arg172 which is located within ECL2 (Al Mahmud et al., 2017). Thus, there are two different

suggested binding models. Compound 271 interacts with Arg172 of human GPR84 in one model, whilst there is no such interaction in the other model (**Figure 3.5 B**). To study which model might be correct, mutant which alter Arg172 to Ala was generated and the potency of compound 271 against this mutant was studied.

(A)

Human GPR84   Mouse GPR84
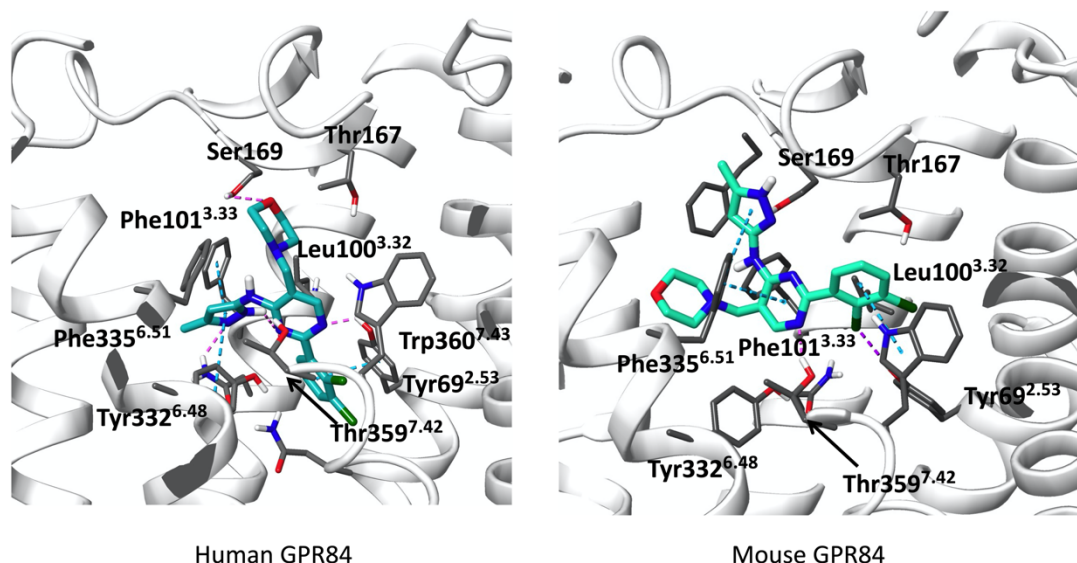
(B)   Docking Poses of Compound 271 in GPR84 Alphafold Model
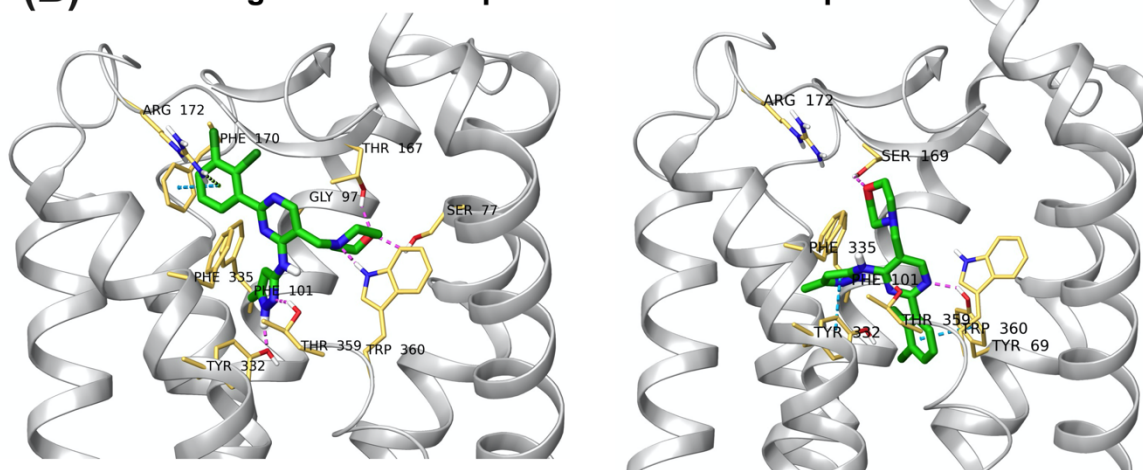
Figure 3.5 Docking of compound 271 into human and mouse GPR84.
A) Amino acids from human and mouse GPR84 are shown respectively and residues are labelled using Ballesteros-Weinstein residue location numbering. B) Two different suggested docking models into human GPR84. Non-conserved residues and their counterparts in interhelical hydrogen bonding are shown in stick-like representation. Hydrogen bonds are shown as dashed lines.

To study which docking model of compound 271 in human GPR84 might be correct, a stable cell line able to induce the expression of hGPR84-R172A-eYFP was generated. As alteration of Arg172 prevents activation of GPR84 by most orthosteric agonists (Al Mahmud et al., 2017), the allosteric agonist PSB-16671 was used as agonist to activate the receptor and the potency of compound 271 to block hGPR84-eYFP and hGPR84-R172A-eYFP was studied. At both these forms compound 271 was able to block activation by PSB-16671 and with similar potency (pIC_{50} 5.87±0.30 and 6.01±0.52 respectively) (**Figure 3.6**). As alteration of Arg172 to Ala did not reduce the binding of compound 271, this suggests that the docking pose showing no interaction between compound 271 and Arg172 of human GPR84 would be the more reasonable one.
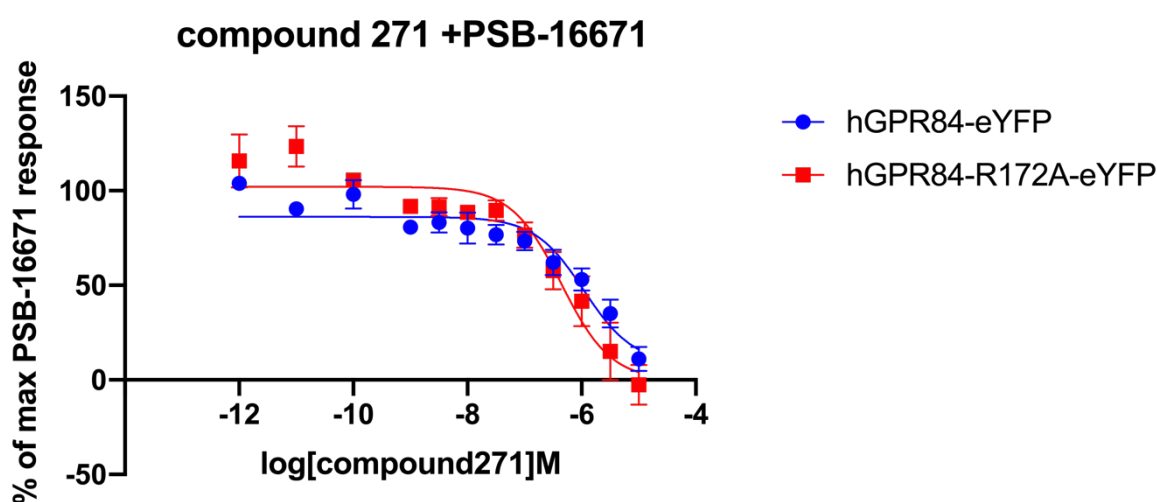
Figure 3.6 Mutation of Arg172 of hGPR84 does not affect the binding of compound 271.
Membranes prepared from Flp-In TREx 293 cells induced to express hGPR84-eYFP or hGPR84-R172A-eYFP were incubated with varying concentrations of compound 271 for 15mins before addition of a of 2-HTP (EC_{80}, calculated from agonist concentration-response curve) for 1h at 30°C. The lowest concentration of compounds displayed on the X-axis is actually 0M (vehicle only). The incorporation of [^{35}S]GTPγS was measured. Response was normalised separately for each cell line. Experiments were performed three times (n=3).

3.2.3 Screening of a cluster of compounds based on compound 210

Initial screens revealed that compound 210 also blocked the activation of human and mouse GPR84 even though it showed lower potency than compound 271. The affinity of compound 210 to block 2-HTP-induced regulation of cAMP was further explored. The Flp-In T-REx 293 cell lines stably expressing HA-human GPR84 or HA-mouse GPR84 were firstly pre-incubated with the potential antagonists for

15mins, then incubated with 2-HTP for 15mins and finally incubated with 1 µM forskolin for 1h. It was found that compound 210 blocked the response of HA-human GPR84 stimulated by 2-HTP with pIC_{50} of 5.48 ± 0.16 (mean±SEM, n=3), but did not show obvious inhibition of HA-mouse GPR84 (**Figure 3.7 A**). To this end, a 'Schild' assay was applied using compound 210 and 2-HTP. Compound 210 shifted the agonist concentration-response curve at human GPR84 which means that compound 210 was a competitive antagonist at HA-human GPR84 with estimated affinity of (pA_2) 6.7 and 'Schild' slope of 1.22 (**Figure 3.7 B**). However, compound 210 only shifted the agonist concentration-response curve at mouse GPR84 to a limited extent and such data was challenging to analyse as a pA_2 value (**Figure 3.7 C**). Thus, although compound 210 is an orthosteric competitive antagonist at human GPR84, it is, at best, a very weak antagonist at the mouse orthologue.
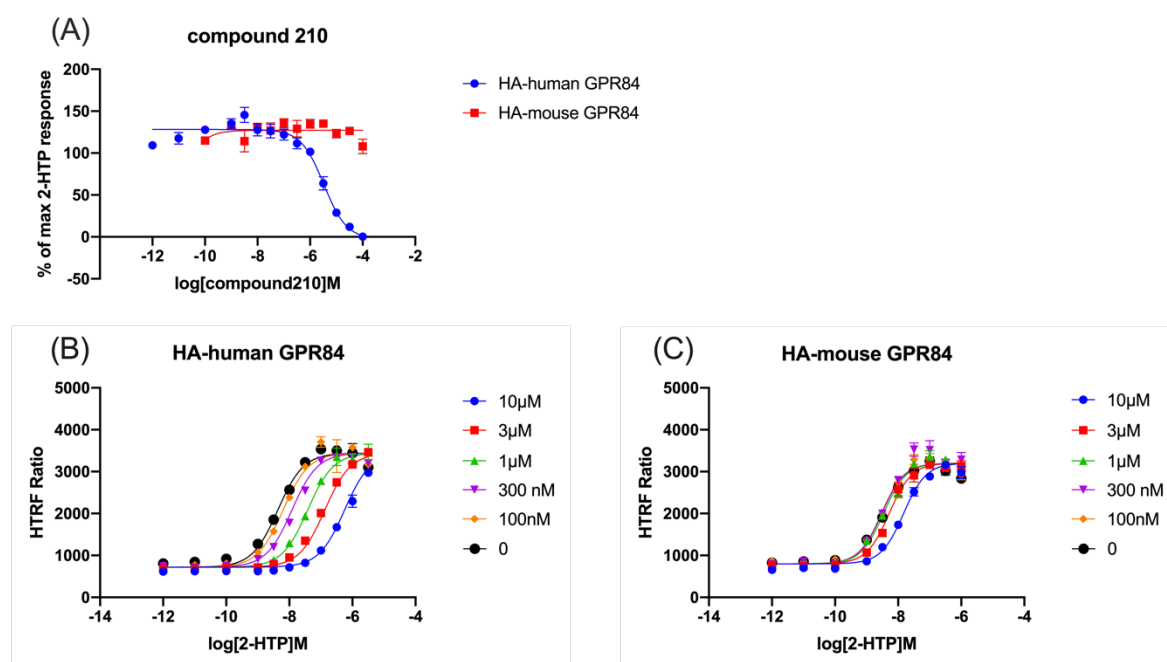
Figure 3.7 Compound 210 is an orthosteric competitive antagonist at human GPR84.
Flp-In TREx 293 cells were induced to express HA-human GPR84 or HA-mouse GPR84 by treatment overnight with 100ng/ml doxycycline. 5000cells/well were plated in low-volume 384-well plates followed by incubation with various concentrations of compound 210 for 15mins, followed by incubation with A) the EC_{80} concentration of 2-HTP or B, C) various concentrations of 2-HTP for 15mins. Subsequently, 1 µM forskolin was added and further incubated for 1h. The lowest concentration of compounds displayed on the X-axis is actually 0M (vehicle only). Response was normalised separately for each cell line. The inhibition experiment was applied three times at human GPR84 (n=3) and one time at mouse GPR84 (n=1). 'Schild' experiments was performed in triplicate. Data are from a single experiment (n=1).

In order to discover novel compounds that block human and mouse GPR84 more potently, a new compound, compound 78, was designed and synthesized by

docking compound 210 into a predicted GPR84 structure. Similar experiments were performed with compound 78, following the same protocol as the experiment with compound 210 (**Figure 3.8**). Compound 78 blocked the stimulated by 2-HTP of HA-human GPR84 with pIC_{50} of 6.63 and at HA-mouse GPR84 by with lower potency (pIC_{50} of 5.15) (**Figure 3.8 A**). To study the affinity of compound 78, a 'Schild' experiment at human and mouse GPR84 was performed, generating estimated pA_2 of 7.0 and 6.79 respectively, and 'Schild' slope of 1.18 and 0.56 respectively (**Figure 3.8 B, C**). The shifted concentration-response curves of 2-HTP suggest that compound 78 is a competitive antagonist to 2-HTP.
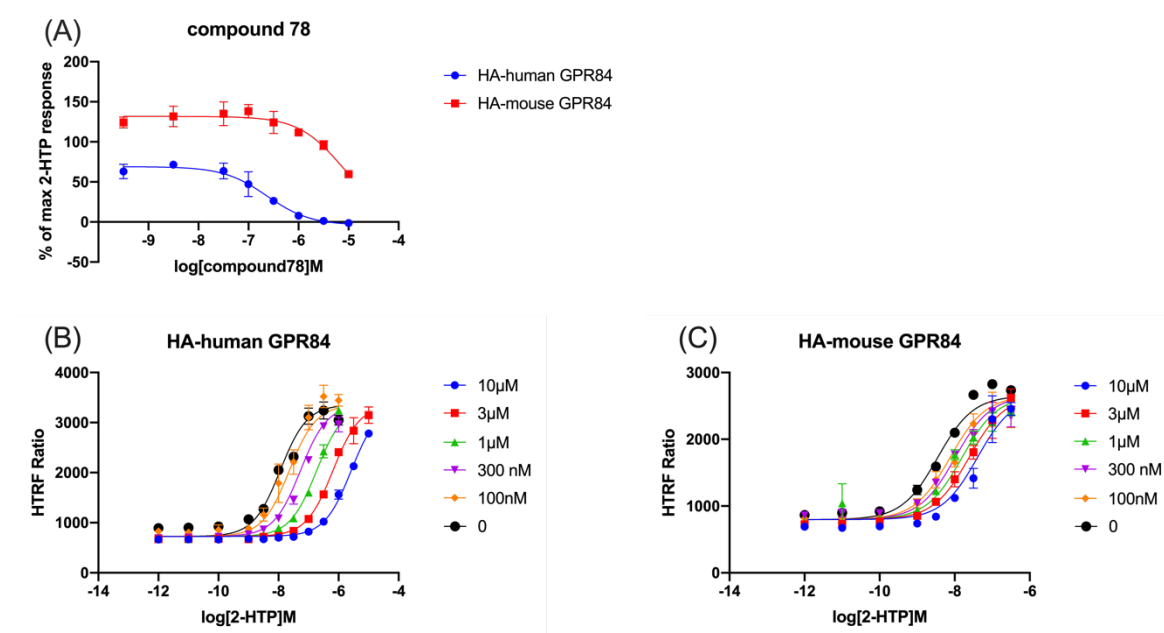
Figure 3.8 Compound 78 is an orthosteric competitive antagonist at human GPR84.
Flp-In TREx 293 cells were induced to express HA-human GPR84 or HA-mouse GPR84 by treatment overnight with 100ng/ml doxycycline. 5000cells/well were plated in low-volume 384-well plates followed by incubation with various concentrations of compound 78 for 15mins, followed by incubation with A) the EC_{80} concentration of 2-HTP or B, C) various concentrations of 2-HTP for 15mins. Subsequently, 1 μM forskolin was added and further incubated for 1h. The lowest concentration of compounds displayed on the X-axis is actually 0M (vehicle only). Single experiments were performed.

3.3 Discussion

GPR84 is attracting considerable interest as a potential therapeutic target because of the increased expression in proinflammatory conditions (Jenkins et al., 2021, Marsango and Milligan, 2023). The best-characterized high-affinity GPR84 antagonist, GLPG1205, has been assessed clinically in ulcerative colitis and idiopathic pulmonary fibrosis (Labéguère et al., 2020, Strambu et al., 2023).

Although the clinical results did not achieve the predicted results, GLPG1205 still displays the treatment effect on idiopathic pulmonary fibrosis in early studies (Jenkins et al., 2021). There would be many aspects that affect the results of clinical trials, and inadequate early research would be a possible reason because of the low affinity of GLPG1205 against mouse GPR84. Therefore, searching distinct and selective high affinity antagonists targeting human and mouse GPR84 would be important.

Following previous studies in our lab (Jenkins et al., 2021), several drug-like potent antagonists were retested against mouse GPR84 and human GPR84. It was found that compound 271 is an orthosteric competitive antagonist at both human and mouse GPR84, which displays higher inhibition potency at human GPR84 than mouse GPR84. Except for compound 271, compound 210 is also a potent antagonist targeting human GPR84. Therefore, a new compound based on the structure of compound 210 was designed and synthesized, which is named as compound 78. It was found that both compound 210 and compound 78 are orthosteric competitive antagonists at human GPR84. However, compound 78 cannot block the activation of mouse GPR84 as potent as blocks human GPR84. Therefore, more studies on understanding the binding sites of different available antagonists into human and mouse GPR84 need to be applied, and hopefully more novel compounds could be screened in order to find novel potent antagonists to human and mouse GPR84.

Although there are no available cryo-EM structures of GPR84 bound with antagonists, there are published structures of GPR84 bound with LY-237 (Liu et al., 2023). LY-237 (6-nonylpyridine-2,4-diol) is a potent orthosteric agonist of GPR84 that is closely related to agonist TUG-2097 used in this chapter. LY-237 has a hydrophilic head and a highly hydrophobic alkyl tail, which is similar to the potential endogenous ligands MCFAs (Liu et al., 2016). The orthosteric pocket of GPR84 is formed by a polar region at the top and a deep hydrophobic cavity below. Residues S169, R172A, Y69 and W360 interact with LY-237, and mutations at these important residues affect the potency of orthosteric agonists (Al Mahmud et al., 2017, Liu et al., 2023, Marsango et al., 2022).

On the basis of these results, the predicted binding model of GPR84 bound with compound 271 was studied, which hopefully could guide us to develop novel potent antagonists targeting mouse GPR84. Based on the predicted binding model and the studies on GPR84 orthosteric binding pocket, we generated a construct in which the Arg172 of human GPR84 was mutated to Ala. It was found that the potency of compound 271 targeting human GPR84 wild type and the mutant is not significantly different. Thus, compound 271 properly not interact with the Arg172 of GPR84. However, compound 271 is competitive to orthosteric agonist 2-HTP and TUG-2097 at both human and mouse GPR84. Therefore, studies on the binding pocket of GPR84 antagonists would be a good way to overcome the gap of lacking tool compounds.

Chapter 4   Characterization of HA-human GPR84, HA-mouse GPR84 and HA-humanised GPR84

4.1 Introduction

As discussed in *Chapter 3*, GPR84 is a poorly characterized pro-inflammatory receptor which suggests that blocking GPR84 could be a potential therapeutic opportunity in treating inflammation-related diseases such as ulcerative colitis, idiopathic pulmonary fibrosis and chronic inflammatory bowel disease (Jenkins et al., 2021, Marsango and Milligan, 2023). However, lack of suitable antagonists directly targeting mouse GPR84 has limited studies on understanding the therapeutic potential to block this receptor. Thus, finding a way to overcome this challenge would be important and necessary. In addition to screening for novel antagonists which directly targets mouse GPR84, generating a transgenic mouse model expressing either human or a 'humanised' form of GPR84 could be a method to fill the gap. Human and mouse GPR84 share about 85% similarity in the extracellular (ECL) regions and transmembrane domains (TMDs) (Jenkins et al., 2021), and most of the different amino acids locate in the ICL3 regions (**Figure 4.1**). If proteins share high similarity in sequence, they are likely to have similar structures. Therefore, four chimeric cDNA constructs were designed and generated by altering different regions to the human sequence in ECL3+TMD7, TMD1+ECL1+TMD3, TMD4+ECL2+TMD5 and all of these different sequences ('humanised' construct). It is expected that these chimeric cDNA constructs will exhibit similar pharmacology and functions as human GPR84 (Jenkins et al., 2021).
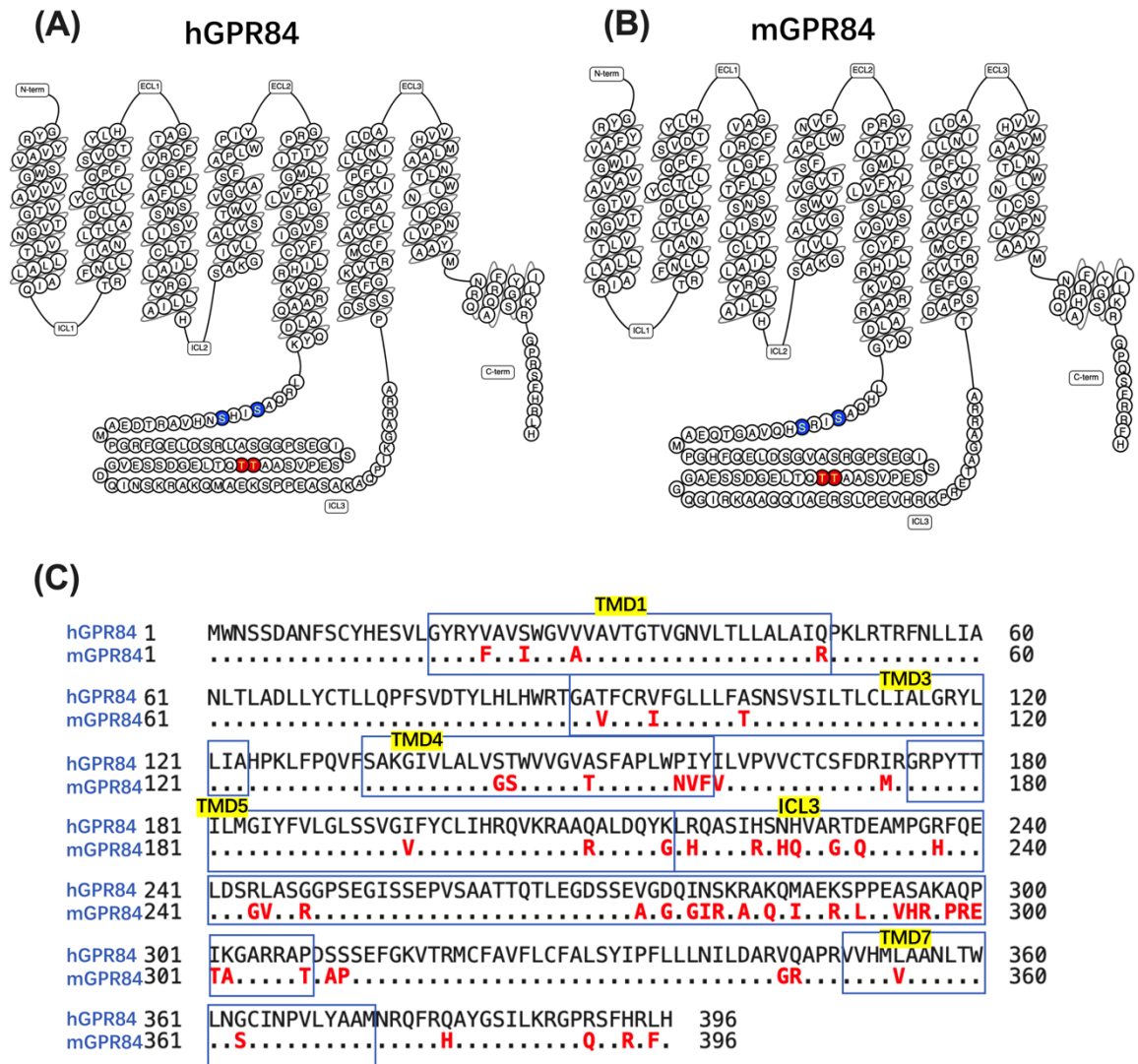
Figure 4.1 Primary amino acid sequences of human GPR84 and mouse GPR84.
Amino acid sequences of A) human GPR84 (hGPR84) and B)mouse GPR84 (mGPR84) were shown with predicted extracellular/ intracellular regions and transmembrane domains in snake plots. C) Different regions between hGPR84 and mGPR84 are highlighted (red). In snake plots, the residues targeted by phosphosite-specific antisera used in this chapter are highlighted in colour: pSer221/pSer224 (blue) and pThr263/pThr264 (red). Snake plots were generated with GPCRdb. This figure suggests that the ECL regions and TMDs of human and mouse GPR84 share high similarity and most of the different amino acids locate in the ICL3 region.

Following the expression in Flp-In T-REx 293 cell lines, each of the above chimeric forms was studied to determine the potency of 2-HTP and the affinity of human GPR84-selective antagonists using a $[^{35}S]$GTPγS binding assay (Jenkins et al., 2021). Among these chimeras, a 'humanised' form in which all residues in the extracellular regions that differ between human and mouse GPR84 were altered to the human sequence within the backbone of mouse GPR84 was explored in detail. In addition, an HA epitope tag was introduced into the extracellular N-terminus of this construct of GPR84 with the anticipation that this would help

facilitate fluorescence-activated cell sorting (FACS) positive immune cells if such a construct was used to generate a transgenic mouse line. In anticipation that this construct might be used to produce such a mouse line, this chimeric receptor was characterized extensively using a Flp-In T-REx 293 cell line in which it was stably expressed. To use such cells, doxycycline was added to induce the expression of the receptor, and the amount of doxycycline can regulate the level of expression. Stable cells expressing each of HA-human GPR84, HA-mouse GPR84 or HA-humanised GPR84 were generated to characterize the pharmacology of these forms and to assess whether HA-humanised GPR84 would display pharmacology and function equivalent to HA-human GPR84.

To evaluate Flp-In T-REx 293 stable cells expressing HA-human GPR84 or HA-mouse GPR84, they were characterized using each of cAMP assays, radioligand binding assays and immunoblotting. cAMP assays help to determine if they show similar or different levels of responses to agonists or antagonists (potency and efficacy). Radioligand binding assays were performed to compare their binding affinity to antagonists. Immunoblotting experiments using phosphosite-specific antisera and GPR84 structural antisera help to understand whether phosphorylation patterns between human and mouse GPR84 are different. Then stable cells expressing HA-humanised GPR84 were characterized using the same methods to compare similarities and differences between these constructs.

4.2 Results

4.2.1 Characterization of stable cell lines expressing HA-human GPR84 or HA-mouse GPR84

Initially, the ability of different agonists to activate HA-human GPR84 (HA-hGPR84) and HA-mouse GPR84 (HA-mGPR84) was explored. A cAMP assay was employed based on a homogenous time-resolved FRET-based detection kit (CisBio). 5000 cells/well were incubated with agonists for 15mins before the addition of 1 μM forskolin for 1h. Forskolin promotes the production of cAMP. As GPR84 is a G_i coupled receptor, the activation of GPR84 stimulated by agonists were anticipated to inhibit cAMP production. Flp-In T-REx 293 cell lines stably expressing HA-hGPR84 or HA-mGPR84 were used to establish the potency of different agonists.

2-HTP and 6-OAU are balanced orthosteric agonists, DL-175 is a G_i-biased orthosteric agonist and PSB-16671 is an allosteric agonist of GPR84 (Marsango et al., 2020, Jenkins et al., 2021). These agonists were used to activate the receptor separately, and non-linear regression curves were fitted to the data (**Figure 4.2**). The pEC_{50} of these agonists at HA-hGPR84 and HA-mGPR84 are listed in **Table 4-1**, and compared by t-test. It was found that the EC_{50} of 2-HTP and PSB-16671 at HA-hGPR84 and HA-mGPR84 were not significantly different, while the EC_{50} of 6-OAU and DL-175 at these two orthologues were significantly different ($p<0.01$). The basal activity of these two orthologues was similar, but the measured E_{max} of HA-hGPR84 was higher than that of HA-mGPR84. However, published work showed that the potency and efficacy of 2-HTP at human GPR84 and mouse GPR84 were similar (Jenkins et al., 2021, Mancini et al., 2019). The different efficacy could be caused by different expression levels of HA-hGPR84 and HA-mGPR84 Flp-In T-REx 293 cell lines. The expression level of a receptor at the plasma membrane is regulated by multiple factors, including transcriptional control, post-translational modifications, and intracellular trafficking (Dong et al., 2007, Sikarwar et al., 2019). Various assays such as saturation binding assays, enzyme-linked immunosorbent assays (ELISA), western blots or even qPCR can be used to evaluate the expression level of a receptor. Further studies will be needed to examine the prediction. If the expression levels of these two orthologues were the same, the higher pEC_{50} and lower efficacy at HA-mGPR84 could reflect that the interaction between HA-mGPR84 and G protein is likely to be weaker than the interaction between HA-hGPR84 and G protein.
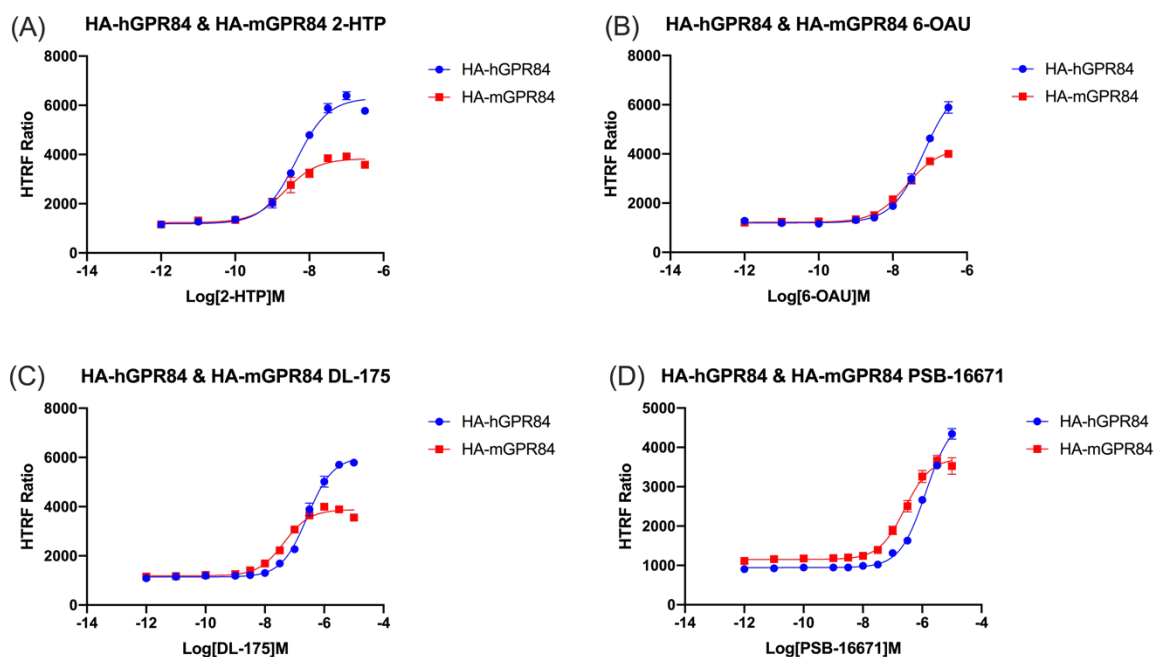
Figure 4.2 GPR84 agonists regulate cAMP levels via HA-hGPR84 and HA-mGPR84 with similar potency.
Flp-In TREx 293 cells were induced to express HA-hGPR84 (blue) or HA-mGPR84 (red) by treatment overnight with 100ng/ml doxycycline. Then 5000cells/well were plated in low-volume 384-well plates followed by incubation with various concentrations of A) 2-HTP, B) 6-OAU, C) DL-175 or D) PSB-16671 for 15mins. Subsequently, 1 μM forskolin was added and further incubated for 1h. The lowest concentration of compounds displayed on the X-axis is actually 0M (vehicle only). Output was measured with a PHERAstar FS plate reader (BMG Labtech). Data are presented as mean±SEM (n=3).

Table 4-1 Potency of different agonists at HA-hGPR84 and HA-mGPR84 in cAMP assays.

	HA-hGPR84 ($pEC_{50} \pm SEM$)	HA-mGPR84 ($pEC_{50} \pm SEM$)
2-HTP	8.36 ± 0.02	8.59 ± 0.23
6-OAU	7.16 ± 0.06	7.63 ± 0.06**
DL-175	6.56 ± 0.10	7.35 ± 0.13**
PSB-16671	6.10 ± 0.18	6.58 ± 0.07

Values were calculated from the HTRF ratio. Data presented as mean±SEM (n=3). **$p<0.01$ by t-test against HA-hGPR84.

Following this, the affinity of different antagonists to block 2-HTP-induced regulation of cAMP was explored. To this end, three previously described antagonists, compound 020 (**Figure 4.3 B**), compound 140 (**Figure 4.3 C**) and compound 837 (**Figure 4.3 D**)(Jenkins et al., 2021) were used in the cAMP assay.

The Flp-In T-REx 293 cell lines stably expressing HA-hGPR84 or HA-mGPR84 were firstly pre-incubated with the different antagonists for 15mins separately, then incubated with 2-HTP (the concentration was the EC_{80} calculated from **Figure 4.2**) for 15mins and finally incubated with 1 µM forskolin for 1h. The graph using various concentrations of 2-HTP can be seen as a positive control of the antagonists inhibition assay (**Figure 4.3 A**). It was found that compound 020, compound 140 and compound 837 blocked the response of HA-hGPR84 stimulated by 2-HTP with pIC_{50} of 5.86±0.20, 5.75±0.23 and 6.57±0.75 respectively, but they did not block the activation of HA-mGPR84 promoted by 2-HTP (**Figure 4.3 B,C,D**). Therefore, these compounds are human GPR84 species selective antagonists. However, the pIC_{50} measured in this chapter was lower than that in published work (Jenkins et al., 2021). The differences might be because the pIC_{50} in this chapter was measured in cAMP assays and the pIC_{50} in the paper was generated using $[^{35}S]GTP\gamma S$. It may also be because the expressed receptor in this chapter was HA-hGPR84 while the receptor in the published work was human GPR84-$G\alpha_{i2}$ fusion protein.
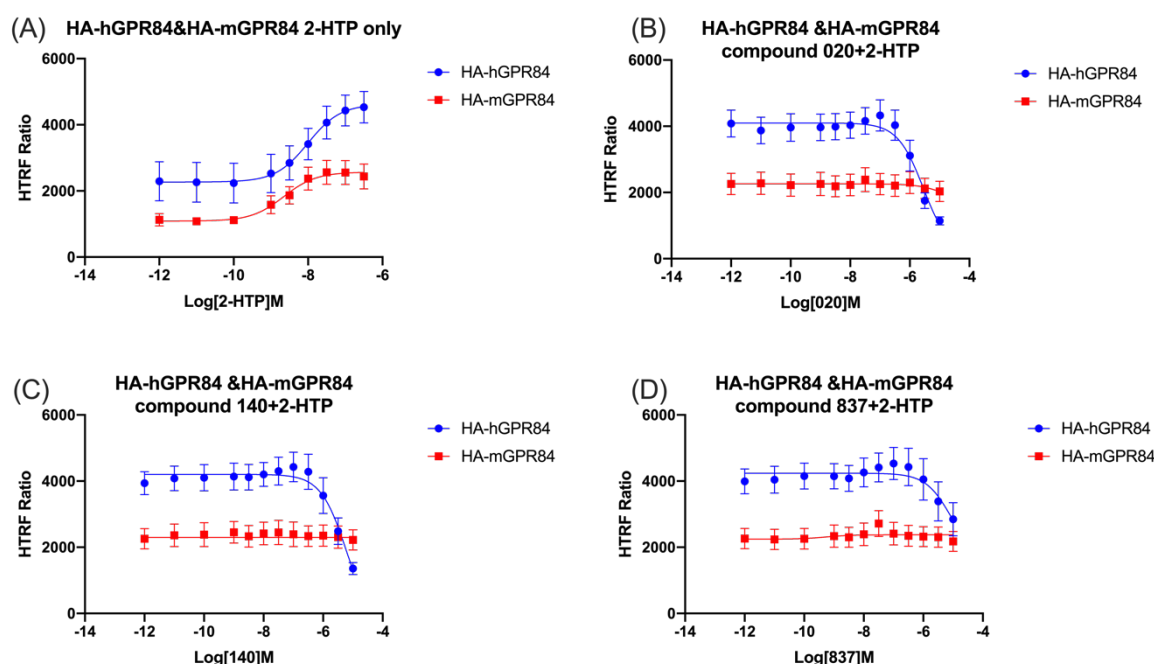
Figure 4.3 The tested compounds inhibit 2-HTP-mediated regulation of cAMP at HA-hGPR84 but not at HA-mGPR84

Flp-In TREx 293 cells were induced to stably express HA-hGPR84 (blue) or HA-mGPR84 (red) by treatment overnight with 100ng/ml doxycycline. Then 5000cells/well were plated in low-volume 384-well plates and pre-incubated with various concentrations of A) vehicle, B) compound 020, C) compound 140 and D) compound 837 for 15mins, followed by incubation with the EC_{80} concentration of 2-HTP for 15mins (EC_{80} calculated from **Figure 4.2**). Then 1 µM forskolin was added and incubated for 1h. The lowest concentration of compounds displayed on the X-axis is actually 0M (vehicle only). The output was measured with a PHERAstar FS plate reader (BMG Labtech). Data are presented as mean±SEM (n=3)

In order to further evaluate the ability of HA-hGPR84 expressed by the Flp-In TREx 293 stable cells to bind various antagonists, radioligand binding assays using [³H]140 were employed following the protocol published previously (Jenkins et al., 2021). Similar experiments on HA-mGPR84 Flp-In TREx 293 stable cells were not performed as compound 140 is not an antagonist for HA-mGPR84. Firstly, saturation binding assays were performed using membranes from HA-hGPR84 Flp-In TREx 293 cells. Membranes were incubated with increasing concentrations of [³H]140 in the presence or absence of 10μM unlabelled GPR84 antagonist compound 837 for 1h at 25°C. Fitting a one-site binding model to the specific binding curve, which was calculated as the difference between total binding and non-specific binding (i.e. that in the presence of compound 837) (**Figure 4.4**), generated K_d =0.96 nM and B_{max} =15.48pmol/mg membrane protein. The K_d is the binding affinity of [³H]140 to HA-hGPR84 and the B_{max} normally reflects the expression level of the receptor.
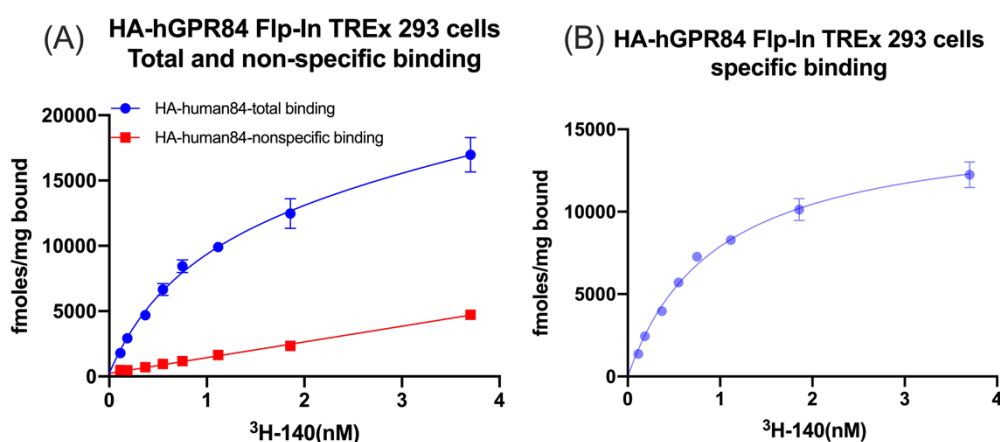
Figure 4.4 Characterization of [³H]140 binding to HA-hGPR84.
A) Membranes prepared from Flp-In T-REx 293 cells stably expressing HA-hGPR84 were incubated with a range of concentrations of [³H]140 for 1h at 25°C, in the absence or presence of 10μM compound 837 to define total and non-specific binding respectively. B) Specific binding of [³H]140 was calculated as the difference between total and non-specific binding. Specific binding with estimated K_d=0.96 nM and B_{max}=15.48 pmol/mg. The experiment was performed in triplicate. Data are from a single experiment (n=1).

Using this information (the affinity of [³H]140 to HA-hGPR84), the affinity of another, chemically distinct GPR84 antagonist, GLPG1205, was studied using competition binding assays because there is no available radioactively labelled

GLPG1205. 0.33nM [^{3}H]140 was incubated with increasing concentrations of unlabelled GLPG1205 (**Figure 4.5**). Binding of [^{3}H]140 to the HA-hGPR84 was competed fully and effectively by the antagonist GLPG1205. Fitting a one-site competition binding equation to the normalized data, the pKi of antagonist GLPG1205 was assessed as 8.1 which is similar to the published pKi=7.52 tested in a competitive radioligand binding assay using [^{3}H]38 at human GPR84 (Labéguère et al., 2020). Compound 140 was characterized as a competitive antagonist of human GPR84 when 2-HTP was used as the activator (Jenkins et al., 2021), and GLPG1205 was characterized as non-competitive blocker of PSB-16671 (Labéguère et al., 2020) and of 2-HTP (PhD thesis from Al Mahmud, Zobaer). This suggests that GLPG1205 binds to a further site that is distinct from that occupied by 2-HTP and PSB-16671 and also different from that occupied by compound 140.
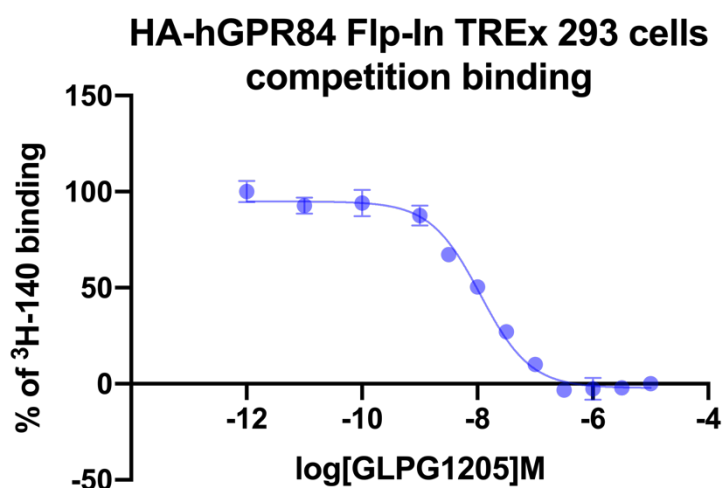
Figure 4.5 Characterization of the affinity of GLPG1205 to HA-hGPR84 using radioligand competition binding assay.
Membranes prepared from Flp-In T-REx 293 cells stably expressing HA-hGPR84 were incubated with 0.33nM [^{3}H]140 and different concentrations of antagonist GLPG1205 for 1h at 25°C. The lowest concentration of compounds displayed on the X-axis is actually 0M (vehicle only). Fitting a one-site competition binding equations to the normalized data gives a log Ki =-8.1 The experiment was performed in triplicate. Data are from a single experiment (n=1).

After this pharmacological characterization, HA-hGPR84 and HA-mGPR84 were characterized using two phosphosite-specific antisera and two GPR84 structural antisera (GPR84, 7TM and mouse ICL3 structural antibody) to understand whether phosphorylation patterns between human and mouse GPR84 are different. The structural antiserum GPR84 (7TM) is designed to recognize the C-terminal of hGPR84 and mouse ICL3 structural antibody is designed to identify the ICL3 of

mGPR84. These phosphosite-specific antibodies were originally characterized using cells expressing human GPR84-eYFP in a published paper and the protocol of using these antisera followed the methodology in that paper (Marsango et al., 2022). Firstly, Flp-In TREx 293 cells were induced to express HA-hGPR84 or HA-mGPR84. Cells were then treated with vehicle or an agonist for 5mins. Following treatment, the HA-tag within the receptor constructs was targeted with an anti-HA agarose trap to enrich the receptor. Samples were eluted by Laemmli buffer, separated on SDS-PAGE gels, and transferred to nitrocellulose membranes. Membranes were incubated with phosphosite-specific antisera, the structural antisera, or with an anti-HA control antibody at 4°C overnight. After washing, fluorescent secondary antibodies were used to visualise primary antisera.

The balanced orthosteric agonist 2-HTP, G_i-biased orthosteric agonist DL-175 and allosteric agonist PSB-16671 were used to treat HA-hGPR84 expressing Flp-In TREx 293 cells. The anti-HA antiserum that detects the HA-tag was used as a control for the expression of HA-hGPR84. After doxycycline induction of HA-hGPR84 Flp-In TREx 293 cells, the anti-HA antiserum recognized the receptor in both the presence and absence of different agonists (**Figure 4.6 A**). The pS221-pS224 GPR84 phosphorylation-site specific antiserum also detected the receptor with or without the presence of agonists (**Figure 4.6 B**), consistent with S221 and/or S224 of human GPR84 being constitutively phosphorylated (Marsango et al., 2022). By contrast, antiserum pT263-pT264, detected the receptor following activation by 2-HTP but did not recognize the receptor either basally or when activated by either the allosteric agonist PSB-16671 or G_i-biased orthosteric agonist DL-175 (**Figure 4.6 C**). It may thus be that phosphorylation of T263 and/or T264 may act as a sensor of GPR84 agonists capable of promoting interactions with arrestins because 2-HTP can promote the interaction between arrestins and GPR84 while DL-175 and PSB-16671 cannot, which is consistent to the results from a published work (Marsango et al., 2022). On this basis, 2-HTP and the phosphorylation-specific antiserum pT263-pT264 were selected for further characterization. In addition to receptor bands migrating between 50kDa and 75kDa, there were also visible bands at lower (37kDa-50kDa) and at higher (100kDa-150kDa) molecular mass sizes. As these bands were not present unless doxycycline had been used to promote expression of the receptor and the 37kDa-50kDa species were only detected by anti-HA and not the phospho-specific antisera, it is reasonable to

suggest these could represent immature receptor and the higher molecular mass bands could represent dimeric or aggregated forms of the receptor. The normalized intensities of receptor bands are displayed in **Figure 4.6**. However, It seems that the pS221-pS224 phosphorylation was increased by treatment with agonists **(Figure 4.6 A, B).** However, these quantification results are preliminary, and the experiment needs to be repeated for further statistical analysis.
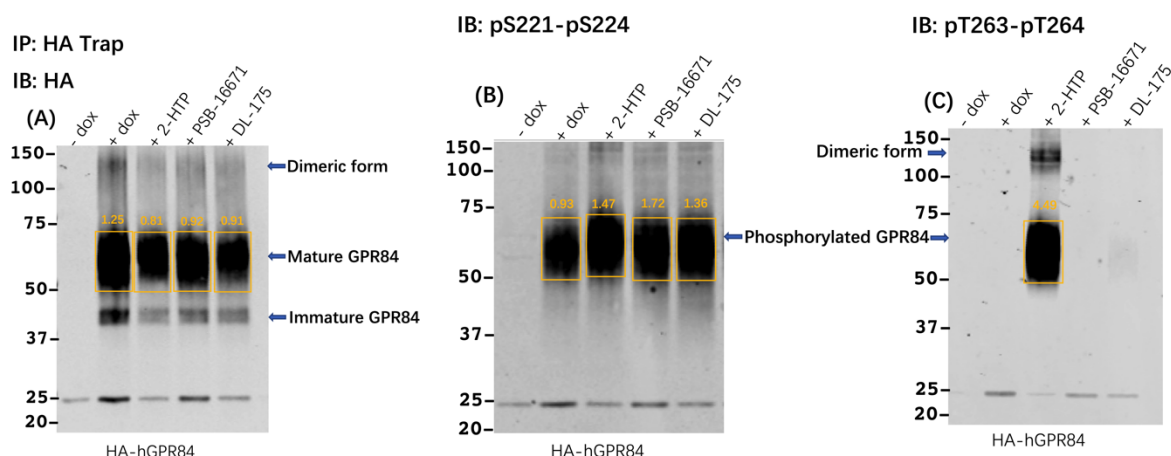
Figure 4.6 Antiserum pT263/pT264 only detects HA-hGPR84 after the activation by the balanced agonist 2-HTP.
Serum-starved Flp-In T-REx 293 stable cells without doxycycline induction or induced to express HA-hGPR84 were treated with vehicle or 5µM 2-HTP/ 13µM PSB-16671/ 98µM DL-175 for 5mins before cell lysis in the presence of protease and phosphatase inhibitors. Lysates were enriched with HA-trap agarose and run on NuPAGE 4-12% Bis-Tris SDSPAGE gels. Proteins were subsequently transferred to nitrocellulose membranes, blocked with TBS with 5% (w/v) BSA and incubated overnight with A) rat anti-HA primary antibody (1:10,000), B) rabbit anti-GPR84-pS221/pS224 (1:2,000) or C) rabbit anti-GPR84-pT263/pT264 (1:2,000). Membranes were finally incubated with goat anti-rat IRDye 800CW (1:10,000) or goat anti-rabbit IRDye 800CW (1:10,000) secondary antibodies, and visualised using the LI-COR Odyssey 9260 gel imaging system. Molecular mass of HA-hGPR84 is between 50-75 kDa. The normalized intensity = intensity of receptor (at 800nm)/ intensity of background (at 700nm). The figure is derived from a single experiment but shows similar outcomes as reported by Marsango et al. (2022).

As these studies identified a suitable phosphosite-specific antiserum and an agonist to promote phosphorylation at these sites, they were used alongside structural antisera (GPR84, from 7TM antibodies and mouse GPR84 ICL3 structural antiserum, generated in-house) to compare similarities and differences between HA-hGPR84 and HA-mGPR84. Although human and mouse GPR84 share over 85% similarity in sequence, there are still considerable differences that presumably lead to species selectivity in pharmacology and function. To determine the potential use of these antisera in *ex vivo* studies in the future, the species orthologue-specificity of the antisera was tested. The anti-HA antiserum detected the HA-tag and confirmed expression of both HA-hGPR84 and HA-mGPR84 (**Figure**

4.7 A, E). Although there are considerable differences between the ICL3 sequences of HA-hGPR84 and HA-mGPR84, the phosphosite-specific antiserum pT263-pT264 recognized the 2-HTP induced phosphorylation of both species (**Figure 4.7 B**). Indeed, alignment of the sequences of mouse and human GPR84 shows these residues to be present in both orthologues, and the residues next to these sites are the same (**Figure 4.1**). The structural antiserum from 7TM antibodies detected the expression of HA-human GPR84 but did not recognize the expression of HA-mGPR84 (**Figure 4.7 C**). This antiserum was designed to recognize the C-terminal tail of human GPR84 and the sequences of the C-terminal region between human and mouse GPR84 are different (**Figure 4.1**). The ICL3 mouse structural antiserum, which was generated against a GST-fusion protein of the peptide sequence of the ICL3 loop of mouse GPR84, recognized both HA-hGPR84 and HA-mGPR84 (**Figure 4.7 D, F**). It is possible that this reflects the antiserum generated using a long polypeptide as the antigen contains a range of different various antibodies including some that identify sequences common or similar between the human and mouse orthologues. Therefore, the polyclonal antibodies could detect HA-hGPR84 even though the ICL3 sequences between human and mouse GPR84 are different in a number of regions. The normalized intensities of receptor bands are displayed in **Figure 4.7**. By normalizing the intensities using structural antisera **(Figure 4.7 C, D, F)** to the intensities using anti-HA antiserum **(Figure 4.7 A, E)**, it suggests that treatment with 2-HTP probably causes conformational changes in the C-terminal and ICL3 of GPR84.

However, whether these changes are observed consistently would require further investigation.
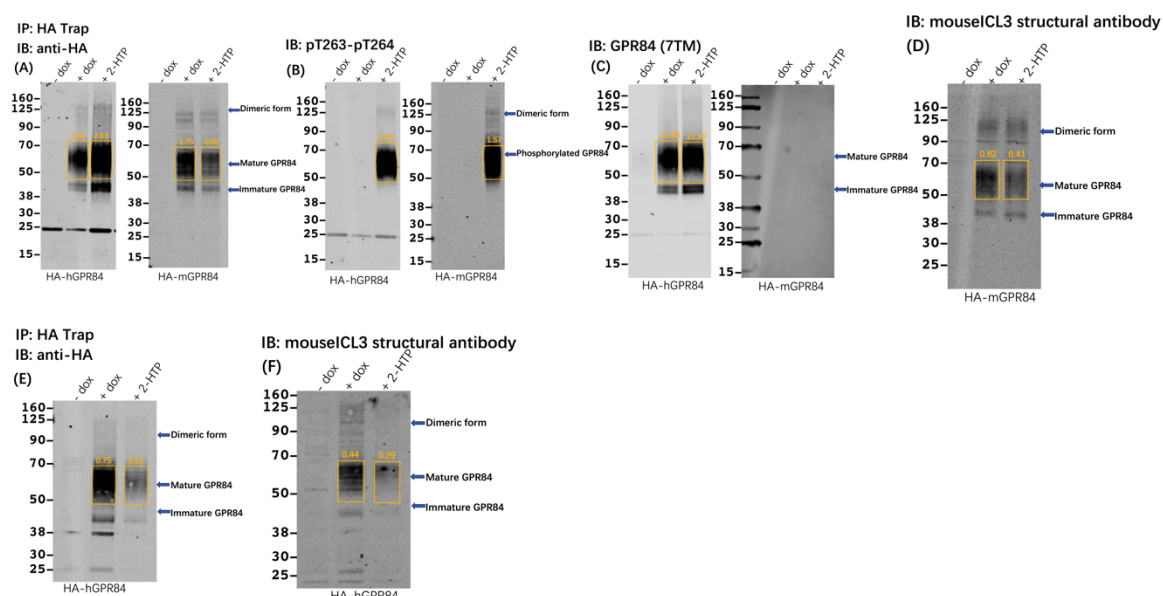
Figure 4.7 Antiserum pT263-pT264 detects the phosphorylation of HA-hGPR84 and HA-mGPR84 in a 2-HTP-depedent manner, while the detection of structural antiserum is species-dependent.

Serum-starved Flp-In T-REx 293 stable cells without doxycycline induction or induced to express HA-hGPR84 or HA-mGPR84 were treated with vehicle or 5μM 2-HTP for 5mins before cell lysis in the presence of protease and phosphatase inhibitors. Lysates were enriched with HA-trap agarose and run on NuPAGE 4-12% Bis-Tris SDSPAGE gels. Proteins were subsequently transferred to nitrocellulose membranes, blocked with TBS supplemented with 5% (w/v) BSA and incubated overnight with A, E) rat anti-HA primary antibody (1:10,000), B) rabbit anti-GPR84-pT263/pT264 (1:2,000), C) rabbit anti-GPR84(7TM) (1:2,000) or D, F) rabbit anti-mouse ICL3 structural antiserum (1:2000). Membranes were finally incubated with goat anti-rat IRDye 800CW (1:10,000) or goat anti-rabbit IRDye 800CW (1:10,000) secondary antibodies, and visualised using the LI-COR Odyssey 9260 gel imaging system. The normalized intensity = intensity of receptor (at 800nm)/ intensity of background (at 700nm). The figure is derived from a single experiment but the blots of HA-hGPR84 shows similar outcomes as reported by Marsango et al. (2022)

To further study whether the phosphorylation of HA-hGPR84 at residues T263-T264 could be affected by antagonists, compound GLPG1205, compound 020 and compound 837 were used in immunoblotting studies. Similar experiments on HA-mGPR84 Flp-In TREx 293 stable cells were not performed because, as I demonstrated earlier, these antagonists are human GPR84 species selective. Flp-In TREx 293 cells were induced to stably express HA-hGPR84 before incubation with 10μM compound GLPG1205/compound 020/compound 837 for 15mins. Then 5μM 2-HTP was added to cells for 5mins. Samples were prepared following the immunoblotting protocol mentioned above. The anti-HA antiserum recognized the expression of HA-hGPR84 after doxycycline induction in the presence or absence of the agonists and antagonists (**Figure 4.8 A, C**). With the treatment of antagonists, the phosphosite-sepecific antiserum pT263/pT264 failed to identify the phosphorylation of HA-hGPR84 (**Figure 4.8 B, D**), consistent with T263 and/or

T264 of human GPR84 being phosphorylated in an agonist-dependent way (Marsango et al., 2022). However, treatment with antagonist GLPG1205 or compound 020 did not obviously affect the structure of ICL3 as the mouse ICL3 structural antiserum still recognized the receptor (**Figure 4.8 E**). Although several blots (**Figure 4.8 C, D, E**) displayed some unusual binding patterns, it is likely to be non-specific interactions because these bands were also present even when Flp-In TREx 293 cells were not induced to express HA-hGPR84. The normalized intensities of receptor bands are displayed in **Figure 4.8**. It appears that treatment with 2-HTP or an antagonist affected the recognition of anti-HA and mouse ICL3 antiserum. Since these quantification results are preliminary, further investigation will be needed to confirm whether this is a consistent observation.
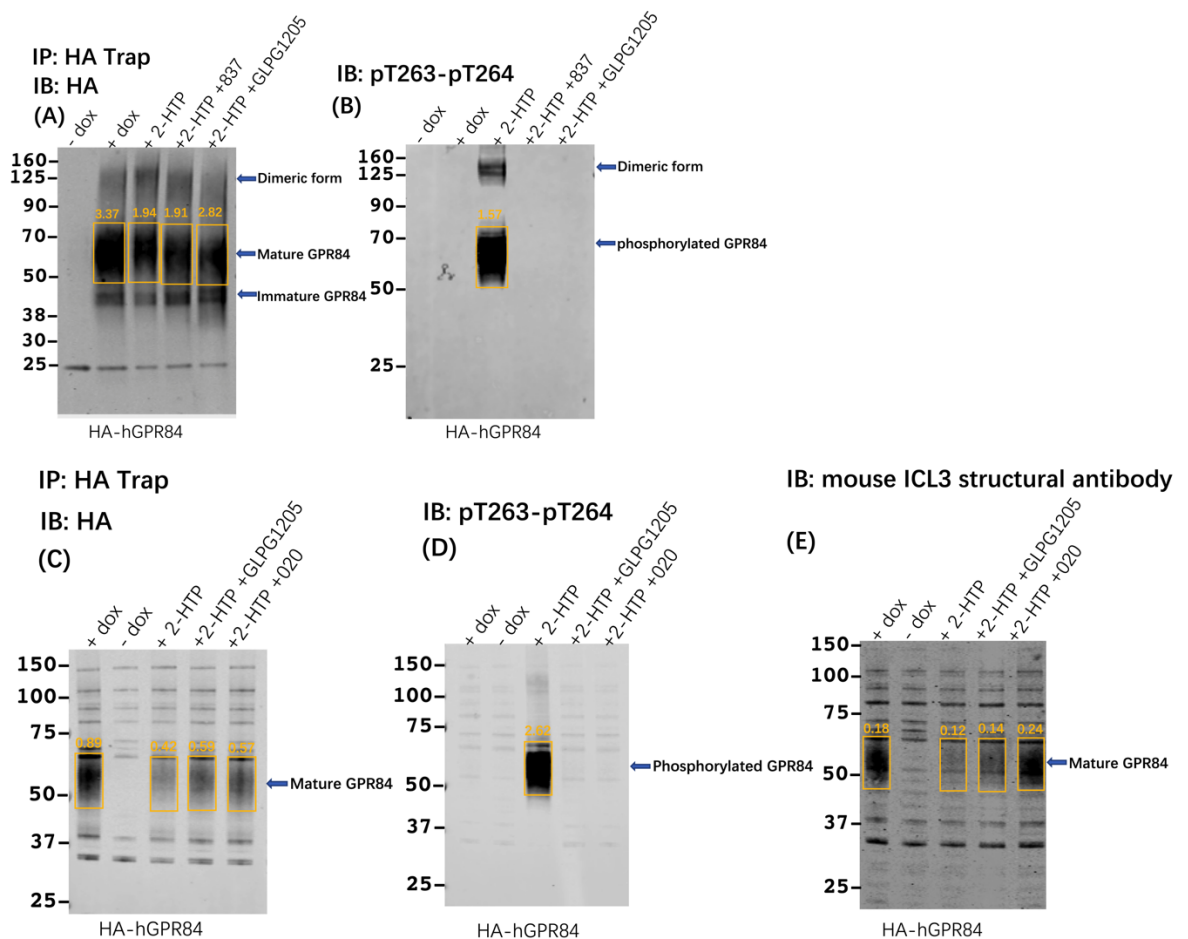
Figure 4.8 GPR84 antagonists inhibit the phosphorylation of HA-hGPR84 at pT263/pT264 without affecting the structure of ICL3.
Serum-starved Flp-In T-REx 293 stable cells without doxycycline induction or induced to express HA-hGPR84 were pre-treated with compound GLPG1205/compound 020/compound 837 for 15mins before adding vehicle or 5µM 2-HTP for 5mins. Then cell lysis was applied in the presence of protease and phosphatase inhibitors. Lysates were enriched with HA-trap agarose and run on NuPAGE 4-12% Bis-Tris SDSPAGE gels. Proteins were subsequently transferred to nitrocellulose membranes, blocked with TBS supplemented with 5% (w/v) BSA and incubated overnight with A,

C) rat anti-HA primary antibody (1:10,000), B, D) rabbit anti-GPR84-pT263/pT264 (1:2,000) or E) rabbit anti-mouseICL3 structural antiserum (1:2000). Membranes were finally incubated with goat anti-rat IRDye 800CW (1:10,000) or goat anti-rabbit IRDye 800CW (1:10,000) secondary antibodies, and visualised using the LI-COR Odyssey 9260 gel imaging system. The normalized intensity = intensity of receptor (at 800nm)/ intensity of background (at 700nm). Representative of 2 blots (n=2 of phosphosite-specific antiserums, and n=1 of structural antiserum).

In order to study whether GRK2 and/or GRK3 were important to the phosphorylation of T263 and/or T264 sites of HA-hGPR84, the GRK2/3 inhibitor compound 101 was used alongside the phosphosite-specific antiserum pT263-pT264. After doxycycline induction of HA-hGPR84 Flp-In TREx 293 cells, cells were pre-incubated with 10µM compound 101 for 30mins before being treated with 5µM 2-HTP for 5mins. The anti-HA antiserum recognized HA-hGPR84 in both the presence and absence of compound 101 after doxycycline induction, but the phosphorylation-specific antiserum pT263-pT264 failed to identify the phosphorylation of HA-hGPR84 after compound 101 treatment (**Figure 4.9**). Therefore, GRK2 and/or GRK3 appear to be essential for the phosphorylation of HA-hGPR84 at T263 and/or T264 sites. Further studies are needed to confirm which individual GRK (GRK2 or GRK3) is necessary to promote phosphorylation of human GPR84. The normalized intensities of receptor bands are displayed in **Figure 4.9**. However, the quantification data might be unreliable since the band of doxycycline induction is unusual (**Figure 4.9 A**). Repeated experiments are needed for further statistical analysis.
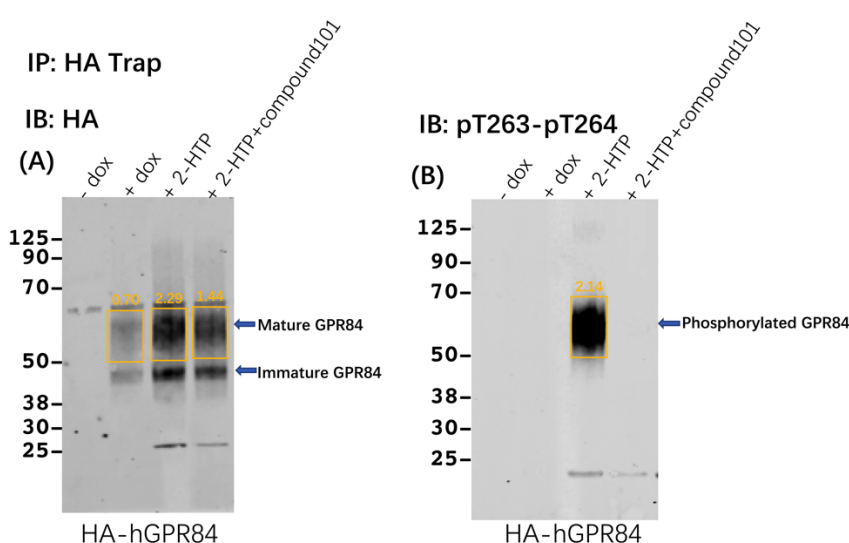
Figure 4.9 Compound 101 blocks phosphorylation at Thr263 and/or Thr264 of HA-hGPR84. Serum-starved Flp-In T-REx 293 stable cells without doxycycline induction or induced to express HA-hGPR84 were treated with vehicle or 10µM compound 101 for 30mins before being treated with vehicle (+dox) or 5µM 2-HTP for 5mins. Then cells were lysed with the presence of protease and

phosphatase inhibitors. Lysates were enriched with HA-trap agarose and run on NuPAGE 4-12% Bis-Tris SDSPAGE gels. Proteins were subsequently transferred to nitrocellulose membranes, blocked with TBS with 5% (w/v) BSA and incubated overnight with A) rat anti-HA primary antibody (1:10,000), B) rabbit anti-GPR84-pT263/pT264 (1:2,000). Membranes were finally incubated with goat anti- IRDye 800CW (1:10,000) or goat anti-rabbit IRDye 800CW (1:10,000) secondary antibodies for 1h. The membranes were scanned using the LI-COR Odyssey 9260 gel imaging system. The figure is derived from a single experiment but shows similar outcomes as reported by Marsango et al. (2022)

4.2.2 Characterization of stable cell lines expressing HA-humanised GPR84

As mentioned in *section 4.1*, the reason for generating the HA-humanised GPR84 (HA-hmGPR84) construct was potentially to produce a transgenic mouse line which has similar pharmacology and functions as human GPR84. In order to compare similarities and differences between the HA-hGPR84, HA-mGPR84 and HA-hmGPR84 constructs, characterization of Flp-In T-REx 293 cells stably expressing HA-hmGPR84 was undertaken using the same methods as described in *section 4.2.1*. Initially, the potency of different agonists to activate Flp-In T-REx 293 cell lines stably expressing HA-hmGPR84 was explored using cAMP assays. 2-HTP, 6-OAU, DL-175 and PSB-16671 were used to activate the receptor separately, and non-linear regression curves were fitted to these data (**Figure 4.10**). The pEC_{50} of these agonists at HA-hmGPR84 is listed in 错误!未找到引用源。**Table 4-2** along with the pEC_{50} of these agonists at HA-hGPR84 and HA-mGPR84 for comparison. It was found that the potency of these agonists at HA-hmGPR84 and HA-hGPR84 were not significantly different, but the potency of 6-OAU and DL-175 at HA-hmGPR84 were significantly different from that at HA-mGPR84 ($p < 0.05$).
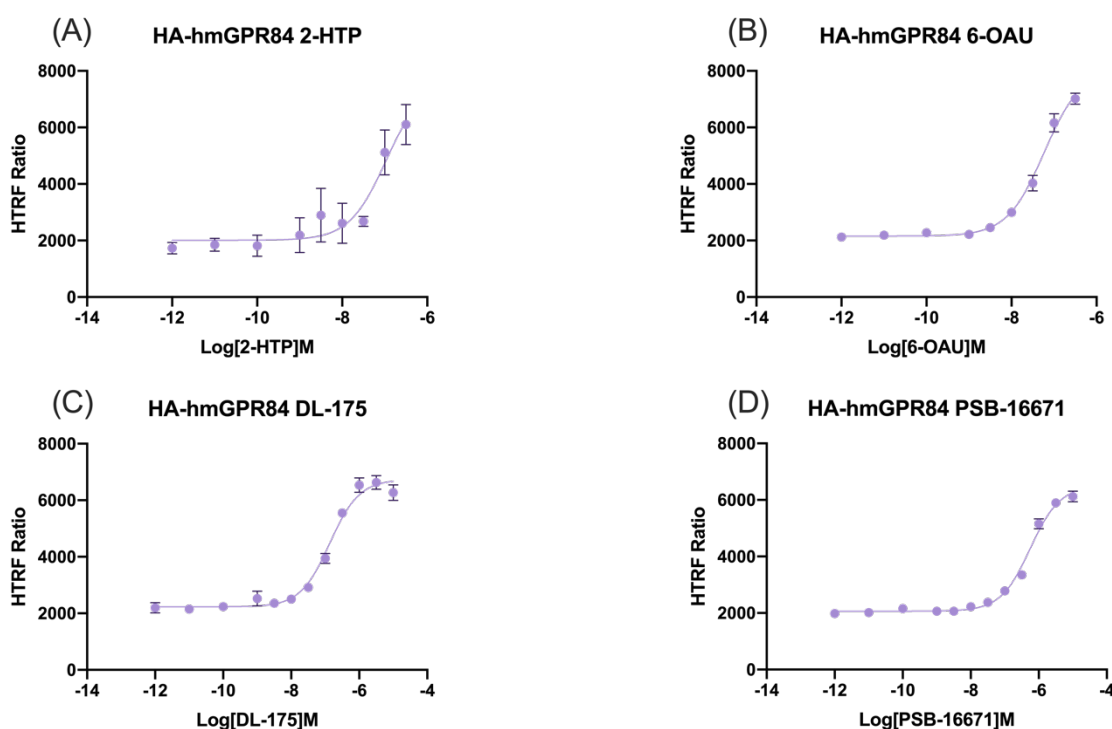
Figure 4.10 GPR84 agonists regulate cAMP levels of HA-hmGPR84
Flp-In TREx 293 cells were induced to stably express HA-hmGPR84 by treatment overnight with 100ng/ml doxycycline. Then 5000cells/well were plated in low-volume 384-well plates followed by incubation with various concentrations of A) 2-HTP, B) 6-OAU, C) DL-175 and D) PSB-16671 for 15mins. Subsequently, 1 μM forskolin was added and cells further incubated for 1h. The lowest concentration of compounds displayed on the X-axis is actually 0M (vehicle only)Output was measured with a PHERAstar FS plate reader (BMG Labtech).Data presented as mean±SEM (n=3).

Table 4-2 Potency of different agonists at HA-hmGPR84, HA-hGPR74 and HA-mGPR84 in cAMP assays.

	HA-hGPR84 (pEC_{50} ± SEM)	HA-mGPR84 (pEC_{50} ± SEM)	HA-hmGPR84 (pEC_{50} ± SEM)
2-HTP	8.36±0.02	8.59±0.23	8.04±0.57
6-OAU	7.16±0.06	7.63 ±0.06**	7.28±0.05*
DL-175	6.56±0.10	7.35±0.13**	6.76±0.10*
PSB-16671	6.10±0.18	6.58±0.07	6.51±0.13

Values were calculated from the ratio of raw data. Data presented as mean±SEM (n=3). The data was analyzed by one-way ANOVA with Tukey's post-hoc multiple comparisons test. **$p<0.01$ against HA-hGPR84, * $p<0.05$ against HA-mGPR84

To compare the differences of E_{max} among HA-hGPR84, HA-mGPR84 and HA-hmGPR84, the concentration-response curves from **Figure 4.2** and **Figure 4.10** were superimposed (**Figure 4.11**). The baseline for each cell line was removed to facilitate a more straightforward and intuitive comparison of E_{max}.
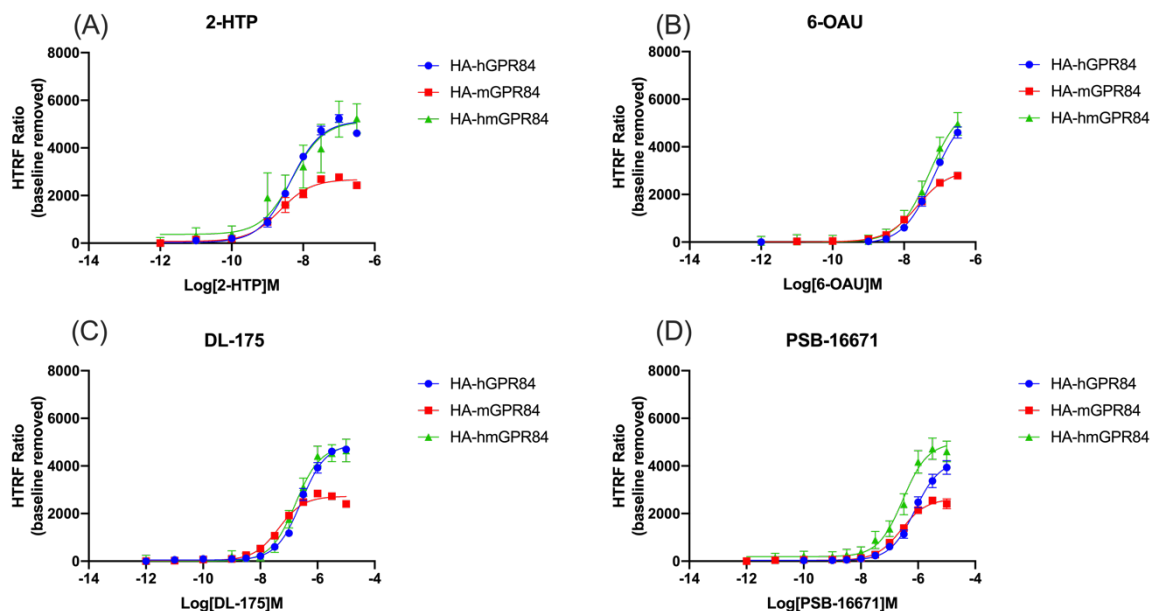
Figure 4.11 The E_{max} of HA-hGPR84 and HA-hmGPR84 are similar and higher than that of HA-mGPR84.
Flp-In TREx 293 cells were induced to stably express HA-hGPR84, HA-mGPR84 or HA-hmGPR84 by treatment overnight with 100ng/ml doxycycline. Then 5000cells/well were plated in low-volume 384-well plates followed by incubation with various concentrations of A) 2-HTP, B) 6-OAU, C) DL-175 and D) PSB-16671 for 15mins. Subsequently, 1 μM forskolin was added and cells further incubated for 1h. The lowest concentration of compounds displayed on the X-axis is actually 0M (vehicle only). Output was measured with a PHERAstar FS plate reader (BMG Labtech). The baseline for each cell line was removed. Data presented as mean±SEM (n=3).

Following this, the affinity of different antagonists to block 2-HTP-induced regulation of cAMP was explored by using antagonists compound 020 (**Figure 4.12 B**), compound 140 (**Figure 4.12 C**) and compound 837 (**Figure 4.12 D**) in the cAMP assay in order to evaluate whether human species-selective GPR84 antagonists can block HA-hmGPR84 . The results using various concentrations of 2-HTP was consistent with the results in **Figure 4.10**, which can be seen as a positive control of the antagonists inhibition assay (**Figure 4.12 A**). Compound 020, compound 140 and compound 837 each blocked the activation of HA-hmGPR84 induced by 2-HTP (**Figure 4.12 B, C, D**). The pIC$_{50}$ of the different antagonists at HA-hmGPR84 and HA-hGPR84 is listed in **Table 4-3**. It is encouraging to see that human GPR84

species selective antagonists blocked the activation of HA-hmGPR84 with similar pIC_{50} as HA-hGPR84.
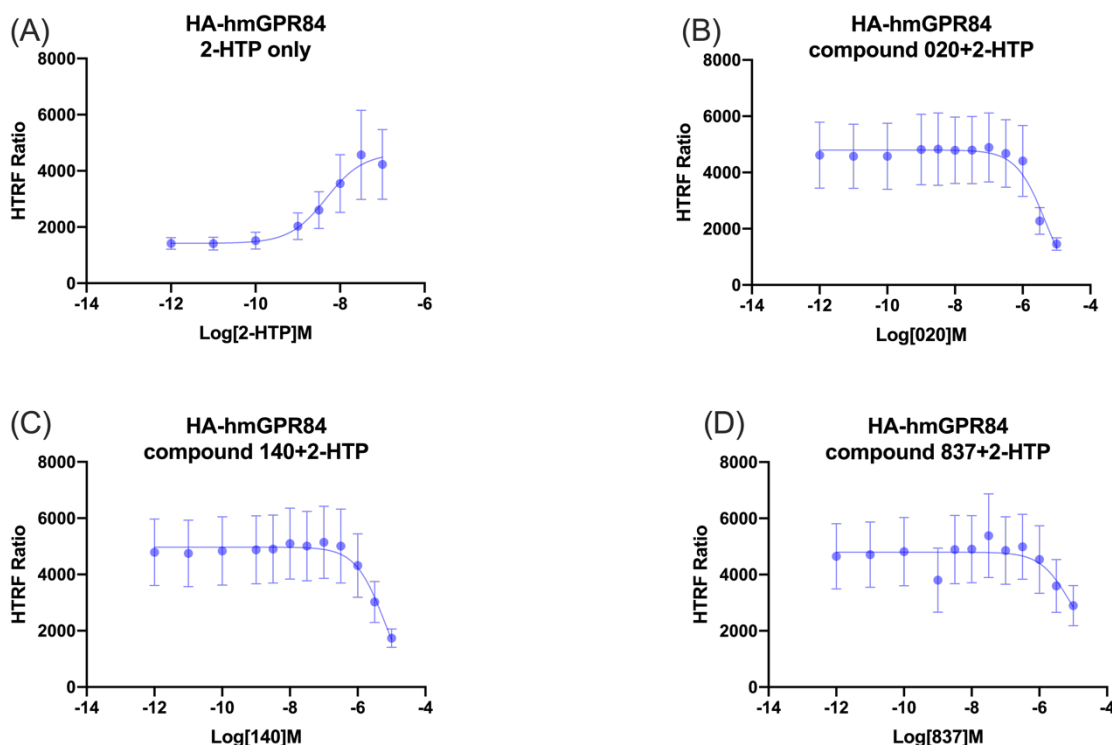
Figure 4.12 Human species-selective GPR84 antagonists affect the 2-HTP-regulated cAMP levels at HA-hmGPR84.
Flp-In TREx 293 cells were induced to stably express HA-hmGPR84 by treatment overnight with 100ng/ml doxycycline. Then 5000cells/well were plated in low-volume 384-well plates following the pre-incubated with various concentrations of A) vehicle, B) compound 020, C) compound 140 and D) compound 837 for 15mins, followed by incubation with the EC80 concentration of 2-HTP (EC80 calculated from **Figure 4.10**) for 15mins. Then 1 μM forskolin was added and incubated for 1h. The lowest concentration of compounds displayed on the X-axis is actually 0M (vehicle only). The output was measured with a PHERAstar FS plate reader (BMG Labtech). Data are presented as mean±range (n=2).

Table 4-3 pIC_{50} of antagonists at HA-hmGPR84 and HA-hGPR84 in cAMP assays.

	HA-hGPR84 (pIC_{50} ± SEM)	HA-hmGPR84 (pIC_{50} ± range)
Compound 020	5.86±0.20	5.45±0.19
Compound 140	5.75±0.23	5.32±0.19
Compound 837	6.57±0.75	5.30±0.14

Values were calculated from the ratio of raw data. Two-tailed p-values in t-test is greater than 0.05.

To compare the ability of HA-hmGPR84 and HA-hGPR84 to bind various antagonists, radioligand binding assays using [^{3}H]140 were employed following the protocol used for HA-hGPR84. Firstly, a saturation binding assay was employed, and data fitted to a one-site binding model. The specific binding curve which was again defined as the difference between total binding and nonspecific binding (i.e. that in the presence of compound 837) generated a K_d =1.04 nM and a B_{max} =8.79 pmol/mg (**Figure 4.13**). Comparison between the K_d of [^{3}H]140 at HA-hmGPR84 and HA-hGPR84 shows that the affinity of these two receptors to bind [^{3}H]140 is very similar. However, the B_{max} at HA-hmGPR84 was about half of the B_{max} at HA-hGPR84. Considering the maximum response of HA-hmGPR84 activated by various agonists was similar to that of HA-hGPR84 **(Figure 4.11)**, it would be reasonable to predict that the sequences in intracellular areas affect the signalling response to compounds.
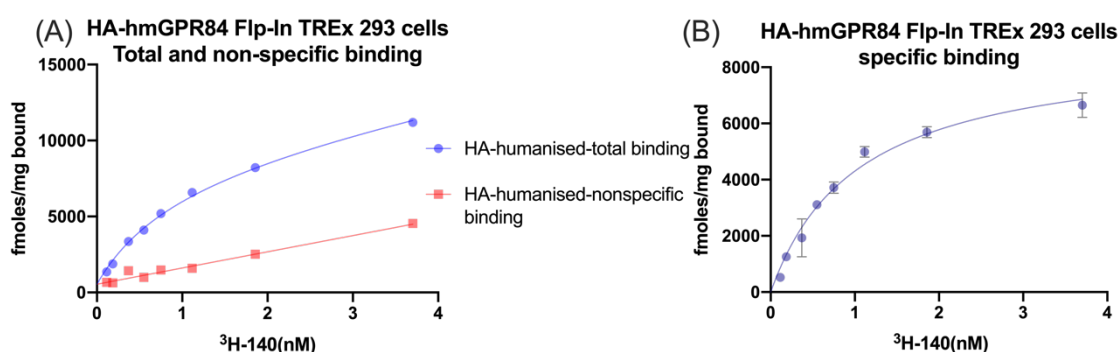
Figure 4.13 Characterization of [^{3}H]140 binding to HA-hmGPR84.
A) Membranes prepared from Flp-In T-REx 293 cells stably expressing HA-hmGPR84 were incubated with a range of concentrations of [^{3}H]140 for 1h at 25°C, in the absence or presence of 10μM compound 837 to define total and non-specific binding respectively. B) Specific binding of [^{3}H]140 was calculated as the difference between total and non-specific binding. Specific binding with estimated K_d=1.04 nM and B_{max}=8.79 pmol/mg (n=1).

Based on previous information (the affinity of [^{3}H]140 to HA-hmGPR84), the affinity of antagonist GLPG1205 to bind to HA-hmGPR84 was studied using competition radioligand binding assays. 0.33nM [^{3}H]140 was incubated with increasing concentrations of the unlabelled antagonist GLPG1205 (**Figure 4.14**). Binding of [^{3}H]140 to the HA-hmGPR84 was competed fully and effectively by the antagonist GLPG1205. Fitting a one-site competition binding equation to the normalized data, the pK_i of antagonist GLPG1205 assessed as 8.2, which was similar to that for HA-hGPR84. Based on these results, it is encouraging to find

that the ability of chimeric construct HA-hmGPR84 to bind agonists and antagonists was very similar to HA-hGPR84.
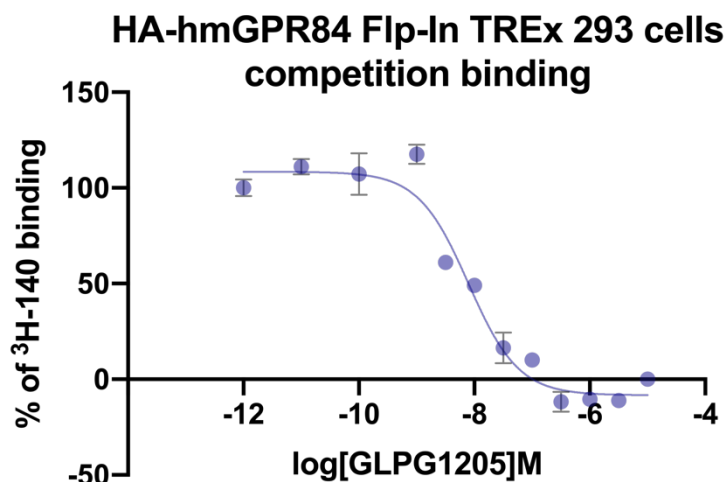
Figure 4.14 Characterization of the affinity of GLPG1205 for HA-hmGPR84 using a radioligand competition binding assay.
Membranes prepared from Flp-In T-REx 293 cells stably expressing HA-hmGPR84 were incubated with 0.33nM [^{3}H]140 and different concentrations of antagonist GLPG1205 for 1h at 25°C. The lowest concentration of compounds displayed on the X-axis is actually 0M (vehicle only). Fitting a one-site competition binding equations to the normalized data gives a logKi =-8.2 (n=1, 3 repeated wells in one experiment).

As mentioned, the longer term plan was to generate a transgenic mouse line expressing HA-hmGPR84 if the HA-hmGPR84 construct displayed similar pharmacology and function as the wild type human receptor. Thus, characterization using the two phosphosite-specific antisera and two GPR84 structural antisera at HA-hmGPR84 was used to predict outcomes in *ex vivo* studies using such a mouse line. The protocol of using these antisera at HA-hmGPR84 was the same for HA-hGPR84 and HA-mGPR84. Firstly, the effect of agonists on HA-hmGPR84 phosphorylation was studied using the ligands 2-HTP, DL-175 and PSB-16671. The anti-HA antiserum detected HA-tag was used as a control for the expression of HA-hmGPR84. After doxycycline induction of HA-hmGPR84 Flp-In TREx 293 cells, the anti-HA antiserum recognized the receptor in both the presence and absence of the different agonists (**Figure 4.15 A**). It was surprisingly found that phosphorylation antiserum pS221-pS224 only detected this receptor construct following treatment with 2-HTP (**Figure 4.15 B**). However, antiserum pT263-pT264, also only detected this receptor construct following activation by the balanced agonist 2-HTP (**Figure 4.15 C**). Although amino acids S221 and S224

exist in both HA-hGPR84 and HA-hmGPR84, the amino acids next to site S221 at HA-hmGPR84 are different from the amino acids at HA-hGPR84, which might be the reason that antiserum pS221-pS224 detected the phosphorylation of HA-hmGPR84 in a 2-HTP dependent way. However, it appears that recognition by pS221-pS224 antiserum was not as effective as when using the pT263-pT264 antiserum. In addition to receptor bands migrating between 50kDa and 75kDa, there were also visible bands at lower (37kDa-50kDa) and at higher (100kDa-150kDa) molecular mass sizes. As these bands were not present unless doxycycline had been used to promote expression of the receptor and the 37kDa-50kDa species were only detected by anti-HA and not the phospho-specific antisera, it is reasonable to suggest these could represent immature receptor and the higher molecular mass bands could represent dimeric or aggregated forms. The normalized intensities of receptor bands are displayed, and repeated experiments are required for further statistical analysis.
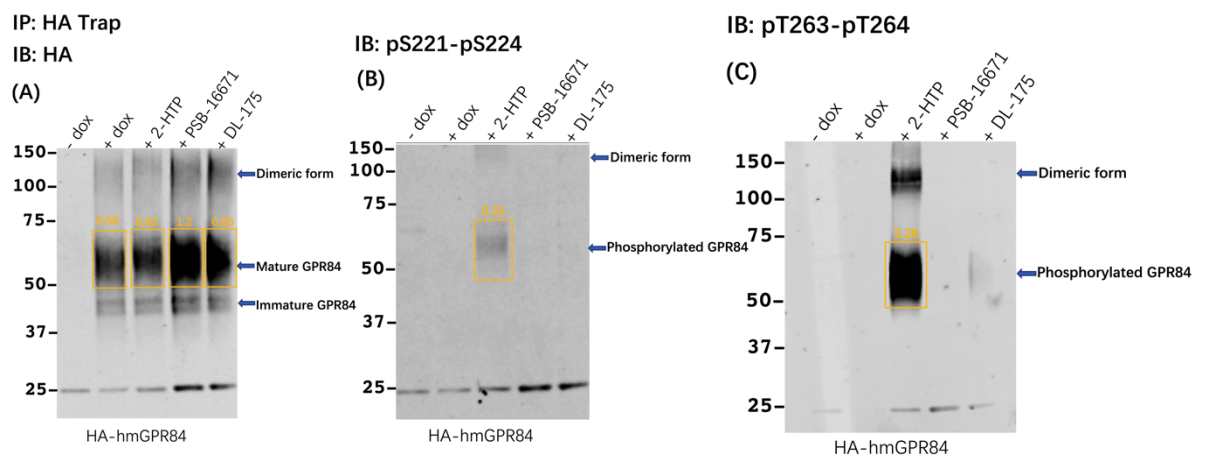
Figure 4.15 Antisera pT263/pT264 and pS221/pS224 only detects HA-hmGPR84 after the activation by the balanced agonist 2-HTP.
Serum-starved Flp-In T-REx 293 stable cells without doxycycline induction or induced to express HA-hmGPR84 were treated with vehicle or 5μM 2-HTP/ 13μM PSB-16671/ 98μM DL-175 for 5mins before cell lysis in the presence of protease and phosphatase inhibitors. Lysates were enriched with HA-trap agarose and run on NuPAGE 4-12% Bis-Tris SDSPAGE gels. Proteins were subsequently transferred to nitrocellulose membranes, blocked with TBS with 5% (w/v) BSA and incubated overnight with A) rat anti-HA primary antibody (1:10,000), B) rabbit anti-GPR84-pS221/pS224 (1:2,000) or C) rabbit anti-GPR84-pT263/pT264 (1:2,000). Molecular mass of HA-hmGPR84 is between 50-75 kDa. The normalized intensity = intensity of receptor (at 800nm)/ intensity of background (at 700nm). The figure is derived from a single experiment.

As these results identified a suitable phosphosite-specific antiserum and an agonist to promote phosphorylation at these sites of HA-hmGPR84, the structural antiserum GPR84 (7TM) and mouse ICL3 structural antiserum were characterized

in order to find a reagent that could identify the presence of HA-hmGPR84 in longer term *ex vivo* studies. The anti-HA antiserum still detected the HA-tag and confirmed expression of HA-hmGPR84 (**Figure 4.16 A, E**). The phosphosite-specific antisera pS221-pS224 and antiserum pT263-pT264 both recognized the phosphorylation of HA-hmGPR84 promoted by 2-HTP, but antiserum pT263-pT264 identified the receptor phosphorylation better than antisera pS221-pS224 (**Figure 4.16 B, C**), which was consistent with the results above. Structural antiserum GPR84 (7TM) failed to detect the expression of HA-hmGPR84 but the mouse ICL3 structural antiserum did recognize the existence of HA-hmGPR84 (**Figure 4.16 D, F**), which was anticipated because the intracellular regions of HA-hmGPR84 and HA-mGPR84 are the same. The normalized intensities of receptor bands are displayed. It seems that treatment with 2-HTP affected the recognition of anti-HA and mouse ICL3 antiserum although the data in panel A of **Figure 4.16** does not really support this hypothesis.
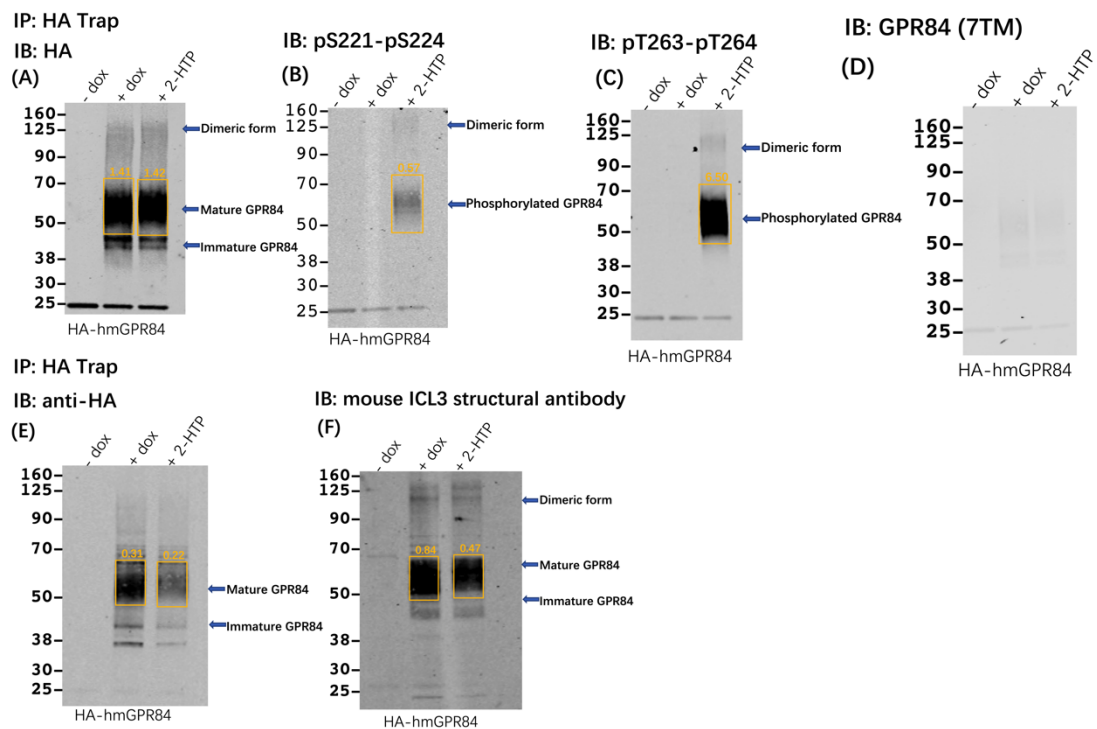
Figure 4.16 Characterization of structural antisera to detect HA-hmGPR84.
Serum-starved Flp-In T-REx 293 stable cells without doxycycline induction or induced to express HA-hmGPR84 were treated with vehicle or 5µM 2-HTP for 5mins before cell lysis in the presence of protease and phosphatase inhibitors. Lysates were enriched with HA-trap agarose and run on NuPAGE 4-12% Bis-Tris SDSPAGE gels. Proteins were subsequently transferred to nitrocellulose membranes, blocked with TBS supplemented with 5% (w/v) BSA and incubated overnight with A, E) rat anti-HA primary antibody (1:10,000), B) rabbit anti-GPR84-pS221/pS224 (1:2,000), C) rabbit anti-GPR84-pT263/pT264 (1:2,000), D) rabbit anti-GPR84(7TM) (1:2,000) or F) rabbit anti-mouse ICL3 structural antiserum (1:2000). Membranes were finally incubated with goat anti-rat IRDye 800CW (1:10,000) or goat anti-rabbit IRDye 800CW (1:10,000) secondary antibodies, and visualised

using the LI-COR Odyssey 9260 gel imaging system. The normalized intensity = intensity of receptor (at 800nm)/ intensity of background (at 700nm). Representative of 2 blots (n=2).

To further study whether human GPR84 species selective antagonists could block the phosphorylation of HA-hmGPR84, immunoblotting using both phosphosite-sepecific antisera and the mouse ICL3 structural antiserum was applied. Antagonists GLPG1205, compound 020 and compound 837 were used to potentially block the activation of HA-hmGPR84 promoted by 2-HTP. The samples were prepared following the same immunoblotting protocol as used on HA-hGPR84. Anti-HA antibody detected the expression of HA-hmGPR84 after doxycycline induction no matter whether cells were treated with agonists or antagonists (**Figure 4.17 A, D**). After the treatment with antagonists, antiserum pS221/pS224 and pT263/pT264 failed to identify the phosphorylation of HA-hmGPR84 (**Figure 4.17 B, C, E**), which means that the phosphorylation of HA-hmGPR84 at sites S221 and/or S224 as well as sites T263 and/or T264 can be inhibited by human GPR84 species selective antagonists. Also, the treatment of antagonist GLPG1205 or compound020 did not obviously affect the structure of ICL3 as the mouseICL3 structural antiserum still recognized the receptor (**Figure 4.17 F**). Although several blots (**Figure 4.17 D, E, F**) using antagonists displayed some unusual binding patterns, these are likely non-specific interactions because these bands were also present when Flp-In TREx 293 cells were not induced to express HA-hmGPR84. The normalized intensities of receptor bands are displayed, and repeated experiments are required for further statistical analysis.
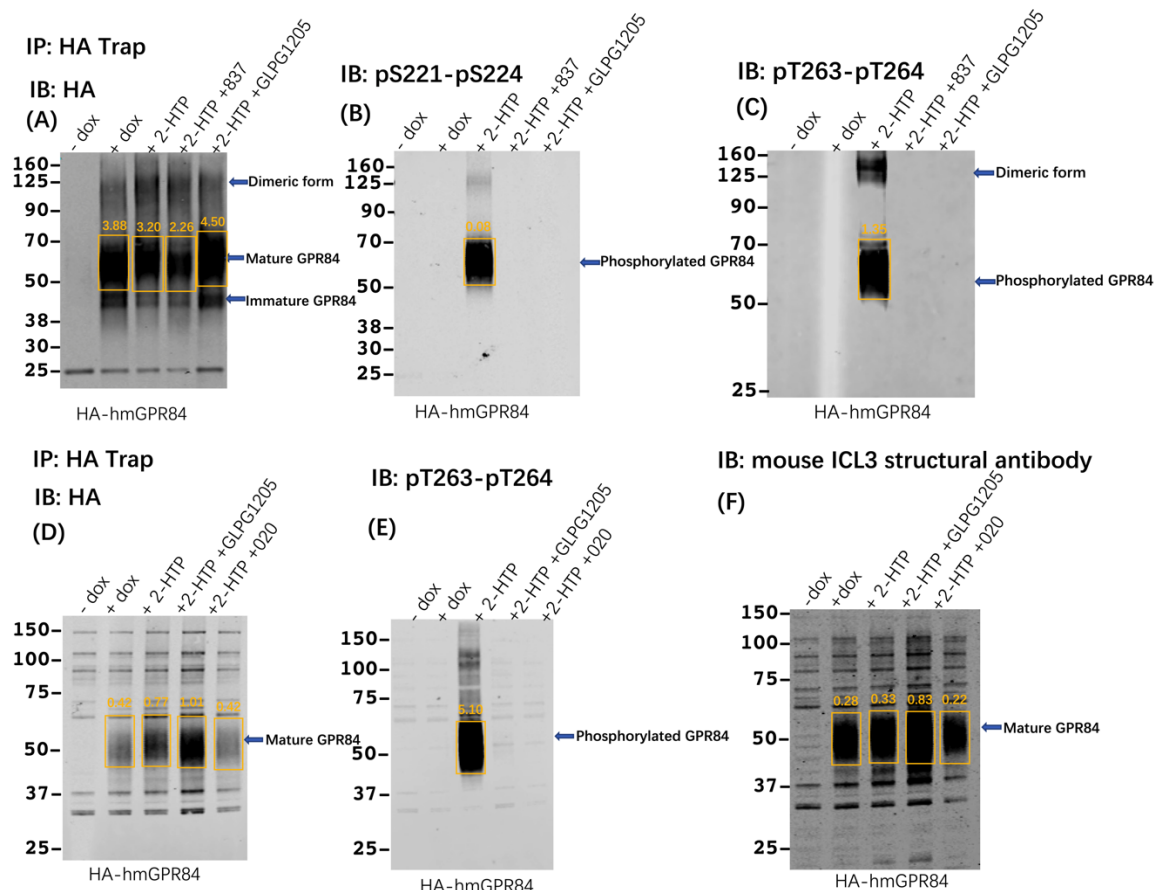
**Figure 4.17 The treatment of GPR84 antagonists block the phosphorylation of HA-hmGPR84 at sites 221/224 and 263/264 without affecting the structure of ICL3**

Serum-starved Flp-In T-REx 293 stable cells without doxycycline induction or induced to express HA-hmGPR84 were pre-treated with antagonist GLPG1205/compound 020/compound 837 for 15mins before adding vehicle or 5µM 2-HTP for 5mins. Then cell lysis was applied in the presence of protease and phosphatase inhibitors. Lysates were enriched with HA-trap agarose and run on NuPAGE 4-12% Bis-Tris SDSPAGE gels. Proteins were subsequently transferred to nitrocellulose membranes, blocked with TBS supplemented with 5% (w/v) BSA and incubated overnight with A, D) rat anti-HA primary antibody (1:10,000), B) rabbit anti-GPR84-pS221/pS224 (1:2,000), C, E) rabbit anti-GPR84-pT263/pT264 (1:2,000) or F) rabbit anti-mouseICL3 structural antiserum (1:2000). Membranes were finally incubated with goat anti-rat IRDye 800CW (1:10,000) or goat anti-rabbit IRDye 800CW (1:10,000) secondary antibodies, and visualised using the LI-COR Odyssey 9260 gel imaging system. The normalized intensity = intensity of receptor (at 800nm)/ intensity of background (at 700nm). Representative of 2 blots (n=2 of phosphosite-specific antiserums, and n=1 of structural antiserum)

Previous chapters showed that the pharmacology of HA-hmGPR84 is similar to the pharmacology of HA-hGPR84, so whether GRK2/3 are responsible for the phosphorylation of HA-hmGPR84 was studied. Flp-In T-REx 293 stable cells induced to express HA-hmGPR84 were preincubated with 10µM compound 101 for 30mins before treated with 5µM 2-HTP for 5mins. The immunoblotting results showed that compound 101 blocked the phosphorylation of HA-hmGPR84 at T263 and/or T264 sites induced by 2-HTP (**Figure 4.18**), which further confirmed that the pharmacology of HA-hmGPR84 and HA-hGPR84 is very similar. The normalized

intensities of receptor bands are displayed which suggests that treatment of compound 101 reduced the recognition of anti-HA antiserum **(Figure 4.18 A)**. However, whether these changes are observed consistently would require further investigation.
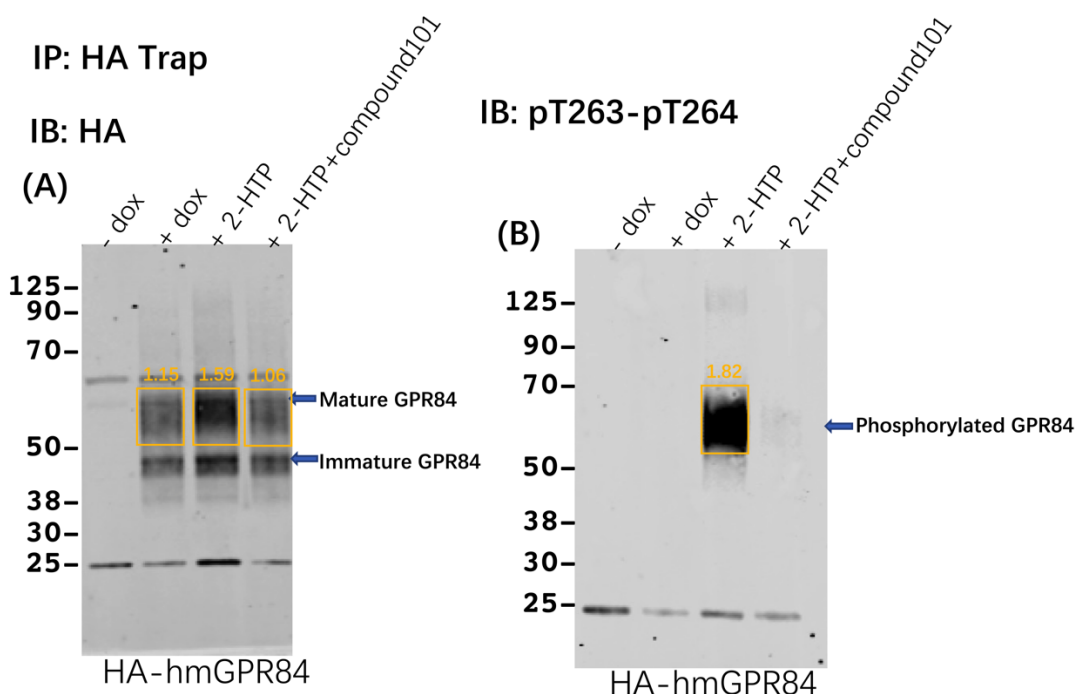
Figure 4.18 Compound 101 blocks agonist-induced phosphorylation of Thr263/Thr264 at HA-hmGPR84.
Serum-starved Flp-In T-REx 293 stable cells without doxycycline induction or induced to express HA-hmGPR84 were treated with vehicle or 10µM compound 101 for 30 mins before being treated with vehicle (+dox) or 5µM 2-HTP for 5mins. Then cells were lysed with the presence of protease and phosphatase inhibitors. Lysates were enriched with HA-trap agarose and run on NuPAGE 4-12% Bis-Tris SDSPAGE gels. Proteins were subsequently transferred to nitrocellulose membranes, blocked with TBS with 5% (w/v) BSA and incubated overnight with A) rat anti-HA primary antibody (1:10,000), B) rabbit anti-GPR843-pT263/pT264 (1:2,000) antiserum. Membranes were finally incubated with goat anti- IRDye 800CW (1:10,000) or goat anti-rabbit IRDye 800CW (1:10,000) secondary antibodies for 1h. The membranes were scanned using the LI-COR Odyssey 9260 gel imaging system. A single experiment was performed (n=1).

In order to further evaluate the possibility of using the phosphosite-specific antiserum pT263/pT264 to visualise the phosphorylation of HA-hmGPR84 in *ex vivo* studies, a series of immunocytochemical staining experiments were performed. In all these following experiments, Flp-In T-REx 293 cells induced to express HA-hmGPR84 were utilized. Staining with DAPI indicated the position of cell nuclei and the anti-HA antibody confirmed the expression of HA-hmGPR84 after doxycycline induction. Indeed, after doxycycline induction of HA-hmGPR84 Flp-In TREx 293 cells, the anti-HA antiserum recognized the receptor on membranes in

both the presence or absence of 2-HTP treatment. The phosphosite-specific antiserum pT263/pT264 showed strong binding to the membranes of 2-HTP-treated cells with little discernible staining in untreated cells, which supports previous data that antiserum pT263/pT264 recognised the phosphorylation of HA-hmGPR84 in a 2-HTP dependent manner in immunoblotting studies. (**Figure 4.19**).
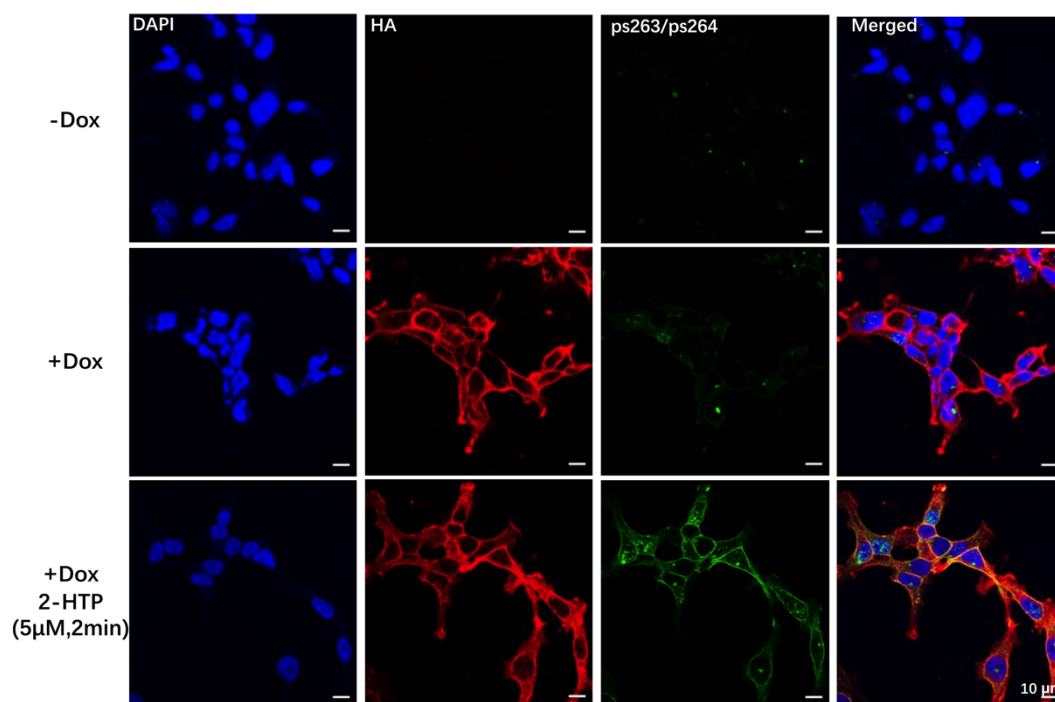
Figure 4.19 Immunocytochemical detection of HA-hmGPR84 phosphorylation induced by 2-HTP.
Serum-starved Flp-In T-REx 293 stable cells without doxycycline induction or induced to express HA-hmGPR84 were treated with vehicle (+dox) or 5μM 2-HTP for 2 mins before fixed with 4% paraformaldehyde. Then cells were incubated with rat anti-HA primary antibody (1:250) or rabbit anti-GPR843-pT263/pT264 (1:250) antiserum overnight at 4 °C. Cells were subsequently incubated with anti-rat IgG AlexaFluor-594 or anti-rabbit IgG AlexaFluor-488 secondary antibody (1:250) for 1h at room temperature. Nuclear DNA was labelled with DAPI (blue). Images were taken with 63× objective of Zeiss 880 Laser Scanning Confocal Microscope. Scale bar represents 10μm. Representative of 2 fields of view each from 2 separate experiments (n=2).

After the initial characterization of using antiserum pT263/pT264 in ICC, the phosphorylation of HA-hmGPR84 was studied in a time-depended manner (**Figure 4.20**). Cells expressing HA-hmGPR84 were treated with 5μM 2-HTP for 2 mins, 5 mins and 10 mins. With the time of 2-HTP treatment increasing, the staining of anti-HA and anti-pT263/pT264 on cell membranes decreased while the staining of anti-pT263/pT264 in intracellular areas increased. However, the colocalised staining of these two antisera only can be seen on cell membranes which makes it

difficult to distinguish between the internalized receptors and non-specific binding inside the cells.
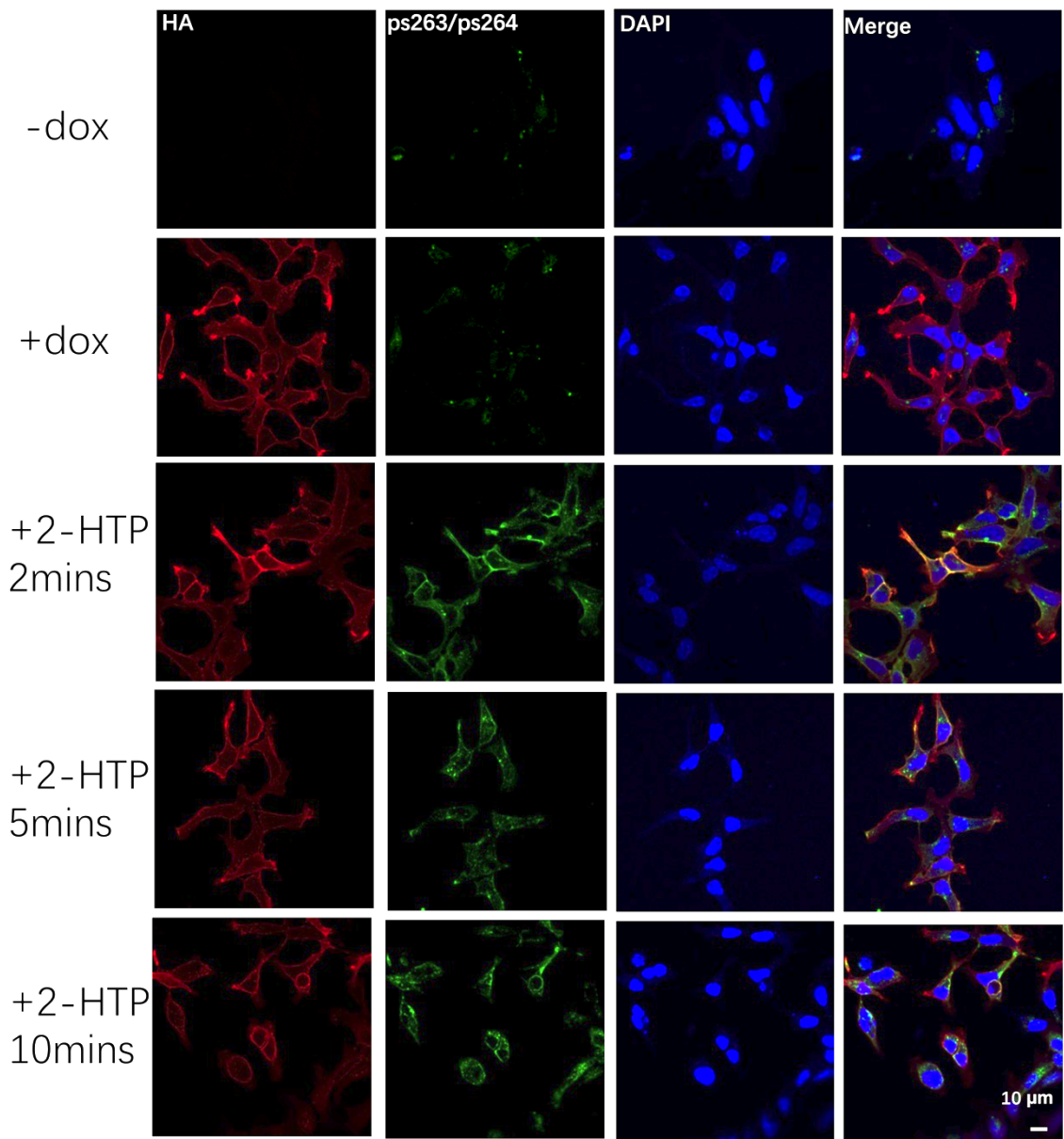
Figure 4.20 Immunocytochemical detection of HA-hmGPR84 phosphorylation over time-on agonist treatment.
Serum-starved Flp-In T-REx 293 stable cells without doxycycline induction or induced to express HA-hmGPR84 were treated with vehicle (+dox) or 5µM 2-HTP for 2 mins, 5 mins or 10 mins before fixed with 4% paraformaldehyde. Then Cells were incubated with rat anti-HA primary antibody (1:250) or rabbit anti-GPR843-pT263/pT264 (1:250) antiserum overnight at 4 ˚C. Cells were subsequently incubated with anti-rat IgG AlexaFluor-594 or anti-rabbit IgG AlexaFluor-488 secondary antibody (1:250) for 1h at room temperature. Nuclear DNA was labelled with DAPI (blue). Images were taken with 63× objective of Zeiss 880 Laser Scanning Confocal Microscope. Scale bar represents 10µm. Representative of 2 fields of view each from one experiment (n=1)

To explore the effects of antagonists on HA-hmGPR84 phosphorylation in a time-depended manner, Flp-In T-REx 293 cells induced to express HA-hmGPR84 were

pre-incubated with 10μM antagonist compound 020 (**Figure 4.21**) or compound 140 (**Figure 4.22**) for 10 mins, 30 mins and 60 mins before addition of 5μM 2-HTP for 10 mins. The phosphorylation staining on cell membranes decreased with increasing incubation time of antagonists. The colocalised staining of anti-HA and anti-pT263/pT264 still only can be detected on cell membranes.
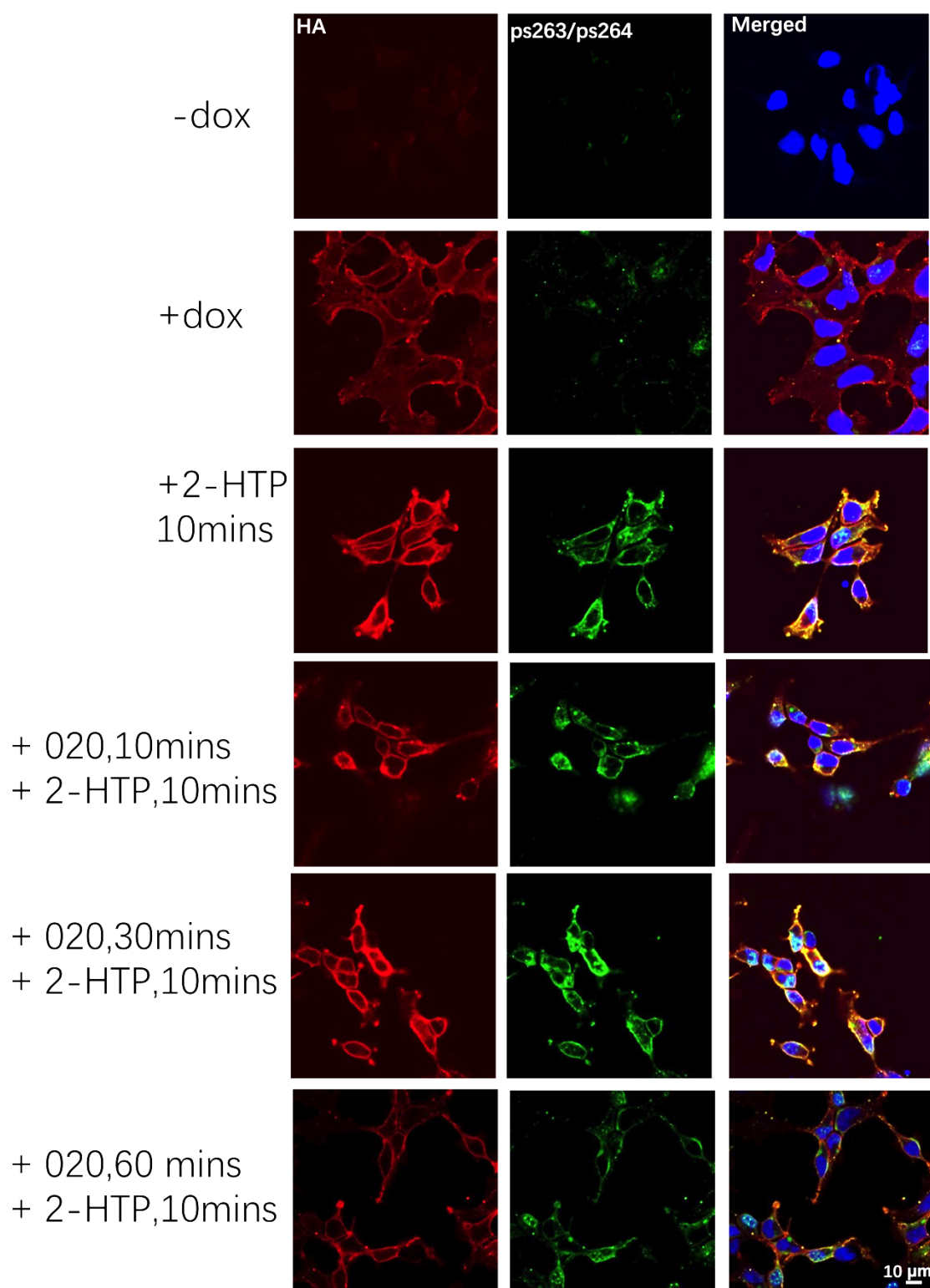
Figure 4.21 Antagonist compound 020 inhibits agonist-induced HA-hmGPR84 phosphorylation in a time-dependent manner.
Serum-starved Flp-In T-REx 293 stable cells without doxycycline induction or induced to express HA-hmGPR84 were pretreated with 10μM compound 020 for 10mins, 30 mins and 60 mins before incubation with 5μM 2-HTP for 10 mins. Cells were then fixed with 4% paraformaldehyde before incubated with rat anti-HA primary antibody (1:250) or rabbit anti-GPR843-pT263/pT264 (1:250)

antiserum overnight at 4 °C. Then cells were incubated with anti-rat IgG AlexaFluor-594 or anti-rabbit IgG AlexaFluor-488 secondary antibody (1:250) for 1h at room temperature. Nuclear DNA was labelled with DAPI (blue). Images were taken with 63× objective of Zeiss 880 Laser Scanning Confocal Microscope. Scale bar represents 10µm. Representative of 2 fields of view each from one experiment (n=1)
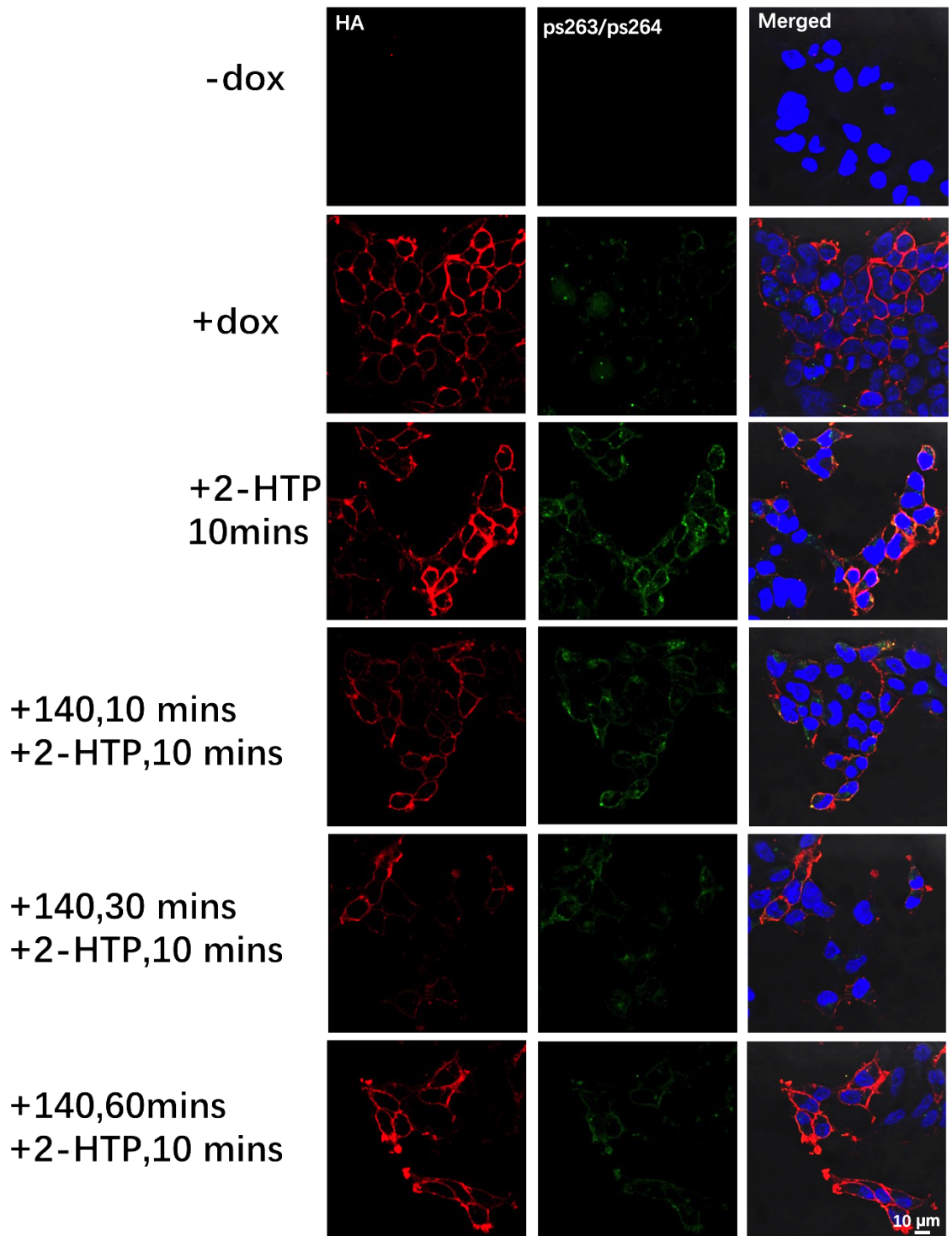
Figure 4.22 As for figure 4.20, antagonist compound 140 inhibited HA-hmGPR84 phosphorylation in a time-dependent manner.
Serum-starved Flp-In T-REx 293 stable cells without doxycycline induction or induced to express HA-hmGPR84 were pretreated with 10µM compound 140 for 10mins, 30 mins and 60 mins before incubation with 5µM 2-HTP for 10 mins. Cells were then fixed with 4% paraformaldehyde before incubated with rat anti-HA primary antibody (1:250) or rabbit anti-GPR843-pT263/pT264 (1:250) antiserum overnight at 4 °C. Then cells were incubated with anti-rat IgG AlexaFluor-594 or anti-

rabbit IgG AlexaFluor-488 secondary antibody (1:250) for 1h at room temperature. Nuclear DNA was labelled with DAPI (blue). Images were taken with 63× objective of Zeiss 880 Laser Scanning Confocal Microscope. Scale bar represents 10μm. Representative of 2 fields of view each from one experiment (n=1)

4.3 Discussion

In anticipation that the construct HA-hmGPR84 might be used to produce a new transgenic mouse line, this chimeric receptor was characterized extensively using a Flp-In T-REx 293 cell line in which it was stably expressed. To compare similarities and differences between HA-hmGPR84 and HA-hGPR84/HA-mGPR84, stable cells expressing each of these constructs were generated to characterize the pharmacology of them. The pharmacology of these Flp-In T-REx 293 cell lines was characterized using each of the cAMP assays, radioligand binding assays and immunoblotting.

It was found that the potency of 2-HTP and PSB-16671 at HA-hGPR84, HA-mGPR84 and HA-hmGPR84 was not significantly different, while the potency of 6-OAU and DL-175 at these constructs were significantly different in cAMP assays. Encouragingly, human GPR84 species selective antagonists compound 020, compound 140 and compound 837 could block the activation of HA-hmGPR84 induced by 2-HTP, and the ability of these antagonists to block HA-hGPR84 and HA-hmGPR84 was similar. Moreover, the affinity of [^{3}H]140 and antagonist GLPG1205 to bind HA-hGPR84 and HA-hmGPR84 was also similar. Therefore, the designed chimeric construct HA-hmGPR84 has similar pharmacology to HA-hGPR84. However, the IC$_{50}$ of antagonists at HA-hGPR84 was less than that in the published paper (Jenkins et al., 2021). These differences are probably because they were tested using different experiment assays, and different experiment assays test different processes of signaling. After the activation of the receptor, eponymous heterotrimeric G proteins are recruited to the intracellular regions of the receptor. Guanosine diphosphate (GDP) is then exchanged for guanosine triphosphate (GTP) on the G protein α-subunit (Simon et al., 1991b). As the downstream signaling of orphan GPR84 mainly depends on Gαi, adenylyl cyclase will be inhibited which causes a decrease in the level of intracellular cyclic adenosine monophosphate (cAMP). The cAMP assay used in this chapter measured the ability of agonists to

inhibit cAMP production. For the $[^{35}S]GTP\gamma S$ assay used in the published paper, the nucleotide exchange process was monitored (Jenkins et al., 2021, Milligan, 2003). Compared to the principles between cAMP and $[^{35}S]GTP\gamma S$ assay, $[^{35}S]GTP\gamma S$ assay measures a very early event in the signal transduction while cAMP assay measures the levels of second messengers. Therefore, the IC_{50} of antagonists tested by cAMP assays could be less than the IC_{50} tested by $[^{35}S]GTP\gamma S$ assay. Except for the effects of using different assays, the receptor used in the published paper is human GPR84-$G_{\alpha i2}$ while the receptor in this chapter is HA-human GPR84. As the downstream signaling of orphan GPR84 mainly depends on $G\alpha i$, it would be reasonable that the tested affinity using human GPR84-$G_{\alpha i2}$ is higher. Besides, the HA-tag on the N-terminal of GPR84 may also affect the binding of compounds to GPR84. According to the binding structure GPR84-Gi signalling complex with 6-OAU (Zhang et al., 2023b), orthosteric antagonists are likely to bind to a similar position as 6-OAU, which means the HA-tag on the N-terminal of GPR84 probably would obstruct the binding of antagonists to the receptor and decrease the tested affinity.

The maximum response of HA-mGPR84 was lower than the maximum response of HA-hGPR84 which could be caused by different expression levels of these Flp-In T-REx 293 stable cell lines at the plasma membrane. The expression level of a receptor at the plasma membrane is regulated by multiple factors, including transcriptional control, post-translational modifications, and intracellular trafficking (Dong et al., 2007, Sikarwar et al., 2019). At the transcriptional level, promoter activity, epigenetic modifications, and transcription factor binding affect mRNA synthesis. Even if receptors have the same transcription levels, the number of receptors may differ due to mRNA stability, translation efficiency and post-translational modifications including glycosylation, phosphorylation, and palmitoylation. Receptor folding within the endoplasmic reticulum (ER) plays an important role because misfolded receptors are often retained in the ER (MM and AA., 2007). Moreover, receptor trafficking mechanisms, including vesicular transport from the Golgi apparatus and endocytosis-mediated recycling or degradation, also affect receptor expressions at the plasma membrane (Dong et al., 2007). The expression level of Flp-In T-REx 293 stable cell lines was

determined by the amount of doxycycline. Therefore, the expression levels of these cell lines are very likely to be the same as the same amount of doxycycline was used at them. If the expression levels of these two orthologues were the same, the higher potency and lower efficacy at HA-mGPR84 could reflect that the interaction between HA-mGPR84 and G protein is likely to be worse than the interaction between HA-hGPR84 and G protein. Considering the B_{max} of HA-hmGPR84 measured in the saturation assay was less than that of HA-hGPR84, it would be possible that the intracellular sequences affect the signaling of GPR84 as the intracellular sequences of HA-hmGPR84 are the same as HA-mGPR84. Since these hypotheses are based on the assumption that these receptors have similar expression levels at the plasma membrane, it is crucial to measure their expression levels to validate this assumption. In order to detect the expression levels of these cell lines, saturation binding assays, the enzyme-linked immunosorbent assay (ELISA), western blots or even qPCR can be used.

In order to use antiserum to identify the existence and the phosphorylation of HA-hmGPR84 in *ex vivo* studies in the future, the characterization of two phosphosite-sepecific antiserum and two GPR84 structural antiserum was applied on HA-hGPR84, HA-mGPR84 and HA-hmGPR84 Flp-In T-REx 293 stable cell lines. Antiserum pT263-pT264 detected the phosphorylation of HA-hGPR84, HA-mGPR84 and HA-hmGPR84 promoted by 2-HTP. However, antiserum pS221-pS224 detected the phosphorylation HA-hGPR84 in the presence or absence of agonists while it detected the phosphorylation of HA-hmGPR84 in a 2-HTP dependent way. Although T263-T264 and S221-S224 sites exist in HA-hGPR84 and HA-hmGPR84, the different amino acids next to site S224 properly would affect the recognition of phosphosite-sepecific antiserum. The differences may be also caused by different structures at the ICL3 of HA-hGPR84 and HA-hmGPR84 as most of the different sequences between them are located in ICL3 regions (**Figure 4.1**). Structural antiserum GPR84(7TM) only detected the existence of HA-hGPR84, but mouse ICL3 structural antibody detected the expression of HA-hGPR84, HA-mGPR84 and HA-hmGPR84. Structural antiserum GPR84(7TM) was designed to target the C-terminal of human GPR84, and the C-terminal of human GPR84 is different from mouse GPR84/humanised GPR84. Although the mouse ICL3 structural antibody was designed to target the ICL3 of mouse GPR84, the home-made antisera properly

contains many antibodies targeting different peptide sequences in ICL3, which enables this antisera to identify the existence of HA-hGPR84, HA-mGPR84 and HA-hmGPR84.

In order to visualize and track the phosphorylation of HA-hmGPR84 *in vitro* and *ex vivo* in the future, the ability of the phosphosite-specific antisera pT263-pT264 to bind activated receptors was studied. However, anti-HA antibody can only detect the receptor on cell membranes which means it would be difficult to confirm whether the binding of antisera pT263-pT264 in intracellular areas was specific binding or non-specific binding because no colocalised staining of these two antisera could be seen. To better understand the phosphorylation and internalization of GPR84, a new stable cell line induced to express HA-Halo-human GPR84 was generated to overcome the limitations of using phosphorylation antiserum in time-cost ICC studies (studied in *Chapter 5*). Interestingly, it was found that GRK2/3 inhibitor compound 101 blocked the phosphorylation of HA-hGPR84 and HA-hmGPR84 promoted by 2-HTP. Following this result, the effect of individual GRKs on GPR84 phosphorylation and internalization was studied in *Chapter 5.*

Chapter 5 Studies on the impact of individual GRKs on GPR84 phosphorylation and internalization

5.1 Introduction

Most activated GPCRs can engage both G protein and β-arrestin signalling pathways. It is generally believed that the primary function of β-arrestin interactions is to inhibit G protein signalling by blocking the interaction between G proteins and the GPCR. In addition to inhibition of G protein signalling, β-arrestins can also regulate GPCR trafficking, desensitization and internalization. These functions rely on the affinity of β-arrestin for clathrin and its adaptor complex AP2 which helps the receptor move into endocytic vesicles through clathrin-coated pits (Kang et al., 2014, Stéphane A. Laporte, 1999). Numerous studies have found that β-arrestin 1 and β-arrestin 2 can interact with many activated GPCRs and may lead to different responses. The 'barcode hypothesis' was developed to explain such observations: Following the activation of receptor, conformational changes in the receptor will be recognized by one or more G protein kinases (GRKs) that phosphorylate the receptor within the 3rd intracellular loop and/or C-terminal tail. Depending on the kinase, the cell or tissue or the GPCR-activating ligand this can result in distinct patterns of phosphorylation that have been designated 'phosphorylation barcodes'. Recruited β-arrestin can 'read' the unique 'phosphorylation barcode' and this process is suggested to lead to different functional consequences (Tobin et al., 2008, Maharana et al., 2023). Although GRK1 and GRK7 are "visual" GRKs, and GRK4 is mostly expressed in the testis, GRK2, 3, 5 and 6 are widely expressed. After the activation of receptor and dissociation of G protein, GRK2 and GRK3 are recruited through their pleckstrin homology (PH) domain by binding to Gβγ. GRK5 non-specifically binds to membrane lipids through its polybasic/hydrophobic domain whilst GRK6 is anchored to the membrane (Palmer et al., 2022, DebBurman et al., 1995)

Although both 2nd messenger-activated and other kinases can play roles in GPCR phosphorylation only the GRKs do so in a manner dependent on agonist activation of the receptor. Hence, studying which GRK(s) might be involved in a specific signalling pathway and how the GRKs respond to the pharmacology of a receptor

is important for further understanding the signalling of a GPCR. In the following studies I used both balanced orthosteric (2-HTP and 6-OAU), and Gi-biased (DL-175) agonists of GPR84 as well as the allosteric agonist PSB-16671 to test whether they have different effects on the recruitment of GRKs to ligand-occupied GPR84. Only GRK2, GRK3, GRK5 and GRK6 were studied in the following research because GPR84 is mainly expressed by immune cells. I selected these four agonists because they have been used in a published paper to assess the relationship between different agonists and GPR84 phosphorylation (Marsango et al., 2022, Marsango and Milligan, 2023). These earlier studies indicated that β-arrestin 2 was only recruited when the receptor was activated by 2-HTP or 6-OAU but not by DL-175 or PSB-16671. Moreover, phosphorylation caused by 2-HTP or 6-OAU could be detected by the incorporation of [^{32}P] (from [^{32}P]ATP) but activation of GPR84 by DL-175 or PSB-16671 could not be detected in this assay. Therefore, it appears that 2-HTP and 6-OAU can promote the phosphorylation of GPR84 while DL-175 or PSB-16671 cannot.

Although it is known that GRKs play an important role in the phosphorylation and regulation of many GPCRs, the specific contribution of individual GRKs to the phosphorylation of many receptors has been poorly studied. To study GRK involvement in the phosphorylation of GPR84, a Nanoluciferase Binary Technology (NanoBit) which detects the recruitment of GRKs to the receptor was developed (**Figure 5.1**). In this assay the N-terminal of GRK was tagged with a fragment of the Nanoluciferase (NLuc) enzyme called LargeBIT (LgBit), while the C-terminal of GPR84 was tagged with the complementary 11-residue fragment named SmallBIT (SmBit). After the activation of GPCR and the association of G protein, the binding of a specific tagged GRK allows the complementation of NLuc which produces strong bioluminescence following addition of an NLuc substrate (Palmer et al., 2022). The generated bioluminescence was detected using a Clariostar plate reader and reflects the extent of GRKs recruitment (Palmer et al., 2022).

The aim of this chapter was to study which GRK(s) contribute to the phosphorylation of GPR84, at least when expressed in a HEK293-derived cell line,

and how GRK recruitment was affected by the presence of GPR84 antagonists or subtype-selective GRK inhibitors. In the light of the results, the effect of PTX on the recruitment of GRKs and ß-arrestin 2 to GPR84 was also investigated. Finally, internalization of GPR84 was studied using both a 'bystander'-based assay and immunocytochemistry to assess whether different agonists resulted in internalization of GPR84.
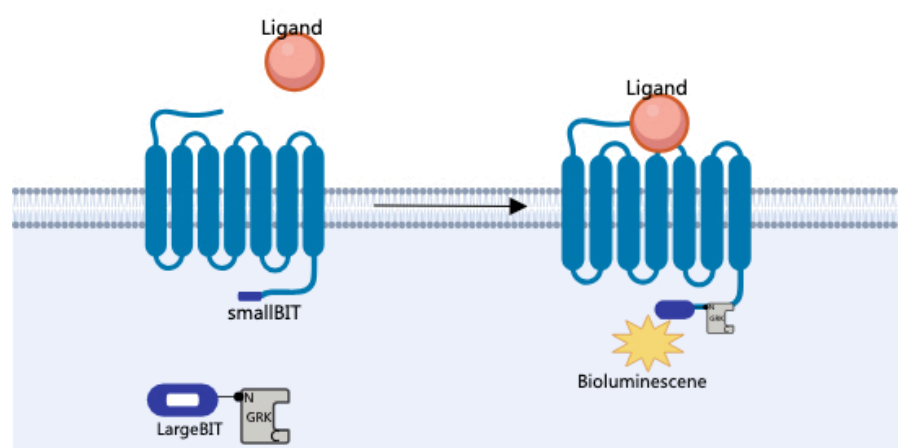
Figure 5.1 The principle of NanoBit assay.
The N-terminal of GRK is tagged with a fragment of the Nanoluciferase (NLuc) enzyme called LargeBIT (LgBit), while the C-terminal of GPR84 is tagged with the complementary fragment named smallBIT (SmBit). After the binding of ligand, a specific GRK may interact with the receptor and, if so, allows the complementation of the NLuc enzyme. NLuc substrate is then added and generates bioluminescence that was measured by a Clariostar plate reader. It was adapted from Palmer et al. (2022)

5.2 Results

The NanoBit assay illustrated in **Figure 5.1** was used to study if agonist activation of GPR84 resulted in recruitment of individual GRKs. To establish the protocol, HA-hGPR84-SmBit and LgBit-GRK2 or wild type GRK2 were co-transfected into GRK knock out (GRK KO) cells. GRK KO were engineered to lack expression of all GRKs, therefore these cells only express the GRKs transfected in (GRK KO cells are gifts from another group, and can refer to Burghi et al. (2023)). GRK2 was used to optimize the assay because inhibitor studies had suggested that GRK2/3 should be involved in GPR84 phosphorylation (Marsango et al., 2022). Orthosteric agonists 2-HTP (**Figure 5.2 A**), 6-OAU (**Figure 5.2 B**), the biased orthosteric agonist DL-175 (**Figure 5.2 C**) and the allosteric agonist PSB-16671 (**Figure 5.2 D**) were used to activate the receptor. All of these ligands promoted the recruitment of LgBit-GRK2. Therefore, the assay can be used to test the recruitment of specific GRKs

as the bioluminescence can only be detected after the combination of LgBit and SmBit. However, it was surprising to see that the G_i biased agonist DL-175 and allosteric agonist PSB-16671 also increased the recruitment of LgBit-GRK2 as these ligands do not phosphorylate GPR84, as least at sites assessed by (Marsango et al., 2022). Since GRK recruitment is typically associated with GPCR phosphorylation, the mechanisms underlying GRK recruitment to non-phosphorylated receptors deserve further investigation.
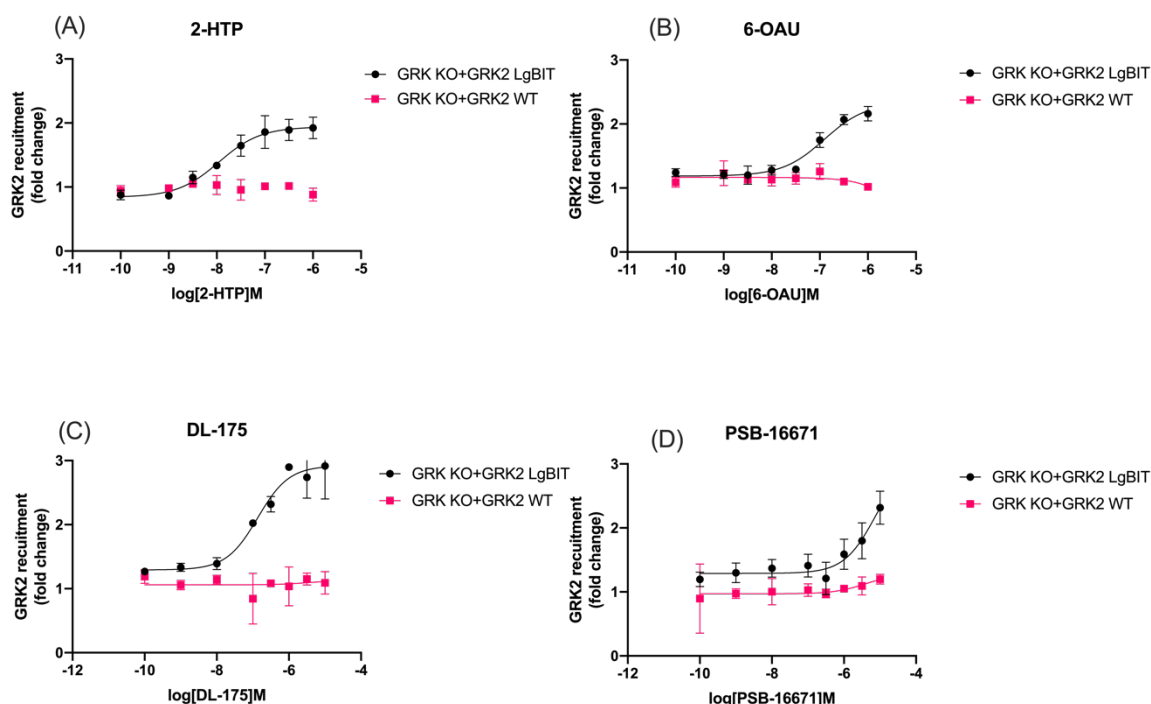
Figure 5.2 The recruitment of LgBit-GRK2 can be detected while the recruitment of GRK WT cannot
Plasmids encoding HA-human GPR84-SmBit and LgBit-GRK2 or GRK2 wild type were co-transfected into GRK KO HEK293 cells overnight. The transfected cells were cultured in polyD-lysine-coated (Palmer et al., 2022) 96-well plates overnight. Cells were pre-incubated with Nano-Glo Luciferase substrate for 10mins and fluorescence then measured using a Clariostar plate reader. Cells were then treated with increasing concentrations of ligands A) 2-HTP, B) 6-OAU, C) DL-175 and D) PSB-16671 for 5 mins. The lowest concentration of compounds displayed on the X-axis is actually 0M (vehicle only). Endpoint BRET luminescence was then measured. The ratio of raw data before and after adding agonists was plotted. Data presented as mean±SEM (n=1, 3 replicate wells in a single experiment).

After the initial characterization, potential differences between using GRK KO and parental HEK293 cells (that express wild type GRKs) were studied which evaluate the effect of wild type GRKs on this assay. HA-hGPR84-SmBit and LgBit-GRK2 were co-transfected into GRK KO cells or parental HEK293 cells (**Figure 5.3**). The balanced agonists 2-HTP, 6-OAU and the G_i-biased agonists DL-175 and PSB-16671 were used to assess the recruitment of the tagged GRK2. The response window in

GRK KO cells was higher than that in parental HEK293 cells. This may reflect that wild type GRKs expressed by the parental cells compete to bind to the receptor with the LgBit labeled GRK. To ensure greatest sensitivity to detect the recruitment of GRKs, only GRK KO cells were then used in subsequent studies.
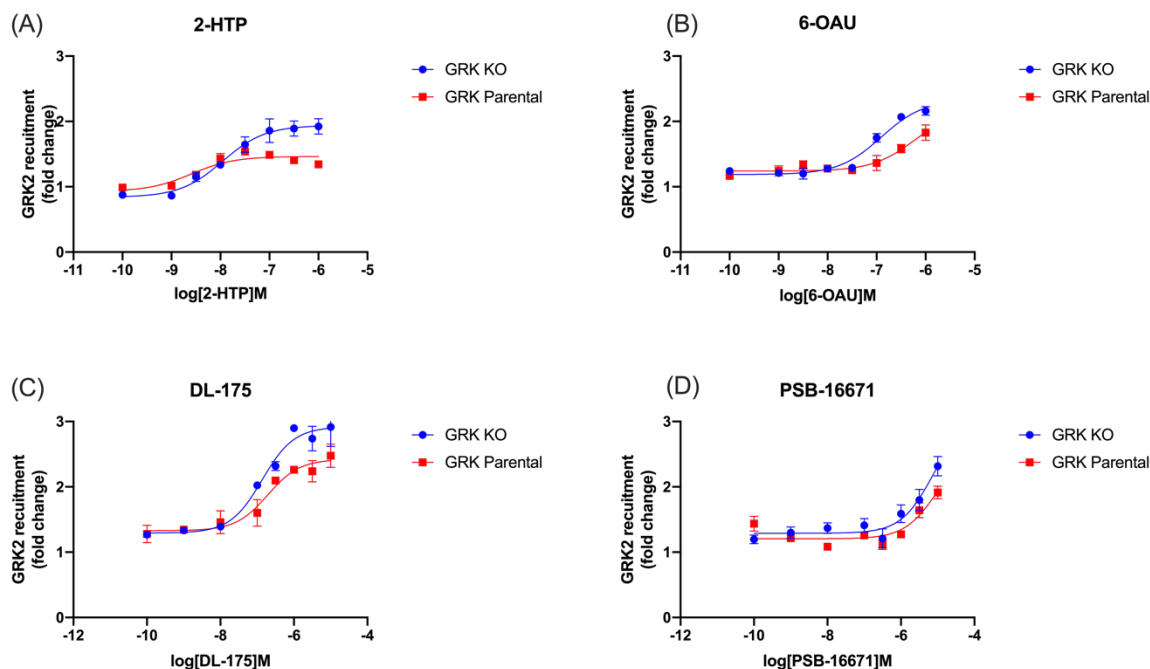
Figure 5.3 The response window in GRK KO cells was higher than that in parental HEK293 cells
Plasmid HA-hGPR84-SmBit and LgBit-GRK2 were co-transfected into GRK KO or GRK parental HEK293 cells overnight. Then transfected cells were cultured in polyD-lysine-coated 96-well plates overnight. Cells were pre-incubated with Nano-Glo Luciferase substrate for 10mins and fluorescence was measured using a Clariostar plate reader. Cells were then treated with increasing concentrations of agonists A) 2-HTP, B) 6-OAU, C) DL-175 and D) PSB-16671 for 5 mins. Endpoint BRET luminescence was then measured. The ratio of raw data before and after adding agonists was plotted. Data presented as mean±SD (n=1, 3 replicate wells in a single experiment).

Following the basic characterization of the NanoBit assay, studies on the interaction between individual GRKs and GPR84 were carried out. The balanced agonist 2-HTP and G$_i$-biased agonist DL-175 were used as representative agonists because 2-HTP can activate both G protein signaling and β-arrestin interactions while DL-175 only activates G protein signalling. Each of LgBit-GRK2/3/5/6 was co-transfected with HA-hGPR84-SmBit into GRK KO cells separately. The recruitment of LgBit-GRK2/3 was increased with increasing concentrations of 2-HTP or DL-175, while GRK5/6 were not recruited by increasing concentrations of agonists (**Figure 5.4**). Therefore, it appeared that LgBit-GRK2/3 was more

important for the activation of GPR84 than LgBit-GRK5/6. The potency of 2-HTP and DL-175 to promote the recruitment of GRK2 and GRK3 are listed in **Table 5-1.**
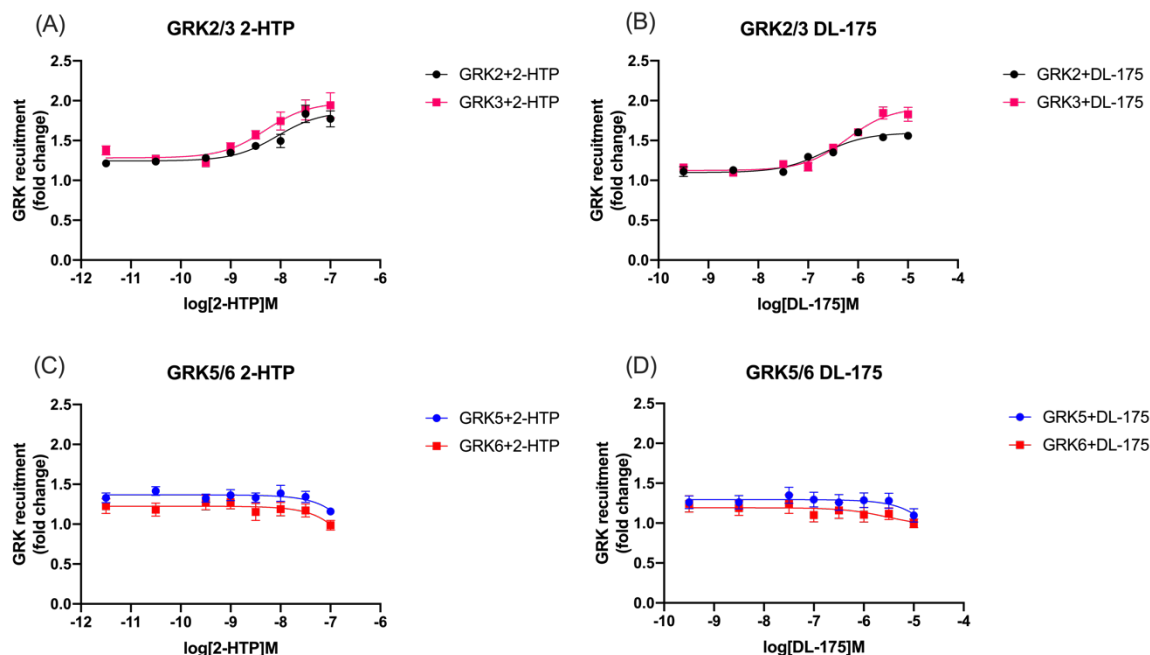
Figure 5.4 GRK2/3 are related to the activation progress of GPR84 while GRK5/6 are not.
HA-hGPR84-SmBit and LgBit-GRK2/3/5/6 were co-transfected into GRK KO cells overnight. Then transfected cells were cultured in polyD-lysine-coated 96-well plates overnight. Cells were pre-incubated with Nano-Glo Luciferase substrate for 10mins and fluorescence then measured using a Clariostar plate reader. Cells were then treated with increasing concentrations of agonists A, C) 2-HTP, B, D) DL-175 for 5 mins. The lowest concentration of compounds displayed on the X-axis is actually 0M (vehicle only). Endpoint BRET luminescence was then measured. The ratio of raw data before and after adding agonists was plotted. Data presented as mean±SEM (from n=3 separate experiments).

Table 5-1 Potency of 2-HTP and DL-175 to promote the recruitment of GRK2/GRK3 to HA-hGPR84-SmBit.

	GRK2 recruitment (pEC$_{50}$ ± SEM)	GRK3 recruitment (pEC$_{50}$ ± SEM)
2-HTP	8.07±0.06	8.36±0.11
DL-175	6.67±0.13	6.20±0.16

Values were calculated from the ratio of raw data. Data presented as mean±SEM (n=3).

To study how GPR84 antagonists affect the recruitment of GRKs, orthosteric antagonist compound 020 was used. Since compound 020 inhibits the phosphorylation of GPR84 at pT263/pT264, its effects on GRK recruitment should be investigated. Transfected cells were pretreated with compound 020 for 15mins

before adding substrate and agonists. Results indicated that compound 020 blocked the recruitment of LgBit-GRK2/3 caused by 2-HTP and DL-175 (**Figure 5.5 A, B**). Compound 020 also did not improve or block the recruitment of LgBit-GRK5/6 as they were not involved in the activation of GPR84 (**Figure 5.5 C, D**). These results also indicated that the recruitment of LgBit-GRK2/3 was improved by the interaction between agonist and receptor. Once the binding between agonists and receptors was blocked, the recruitment of LgBit-GRK2/3 decreased. The pIC_{50} of compound 020 block GRK2 and GRK3 recruitment caused by 2-HTP and DL-175 are listed in **Table 5-2**.
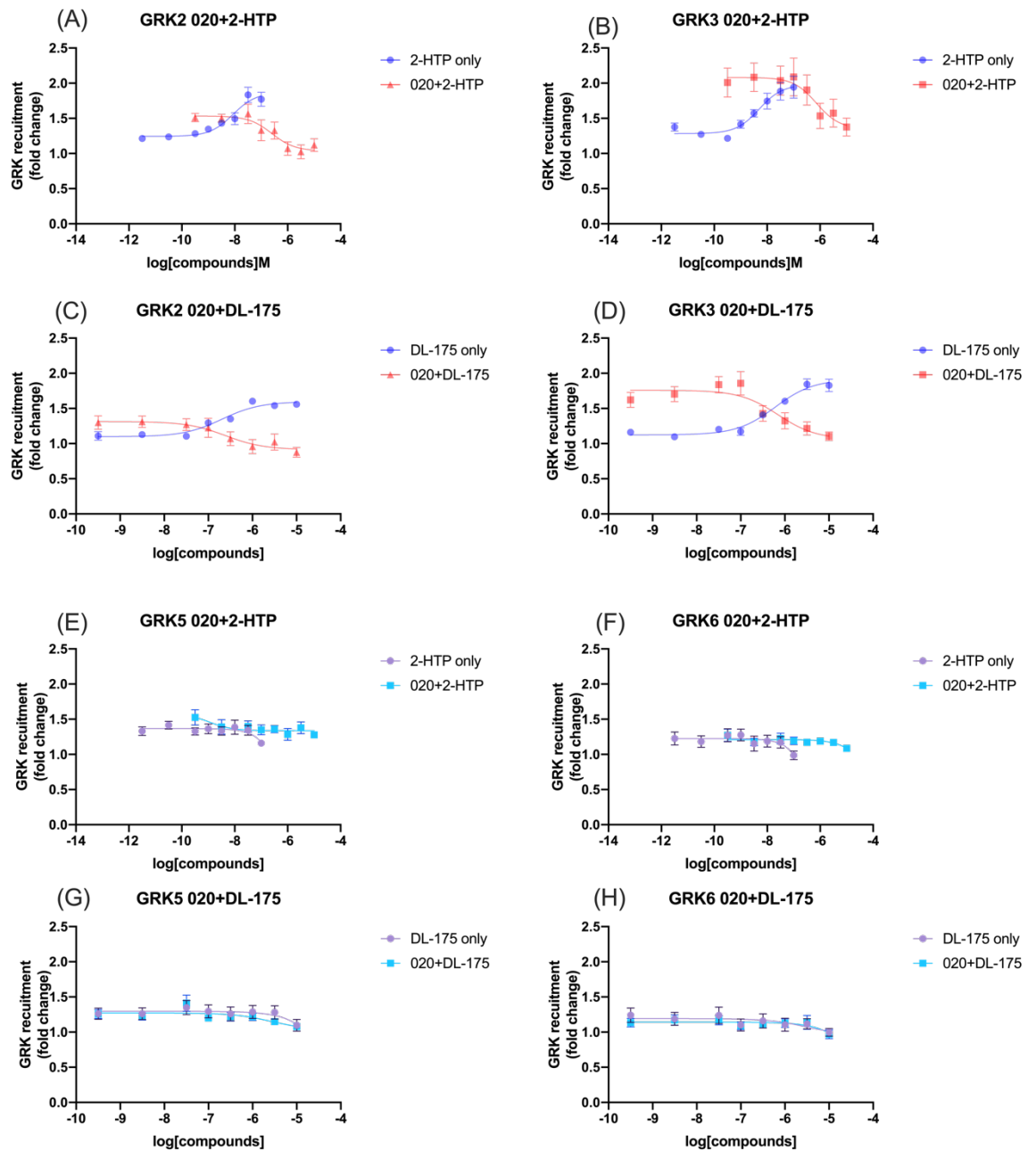
Figure 5.5 GPR84 antagonist compound 020 blocks the recruitment of GRK2/3 induced by 2-HTP and DL-175.
HA-hGPR84-SmBit and LgBit-GRK2/3/5/6 were co-transfected into GRK KO cells overnight. Then transfected cells were cultured in polyD-lysine-coated 96-well plates overnight. Cells were pre-incubated with antagonist compound 020 for 15mins before incubation with Nano-Glo Luciferase substrate for 10mins. For the curves of 2-HTP/DL-175-only, the X-axis present the concentrations of 2-HTP or DL-175. Otherwise, the X-axis present the concentrations of compound 020. The lowest concentration of compounds displayed on the X-axis is actually 0M (vehicle only). Fluorescence was then measured using a Clariostar plate reader. After that cells were treated with increasing concentrations of agonists A, B,E,F) 2-HTP or C,D,G,H) DL-175 for 5 mins. Endpoint BRET luminescence was measured. The ratio of raw data before and after adding agonists was plotted. Data presented as mean±SEM from n=3 separate experiments.

Table 5-2 The pIC$_{50}$ of compound 020 block GRK2 and GRK3 recruitment caused by 2-HTP and DL-175.

the pIC$_{50}$ of compound 020	GRK2 (pIC$_{50}$ ± SEM)	GRK3 (pIC$_{50}$ ± SEM)
2-HTP as the agonist	6.78±0.42	6.29±0.37
DL-175 as the agonist	6.55±0.44	6.08±0.30

Values were calculated from the ratio of raw data. Data presented as mean±SEM (n=3).

As it was shown that GPR84 antagonist compound 020 blocked the recruitment of LgBit-GRK2/3, I wanted to know whether selective GRK inhibitors affect the recruitment of GRK(s). Compound 101 is an inhibitor of GRK2/3 and compound 19 is an inhibitor of GRK5/6. The working concentration of GRK inhibitors was 10 μM (Marsango et al., 2022). As the agonists did not promote recruitment of LgBit-GRK5/6 then compound 19 was not expected to affect this (**Figure 5.6 E-H**). Interestingly, GRK2/3 inhibitor compound 101 did not reduce agonist-promoted recruitment of GRK2/3 (**Figure 5.6 A-D**) but rather slightly increased the recruitment of LgBit-GRK2/3. And the effect of GRKs inhibitors was the same nevertheless 2-HTP or DL-175 was used as the agonist. This suggests that GRK2/3 can be recruited to GPR84 in an agonist-dependent manner in the presence of compound 101 but is then unable to cause receptor phosphorylation.
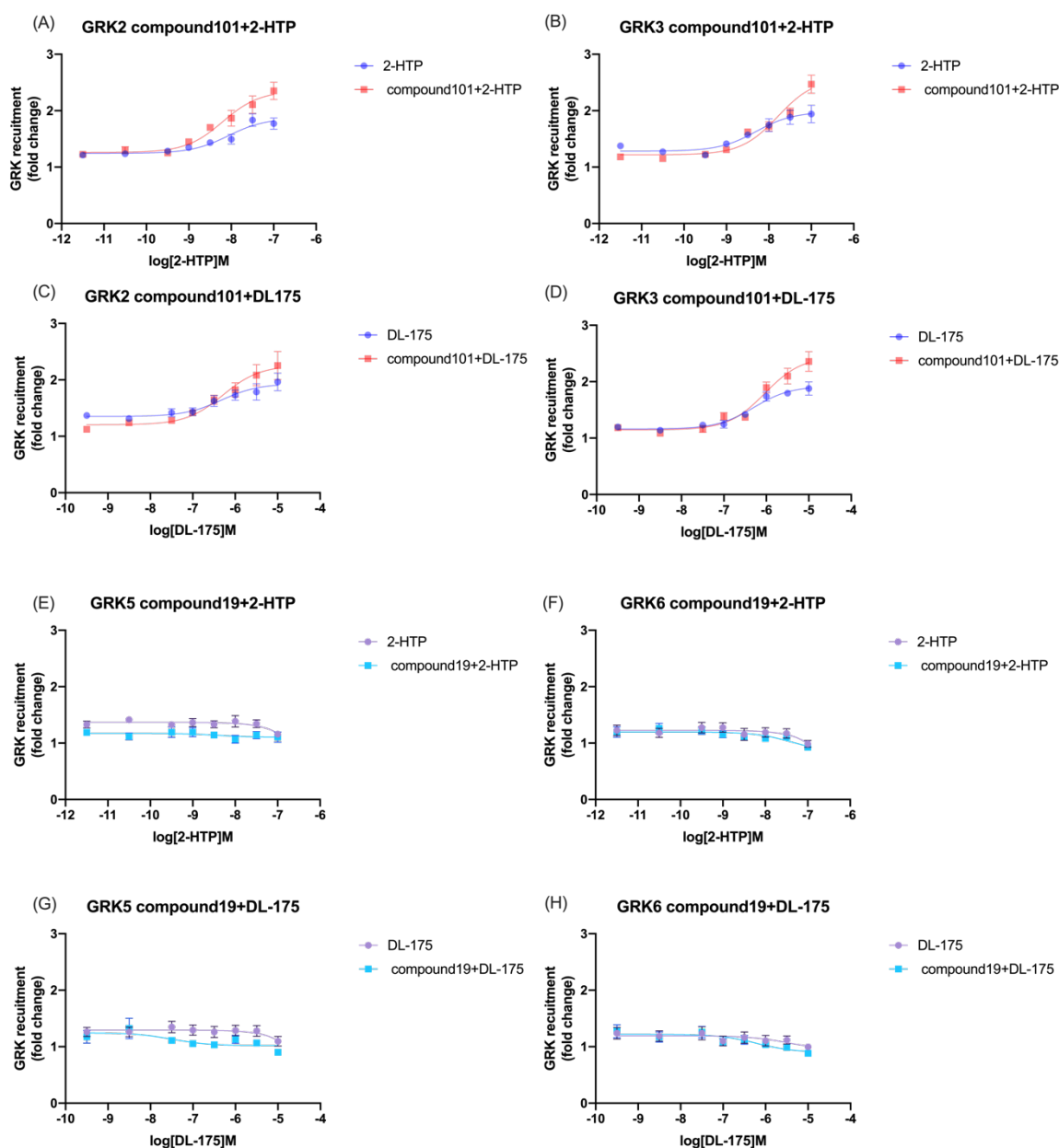
Figure 5.6 GRK2/3 inhibitor compound 101 did not block the interaction between these GRKs and GPR84.
Plasmid HA-GPR84-SmBit and LgBit-GRK2/3/5/6 were co-transfected into GRK KO cells overnight. Then transfected cells were cultured in polyD-lysine-coated 96-well plates overnight. Transfected cells were pre-incubated with 10 μM compound 101 (A-D) or compound 19 (E-H) for 30 mins before incubating with Nano-Glo Luciferase substrate for 10mins. Fluorescence was then measured using a Clariostar plate reader. Cells were then treated with increasing concentrations of agonists A, B, E, F) 2-HTP or C, D, G, H) DL-175 for 5 mins. Endpoint BRET luminescence was measured. The ratio of raw data before and after adding agonists was plotted. Data presented as mean±SEM (n=3).

5.2.1 Studies on effects of PTX on GRK recruitment and GPR84 phosphorylation

From the NanoBit results above, it is not clear why the Gi-biased agonist DL-175 improved the interaction between GRKs and GPR84 but did not promote the

recruitment of arrestin 3 to GPR84 (Marsango et al., 2022). Thus, the Gi signalling inhibitor PTX was used to study whether the recruitment of GRKs induced by DL-175 is related to Gi signalling. 25ng/ml PTX was added to the transfected cells when transferring cells to 96-well plates and left overnight. Then the assay was applied following the characterized NanoBit assay protocol. PTX blocked the recruitment of LgBit-GRK2/GRK3 induced by both 2-HTP and DL-175 and did not modify the lack of recruitment of LgBit-GRK5/6 (**Figure 5.7**). This result suggests that GRK2/3 recruitment to GPR84 is G_i-dependent.
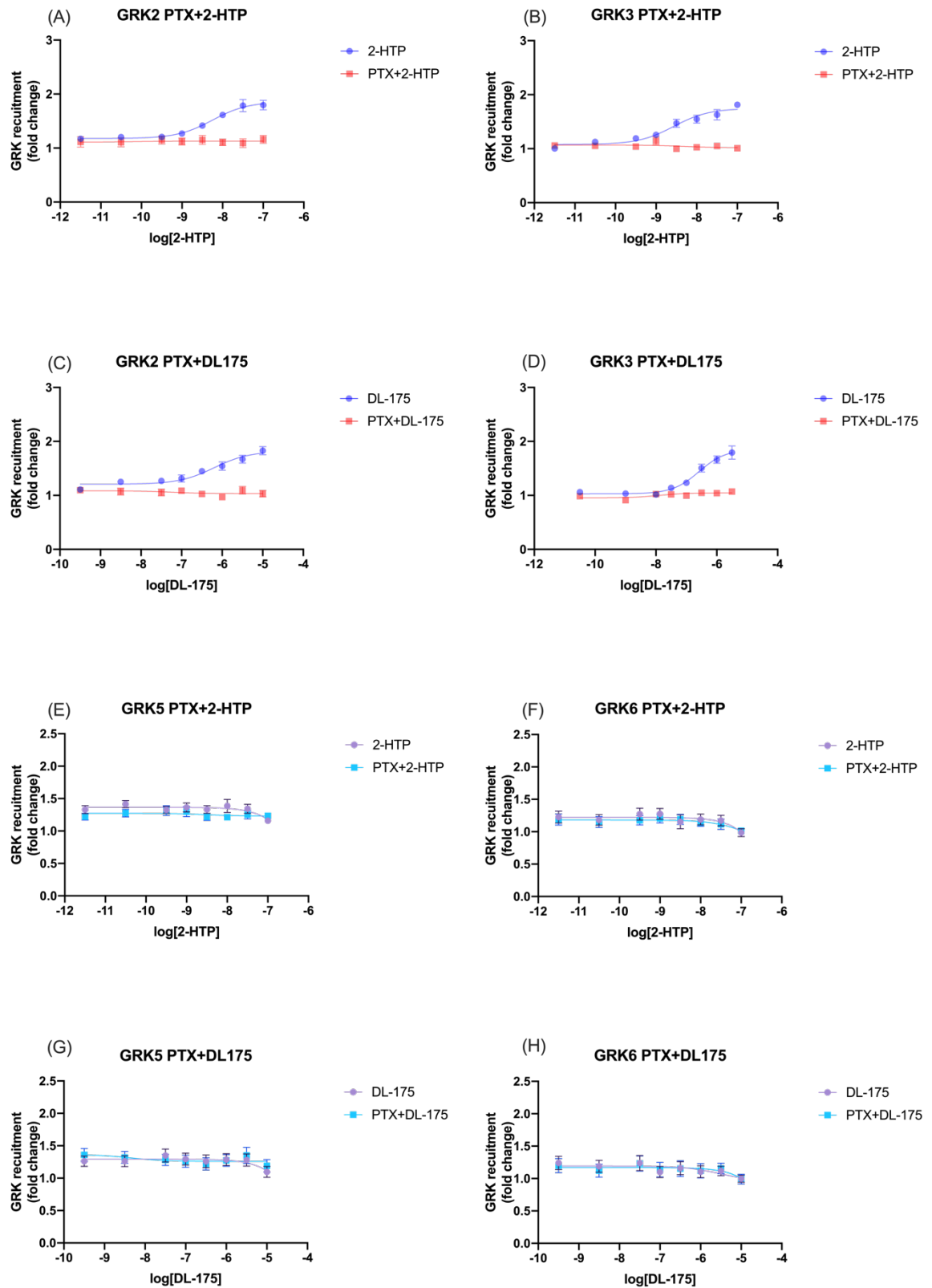
Figure 5.7 Gi signaling inhibitor PTX prevents recruitment of GRK2 and GRK3 to GPR84.
Plasmid HA-hGPR84-SmBit and LgBit-GRK2/3/5/6 were co-transfected into GRK KO cells overnight. Transfected cells were cultured in polyD-lysine-coated 96-well plates with 25ng/ml PTX overnight. Transfected cells were then incubated with Nano-Glo Luciferase substrate for 10mins. Fluorescence was measured using a Clariostar plate reader. After that cells were treated with increasing concentrations of agonists A, B, E, F) 2-HTP or C, D, G, H) DL-175 for 5 mins. Endpoint BRET luminescence was then measured. The ratio of raw data before and after adding agonists was plotted. Data presented as mean±SEM (n=3).

To further assess whether G_i is essential for β-arrestin 2 recruitment to GPR84, β-arrestin 2 recruitment BRET experiments were performed. HEK 293T cells (**Figure 5.8 A**) and G protein-expressing parental HEK293 cells (**Figure 5.8 B**) or G protein knock out cells (**Figure 5.8 C**) were used in this assay. The G protein knock out cells lack of G_s, G_o, G_q, G_{12} and G_{13} but still express members of the G_i family. PTX partially blocked the β-arrestin 2 recruitment in response to 2-HTP, and compound 101+PTX blocked most of the β-arrestin 2 recruitment in each of these three types of cells. These results indicated that G_i affected the recruitment of β-arrestin 2 but it was not necessary for such interactions. However, GRK2/3 played an important role in the recruitment of β-arrestin 2. Moreover, the β-arrestin 2 recruitment to GPR84 has a G protein independent component ('βarr recruitment at zero functional G') (Grundmann et al., 2018).
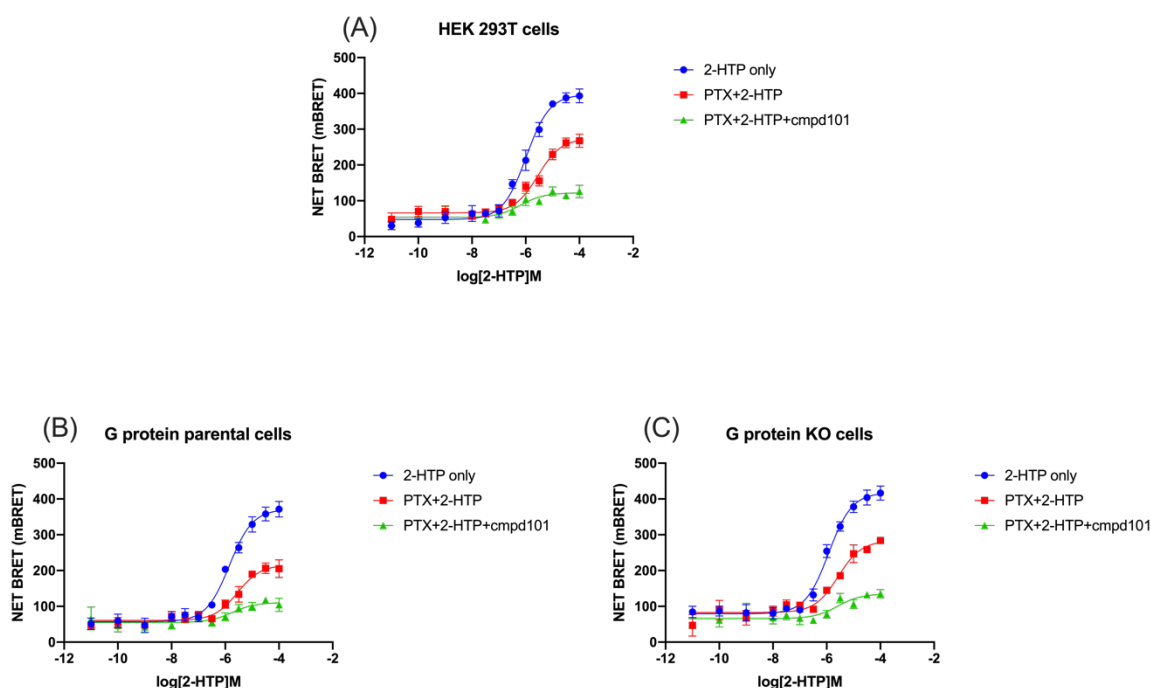
Figure 5.8 PTX partially and compound 101+PTX treatment largely blocks β-arrestin 2 recruitment to GPR84.
A) HEK293T cells, B) G protein parental cells and C) G protein KO cells were transiently transfected to express NLuc-tagged β-arrestin 2 with/without hGPR84-eYFP. Transfected cells were cultured in poly-D-lysine-coated 96-well plates with/without PTX overnight. Then cells were treated with 10 μM compound 101 or vehicle for 30mins before being incubated with Nano-Glo Luciferase substrate for 10mins. Subsequently, cells were incubated with 2-HTP for 5 mins and the endpoint BRET luminescence of eYFP and NLuc was measured using the PHERAstar FS plate reader at 535nm and 475nm respectively. Raw data baseline was adjusted to NLuc-ß-arrestin 2 control. Data presented as mean±SEM (n=3).

To study whether PTX affects the phosphorylation of GPR84, a western blot was applied using phospho-antiserum (optimized in *Chapter 4*). The anti-HA antiserum that detects the HA-tag was used as a control for the expression of HA-hGPR84. After doxycycline induction of HA-hGPR84 Flp-In TREx 293 cells, the anti-HA antiserum recognized the receptor in both the presence and absence of PTX (**Figure 5.9 A**). Phosphorylation-site specific antiserum pT263-pT264 and pS221-pS224 detected GPR84 phosphorylation in both the presence and absence of PTX (**Figure 5.9 B, C**). In conclusion, PTX cannot block the phosphorylation of GPR84 but can totally block the recruitment of GRK2/3 promoted by 2-HTP/DL-175. These results indicate that the phosphorylation of GPR84 can occur in a GRK2/3 independent manner.
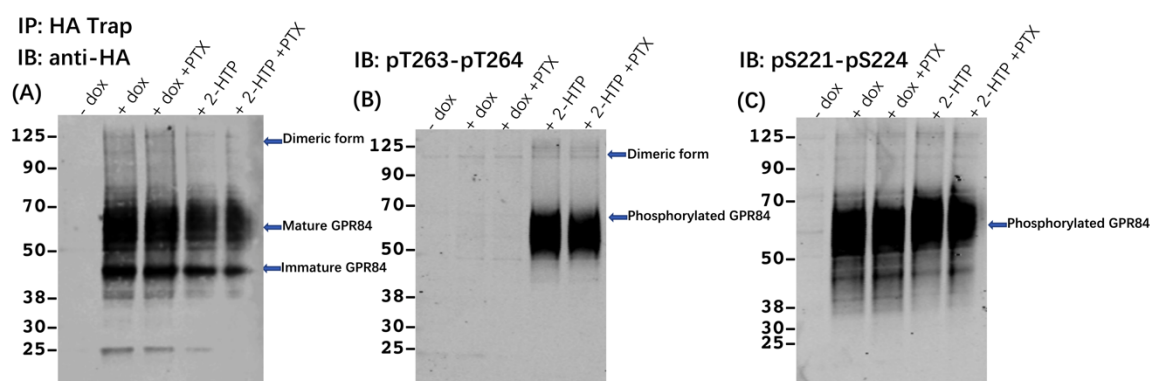
Figure 5.9 PTX does not affect the phosphorylation of GPR84 at pT263/pT264 and pS221/pS224.
Serum-starved Flp-In T-REx 293 stable cells without doxycycline induction or induced to express HA-hGPR84 were treated with vehicle/ vehicle + PTX/ 2-HTP /2-HTP+PTX before cell lysis in the presence of protease and phosphatase inhibitors. Lysates were enriched with HA-trap agarose and run on NuPAGE 4-12% Bis-Tris SDSPAGE gels. Proteins were subsequently transferred to nitrocellulose membranes, blocked with TBS with 5% (w/v) BSA and incubated overnight with A) rat anti-HA primary antibody (1:10,000), B) rabbit anti-GPR84-pT263/pT264 (1:2,000), C) rabbit anti-GPR84-pS221/pS224 (1:2,000). Membranes were finally incubated with goat anti-rat IRDye 800CW (1:10,000) or goat anti-rabbit IRDye 800CW (1:10,000) secondary antibodies, and visualised using the LI-COR Odyssey 9260 gel imaging system. Molecular mass of HA-hGPR84 is between 50-75 kDa. The figure is derived from a single experiment.

5.2.2 Studies on the internalization of GPR84

Based on previous studies that related to the phosphorylation of GPR84, receptor internalization was studied using a 'Bystander' BRET assay. In this assay, human GPR84-Nluc and mNeonGREEN-ZNF-FYVE were co-transfected into GRK parental 293 cells. The FYVE domain associates with phosphatidylinositol 3-phosphate [PtdIns(3)P] which is located on membranes of early endosomes (Raiborg et al.,

2001). If the receptor internalizes into early endosomes, the Nluc on the C-terminal of GPR84 will be in proximity to mNeonGreen on the membranes of early endosomes and then generate BRET which can be measured by a plate reader (**Figure 5.10**). The effects of G_i inhibitor PTX and/or GRK2/3 inhibitor compound 101 on the internalization of GPR84 were studied.
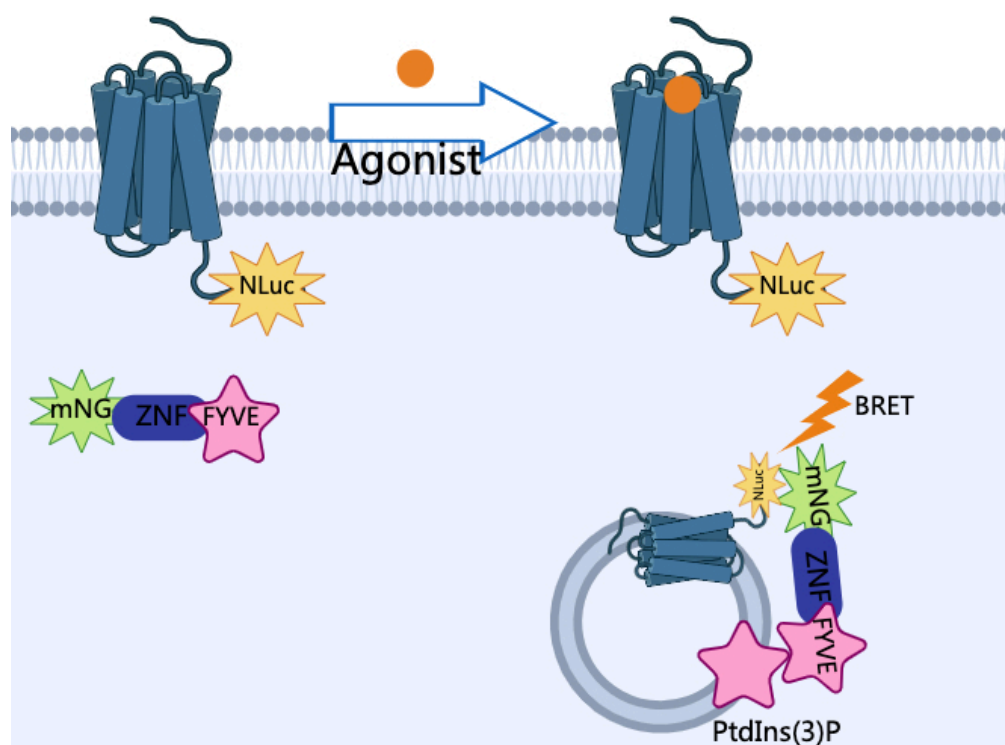
Figure 5.10 The principle of the internalization assay.
The N-terminal of human GPR84 was tagged with Nanoluciferase (NLuc), and the FYVE was tagged with mNeonGreen. After the binding of a suitable agonist ligand, the receptor will be phosphorylated, interact with an arrestin and potentially become internalized. If the receptor internalizes into the early endosomes, the mNeonGreen-ZNF-FYVE which binds to the PtdIns(3)P on the early endosomes will come into proximity with GPR84-NLuc and generate BRET that can be detected by a PHERAstar FS plate reader.

2-HTP induced internalization of GPR84 to the early endosomes in a concentration dependent manner (**Figure 5.11 A**). G protein inhibitor PTX decreased the speed and degree of GPR84 internalization and the GRK2/3 inhibitor compound 101 inhibited substantially the internalization of GPR84 to the point that internalization was almost completely prevented (**Figure 5.11 B C**). When PTX and compound 101 were used together, internalization was still blocked (**Figure 5.11 D**). A time point of 60mins after addition of 2-HTP was selected from graphs A, B, C and D, and agonist concentration-response curves generated (**Figure 5.11**

E). The result of this internalization assay is consistent with the findings related to β-arrestin 2 recruitment **(Figure 5.8)**.
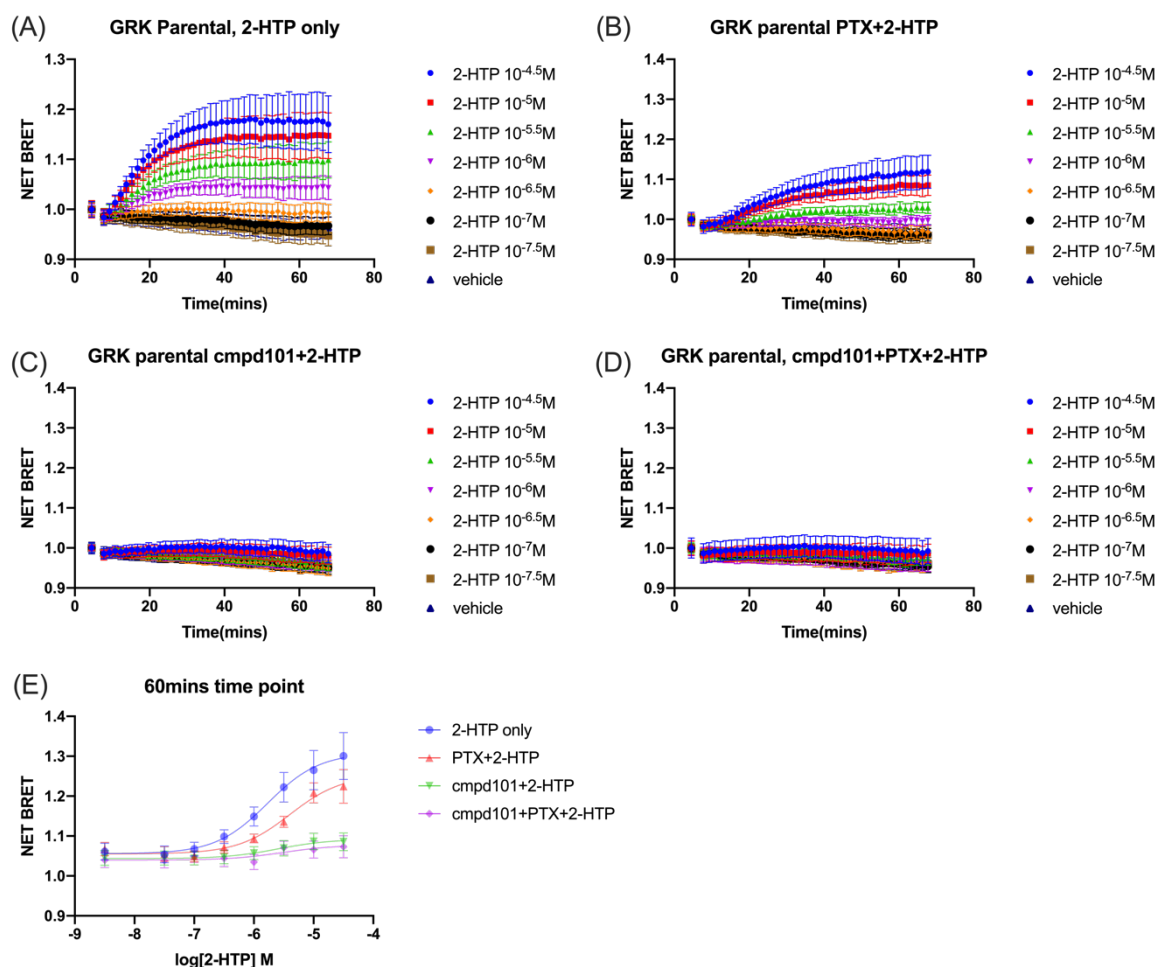
Figure 5.11 Time-dependent trafficking of GPR84 measured by 'Bystander' BRET.
GRK parental cells were transiently co-transfected with GPR84-NLuc and mNeonGreen-ZNF-FYVE. Transfected cells were cultured in poly-D-lysine-coated 96-well plates with or without PTX overnight. Then cells were treated with 10 µM compound 101 or vehicle for 30mins before being incubated with Nano-Glo Luciferase substrate for 10mins. Subsequently, cells were treated with different concentrations of 2-HTP for 1h. E) The 60 min time point was plotted separately to compare the extent of internalization in different conditions. Raw BRET ratios were measured by PHERAstar FS plate reader at 535nm and 475nm respectively. Data presented as mean±SEM (n=3).

Because previous studies showed that PSB-16671 cannot cause the recruitment of arrestin-3 to GPR84 (Marsango et al., 2022), whether this compound will promote the receptor trafficking to the early endosomes was studied. The movement of a receptor to the early endosomes normally happens after the recruitment of arrestins, and it is related to 'sustained signaling' **(Figure 1.6)**. To better understanding the signalling mechanisms of GPR84, studying the movement of GPR84 would be important. 2-HTP still induced internalization of GPR84 to the

early endosomes in a concentration dependent manner (**Figure 5.12 A**), which is a positive control of this experiment. PSB-16671 did not promote GPR84 internalize to the early endosomes (**Figure 5.12 B**). A time point of 30mins after addition of agonists was selected from graphs A and B to generate agonist concentration-response curves (**Figure 5.12 C**).
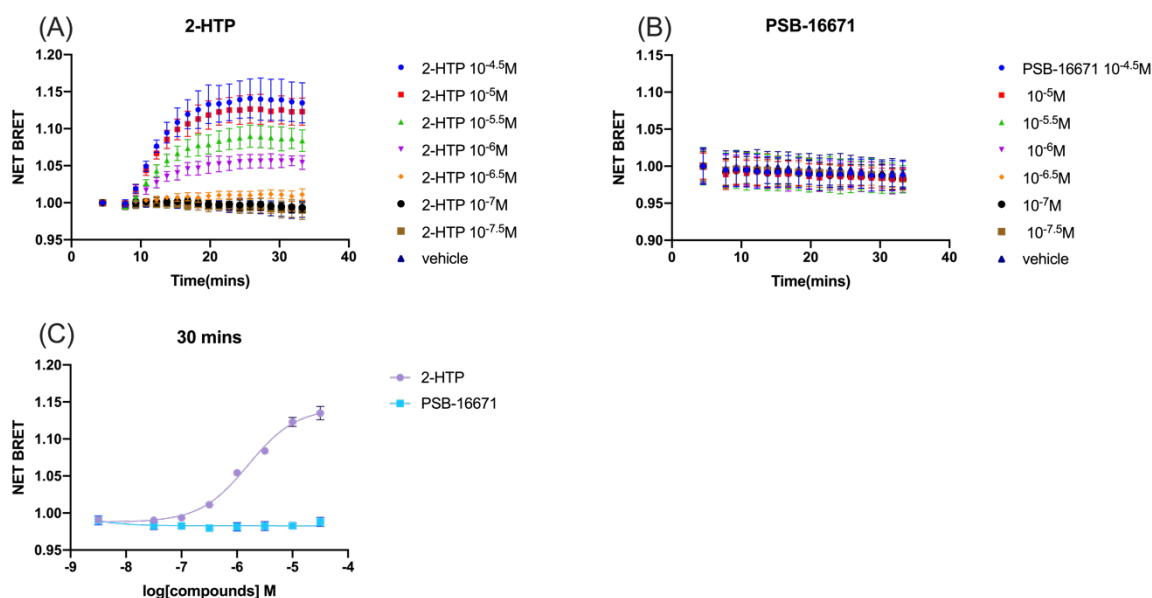
Figure 5.12 Time-dependent trafficking of GPR84 measured by 'Bystander' BRET.
GRK parental cells were transiently co-transfected with GPR84-NLuc and mNeonGreen-ZNF-FYVE. Transfected cells were cultured in poly-D-lysine-coated 96-well plates overnight. Then cells were incubated with Nano-Glo Luciferase substrate for 10mins. Subsequently, cells were treated with different concentrations of A) 2-HTP or B) PSB-16671 for 1h. C) The 30 min time point was plotted separately to compare the extent of internalization in different conditions. Raw BRET ratios were measured by PHERAstar FS plate reader at 535nm and 475nm respectively. Data presented as mean±SEM (n=3).

After using the Bystander assay to quantify the internalization of GPR84, immunocytochemical staining was used to visualize this progress. To apply the immunocytochemical staining, a new stable cell line expressing HA-HALO-human GPR84 was generated. It enables the tracking of GPR84 movement in live cells, rather than in fixed cells. Besides, the binding of HALO-Tag ligand to HALO-Tag is highly specific which minimizes the effects of non-specific binding. A cell-impermeant HALO-Tag ligand was used to label receptors on the surface membrane of live cells and HALO-Tag ligand dye was excited using the 488-nm laser line. Cells were always imaged at 0min and 5mins before treated with vehicle or ligands and these were used as a baseline. Then the movement of receptor was tracked for 30mins after treatment with ligands.

To ensure effective internalization (if this were to occur), the concentration of 2-HTP used in these assays was determined by calculating the EC_{90} concentration from the β-arrestin 2 recruitment assays. In contrast, the concentrations of DL-175 and PSB-16671, which do not promote effective interactions with β-arrestin 2, were set at 100 times EC_{90} from $[^{35}S]GTP\gamma S$ binding studies (Marsango et al., 2022). 1% DMSO was used as vehicle: this did not result in internalization of GPR84 (**Figure 5.13 A**). 2-HTP caused obvious internalization after 10min treatment, and the extent of internalization degree visually increased with time (**Figure 5.13 B**). DL-175 caused limited internalization treatment (**Figure 5.13 C**). whilst PSB-16671 promoted a limited degree of internalization of compared to 2-HTP (**Figure 5.13 D**). When comparing the images of treatment with 2-HTP and PSB-16671, it appeared that internalization caused by the orthosteric agonists and the allosteric agonist had different kinetics **(Figure 5.13 B, D)**. It is also possible that the receptor moved to different areas of the cells after activation with different agonists. Further studies will however need to be performed to provide support for this concept.

(A)

UT, 0 min. | UT, 5 min. | + Veh, 5 min. | + Veh, 10 min.

+ Veh, 15 min. | + Veh, 20 min. | + Veh, 25 min. | + Veh, 30 min.

25 µm

(B)

UT, 0 min. | UT, 5 min. | + 2-HTP 3.7 µM, 5 min. | + 2-HTP 3.7 µM, 10 min.

+ 2-HTP 3.7 µM, 15 min. | + 2-HTP 3.7 µM, 20 min. | + 2-HTP 3.7 µM, 25 min. | + 2-HTP 3.7 µM, 30 min.

25 µm

(C)

UT, 0 min. | UT, 5 min. | + DL-175, 98 µM, 5 min. | + DL-175, 98 µM, 10 min.

+ DL-175, 98 µM, 15 min. | + DL-175, 98 µM, 20 min. | + DL-175, 98 µM, 25 min. | + DL-175, 98 µM, 30 min.

(D)

UT, 0 min. | UT, 5 min. | + PSB-16671, 13 µM, 5 min. | + PSB-16671, 13µM, 10 min.

+ PSB-16671 µM, 15 min. | + PSB-16671, 13 µM, 20 min. | + PSB-16671, 13 µM, 25 min. | + PSB-16671, 13 µM, 30 min.

25 µm

Figure 5.13 Immunohistochemical detection of HA-HALO-hGPR84 internalization.
Flp-In T-REx 293 cells stably express HA-HALO human GPR84 were cultured on poly-D-lysine-coated 30-mm round coverslips in 6-well plates and incubated for 24 h at 37 °C. After that, a final concentration of 100ng/mL doxycycline was used to treat the cells overnight. Then cells were labelled with a HALOTag ligands labelled with Alexa Fluor 488 (1 mM, diluted 1:1000 in culture medium) for 15mins at 37 °C before washing twice with HBSS. Subsequently, coverslips were placed in a microscope chamber containing HBSS and images were acquired before and 15mins after agonist treatment using a Zeiss LSM 980 confocal equipped with a 63x/1.4 NA Plan Apochromat oil-immersion objective. HALO-Tag ligand dye was excited using the 488-nm laser line and the emission light was detected over the wavelength range 500 to 560 nm using a GaASP detector. 3D best focus z stacks were created using Metamorph software to visualise the degree of receptor protein internalization evoked for each treatment ligand. Representative images from n=3 experiments are shown.

Then we want to study the specific sites of GPR84 which will affect the internalization of it. Previous studies show that if the Arg 172 of GPR84 was mutated to Ala, 2-HTP cannot activate GPR84 while G_i biased agonist DL-175 could promote the recruitment of arrestin 3 to GPR84 (Marsango et al., 2022). Therefore, a stable cell line expressing HA-HALO-human GPR84-R172A was generated. It was found that the internalization of GPR84 caused by 2-HTP was totally blocked while DL-175 could result the internalization (**Figure 5.14**). Compare to the internalization of HA-HALO-hGPR84 induced by DL-175, the internalization of HA-HALO-hGPR84-R172A caused by DL-175 is faster and likely more extensive.
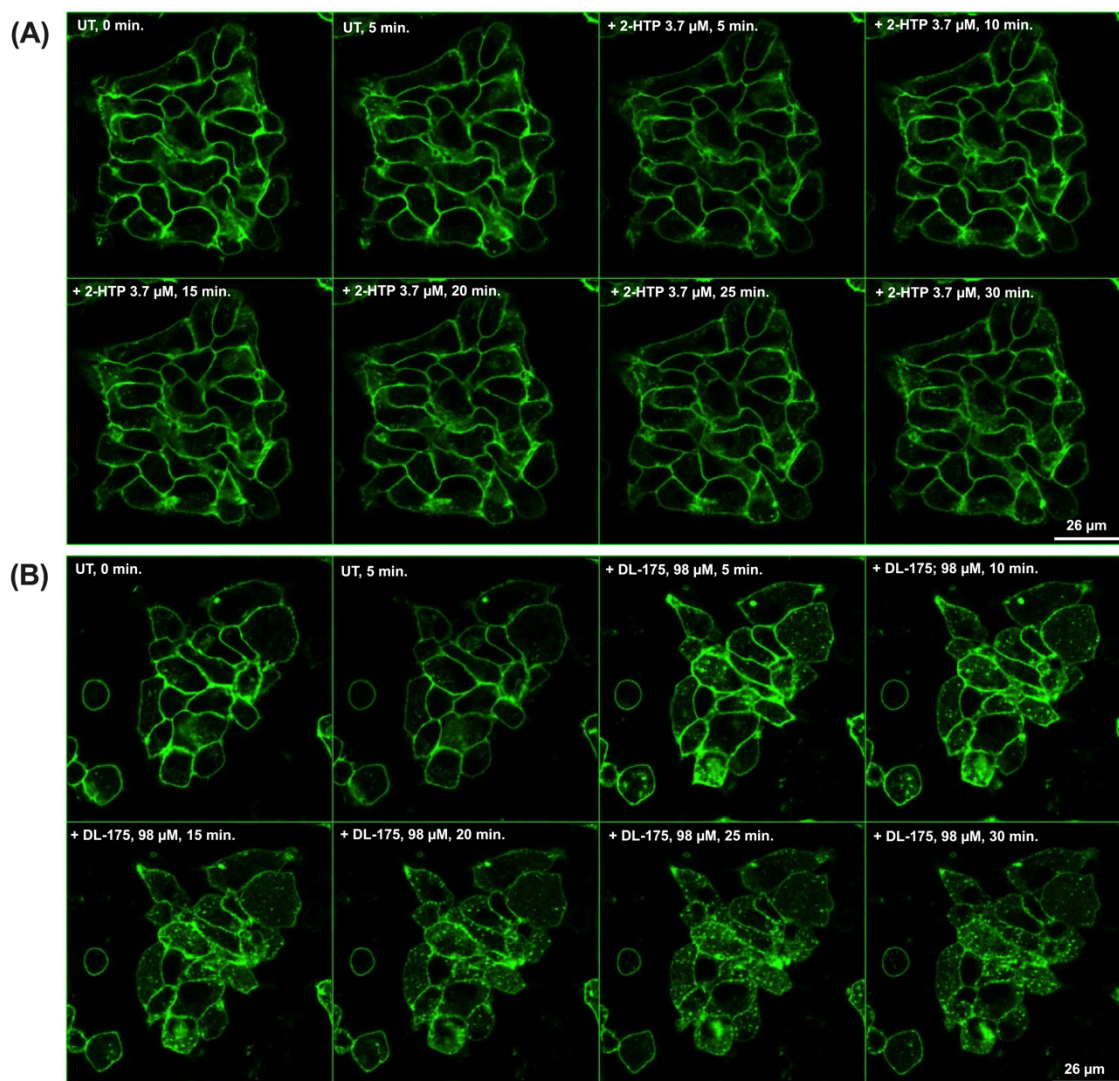
Figure 5.14 Immunohistochemical detection of HA-HALO-hGPR84-R172A internalization.
Flp-In T-REx 293 cells stably express HA-HALO human GPR84-R172A were cultured on poly-D-lysine-coated 30-mm round coverslips in 6-well plates and incubated for 24 h at 37 °C. After that, a final concentration of 100ng/mL doxycycline was used to treat the cells overnight. Then cells were labelled with a HALO-Tag ligands labelled with Alexa Fluor 488 (1 mM, diluted 1:1000 in culture medium) for 15mins at 37 °C before washing twice with HBSS. Subsequently, coverslips were placed in a microscope chamber containing HBSS and images were acquired before and 15mins after agonist treatment using a Zeiss LSM 980 confocal equipped with a 63x/1.4 NA Plan Apochromat oil-immersion objective. HALO-Tag ligand dye was excited using the 488-nm laser line and the emission light was detected over the wavelength range 500 to 560 nm using a GaASP detector. 3D best focus z stacks were created using Metamorph software to visualise the degree of receptor protein internalization evoked for each treatment ligand. Representative images from single experiment are shown.

5.3 Discussion

Alongside classical G-protein-mediated signaling, interactions with arrestins and potential "ß-arrestin–mediated signaling" can play an important role in receptor-mediated cellular function and physiology by regulating various steps including GPCR trafficking, desensitization and internalization. Following the activation of GPCRs, in many cases receptors are phosphorylated by G protein kinases which

can result in different functional consequences. To fully understand the signaling of the orphan receptor GPR84, studying the specific contribution of individual GRKs in GPR84 signaling is important. Also, studying the internalization after phosphorylation can help to better understand the movement of the receptor in cells.

Previous [^{32}P] incorporation assays showed that GPR84 agonists 2-HTP and 6-OAU promote the phosphorylation of GPR84 whereas DL-175 or PSB-16671 we unable to do so (Marsango et al., 2022). However, when using these four agonists to optimize the NanoBit GRK recruitment assay, it is found that all of them promoted recruitment of LgBit-GRK2. 2-HTP and 6-OAU are balanced orthosteric agonists which activate both G protein signalling and ß-arrestin recruitment. DL-175 is a Gi-biased orthosteric agonist and PSB-16671 is an allosteric agonist (Marsango et al., 2020). It is possible that agonists that bind at different sites of the receptor may lead to different conformational changes. Based on the 'phosphorylation barcode' theory (Tobin et al., 2008), GRK(s) should recognise the conformational changes and then produce a unique 'phosphorylation barcode'. If the recruited GRK cannot recognise the conformational changes, the following phosphorylation would not happen. However, further studies needed to prove this prediction. 2-HTP and DL-175 both enhanced recruitment of LgBit-GRK2/3 in a concentration-manner way neither improved the recruitment of LgBit-GRK5/6. The recruitment of LgBit-GRK2/3 by agonists 2-HTP/DL-175 was prevented with increasing concentration of the GPR84 orthosteric antagonist compound 020 indicating these effects of the agonists were indeed generated via the receptor. These two results proved that the recruitment of LgBit-GRK2/3 was caused by the binding between GPR84 and agonists 2-HTP or DL-175. Also, when DL-175 and PSB-16671 were used to activate HA-HALO-hGPR84, both of them caused the internalization of the receptor. Therefore, it is likely that these two compounds could promote GPR84 phosphorylation at sites we have never studied although the direct [^{32}P] incorporation assays do not really support it (Marsango et al., 2022).

GRK2/3 inhibitor compound 101 did not block the recruitment of GRK(s) but slightly increased that, and GRK5/6 inhibitor compound 19 did not promote or inhibit the recruitment of GRK5/6. However, earlier studies using immunoblotting showed that compound 101 blocks the phosphorylation of residues Thr263/Thr264 sites in GPR84 (*chapter 4*)(Marsango et al., 2022). In conclusion, compound 101 did not reduce the recruitment of GRK2/3 but blocked the phosphorylation of GPR84 probably which reflects the working principle of GRK inhibitors. GRK inhibitors normally block kinase activity to inhibit GPCR phosphorylation (Sulon and Benovic, 2021). Therefore, even though the relevant GRKs were recruited, the receptor cannot be phosphorylated by the inhibitor-bound inactive GRKs.

G_i signalling inhibitor PTX blocked the recruitment of GRK2/3 and did not promote the recruitment of GRK5/6. PTX also partially blocked the recruitment of β-arrestin 2 and partially blocked GPR84 internalization to the early endosomes. However, PTX cannot block GPR84 phosphorylation in the western blot using phospho-site specific antiserum. These results suggest that GPR84 may be phosphorylated independently of GRKs, or that the GRKs responsible for promoting GPR84 phosphorylation were not investigated in this chapter. Other work has indicated that for the β2AR receptor, the recruitment of β-arrestin 1 and β-arrestin 2 to β2AR in $G\alpha$s knock out cells are significantly decreased compared to that in the wild type cells, and Gαs protein dictates the GRK isoforms involved in ß-arrestin recruitment (Burghi et al., 2023). It is hence reasonable to predict that Gi is related to the recruitment of β-arrestin 2 and affects GRK selectivity for Gi-coupled receptors such as GPR84. Further studies needed to detect the relationship between G_i and GPR84 phosphorylation or internalization.

Previous studies showed that agonist PSB-16671 cannot mediate the recruitment of ß-arrestin 2 (Marsango et al., 2022) and cannot promote GPR84 internalization to the early endosomes. However, the immunocytochemical staining showed that allosteric agonist PSB-16671 may cause some internalization of GPR84 but this appeared to be distinct from the effect of 2-HTP and may hence be ß-arrestin independent. To study whether GPR84 internalization happens in a ß-arrestin

independent way, β-arrestins knock out cells could be generated to study this prediction.

Chapter 6   Final discussion

The GPCR family is a group of cell surface receptors that are involved in many physiological processes. Consequently, GPCRs have been a major focus as drug targets for decades, with approximately 34% of marketed drugs aimed at these receptors (Addis et al., 2024, Yang et al., 2021). However, there is still a lot of therapeutic potential of GPCRs that needs to be explored. Among them, pro-inflammatory orphan receptor GPR84 has been identified as a potential therapeutic target. Although the basal expression of GPR84 in immune cells is low, GPR84 transcript and expression are up regulated in many pro-inflammatory conditions (Marsango et al., 2020, Luscombe et al., 2020, Jenkins et al., 2021). Thus, blocking GPR84 could be a potential therapeutic approach for the treatment of inflammation-related and/or fibrosis-associated diseases such as ulcerative colitis, idiopathic pulmonary fibrosis, inflammatory bowel diseases (IBD) and chronic neuropathic pain (Marsango and Milligan, 2023, Marsango et al., 2020, Wang et al., 2023, Labéguère et al., 2020, Gagnon et al., 2018, Gaidarov et al., 2018). Regardless of these therapeutic possibilities, GPR84 is still identified as 'orphan' receptor as the possible endogenous ligands, medium-chain fatty acids 9 MCFAs), display modest potency in activating the receptor. Therefore, whether the concentrations of MCFAs under physiological conditions could activate the receptor still need to be further studied. Moreover, the model of GPR84-ligands interactions, the signalling pathways of GPR84 and the physiological functions of GPR84 are still poorly characterized.

To date, there is still a significant lack of GPR84 compounds from mouse model studies to in-human clinical trials. Although some potent synthetic agonists such as 2-HTP, 6-OAU, LY-237 and TUG-2099 have been published (Ieremias et al., 2024, Liu et al., 2016, Zhang et al., 2016, Suzuki et al., 2013), only limited GPR84 antagonists are available which consequently limits studies on the understanding of the pathophysiological roles of GPR84. Thus, searching for mouse GPR84 antagonists is necessary for understanding the function of GPR84 and developing potential treatments for inflammatory diseases. The most widely used GPR84 antagonist, GLPG1205, displayed a lower affinity at mouse GPR84 than at human GPR84 but it has not achieved positive primary clinical endpoints (Jenkins et al.,

2021, Marsango and Milligan, 2023). Therefore, differences in receptor affinity between species should be considered carefully when extrapolating preclinical findings to human contexts. One of the aims of this thesis is to test antagonists targeting both human and mouse GPR84 with similar affinity in pharmacological assays to study the model of GPR84-antagonist interactions. Compound 271 was characterized as a competitive orthosteric antagonist for both human GPR84 and mouse GPR84, displaying 10 times lower affinity at mouse GPR84. A molecular docking study was carried out in attempt to study the binding modes of GPR84 antagonists. The human GPR84 structure was generated by the AlphaFold deep learning algorithm, and it has been used effectively in previous docking of agonists (Marsango et al., 2022). In the cryo-EM structures and mutagenesis studies, Arg172 within the ECL2 of GPR84 is an important residue that interact with orthosteric agonists (Zhang et al., 2023b, Liu et al., 2023, Al Mahmud et al., 2017). A construct in which Arg172 was altered to Ala was generated, and compound 271 targeting this mutant did not display significantly different affinity compared to wild type GPR84. Therefore, compound 271 probably not interact with residue Arg172 of GPR84. However, the potency of 2-HTP and LY-237 (similar to TUG-2097 in *Chapter 3*) were reduced targeting this mutant compared to WT GPR84 (Marsango et al., 2022, Liu et al., 2023, Al Mahmud et al., 2017), which means that these two orthosteric agonists interact with residue Arg172 of GPR84. Thus, even though antagonist compound 271 is competitive to orthosteric agonists of GPR84, they probably do not bind to the same residues. Further studies on the binding pocket of GPR84 antagonists would be a good method to solve the problem of lacking tool GPR84 antagonists.

It is generally agreed that animal models are powerful tools in understanding the pharmacology of a GPCR. As discussed in *Chapter 1*, GPR84 plays a role in mediating inflammatory responses and blocking GPR84 could be a therapeutic strategy to treat inflammation-related diseases. The lower affinity of antagonists at mouse GPR84 than human GPR84 has presented a challenge in studying the pharmacology and functions of GPR84 in mouse models (Marsango et al., 2020, Jenkins et al., 2021, Marsango and Milligan, 2023). Screening novel mouse GPR84 antagonists and studying the binding mode of available antagonists would be the direct way to fill this gap. However, this research approach requires a lot of time.

Therefore, generating a chimeric construct or even mouse line that displays "human orthologue-like" pharmacology and can be blocked by available GPR84 antagonists could be a more time-saving method. Following the studies from Jenkins et al. (2021), stable cells induced to express HA-humanised GPR84 (HA-hmGPR84), HA-human GPR84 (HA-hGPR484) and HA-mouse GPR84 (HA-mGPR84) were generated and characterized using each of the cAMP assays, radioligand binding assays and immunoblotting. Encouragingly, human GPR84 species selective antagonists compound 020, compound 140 and compound 837 could block the activation of HA-hmGPR84 induced by 2-HTP, and the ability of these antagonists to block HA-hGPR84 and HA-hmGPR84 was similar, which is consistent with the results in (Jenkins et al., 2021). In order to use antiserum to identify the existence and the phosphorylation of HA-hmGPR84 in *ex vivo* studies in the future, the characterization of two phosphosite-specific antiserum and two GPR84 structural antiserum was applied. However, phosphosite-specific antiserum pS221-pS224 and structural antiserum GPR84(7TM) were found to detect phosphorylation and the presence of HA-hGPR84, but not HA-hmGPR84. These results suggest that although chimeric construct HA-hmGPR84 displays similar pharmacology to HA-hGPR84, the differences between them still need to be considered carefully.

In addition to characterizing novel GPR84 antagonists for drug discovery and generating 'chimeric' constructs for pre-clinical models, basic research around GPR84 signalling also need to be improved. Phosphorylation is an important process of GPCR signalling which is normally followed by the desensitization and internalization of receptors, and these signalling processes could be regulated by GRKs (Tobin et al., 2008, Gurevich et al., 2012, Marsango and Milligan, 2023). Thus, studying which GRK(s) might be involved in GPR84 signalling pathway and how the GRKs respond to the pharmacology of GPR84 is important for further understanding the signalling of the receptor. Previous studies found that balanced agonists 2-HTP or 6-OAU resulted in GPR84 phosphorylation which is detected by the incorporation of $[^{32}P]$ (from $[^{32}P]$ATP) but G_i-biased agonist DL-175 or allosteric agonist PSB-16671 could not promote GPR84 phosphorylation in this assay. Immunoblotting results using GRK2 and GRK3 inhibitor, compound 101, have revealed that GRK2 and/or GRK3 are related to GPR84 phosphorylation (Marsango et al., 2022). Inhibitor studies also have highlighted a crucial role for GRK2 family

kinases in regulating GPR84 in human neutrophils (Fredriksson et al., 2022). On the basis of these findings, 2-HTP and DL-175 were selected as representative compounds in NanoBit assays to detect the recruitment of GRKs to the receptor using GRKs knock out cells (*Chapter 5*). Both balanced agonist 2-HTP and G_i-biased agonist DL-175 promoted the recruitment of GRK2 and GRK3 but did not cause GRK5 and GRK6 recruitment. The recruitment of GRK2/3 caused by agonists can be reduced by GPR84 antagonists. These results indicate that GRK2 and GRK3 are likely to be involved in GPR84 phosphorylation stimulated by agonists. Interestingly, the G_i-biased agonist DL-175 improved GRK2/3 recruitment but cannot improve β-arrestins recruitment and GPR84 phosphorylation (Marsango et al., 2022) as well as GPR84 internalization. It has been discovered that biased ligands can achieve unique signalling outcomes by influencing the range of receptor conformations (Gurevich and Gurevich, 2020, Wingler and Lefkowitz, 2020). In the case of GPR84, it is probably because the conformational changes of GPR84 caused by DL-175 binding cannot be recognized by recruited GRK2/3. If recruited GRKs cannot phosphorylate GPR84, the following β-arrestins recruitment should not happen ('phosphorylation barcode' theory) (Tobin, 2008). This prediction still needs to be proved by further studies on GPR84 structures and GPR84 conformational changes.

Although compound 101 block the activity of GRK2 and GRK3 (Sulon and Benovic, 2021), it did not reduce the recruitment of these GRKs. However, immunoblotting studies showed that compound 101 blocked the phosphorylation of residues Thr263/Thr264 sites in GPR84 activated by 2-HTP (Marsango et al., 2022), and almost totally block GPR84 internalization to the early endosomes. However, compound 101 did not completely prevent the recruitment of arrestin 3. These results suggest that GPR84 probably could be phosphorylated without the involvement of GRKs, or arrestin 3 can recruit to active but non-phosphorylated GPR84. Although these results are not in line with the classical mechanism that β-arrestins are recruited to GPCR phosphorylated by GRKs, there are evidence that arrestins can bind to non-phosphorylated receptors through specific interaction interfaces. Studies on D2 receptors showed that GRK phosphorylation within ICL3 does not seem to be required for the arrestin 3 binding (Namkung et al., 2009). In

contrast, GRK phosphorylation within the ICL3 of M2 muscarinic receptor is necessary for the arrestin binding (Lee et al., 2000). As both constitutive and agonist-regulated phosphorylation sites of human GPR84 are present within IL3, it is reasonably to predict that the recruitment and binding of arrestin 3 to the receptor do not rely on GPR84 phosphorylation although the functions of arrestin 3 recruitment to GPR84 still need to be explored.

Gi signalling inhibitor PTX blocked GRK2/3 recruitment but cannot block GPR84 phosphorylation at sites pT263-pT264 and pS221-pS224. Moreover, PTX only partially block arrestin 3 recruitment to GPR84 and partially block the internalization of GPR84 to the early endosomes. These results indicate that GPR84 probably could be phosphorylated without the involvement of GRKs, or that the GRKs involved in promoting GPR84 phosphorylation were not explored in this thesis. However, previous results showed that GRK2/3 are necessary for the phosphorylation at sites pT263-pT264 (Marsango et al., 2022) and GPR84 internalization to the early endosomes. Therefore, it is likely that $G\alpha_i$ influences the GRK subtypes that phosphorylate GPR84, or there may be other effectors capable of phosphorylating GPR84 when Gαi is inhibited. In the case of β2AR receptor, the recruitment of β-arrestin 1 and β-arrestin 2 to β2AR in $G\alpha_s$ knock out cells are significantly decreased compared to that in the wild type cells, and $G\alpha_s$ protein dictates the GRK isoforms involved in β-arrestin recruitment (Burghi et al., 2023). Although the recruitment of GRK5/6 were not detected in the presence of PTX, this probably because of the membrane-anchored localization of GRK5/6 which could constitutively interact with the receptor (Palmer et al., 2022). This hypothesis should be better studied in the future with more sensitive and specific approaches to determine the role of G_i in GPR84 phosphorylation and the relationship between G protein and GRK isoforms selectivity.

Following GPR84 phosphorylation, the internalization of this receptor was also studied because receptor internalization is considered as one of the important processes in GPCR regulation (Moller et al., 2024, Calebiro and Godbole, 2018, Ferguson, 2001). BRET-based 'Bystander' assays were utilized to detect the internalization of GPR84 to the early endosomes. Although the internalization of

GPR84 caused by embelin and 2-HTP has been reported (Gaidarov et al., 2018, Marsango et al., 2022, Zhang et al., 2016), the location where the receptor internalizes within the cell remains unclear. The results in *Chapter 5* showed that 2-HTP promoted the internalization of GPR84 to the early endosomes in a concentration dependent manner, while PSB-16671 did not have such effects. This result is consistent with the published result that 2-HTP caused GPR84 phosphorylation while PSB-16671 did not (Marsango et al., 2022). The limitation of this assay is whether GPR84 internalization via other organelles cannot be detected. To visualize the whole process of GPR84 internalization, a series of immunocytochemical staining experiments were performed using characterized phosphosite-sepecific antiserum pT263/pT264 in HA-hmGPR84 stable cells. These images illustrate colocalization of anti-pT263/pT264 and anti-HA, which reflected the distribution of phosphorylated GPR84. It was obvious that 2-HTP phosphorylated GPR84 on cell membranes decreased while the staining of phosphorylated GPR84 in intracellular areas increased in a time-dependent pattern. Similarly, antagonist compound 140 and compound 020 also regulate GPR84 phosphorylation in a time-dependent way. The limitations of these series of images is that the colocalization of these two antiserum in intracellular regions was not observed, and the anti-serum pT263/pT264 displayed strong nucleus staining even in cells that have not been induced to express. To overcome these limitations and tracking the process of GPR84 internalization for longer time, a cell line stably expressing HA-HALO-human GPR84 was generated for immunocytochemical staining in which the HALO ligand bound is highly specific and can be applied in live cells. 2-HTP caused GPR84 internalization rapidly in a time-dependent way, and Arg172 of GPR84 is necessary for this process which is consistent with previous results. Long-term treatment of DL-175 causeed GPR84 internalization, while the internalization of mutant HA-HALO-hGPR84-R172A caused by DL-175 was quicker than wild type (Marsango et al., 2022, Al Mahmud et al., 2017). However, PSB-16671, which did not significantly promote the interaction between arrestin 3 and GPR84, still caused the internalization of GPR84 (Marsango et al., 2022). This result shows that GPR84 internalization could happen in arrestin-independent pathways. Similar results were also observed by other groups (Peters et al., 2020, Luscombe et al., 2023). Although GPCR internalization is typically associated with arrestins binding to phosphorylated receptors, there are many examples of arrestin-independent GPCR internalization

upon agonist stimulation through alternative mechanisms (Moo et al., 2021). The alternative mediators could be caveolae and endophilin. However, the mechanisms of GPR84 internalization still need to be further studied.

In conclusion, the novel compounds and tools characterized in this thesis have the potential to make contributions to the studies on GPR84. By screening novel antagonists targeting both human and mouse GPR84 with similar affinity and docking antagonists to the receptor, the problem of lacking tool compounds in mouse model studies can be overcome. By characterizing HA-humanised construct which displayed 'human orthologue-like' pharmacology would be helpful further understanding functions of blocking GPR84 in mouse models. In addition, understandings on the mechanism of GPR84 phosphorylation and internalization provide fundamental knowledge for further research on GPR84.

References

ABDEL-AZIZ, H., SCHNEIDER, M., NEUHUBER, W., MEGUID KASSEM, A., KHAILAH, S., MULLER, J., GAMAL ELDEEN, H., KHAIRY, A., M, T. K., SHCHERBAKOVA, A., EFFERTH, T. & ULRICH-MERZENICH, G. 2016. GPR84 and TREM-1 Signaling Contribute to the Pathogenesis of Reflux Esophagitis. *Mol Med,* 21, 1011-1024.

ADDIS, P., BALI, U., BARON, F., CAMPBELL, A., HARBORNE, S., JAGGER, L., MILNE, G., PEARCE, M., ROSETHORNE, E. M., SATCHELL, R., SWIFT, D., YOUNG, B. & UNITT, J. F. 2024. Key aspects of modern GPCR drug discovery. *SLAS Discov,* 29, 1-22.

AL MAHMUD, Z., JENKINS, L., ULVEN, T., LABEGUERE, F., GOSMINI, R., DE VOS, S., HUDSON, B. D., TIKHONOVA, I. G. & MILLIGAN, G. 2017. Three classes of ligands each bind to distinct sites on the orphan G protein-coupled receptor GPR84. *Sci Rep,* 7, 17953.

ALEXANDER, S. P. H., CHRISTOPOULOS, A., DAVENPORT, A. P., KELLY, E., MARRION, N. V., PETERS, J. A., FACCENDA, E., HARDING, S. D., PAWSON, A. J., SHARMAN, J. L., SOUTHAN, C. & DAVIES, J. A. 2017. THE CONCISE GUIDE TO PHARMACOLOGY 2017/18: G protein – coupled receptors. *British Journal of Pharmacology,* 174.

ALVAREZ-CURTO, E. & MILLIGAN, G. 2016. Metabolism meets immunity: The role of free fatty acid receptors in the immune system. *Biochem Pharmacol,* 114, 3-13.

ARSHAVSKY, V. Y., LAMB, T. D. & PUGH, E. N., JR. 2002. G proteins and phototransduction. *Annu Rev Physiol,* 64, 153-87.

AUDOY-REMUS, J., BOZOYAN, L., DUMAS, A., FILALI, M., LECOURS, C., LACROIX, S., RIVEST, S., TREMBLAY, M. E. & VALLIERES, L. 2015. GPR84 deficiency reduces microgliosis, but accelerates dendritic degeneration and cognitive decline in a mouse model of Alzheimer's disease. *Brain Behav Immun,* 46, 112-20.

BENOVIC, J. L. 2021. Historical Perspective of the G Protein-Coupled Receptor Kinase Family. *Cells,* 10.

BOUCHARD, C., PAGE, J., BEDARD, A., TREMBLAY, P. & VALLIERES, L. 2007. G protein-coupled receptor 84, a microglia-associated protein expressed in neuroinflammatory conditions. *Glia,* 55, 790-800.

BRISCOE, C. P., TADAYYON, M., ANDREWS, J. L., BENSON, W. G., CHAMBERS, J. K., EILERT, M. M., ELLIS, C., ELSHOURBAGY, N. A., GOETZ, A. S., MINNICK, D. T., MURDOCK, P. R., SAULS, H. R., JR., SHABON, U., SPINAGE, L. D., STRUM, J. C., SZEKERES, P. G., TAN, K. B., WAY, J. M., IGNAR, D. M., WILSON, S. & MUIR, A. I. 2003. The orphan G protein-coupled receptor GPR40 is activated by medium and long chain fatty acids. *J Biol Chem,* 278, 11303-11.

BURGHI, V., PARADIS, J. S., OFFICER, A., ADAME-GARCIA, S. R., WU, X., MATTHEES, E. S. F., BARSI-RHYNE, B., RAMMS, D. J., CLUBB, L., ACOSTA, M., TAMAYO, P., BOUVIER, M., INOUE, A., VON ZASTROW, M., HOFFMANN, C. & GUTKIND, J. S. 2023. Gαs is dispensable for ß-arrestin coupling but dictates GRK selectivity and is predominant for gene expression regulation by ß2-adrenergic receptor. *Journal of Biological Chemistry,* 299.

CALEBIRO, D. & GODBOLE, A. 2018. Internalization of G-protein-coupled receptors: Implication in receptor function, physiology and diseases. *Best Pract Res Clin Endocrinol Metab,* 32, 83-91.

CALEBIRO, D., NIKOLAEV, V. O., GAGLIANI, M. C., DE FILIPPIS, T., DEES, C., TACCHETTI, C., PERSANI, L. & LOHSE, M. J. 2009. Persistent cAMP-signals triggered by internalized G-protein-coupled receptors. *PLoS Biol,* 7, e1000172.

CARPENTIER, Y. A., PORTOIS, L. & MALAISSE, W. J. 2006. n-3 fatty acids and the metabolic syndrome. *Am J Clin Nutr,* 83, 1499S-1504S.

CARRONI, M. & SAIBIL, H. R. 2016. Cryo electron microscopy to determine the structure of macromolecular complexes. *Methods,* 95, 78-85.

CHEN, C. J., JIANG, C., YUAN, J., CHEN, M., CUYLER, J., XIE, X. Q. & FENG, Z. 2022a. How Do Modulators Affect the Orthosteric and Allosteric Binding Pockets? *ACS Chem Neurosci,* 13, 959-977.

CHEN, L. H., ZHANG, Q., XIAO, Y. F., FANG, Y. C., XIE, X. & NAN, F. J. 2022b. Phosphodiesters as GPR84 Antagonists for the Treatment of Ulcerative Colitis. *J Med Chem,* 65, 3991-4006.

CHENG, L., SUN, S., WANG, H., ZHAO, C., TIAN, X., LIU, Y., FU, P., SHAO, Z., CHAI, R. & YAN, W. 2023. Orthosteric ligand selectivity and allosteric probe dependence at Hydroxycarboxylic acid receptor HCAR2. *Signal Transduct Target Ther,* 8, 364.

CONN, P. J., CHRISTOPOULOS, A. & LINDSLEY, C. W. 2009. Allosteric modulators of GPCRs: a novel approach for the treatment of CNS disorders. *Nat Rev Drug Discov,* 8, 41-54.

DEBBURMAN, S. K., PTASIENSKI, J., BOETTICHER, E., LOMASNEY, J. W., BENOVIC, J. L. & HOSEY, M. M. 1995. Lipid-mediated regulation of G protein-coupled receptor kinases 2 and 3. *J Biol Chem,* 270, 5742-7.

DEN BESTEN, G., VAN EUNEN, K., GROEN, A. K., VENEMA, K., REIJNGOUD, D. J. & BAKKER, B. M. 2013. The role of short-chain fatty acids in the interplay between diet, gut microbiota, and host energy metabolism. *J Lipid Res,* 54, 2325-40.

DEWIRE, S. M., AHN, S., LEFKOWITZ, R. J. & SHENOY, S. K. 2007. Beta-arrestins and cell signaling. *Annu Rev Physiol,* 69, 483-510.

DINGUS, J., WELLS, C. A., CAMPBELL, L., CLEATOR, J. H., ROBINSON, K. & HILDEBRANDT, J. D. 2005. G Protein ßγ Dimer Formation: Gß and Gγ Differentially Determine Efficiency of in Vitro Dimer Formation. *Biochemistry* Biochemistry 2005, 44, 35, 11882–11890.

DONG, C., FILIPEANU, C. M., DUVERNAY, M. T. & WU, G. 2007. Regulation of G protein-coupled receptor export trafficking. *Biochim Biophys Acta,* 1768, 853-70.

DU TOIT, E., BROWNE, L., IRVING-RODGERS, H., MASSA, H. M., FOZZARD, N., JENNINGS, M. P. & PEAK, I. R. 2018. Effect of GPR84 deletion on obesity and diabetes development in mice fed long chain or medium chain fatty acid rich diets. *Eur J Nutr,* 57, 1737-1746.

EISHINGDRELO, H., SUN, W., LI, H., WANG, L., EISHINGDRELO, A., DAI, S., MCKEW, J. C. & ZHENG, W. 2015. ERK and beta-arrestin interaction: a converging point of signaling pathways for multiple types of cell surface receptors. *J Biomol Screen,* 20, 341-9.

FERGUSON, S. S. 2001. Evolving concepts in G protein-coupled receptor endocytosis: the role in receptor desensitization and signaling. *Pharmacol Rev,* 53, 1-24.

FORD, C. E., SKIBA, N. P., BAE, H., DAAKA, Y., REUVENY, E., SHEKTER, L. R., ROSAL, R., WENG, G., YANG, C.-S., IYENGAR, R., MILLER, R. J., JAN, L. Y., LEFKOWITZ, R. J. & HAMM, H. E. 1998. Molecular basis for interactions of G protein ßγ subunits with effectors. *Science,* 280 (5367), 1271-1274.

FREDRIKSSON, J., HOLDFELDT, A., MARTENSSON, J., BJORKMAN, L., MOLLER, T. C., MULLERS, E., DAHLGREN, C., SUNDQVIST, M. & FORSMAN, H. 2022. GRK2 selectively attenuates the neutrophil NADPH-oxidase response triggered by beta-arrestin recruiting GPR84 agonists. *Biochim Biophys Acta Mol Cell Res,* 1869**,** 119262.

FREDRIKSSON, R., LAGERSTROM, M. C., LUNDIN, L. G. & SCHIOTH, H. B. 2003. The G-Protein-Coupled Receptors in the Human Genome
Form Five Main Families. Phylogenetic Analysis, Paralogon
Groups, and Fingerprints. *Phylogenetic analysis, paralogon groups, and fingerprints. Mol. Pharmacol. 63, 1256-1272.*

FRIESNER, R. A., JAY L BANKS, ROBERT B MURPHY, THOMAS A HALGREN, JASNA J KLICIC, DANIEL T MAINZ, MATTHEW P REPASKY, ERIC H KNOLL, MEE SHELLEY, JASON K PERRY, DAVID E SHAW, PERRY FRANCIS & SHENKIN, P. S. 2004. Glide: A new approach for rapid, accurate docking and scoring. 1. Method and assessment of docking accuracy. *J. Med. Chem.,* 47:1739–1749.

FUJITA, T., MATSUOKA, T., HONDA, T., KABASHIMA, K., HIRATA, T. & NARUMIYA, S. 2011. A GPR40 agonist GW9508 suppresses CCL5, CCL17, and CXCL10 induction in keratinocytes and attenuates cutaneous immune inflammation. *J Invest Dermatol,* 131**,** 1660-7.

GAGNON, L., LEDUC, M., THIBODEAU, J. F., ZHANG, M. Z., GROUIX, B., SARRA-BOURNET, F., GAGNON, W., HINCE, K., TREMBLAY, M., GEERTS, L., KENNEDY, C. R. J., HEBERT, R. L., GUTSOL, A., HOLTERMAN, C. E., KAMTO, E., GERVAIS, L., OUBOUDINAR, J., RICHARD, J., FELTON, A., LAVERDURE, A., SIMARD, J. C., LETOURNEAU, S., CLOUTIER, M. P., LEBLOND, F. A., ABBOTT, S. D., PENNEY, C., DUCEPPE, J. S., ZACHARIE, B., DUPUIS, J., CALDERONE, A., NGUYEN, Q. T., HARRIS, R. C. & LAURIN, P. 2018. A Newly Discovered Antifibrotic Pathway Regulated by Two Fatty Acid Receptors: GPR40 and GPR84. *Am J Pathol,* 188**,** 1132-1148.

GAIDAROV, I., ANTHONY, T., GATLIN, J., CHEN, X., MILLS, D., SOLOMON, M., HAN, S., SEMPLE, G. & UNETT, D. J. 2018. Embelin and its derivatives unravel the signaling, proinflammatory and antiatherogenic properties of GPR84 receptor. *Pharmacol Res,* 131**,** 185-198.

GENEROSO, J. S., GIRIDHARAN, V. V., LEE, J., MACEDO, D. & BARICHELLO, T. 2021. The role of the microbiota-gut-brain axis in neuropsychiatric disorders. *Braz J Psychiatry,* 43**,** 293-305.

GOODMANJR, O. B., KRUPNICK, J. G., SANTINI, F., GUREVICH, V. V., PENN, R. B., GAGNON, A. W., KEEN, J. H. & BENOVIC, J. L. 1996. ß-Arrestin acts as a clathrin adaptor in endocytosis of the ß2-adrenergic recepto. *Nature,* 383, 447–450.

GRUNDMANN, M., MERTEN, N., MALFACINI, D., INOUE, A., PREIS, P., SIMON, K., RUTTIGER, N., ZIEGLER, N., BENKEL, T., SCHMITT, N. K., ISHIDA, S., MULLER, I., REHER, R., KAWAKAMI, K., INOUE, A., RICK, U., KUHL, T., IMHOF, D., AOKI, J., KONIG, G. M., HOFFMANN, C., GOMEZA, J., WESS, J. & KOSTENIS, E. 2018. Lack of beta-arrestin signaling in the absence of active G proteins. *Nat Commun,* 9**,** 341.

GUO, S., ZHAO, T., YUN, Y. & XIE, X. 2022. Recent progress in assays for GPCR drug discovery. *Am J Physiol Cell Physiol,* 323**,** C583-C594.

GUREVICH, E. V. & GUREVICH, V. V. 2006. Arrestins: ubiquitous regulators of cellular signaling pathways. *Genome Biol,* 7**,** 236.

GUREVICH, E. V., TESMER, J. J., MUSHEGIAN, A. & GUREVICH, V. V. 2012. G protein-coupled receptor kinases: more than just kinases and not only for GPCRs. *Pharmacol Ther,* 133**,** 40-69.

GUREVICH, V. V. & GUREVICH, E. V. 2019. GPCR Signaling Regulation: The Role of GRKs and Arrestins. *Front Pharmacol,* 10**,** 125.

GUREVICH, V. V. & GUREVICH, E. V. 2020. Biased GPCR signaling: Possible mechanisms and inherent limitations. *Pharmacol Ther,* 211**,** 107540.

GURWITZ, D., HARING, R., HELDMAN, E., FRASER, C. M., MANOR, D. & FISHER, A. 1994. Discrete activation of transduction pathways associated with acetylcholine m1 receptor by several muscarinic ligands. *European Journal of Pharmacology: Molecular Pharmacology,* 267(1), 21-31.

HAKAK, Y., UNETT, D. J., GATLIN, J. & LIAW, C. W. 2007. Human G protein-coupled receptor and modulators thereof for the treatment of atherosclerosis and atherosclerotic disease and for the treatment of conditions related to MCP-1 expression. *International patent application.,* WO/2007/027661.

HAMANN, J., AUST, G., ARAC, D., ENGEL, F. B., FORMSTONE, C., FREDRIKSSON, R., HALL, R. A., HARTY, B. L., KIRCHHOFF, C., KNAPP, B., KRISHNAN, A., LIEBSCHER, I., LIN, H. H., MARTINELLI, D. C., MONK, K. R., PEETERS, M. C., PIAO, X., PROMEL, S., SCHONEBERG, T., SCHWARTZ, T. W., SINGER, K., STACEY, M., USHKARYOV, Y. A., VALLON, M., WOLFRUM, U., WRIGHT, M. W., XU, L., LANGENHAN, T. & SCHIOTH, H. B. 2015. International Union of Basic and Clinical Pharmacology. XCIV. Adhesion G protein-coupled receptors. *Pharmacol Rev,* 67**,** 338-67.

HAN, B., SALITURO, F. G. & BLANCO, M. J. 2020. Impact of Allosteric Modulation in Drug Discovery: Innovation in Emerging Chemical Modalities. *ACS Med Chem Lett,* 11**,** 1810-1819.

HAUSER, A. S., ATTWOOD, M. M., RASK-ANDERSEN, M., SCHIOTH, H. B. & GLORIAM, D. E. 2017. Trends in GPCR drug discovery: new agents, targets and indications. *Nat Rev Drug Discov,* 16**,** 829-842.

HE, X., NI, D., LU, S. & ZHANG, J. 2019. Characteristics of Allosteric Proteins, Sites, and Modulators. *In: Zhang, J., Nussinov, R. (eds) Protein Allostery in Drug Discovery. Advances in Experimental Medicine and Biology,,* 1163.

HEO, L. & FEIG, M. 2022. Multi-state modeling of G-protein coupled receptors at experimental accuracy. *Proteins,* 90**,** 1873-1885.

HICKS, C., GARDNER, J., EIGER, D. S., CAMARDA, N. D., PHAM, U., DHAR, S., RODRIGUEZ, H., CHUNDI, A. & RAJAGOPAL, S. 2024. ACKR3 Proximity Labeling Identifies Novel G protein- and beta-arrestin-independent GPCR Interacting Proteins. *bioRxiv*.

HIDALGO, M. A., CARRETTA, M. D. & BURGOS, R. A. 2021. Long Chain Fatty Acids as Modulators of Immune Cells Function: Contribution of FFA1 and FFA4 Receptors. *Front Physiol,* 12**,** 668330.

HO, J. D., CHAU, B., RODGERS, L., LU, F., WILBUR, K. L., OTTO, K. A., CHEN, Y., SONG, M., RILEY, J. P., YANG, H. C., REYNOLDS, N. A., KAHL, S. D., LEWIS, A. P., GROSHONG, C., MADSEN, R. E., CONNERS, K., LINESWALA, J. P., GHEYI, T., SAFLOR, M. D., LEE, M. R., BENACH, J., BAKER, K. A., MONTROSE-RAFIZADEH, C., GENIN, M. J., MILLER, A. R. & HAMDOUCHI, C. 2018. Structural basis for GPR40 allosteric agonism and incretin stimulation. *Nat Commun,* 9**,** 1645.

HOLLIDAY, N. D., WATSON, S. J. & BROWN, A. J. 2011. Drug discovery opportunities and challenges at g protein coupled receptors for long chain free Fatty acids. *Front Endocrinol (Lausanne),* 2**,** 112.

HUDSON, B. D., SHIMPUKADE, B., MACKENZIE, A. E., BUTCHER, A. J., PEDIANI, J. D., CHRISTIANSEN, E., HEATHCOTE, H., TOBIN, A. B., ULVEN, T. & MILLIGAN, G. 2013. The pharmacology of TUG-891, a potent and selective agonist of the free fatty acid receptor 4 (FFA4/GPR120), demonstrates both potential

opportunity and possible challenges to therapeutic agonism. *Mol Pharmacol,* 84**,** 710-25.

HULME, E. C. & TREVETHICK, M. A. 2010. Ligand binding assays at equilibrium: validation and interpretation. *Br J Pharmacol,* 161**,** 1219-37.

HUSTED, A. S., EKBERG, J. H., TRIPP, E., NISSEN, T. A. D., MEIJNIKMAN, S., O'BRIEN, S. L., ULVEN, T., ACHERMAN, Y., BRUIN, S. C., NIEUWDORP, M., GERHART-HINES, Z., CALEBIRO, D., DRAGSTED, L. O. & SCHWARTZ, T. W. 2020. Autocrine negative feedback regulation of lipolysis through sensing of NEFAs by FFAR4/GPR120 in WAT. *Mol Metab,* 42**,** 101103.

IEREMIAS, L., KASPERSEN, M. H., MANANDHAR, A., SCHULTZ-KNUDSEN, K., VRETTOU, C. I., POKHREL, R., HEIDTMANN, C. V., JENKINS, L., KANELLOU, C., MARSANGO, S., LI, Y., BRAUNER-OSBORNE, H., REXEN ULVEN, E., MILLIGAN, G. & ULVEN, T. 2024. Structure-Activity Relationship Studies and Optimization of 4-Hydroxypyridones as GPR84 Agonists. *J Med Chem,* 67**,** 3542-3570.

INOUE, D., KIMURA, I., WAKABAYASHI, M., TSUMOTO, H., OZAWA, K., HARA, T., TAKEI, Y., HIRASAWA, A., ISHIHAMA, Y. & TSUJIMOTO, G. 2012. Short-chain fatty acid receptor GPR41-mediated activation of sympathetic neurons involves synapsin 2b phosphorylation. *FEBS Lett,* 586**,** 1547-54.

JENKINS, L., MARSANGO, S., MANCINI, S., MAHMUD, Z. A., MORRISON, A., MCELROY, S. P., BENNETT, K. A., BARNES, M., TOBIN, A. B., TIKHONOVA, I. G. & MILLIGAN, G. 2021. Discovery and Characterization of Novel Antagonists of the Proinflammatory Orphan Receptor GPR84. *ACS Pharmacol Transl Sci,* 4**,** 1598-1613.

KAKU, K., ENYA, K., NAKAYA, R., OHIRA, T. & MATSUNO, R. 2015. Efficacy and safety of fasiglifam (TAK-875), a G protein-coupled receptor 40 agonist, in Japanese patients with type 2 diabetes inadequately controlled by diet and exercise: a randomized, double-blind, placebo-controlled, phase III trial. *Diabetes Obes Metab,* 17**,** 675-81.

KALITA, M., PARK, J. H., KUO, R. C., HAYEE, S., MARSANGO, S., STRANIERO, V., ALAM, I. S., RIVERA-RODRIGUEZ, A., PANDRALA, M., CARLSON, M. L., REYES, S. T., JACKSON, I. M., SUIGO, L., LUO, A., NAGY, S. C., VALOTI, E., MILLIGAN, G., HABTE, F., SHEN, B. & JAMES, M. L. 2023. PET Imaging of Innate Immune Activation Using (11)C Radiotracers Targeting GPR84. *JACS Au,* 3**,** 3297-3310.

KAMBER, R. A., NISHIGA, Y., MORTON, B., BANUELOS, A. M., BARKAL, A. A., VENCES-CATALAN, F., GU, M., FERNANDEZ, D., SEOANE, J. A., YAO, D., LIU, K., LIN, S., SPEES, K., CURTIS, C., JERBY-ARNON, L., WEISSMAN, I. L., SAGE, J. & BASSIK, M. C. 2021. Inter-cellular CRISPR screens reveal regulators of cancer cell phagocytosis. *Nature,* 597**,** 549-554.

KANG, D. S., TIAN, X. & BENOVIC, J. L. 2014. Role of beta-arrestins and arrestin domain-containing proteins in G protein-coupled receptor trafficking. *Curr Opin Cell Biol,* 27**,** 63-71.

KARLSSON, F., TREMAROLI, V., NIELSEN, J. & BACKHED, F. 2013. Assessing the human gut microbiota in metabolic diseases. *Diabetes,* 62**,** 3341-9.

KARMOKAR, P. F. & MONIRI, N. H. 2022. Oncogenic signaling of the free-fatty acid receptors FFA1 and FFA4 in human breast carcinoma cells. *Biochem Pharmacol,* 206**,** 115328.

KARPE, F., DICKMANN, J. R. & FRAYN, K. N. 2011. Fatty acids, obesity, and insulin resistance: time for a reevaluation. *Diabetes,* 60**,** 2441-9.

KENAKIN, T. 2004. Principles: receptor theory in pharmacology. *Trends Pharmacol Sci,* 25**,** 186-92.

KENAKIN, T. 2013. New concepts in pharmacological efficacy at 7TM receptors: IUPHAR review 2. *Br J Pharmacol,* 168**,** 554-75.

KENAKIN, T., JENKINSON, S. & WATSON, C. 2006. Determining the potency and molecular mechanism of action of insurmountable antagonists. *J Pharmacol Exp Ther,* 319**,** 710-23.

KENAKIN, T. & STRACHAN, R. T. 2018. PAM-Antagonists: A Better Way to Block Pathological Receptor Signaling? *Trends Pharmacol Sci,* 39**,** 748-765.

KENAKIN, T. P. 2017. Allosteric Drug Effects. *Pharmacology in Drug Discovery and Development.*

KHALIL, N., MANGANAS, H., RYERSON, C. J., SHAPERA, S., CANTIN, A. M., HERNANDEZ, P., TURCOTTE, E. E., PARKER, J. M., MORAN, J. E., ALBERT, G. R., SAWTELL, R., HAGERIMANA, A., LAURIN, P., GAGNON, L., CESARI, F. & KOLB, M. 2019. Phase 2 clinical trial of PBI-4050 in patients with idiopathic pulmonary fibrosis. *Eur Respir J,* 53.

KOLB, P., KENAKIN, T., ALEXANDER, S. P. H., BERMUDEZ, M., BOHN, L. M., BREINHOLT, C. S., BOUVIER, M., HILL, S. J., KOSTENIS, E., MARTEMYANOV, K. A., NEUBIG, R. R., ONARAN, H. O., RAJAGOPAL, S., ROTH, B. L., SELENT, J., SHUKLA, A. K., SOMMER, M. E. & GLORIAM, D. E. 2022. Community guidelines for GPCR ligand bias: IUPHAR review 32. *Br J Pharmacol,* 179**,** 3651-3674.

KOMOLOV, K. E. & BENOVIC, J. L. 2018. G protein-coupled receptor kinases: Past, present and future. *Cell Signal,* 41**,** 17-24.

KOSE, M., PILLAIYAR, T., NAMASIVAYAM, V., DE FILIPPO, E., SYLVESTER, K., ULVEN, T., VON KUGELGEN, I. & MULLER, C. E. 2020. An Agonist Radioligand for the Proinflammatory Lipid-Activated G Protein-Coupled Receptor GPR84 Providing Structural Insights. *J Med Chem,* 63**,** 2391-2410.

LABÉGUÈRE, F., ALVEY, L., NEWSOME, G., SANIERE, L. & FLETCHER, S. 2014. Novel dihydropyrimidinoisoquinolinones and pharmaceutical compositions thereof for the treatment of inflammatory disorders. . *WO 2013/092791A1.*

LABÉGUÈRE, F., DUPONT, S., ALVEY, L., SOULAS, F., NEWSOME, G., TIRERA, A., QUENEHEN, V., MAI, T. T. T., DEPREZ, P., BLANQUE, R., OSTE, L., LE TALLEC, S., DE VOS, S., HAGERS, A., VANDEVELDE, A., NELLES, L., VANDERVOORT, N., CONRATH, K., CHRISTOPHE, T., VAN DER AAR, E., WAKSELMAN, E., MERCIRIS, D., COTTEREAUX, C., DA COSTA, C., SANIERE, L., CLEMENT-LACROIX, P., JENKINS, L., MILLIGAN, G., FLETCHER, S., BRYS, R. & GOSMINI, R. 2020. Discovery of 9-Cyclopropylethynyl-2-((S)-1-[1,4]dioxan-2-ylmethoxy)-6,7-dihydropyrimido[6,1-a]isoquinolin-4-one (GLPG1205), a Unique GPR84 Negative Allosteric Modulator Undergoing Evaluation in a Phase II Clinical Trial. *J Med Chem,* 63**,** 13526-13545.

LAGERSTROM, M. C. & SCHIOTH, H. B. 2008. Structural diversity of G protein-coupled receptors and significance for drug discovery. *Nat Rev Drug Discov,* 7**,** 339-57.

LATORRACA, N. R., VENKATAKRISHNAN, A. J. & DROR, R. O. 2017. GPCR Dynamics: Structures in Motion. *Chem Rev,* 117**,** 139-155.

LE POUL, E., LOISON, C., STRUYF, S., SPRINGAEL, J. Y., LANNOY, V., DECOBECQ, M. E., BREZILLON, S., DUPRIEZ, V., VASSART, G., VAN DAMME, J., PARMENTIER, M. & DETHEUX, M. 2003. Functional characterization of human receptors for short chain fatty acids and their role in polymorphonuclear cell activation. *J Biol Chem,* 278**,** 25481-9.

LEE, J. H., O'KEEFE, J. H., LAVIE, C. J. & HARRIS, W. S. 2009. Omega-3 fatty acids: cardiovascular benefits, sources and sustainability. *Nat Rev Cardiol,* 6**,** 753-8.

LEE, K. B., PTASIENSKI, J. A., PALS-RYLAARSDAM, R., GUREVICH, V. V. & HOSEY, M. M. 2000. Arrestin binding to the M(2) muscarinic acetylcholine receptor is precluded by an inhibitory element in the third intracellular loop of the receptor. *J Biol Chem,* 275**,** 9284-9.

LEFKOWITZ, R. J. 2004. Historical review: a brief history and personal retrospective of seven-transmembrane receptors. *Trends Pharmacol Sci,* 25**,** 413-22.

LIU, H., ZHANG, Q., HE, X., JIANG, M., WANG, S., YAN, X., CHENG, X., LIU, Y., NAN, F. J., XU, H. E., XIE, X. & YIN, W. 2023. Structural insights into ligand recognition and activation of the medium-chain fatty acid-sensing receptor GPR84. *Nat Commun,* 14**,** 3271.

LIU, Y., ZHANG, Q., CHEN, L. H., YANG, H., LU, W., XIE, X. & NAN, F. J. 2016. Design and Synthesis of 2-Alkylpyrimidine-4,6-diol and 6-Alkylpyridine-2,4-diol as Potent GPR84 Agonists. *ACS Med Chem Lett,* 7**,** 579-83.

LOGOTHETIS, D. E., KURACHI, Y., GALPER, J., NEER, E. J. & CLAPHAM, D. E. 1987. The beta gamma subunits of GTP-binding proteins activate the muscarinic K+ channel in heart. *Nature,* 325**,** 321–326.

LOHSE, M. J. & HOFFMANN, C. 2014. Arrestin interactions with G protein-coupled receptors. *Handbook of Experimental Pharmacology,* 219, 15.

LU, H., WANG, J., WANG, Y., QIAO, L. & ZHOU, Y. 2016. Embelin and Its Role in Chronic Diseases. *Adv Exp Med Biol,* 928:397-418.

LU, Y., ZHANG, Y., ZHAO, X., SHANG, C., XIANG, M., LI, L. & CUI, X. 2022. Microbiota-derived short-chain fatty acids: Implications for cardiovascular and metabolic disease. *Front Cardiovasc Med,* 9**,** 900381.

LUCY, D., PURVIS, G. S. D., ZEBOUDJ, L., CHATZOPOULOU, M., RECIO, C., BATAILLE, C. J. R., WYNNE, G. M., GREAVES, D. R. & RUSSELL, A. J. 2019. A Biased Agonist at Immunometabolic Receptor GPR84 Causes Distinct Functional Effects in Macrophages. *ACS Chem Biol,* 14**,** 2055-2064.

LUNDQUIST, F., TYGSTRUP, N., WINKLER, K., MELLEMGAARD, K. & MUNCK-PETERSEN, S. 1962. Ethanol metabolism and production of free acetate in the human liver. *J Clin Invest,* 41**,** 955-61.

LUSCOMBE, V. B., BAENA-LOPEZ, L. A., BATAILLE, C. J. R., RUSSELL, A. J. & GREAVES, D. R. 2023. Kinetic insights into agonist-dependent signalling bias at the pro-inflammatory G-protein coupled receptor GPR84. *Eur J Pharmacol,* 956**,** 175960.

LUSCOMBE, V. B., LUCY, D., BATAILLE, C. J. R., RUSSELL, A. J. & GREAVES, D. R. 2020. 20 Years an Orphan: Is GPR84 a Plausible Medium-Chain Fatty Acid-Sensing Receptor? *DNA Cell Biol,* 39**,** 1926-1937.

LUTTRELL, L. M. & LEFKOWITZ, R. J. 2002. The role of ß-arrestins in the termination and transduction of G-protein-coupled receptor signals. . *Journal of Cell Science* 115, 455-465.

LUTTRELL, L. M., MAUDSLEY, S. & BOHN, L. M. 2015. Fulfilling the Promise of "Biased" G Protein-Coupled Receptor Agonism. *Mol Pharmacol,* 88**,** 579-88.

MAGGIO, R., FASCIANI, I., CARLI, M., PETRAGNANO, F., MARAMPON, F., ROSSI, M. & SCARSELLI, M. 2021. Integration and Spatial Organization of Signaling by G Protein-Coupled Receptor Homo- and Heterodimers. *Biomolecules,* 11.

MAHARANA, J., SARMA, P., YADAV, M. K., SAHA, S., SINGH, V., SAHA, S., CHAMI, M., BANERJEE, R. & SHUKLA, A. K. 2023. Structural snapshots uncover a key phosphorylation motif in GPCRs driving beta-arrestin activation. *Mol Cell,* 83**,** 2091-2107 e7.

MAHINDRA, A., JENKINS, L., MARSANGO, S., HUGGETT, M., HUGGETT, M., ROBINSON, L., GILLESPIE, J., RAJAMANICKAM, M., MORRISON, A., MCELROY, S., TIKHONOVA, I. G., MILLIGAN, G. & JAMIESON, A. G. 2022. Investigating

the Structure-Activity Relationship of 1,2,4-Triazine G-Protein-Coupled Receptor 84 (GPR84) Antagonists. *J Med Chem,* 65, 11270-11290.

MANCINI, S. J., MAHMUD, Z. A., JENKINS, L., BOLOGNINI, D., NEWMAN, R., BARNES, M., EDYE, M. E., MCMAHON, S. B., TOBIN, A. B. & MILLIGAN, G. 2019. On-target and off-target effects of novel orthosteric and allosteric activators of GPR84. *Sci Rep,* 9, 1861.

MARQUES, M., LAFLAMME, L., BENASSOU, I., CISSOKHO, C., GUILLEMETTE, B. & GAUDREAU, L. 2014. Low levels of 3,3′-diindolylmethane activate estrogen receptor α and induce proliferation of breast cancer cells in the absence of estradiol. *BMC Cancer,* 14, 524.

MARSANGO, S., BARKI, N., JENKINS, L., TOBIN, A. B. & MILLIGAN, G. 2020. Therapeutic validation of an orphan G protein-coupled receptor: The case of GPR84. *Br J Pharmacol,* 179, 3529-3541.

MARSANGO, S. & MILLIGAN, G. 2023. Regulation of the pro-inflammatory G protein-coupled receptor GPR84. *Br J Pharmacol.*

MARSANGO, S., WARD, R. J., JENKINS, L., BUTCHER, A. J., AL MAHMUD, Z., DWOMOH, L., NAGEL, F., SCHULZ, S., TIKHONOVA, I. G., TOBIN, A. B. & MILLIGAN, G. 2022. Selective phosphorylation of threonine residues defines GPR84-arrestin interactions of biased ligands. *J Biol Chem,* 298, 101932.

MARY, S., FEHRENTZ, J. A., DAMIAN, M., VERDIE, P., MARTINEZ, J., MARIE, J. & BANERES, J. L. 2013. How ligands and signalling proteins affect G-protein-coupled receptors' conformational landscape. *Biochem Soc Trans,* 41, 144-7.

MASLOWSKI, K. M., VIEIRA, A. T., NG, A., KRANICH, J., SIERRO, F., YU, D., SCHILTER, H. C., ROLPH, M. S., MACKAY, F., ARTIS, D., XAVIER, R. J., TEIXEIRA, M. M. & MACKAY, C. R. 2009. Regulation of inflammatory responses by gut microbiota and chemoattractant receptor GPR43. *Nature,* 461, 1282-6.

MATTHEES, E. S. F., HAIDER, R. S., HOFFMANN, C. & DRUBE, J. 2021. Differential Regulation of GPCRs-Are GRK Expression Levels the Key? *Front Cell Dev Biol,* 9, 687489.

MILLIGAN, G. 2003. Principles: Extending the utility of [35S]GTPgS binding assays. *TRENDS in Pharmacological Sciences,* Vol.24 No.2.

MILLIGAN, G., ALVAREZ-CURTO, E., HUDSON, B. D., PRIHANDOKO, R. & TOBIN, A. B. 2017a. FFA4/GPR120: Pharmacology and Therapeutic Opportunities. *Trends Pharmacol Sci,* 38, 809-821.

MILLIGAN, G., BARKI, N. & TOBIN, A. B. 2021. Chemogenetic Approaches to Explore the Functions of Free Fatty Acid Receptor 2. *Trends Pharmacol Sci,* 42, 191-202.

MILLIGAN, G. & KOSTENIS, E. 2006. Heterotrimeric G-proteins: a short history. *Br J Pharmacol,* 147 Suppl 1, S46-55.

MILLIGAN, G., SHIMPUKADE, B., ULVEN, T. & HUDSON, B. D. 2017b. Complex Pharmacology of Free Fatty Acid Receptors. *Chem Rev,* 117, 67-110.

MISHRA, S. P., KARUNAKAR, P., TARAPHDER, S. & YADAV, H. 2020. Free Fatty Acid Receptors 2 and 3 as Microbial Metabolite Sensors to Shape Host Health: Pharmacophysiological View. *Biomedicines,* 8.

MIYAUCHI, S., HIRASAWA, A., IGA, T., LIU, N., ITSUBO, C., SADAKANE, K., HARA, T. & TSUJIMOTO, G. 2009. Distribution and regulation of protein expression of the free fatty acid receptor GPR120. *Naunyn Schmiedebergs Arch Pharmacol,* 379, 427-34.

MM, K. & AA., C. 2007. Misfolded proteins traffic from the endoplasmic reticulum (ER) due to ER export signals. *Mol Biol Cell,* 18(2):455-63. .

MOLLER, T. C., MOO, E. V., INOUE, A., PEDERSEN, M. F. & BRAUNER-OSBORNE, H. 2024. Characterization of the real-time internalization of nine GPCRs reveals distinct dependence on arrestins and G proteins. *Biochim Biophys Acta Mol Cell Res,* 1871**,** 119584.

MONTGOMERY, M. K., OSBORNE, B., BRANDON, A. E., O'REILLY, L., FIVEASH, C. E., BROWN, S. H. J., WILKINS, B. P., SAMSUDEEN, A., YU, J., DEVANAPALLI, B., HERTZOG, A., TOLUN, A. A., KAVANAGH, T., COOPER, A. A., MITCHELL, T. W., BIDEN, T. J., SMITH, N. J., COONEY, G. J. & TURNER, N. 2019. Regulation of mitochondrial metabolism in murine skeletal muscle by the medium-chain fatty acid receptor Gpr84. *FASEB J,* 33**,** 12264-12276.

MOO, E. V., VAN SENTEN, J. R., BRAUNER-OSBORNE, H. & MOLLER, T. C. 2021. Arrestin-Dependent and -Independent Internalization of G Protein-Coupled Receptors: Methods, Mechanisms, and Implications on Cell Signaling. *Mol Pharmacol,* 99**,** 242-255.

MOORE, M. N., PERSON, K. L., ALWIN, A., KRUSEMARK, C., FOSTER, N., RAY, C., INOUE, A., JACKSON, M. R., SHEEDLO, M. J., BARAK, L. S., FERNANDEZ DE VELASCO, E. M., OLSON, S. H. & SLOSKY, L. M. 2024. Design of allosteric modulators that change GPCR G protein subtype selectivity. *bioRxiv.*

NAGASAKI, H., KONDO, T., FUCHIGAMI, M., HASHIMOTO, H., SUGIMURA, Y., OZAKI, N., ARIMA, H., OTA, A., OISO, Y. & HAMADA, Y. 2012. Inflammatory changes in adipose tissue enhance expression of GPR84, a medium-chain fatty acid receptor: TNFalpha enhances GPR84 expression in adipocytes. *FEBS Lett,* 586**,** 368-72.

NAJA, K., ANWARDEEN, N., MALKI, A. M. & ELRAYESS, M. A. 2024. Metformin increases 3-hydroxy medium chain fatty acids in patients with type 2 diabetes: a cross-sectional pharmacometabolomic study. *Front Endocrinol (Lausanne),* 15**,** 1313597.

NAMKUNG, Y., DIPACE, C., URIZAR, E., JAVITCH, J. A. & SIBLEY, D. R. 2009. G protein-coupled receptor kinase-2 constitutively regulates D2 dopamine receptor expression and signaling independently of receptor phosphorylation. *J Biol Chem,* 284**,** 34103-15.

NGUYEN, A. H. & LEFKOWITZ, R. J. 2021. Signaling at the endosome: cryo-EM structure of a GPCR-G protein-beta-arrestin megacomplex. *FEBS J,* 288**,** 2562-2569.

NGUYEN, A. H., THOMSEN, A. R. B., CAHILL, T. J., 3RD, HUANG, R., HUANG, L. Y., MARCINK, T., CLARKE, O. B., HEISSEL, S., MASOUDI, A., BEN-HAIL, D., SAMAAN, F., DANDEY, V. P., TAN, Y. Z., HONG, C., MAHONEY, J. P., TRIEST, S., LITTLE, J. T., CHEN, X., SUNAHARA, R., STEYAERT, J., MOLINA, H., YU, Z., DES GEORGES, A. & LEFKOWITZ, R. J. 2019. Structure of an endosomal signaling GPCR-G protein-beta-arrestin megacomplex. *Nat Struct Mol Biol,* 26**,** 1123-1131.

NGUYEN, Q. T., NSAIBIA, M. J., SIROIS, M. G., CALDERONE, A., TARDIF, J. C., FEN SHI, Y., RUIZ, M., DANEAULT, C., GAGNON, L., GROUIX, B., LAURIN, P. & DUPUIS, J. 2020. PBI-4050 reduces pulmonary hypertension, lung fibrosis, and right ventricular dysfunction in heart failure. *Cardiovasc Res,* 116**,** 171-182.

NICOL, L. S., DAWES, J. M., LA RUSSA, F., DIDANGELOS, A., CLARK, A. K., GENTRY, C., GRIST, J., DAVIES, J. B., MALCANGIO, M. & MCMAHON, S. B. 2015. The role of G-protein receptor 84 in experimental neuropathic pain. *J Neurosci,* 35**,** 8959-69.

NIKOLOVSKA-COLESKA, Z., WANG, R., FANG, X., PAN, H., TOMITA, Y., LI, P., ROLLER, P. P., KRAJEWSKI, K., SAITO, N. G., STUCKEY, J. A. & WANG, S.

2004. Development and optimization of a binding assay for the XIAP BIR3 domain using fluorescence polarization. *Anal Biochem,* 332**,** 261-73.

NOHR, M. K., EGEROD, K. L., CHRISTIANSEN, S. H., GILLE, A., OFFERMANNS, S., SCHWARTZ, T. W. & MOLLER, M. 2015. Expression of the short chain fatty acid receptor GPR41/FFAR3 in autonomic and somatic sensory ganglia. *Neuroscience,* 290**,** 126-37.

NUTT, D., STAHL, S., BLIER, P., DRAGO, F., ZOHAR, J. & WILSON, S. 2017. Inverse agonists - What do they mean for psychiatry? *Eur Neuropsychopharmacol,* 27**,** 87-90.

OH, D. Y., TALUKDAR, S., BAE, E. J., IMAMURA, T., MORINAGA, H., FAN, W., LI, P., LU, W. J., WATKINS, S. M. & OLEFSKY, J. M. 2010. GPR120 is an omega-3 fatty acid receptor mediating potent anti-inflammatory and insulin-sensitizing effects. *Cell,* 142**,** 687-98.

PAGE, K. A., WILLIAMSON, A., YU, N., MCNAY, E. C., DZUIRA, J., MCCRIMMON, R. J. & SHERWIN, R. S. 2009. Medium-chain fatty acids improve cognitive function in intensively treated type 1 diabetic patients and support in vitro synaptic transmission during acute hypoglycemia. *Diabetes,* 58**,** 1237-44.

PALMER, C. B., D'UONNOLO, G., LUIS, R., MEYRATH, M., UCHANSKI, T., CHEVIGNE, A. & SZPAKOWSKA, M. 2022. Nanoluciferase-based complementation assay for systematic profiling of GPCR-GRK interactions. *Methods Cell Biol,* 169**,** 309-321.

PAPAMANDJARIS, A. A., MACDOUGALL, D. E. & JONES, P. J. H. 1998. Medium chain fatty acid metabolism and energy expenditure: obesity treatment implications. . *Life Sci.,* 62(14)**,** 1203–1215.

PARK, J. Y., LEE, S. Y., KIM, H. R., SEO, M. D. & CHUNG, K. Y. 2016. Structural mechanism of GPCR-arrestin interaction: recent breakthroughs. *Arch Pharm Res,* 39**,** 293-301.

PATEL, M., KAWANO, T., SUZUKI, N., HAMAKUBO, T., KARGINOV, A. V. & KOZASA, T. 2014. Galpha13/PDZ-RhoGEF/RhoA signaling is essential for gastrin-releasing peptide receptor-mediated colon cancer cell migration. *Mol Pharmacol,* 86**,** 252-62.

PETERS, A., RABE, P., KRUMBHOLZ, P., KALWA, H., KRAFT, R., SCHONEBERG, T. & STAUBERT, C. 2020. Natural biased signaling of hydroxycarboxylic acid receptor 3 and G protein-coupled receptor 84. *Cell Commun Signal,* 18**,** 31.

PILLAIYAR, T., KOSE, M., NAMASIVAYAM, V., SYLVESTER, K., BORGES, G., THIMM, D., VON KUGELGEN, I. & MULLER, C. E. 2018. 6-(Ar)Alkylamino-Substituted Uracil Derivatives: Lipid Mimetics with Potent Activity at the Orphan G Protein-Coupled Receptor 84 (GPR84). *ACS Omega,* 3**,** 3365-3383.

PILLAIYAR, T., KOSE, M., SYLVESTER, K., WEIGHARDT, H., THIMM, D., BORGES, G., FORSTER, I., VON KUGELGEN, I. & MULLER, C. E. 2017. Diindolylmethane Derivatives: Potent Agonists of the Immunostimulatory Orphan G Protein-Coupled Receptor GPR84. *J Med Chem,* 60**,** 3636-3655.

PUENGEL, T., DE VOS, S., HUNDERTMARK, J., KOHLHEPP, M., GULDIKEN, N., PUJUGUET, P., AUBERVAL, M., MARSAIS, F., SHOJI, K. F., SANIERE, L., TRAUTWEIN, C., LUEDDE, T., STRNAD, P., BRYS, R., CLEMENT-LACROIX, P. & TACKE, F. 2020. The Medium-Chain Fatty Acid Receptor GPR84 Mediates Myeloid Cell Infiltration Promoting Steatohepatitis and Fibrosis. *J Clin Med,* 9.

QIN, G., LIU, S., LIU, J., HU, H., YANG, L., ZHAO, Q., LI, C., ZHANG, B. & ZHANG, Y. 2023. Overcoming resistance to immunotherapy by targeting GPR84 in myeloid-derived suppressor cells. *Signal Transduct Target Ther,* 8**,** 164.

QIU, Y., HOU, Y., GOHEL, D., ZHOU, Y., XU, J., BYKOVA, M., YANG, Y., LEVERENZ, J. B., PIEPER, A. A., NUSSINOV, R., CALDWELL, J. Z. K., BROWN, J. M. &

CHENG, F. 2024. Systematic characterization of multi-omics landscape between gut microbial metabolites and GPCRome in Alzheimer's disease. *Cell Rep,* 43**,** 114128.

RAIBORG, C., BREMNES, B., MEHLUM, A., GILLOOLY, D. J., D'ARRIGO, A., STANG, E. & STENMARK, H. 2001 FYVE and coiled-coil domains determine the specific

localisation of Hrs to early endosomes. *Journal of Cell Science 114, 2255-2263.*

RAJAGOPAL, S. & SHENOY, S. K. 2018. GPCR desensitization: Acute and prolonged phases. *Cell Signal,* 41**,** 9-16.

RANKOVIC, Z., BRUST, T. F. & BOHN, L. M. 2016. Biased agonism: An emerging paradigm in GPCR drug discovery. *Bioorg Med Chem Lett,* 26**,** 241-250.

RECIO, C., LUCY, D., PURVIS, G. S. D., IVESON, P., ZEBOUDJ, L., IQBAL, A. J., LIN, D., O'CALLAGHAN, C., DAVISON, L., GRIESBACH, E., RUSSELL, A. J., WYNNE, G. M., DIB, L., MONACO, C. & GREAVES, D. R. 2018. Activation of the Immune-Metabolic Receptor GPR84 Enhances Inflammation and Phagocytosis in Macrophages. *Front Immunol,* 9**,** 1419.

RHEE, S. G. 2001. regulation of phosphoinositide-specific phospholipase c. *Annual Review of Biochemistry,* 70(1), 281-312.

RIOBO, N. A., SAUCY, B., DILIZIO, C. & MANNING, D. R. 2006. Activation of heterotrimeric G proteins by Smoothened. *Proc Natl Acad Sci U S A,* 103**,** 12607-12.

ROSSI, A. M. & TAYLOR, C. W. 2011. Analysis of protein-ligand interactions by fluorescence polarization. *Nat Protoc,* 6**,** 365-87.

SHCHEPINOVA, M. M., HANYALOGLU, A. C., FROST, G. S. & TATE, E. W. 2020. Chemical biology of noncanonical G protein-coupled receptor signaling: Toward advanced therapeutics. *Curr Opin Chem Biol,* 56**,** 98-110.

SIKARWAR, A. S., BHAGIRATH, A. Y. & DAKSHINAMURTI, S. 2019. Effects of Post-translational Modifications on Membrane Localization and Signaling of Prostanoid GPCR-G Protein Complexes and the Role of Hypoxia. *J Membr Biol,* 252**,** 509-526.

SIMON, M. I., STRATHMANN, M. P. & GAUTAM, N. 1991a. Diversity of G Proteins in Signal Transduction. *Science,* 252, 802-808.

SIMON, M. I., STRATHMANN, M. P. & GAUTAM, N. 1991b. Diversity of G-proteins in signal transduction. *Science,* 252, 802-808.

SMITH, J. S. & PACK, T. F. 2021. Noncanonical interactions of G proteins and beta-arrestins: from competitors to companions. *FEBS J,* 288**,** 2550-2561.

SMITH, J. S. & RAJAGOPAL, S. 2016. The beta-Arrestins: Multifunctional Regulators of G Protein-coupled Receptors. *J Biol Chem,* 291**,** 8969-77.

SMITH, N. J. & MILLIGAN, G. 2010. Allostery at G protein-coupled receptor homo- and heteromers: uncharted pharmacological landscapes.

. *Pharmacological Reviews, 62(4), 701-725.*

SOUTHERN, C., COOK, J. M., NEETOO-ISSELJEE, Z., TAYLOR, D. L., KETTLEBOROUGH, C. A., MERRITT, A., BASSONI, D. L., RAAB, W. J., QUINN, E., WEHRMAN, T. S., DAVENPORT, A. P., BROWN, A. J., GREEN, A., WIGGLESWORTH, M. J. & REES, S. 2013. Screening beta-arrestin recruitment for the identification of natural ligands for orphan G-protein-coupled receptors. *J Biomol Screen,* 18**,** 599-609.

SPRANG, S. R., CHEN, Z. & DU, X. 2007. Structural basis of effector regulation and signal termination in heterotrimeric Galpha proteins. *Adv Protein Chem,* 74**,** 1-65.

SRIRAM, K. & INSEL, P. A. 2018. G Protein-Coupled Receptors as Targets for Approved Drugs: How Many Targets and How Many Drugs? *Mol Pharmacol,* 93**,** 251-258.

SRIVASTAVA, A., YANO, J., HIROZANE, Y., KEFALA, G., GRUSWITZ, F., SNELL, G., LANE, W., IVETAC, A., AERTGEERTS, K., NGUYEN, J., JENNINGS, A. & OKADA, K. 2014. High-resolution structure of the human GPR40 receptor bound to allosteric agonist TAK-875. *Nature*, 513, 124-7.

STÉPHANE A. LAPORTE, R. H. O., JIE ZHANG, JASON A. HOLT, STEPHEN S. G. FERGUSON,* MARC G. CARON,† AND LARRY S. BARAK 1999. The ß2-adrenergic receptor/ßarrestin complex recruits the clathrin adaptor AP-2 during endocytosis. *Proc Natl Acad Sci U S A. 1999 Mar 30;96(7):3712-7. doi: 10.1073/pnas.96.7.3712. PMID: 10097102; PMCID: PMC22359.*

STODDART, L. A., BROWN, A. J. & MILLIGAN, G. 2007. Uncovering the pharmacology of the G protein-coupled receptor GPR40: high apparent constitutive activity in guanosine 5'-O-(3-[35S]thio)triphosphate binding studies reflects binding of an endogenous agonist. *Mol Pharmacol*, 71, 994-1005.

STODDART, L. A., SMITH, N. J., JENKINS, L., BROWN, A. J. & MILLIGAN, G. 2008a. Conserved polar residues in transmembrane domains V, VI, and VII of free fatty acid receptor 2 and free fatty acid receptor 3 are required for the binding and function of short chain fatty acids. *J Biol Chem*, 283, 32913-24.

STODDART, L. A., SMITH, N. J. & MILLIGAN, G. 2008b. International Union of Pharmacology. LXXI. Free fatty acid receptors FFA1, -2, and -3: pharmacology and pathophysiological functions. *Pharmacol Rev*, 60, 405-17.

STRAMBU, I. R., SEEMAYER, C. A., FAGARD, L. M. A., FORD, P. A., VAN DER AA, T. A. K., DE HAAS-AMATSALEH, A. A., MODGILL, V., SANTERMANS, E., SONDAG, E. N., HELMER, E. G., MAHER, T. M., COSTABEL, U. & COTTIN, V. 2023. GLPG1205 for idiopathic pulmonary fibrosis: a phase 2 randomised placebo-controlled trial. *Eur Respir J*, 61.

SULON, S. M. & BENOVIC, J. L. 2021. Targeting G protein-coupled receptor kinases (GRKs) to G protein-coupled receptors. *Curr Opin Endocr Metab Res*, 16, 56-65.

SUN, X. N., AN, Y. A., PASCHOAL, V. A., DE SOUZA, C. O., WANG, M. Y., VISHVANATH, L., BUENO, L. M., COBB, A. S., NIETO CARRION, J. A., IBE, M. E., LI, C., KIDD, H. A., CHEN, S., LI, W., GUPTA, R. K. & OH, D. Y. 2023. GPR84-mediated signal transduction affects metabolic function by promoting brown adipocyte activity. *J Clin Invest*, 133.

SUNDQVIST, M., CHRISTENSON, K., HOLDFELDT, A., GABL, M., MARTENSSON, J., BJORKMAN, L., DIECKMANN, R., DAHLGREN, C. & FORSMAN, H. 2018. Similarities and differences between the responses induced in human phagocytes through activation of the medium chain fatty acid receptor GPR84 and the short chain fatty acid receptor FFA2R. *Biochim Biophys Acta Mol Cell Res*, 1865, 695-708.

SUZUKI, M., TAKAISHI, S., NAGASAKI, M., ONOZAWA, Y., IINO, I., MAEDA, H., KOMAI, T. & ODA, T. 2013. Medium-chain fatty acid-sensing receptor, GPR84, is a proinflammatory receptor. *J Biol Chem*, 288, 10684-91.

SYROVATKINA, V., ALEGRE, K. O., DEY, R. & HUANG, X. Y. 2016. Regulation, Signaling, and Physiological Functions of G-Proteins. *J Mol Biol*, 428, 3850-68.

TAKEDA, S., YAMAMOTO, A., OKADA, T., MATSUMURA, E., NOSE, E., KOGURE, K., KOJIMA, S. & HAGA, T. 2003. Identification of surrogate ligands for orphan G protein-coupled receptors. *Life Sci*, 74, 367-77.

TENNAKOON, M., SENARATH, K., KANKANAMGE, D., RATNAYAKE, K., WIJAYARATNA, D., OLUPOTHAGE, K., UBEYSINGHE, S., MARTINS-CANNAVINO, K., HEBERT, T. E. & KARUNARATHNE, A. 2021. Subtype-dependent regulation of Gbetagamma signalling. *Cell Signal*, 82, 109947.

THOMSEN, A. R. B., PLOUFFE, B., CAHILL, T. J., 3RD, SHUKLA, A. K., TARRASCH, J. T., DOSEY, A. M., KAHSAI, A. W., STRACHAN, R. T., PANI, B., MAHONEY, J. P., HUANG, L., BRETON, B., HEYDENREICH, F. M., SUNAHARA, R. K., SKINIOTIS, G., BOUVIER, M. & LEFKOWITZ, R. J. 2016. GPCR-G Protein-beta-Arrestin Super-Complex Mediates Sustained G Protein Signaling. *Cell,* 166, 907-919.

TOBIN, A. B. 2008. G-protein-coupled receptor phosphorylation: where, when and by whom. *Br J Pharmacol,* 153 Suppl 1, S167-76.

TOBIN, A. B., BUTCHER, A. J. & KONG, K. C. 2008. Location, location, location...site-specific GPCR phosphorylation offers a mechanism for cell-type-specific signalling. *Trends Pharmacol Sci,* 29, 413-20.

ULVEN, T. & CHRISTIANSEN, E. 2015. Dietary Fatty Acids and Their Potential for Controlling Metabolic Diseases Through Activation of FFA4/GPR120. *Annu Rev Nutr,* 35, 239-63.

UNSON, C. G., WU, C.-R., JIANG, Y., YOO, B., CHEUNG, C., SAKMAR, T. P. & MERRIFIELD, R. B. 2002. Roles of Specific Extracellular Domains of the Glucagon Receptor in Ligand Binding and Signaling. *Biochemistry, 41,* *11795-11803.*

URIZAR, E., CLAEYSEN, S., DEUPI, X., GOVAERTS, C., COSTAGLIOLA, S., VASSART, G. & PARDO, L. 2005. An activation switch in the rhodopsin family of G protein-coupled receptors: the thyrotropin receptor. *J Biol Chem,* 280, 17135-41.

VENKATAKRISHNAN, A. J., DEUPI, X., LEBON, G., TATE, C. G., SCHERTLER, G. F. & BABU, M. M. 2013. Molecular signatures of G-protein-coupled receptors. *Nature,* 494, 185-94.

VENKATARAMAN, C. & KUO, F. 2005. The G-protein coupled receptor, GPR84 regulates IL-4 production by T lymphocytes in response to CD3 crosslinking. *Immunol Lett,* 101, 144-53.

VIZURRAGA, A., ADHIKARI, R., YEUNG, J., YU, M. & TALL, G. G. 2020. Mechanisms of adhesion G protein-coupled receptor activation. *J Biol Chem,* 295, 14065-14083.

VOGEL, R., MAHALINGAM, M., LUDEKE, S., HUBER, T., SIEBERT, F. & SAKMAR, T. P. 2008. Functional role of the "ionic lock"--an interhelical hydrogen-bond network in family A heptahelical receptors. *J Mol Biol,* 380, 648-55.

WANG, F., MA, L., DING, Y., HE, L., CHANG, M., SHAN, Y., SIWKO, S., CHEN, G., LIU, Y., JIN, Y., PENG, X. & LUO, J. 2021. Fatty acid sensing GPCR (GPR84) signaling safeguards cartilage homeostasis and protects against osteoarthritis. *Pharmacol Res,* 164, 105406.

WANG, J., WU, X., SIMONAVICIUS, N., TIAN, H. & LING, L. 2006. Medium-chain fatty acids as ligands for orphan G protein-coupled receptor GPR84. *J Biol Chem,* 281, 34457-64.

WANG, P., RAJA, A., LUSCOMBE, V. B., BATAILLE, C. J. R., LUCY, D., ROGGA, V. V., GREAVES, D. R. & RUSSELL, A. J. 2024. Development of Highly Potent, G-Protein Pathway Biased, Selective, and Orally Bioavailable GPR84 Agonists. *J Med Chem,* 67, 110-137.

WANG, S. W., ZHANG, Q., LU, D., FANG, Y. C., YAN, X. C., CHEN, J., XIA, Z. K., YUAN, Q. T., CHEN, L. H., ZHANG, Y. M., NAN, F. J. & XIE, X. 2023. GPR84 regulates pulmonary inflammation by modulating neutrophil functions. *Acta Pharmacol Sin,* 1-11.

WANG, T. T., SCHOENE, N. W., MILNER, J. A. & KIM, Y. S. 2012. Broccoli-derived phytochemicals indole-3-carbinol and 3,3'-diindolylmethane exerts concentration-dependent pleiotropic effects on prostate cancer cells:

comparison with other cancer preventive phytochemicals. *Mol Carcinog,* 51**,** 244-56.

WATSON, N., LINDER, M. E., DRUEY, K. M., KEHRL, J. H. & BLUMER, K. J. 1996. RGS family members: GTPase-activating proteins for heterotrimeric G-protein α-subunits. *Nature 383,* 172–175.

WHALEN, E. J., RAJAGOPAL, S. & LEFKOWITZ, R. J. 2011. Therapeutic potential of beta-arrestin- and G protein-biased agonists. *Trends Mol Med,* 17**,** 126-39.

WINGLER, L. M. & LEFKOWITZ, R. J. 2020. Conformational Basis of G Protein-Coupled Receptor Signaling Versatility. *Trends Cell Biol,* 30**,** 736-747.

WITTENBERGER, T., SCHALLER, H. C. & HELLEBRAND, S. 2001. An expressed sequence tag (EST) data mining strategy succeeding in the discovery of new G-protein coupled receptors. *J Mol Biol,* 307**,** 799-813.

WOJCIECHOWICZ, M. L. & MA'AYAN, A. 2020. GPR84: an immune response dial? *Nat Rev Drug Discov,* 19**,** 374.

XIAO, Y., CHEN, J., LI, S., ZHANG, Q., LIU, Y., CHEN, L., SUN, Y., GU, M., XIE, X. & NAN, F. 2024. Discovery of GPR84 Fluorogenic Probes Based on a Novel Antagonist for GPR84 Bioimaging. *J Med Chem,* 67**,** 10875-10890.

YANG, D., ZHOU, Q., LABROSKA, V., QIN, S., DARBALAEI, S., WU, Y., YULIANTIE, E., XIE, L., TAO, H., CHENG, J., LIU, Q., ZHAO, S., SHUI, W., JIANG, Y. & WANG, M. W. 2021. G protein-coupled receptors: structure- and function-based drug discovery. *Signal Transduct Target Ther,* 6**,** 7.

YANG, F., YU, X., LIU, C., QU, C. X., GONG, Z., LIU, H. D., LI, F. H., WANG, H. M., HE, D. F., YI, F., SONG, C., TIAN, C. L., XIAO, K. H., WANG, J. Y. & SUN, J. P. 2015. Phospho-selective mechanisms of arrestin conformations and functions revealed by unnatural amino acid incorporation and (19)F-NMR. *Nat Commun,* 6**,** 8202.

YANG, Z., YANG, F., ZHANG, D., LIU, Z., LIN, A., LIU, C., XIAO, P., YU, X. & SUN, J. P. 2017. Phosphorylation of G Protein-Coupled Receptors: From the Barcode Hypothesis to the Flute Model. *Mol Pharmacol,* 92**,** 201-210.

YONEZAWA, T., KATOH, K. & OBARA, Y. 2004. Existence of GPR40 functioning in a human breast cancer cell line, MCF-7. *Biochem Biophys Res Commun,* 314**,** 805-9.

YOUSEFI, S., COOPER, P. R., POTTER, S. L., MUECK, B. & JARAI, G. 2001. Cloning and expression analysis of a novel G-protein-coupled receptor selectively expressed on granulocytes. *Journal of Leukocyte Biology,* 69**,** 1045-1052.

ZHANG, Q., CHEN, L. H., YANG, H., FANG, Y. C., WANG, S. W., WANG, M., YUAN, Q. T., WU, W., ZHANG, Y. M., LIU, Z. J., NAN, F. J. & XIE, X. 2022. GPR84 signaling promotes intestinal mucosal inflammation via enhancing NLRP3 inflammasome activation in macrophages. *Acta Pharmacol Sin,* 43**,** 2042-2054.

ZHANG, Q., YANG, H., LI, J. & XIE, X. 2016. Discovery and Characterization of a Novel Small-Molecule Agonist for Medium-Chain Free Fatty Acid Receptor G Protein-Coupled Receptor 84. *J Pharmacol Exp Ther,* 357**,** 337-44.

ZHANG, X., GUSEINOV, A. A., JENKINS, L., LI, K., TIKHONOVA, I. G., MILLIGAN, G. & ZHANG, C. 2023a. Structural basis for the ligand recognition and signaling of free fatty acid receptors. *bioRxiv.*

ZHANG, X., WANG, Y., SUPEKAR, S., CAO, X., ZHOU, J., DANG, J., CHEN, S., JENKINS, L., MARSANGO, S., LI, X., LIU, G., MILLIGAN, G., FENG, M., FAN, H., GONG, W. & ZHANG, C. 2023b. Pro-phagocytic function and structural basis of GPR84 signaling. *Nat Commun,* 14**,** 5706.